Targeting C5aR1 to improve radiation response of high-grade glioma

Sze Wing Kelly Lee

The Queen's College

University of Oxford

A thesis submitted for the degree of *Doctor of Philosophy*

Trinity 2025

Supervisor

Dr. Monica Olcina del Molino

Prof. Ester M Hammond

Word count: 40344 (excluding references)

Abstract

High-grade gliomas (HGGs) are aggressive grade III or IV brain tumours originating from glial cells, characterised by rapid growth, poor prognosis and high recurrence rates. Radiotherapy remains the standard of care treatment for HGG, yet, treatment resistance, particularly due to its hypoxic nature, remains a key challenge, and a novel effective therapeutic strategy is needed to improve treatment efficacy. Despite the immunosuppressive tumour microenvironment, the complement receptor C5aR1 is overexpressed in glioblastoma and paediatric HGGs compared to healthy brain tissue. In this study, we identified that C5aR1 expression was upregulated under severe hypoxia in glioblastoma, driven by endoplasmic reticulum stress, and that C5aR1 signalling was critical for glioma cell survival. We also explored the potential of C5aR1 inhibition as a radiosensitising target in both glioblastoma and diffuse midline glioma, given its ability in modulating pro-survival signalling via G-protein coupled receptor activity. Both genetic silencing and pharmacological inhibition of C5aR1 enhanced glioma sensitivity to radiation and potentiated radiation-induced cytotoxicity. Importantly, these anti-survival effects were sustained under hypoxic conditions in 2D culture models, addressing a key barrier to radiotherapy efficacy. In contrast, C5aR1 inhibition in microglia did not reduce cell survival, but instead altered their inflammatory phenotype following irradiation. The suppression of microglia-derived pro-inflammatory factors, IL-1β in particular, was found to improve glioma radiosensitivity, highlighting a dual mechanism by which C5aR1 target may enhance radiation response and outcomes in HGGs.

Acknowledgment

My first thank you goes to my amazing and wonderful supervisor Monica – the brave soul who looked at a confused potato and thought, “Yes, I’ll take this one”. Thank you for taking the bold leap of faith, and even let me stay for a DPhil, I am eternally grateful for all your support, patience and trust in me. You are the most optimistic person I have ever met, always full of positive energies. Thank you for always reminding me to believe in myself. I am always proud to say I have the nicest PI in the universe who cares so much about her students and everyone around her. I am so lucky to have had you as my supervisor, and I would certainly not be where I am now without you. Thank you, Monica!

Ester, you always joke that I am your favourite student, and just so you know, I choose to believe that lie with my whole heart. Thank you for the calmness, the cool vibe, and the reassurances when I was internally combusting. Your humorous comment always makes my day better. Also, I fully expect all the juicy gossip one day. No pressure.

David and Dominika, bless your hearts for dealing with me in my early days when I didn’t know anything about lab work. I was essentially a scientific toddler and thank you so much for your patience and teaching from day one. David, we miss you laugh echoing through the lab and your post-pub rescue missions, still not sure how you carried me and my dignity home. Dominika, your joy is infections. If touchwood, science doesn’t work out, it’s never too late to be an Olympic rower, just saying.

Tatsuya, I have learnt so much from you. Your work ethic is legendary and something I really wish to achieve one day. You taught me the difference between working hard and working smart (although you work both hard and smart). Thank you for being my scientific compass and helping me out all the time. I couldn’t have done half of the DPhil without your help. Don’t forget to take us to your favourite ramen restaurant when we visit you in Japan!

Lolita and Salma, I am so grateful to have you joining the brain team. Thank you for making sure I wasn’t the only one crying about those high-maintenance brain cells while everyone else was happily working with HCT116. You two saved my cell cultures and my sanity countless times. This project is tough, and the cells are horrible to work with, but having you guys as fierce warriors by my side relived a lot of the pressure. Together, let’s see how the project grows.

Jeff, Heather, Ian, and all our visiting students, it was really great fun working with you all. Thank you for never attempting to compete for those miserable Monday 8am TC slots with me. I will always remember the nice time we had punting on the river.

To all the past and current members of the Hammond Lab, especially Tiff, Sophie, Kat, Louise and Ed – it’s amazing to have you all as my lovely colleagues and friends. Without you, I’d have been that awkward person eating lunch on her own. Thank you for letting me be the friendly lab parasite, borrowing endless reagents and stealing your time. Thank you for trusting me to use your hypoxia chamber, I could not have completed any of my hypoxia work without it. Special shoutout to the Bacton – truly the Beyoncé of equipment. The Hammond Lab has a very special vibe, and a big part of that is the willingness to help each other out, and obviously all the laughter and chit chats. Thank you all for letting me be part of your lab.

Tess and Simei, you two are the best desk mates and unofficial therapists I could ever ask for. Thanks for listening to every single rant (I'm aware there were many). It is so lovely to have your company when it was so quiet in the building. Seeing you at 8am and 7pm makes the long working hours a lot more bearable and somewhat fun.

Hala and Nuria, my bus buddies! I couldn't thank you enough for looking after me for the past four years (scientifically and mentally). This lab surely couldn't run without the help from you two, and Kelly would never have made it home at 4am without your navigation, and occasional judgement.

Minn-e, Alexa, Teofanija, Cedric, Aiyan - my MRes crew. You guys made my first year at Oxford so magical. I really miss those days when we would tell each other everything, do all those silly things together and randomly dance at the basement. 2021-2022 was probably one of the best times in my life because of you guys, who then became my life-long friends. I am waiting for the day when we could all meet up again.

Benjamin and Louis, the cutest cats on Earth. Sitting on my laptop during thesis writing and silently judging my procrastination with your side eye, you two were my beloved emotional support, and I love you to bits. I miss you both.

Jacob, thank you so much for everything. You've seen all my blood and tears in the past few years, especially when my mental health absolutely crashed. I wouldn't still be here if it wasn't you holding onto me physically and emotionally through my endless crisis and reminding me that I am a strong and independent woman. I am looking forward to our future adventures together.

Grandma, when I talked to you the very last time, I told you I would become a doctor. This came a few years late, and probably not the kind you expected, but I hope you would still be proud of me. I think of you all the time and I really miss you.

The last and most important thank you goes to my parents who shaped who I am. To my amazing mum, thank you for everything you have provided for me. You are not a scientist, and I know you've never quite understood what my DPhil is about, but you have never doubted me once. I will always remember the one time you said "seeing you pursuing your dream is a wonderful thing, and I just want you to be happy". No words could thank you enough for spending everything on me, I am aware I am indeed a super expensive child to raise. You are the strongest woman I know, and I'll try my best to live up to your strength and selflessness. I love you.

To everyone mentioned, and everyone I forgot to mention but definitely still love — THANK YOU. You made this journey fun, hilarious, and meaningful. I could not have done it without you all.

Love you all! ♡

(written in tears)

Table of Contents

List of Tables

List of Figures

List of Abbreviations

2D	two-dimensional
3D	three-dimensional
ac	acetylation
ACTB	beta-actin
ACVR	activin A, type I
ALS	amyotrophic lateral sclerosis
APC	antigen-presenting cell
ARG1	arginase 1
ATF	activating transcription factor 4
ATF6	activating transcription factor 6
ATP	adenosine triphosphate
APOE	apolipoprotein E
BBB	blood-brain barrier
BiP	binding immunoglobulin protein
BSA	bovine serum albumin
^{0}C	degrees Celsius
C1q	complement component 1q
C3	complement component 3
C3aR	complement component 3a receptor
C5	complement component 5
C5aR1	complement component 5a receptor 1
C5aR2	complement component 5a receptor 2
CA9	carbonic anhydrase IX
CCL2	C-C motif ligand 2
CCL7	C-C motif ligand 7
CD4	cluster of differentiation 4
CD8	cluster of differentiation 8
CD11b	cluster of differentiation 11b
CD40	cluster of differentiation 40
CD55	cluster of differentiation 55
CD59	cluster of differentiation 59

CD68	cluster of differentiation 68
CD80	cluster of differentiation 80
CD86	Cluster of differentiation 86
CD88	cluster of differentiation 88 / complement component 5a receptor 1
CD163	cluster of differentiation 163
CD206	cluster of differentiation 206
CHOP	C/EBP homologous protein
β	conditioned media
CNS	central nervous system
Cocl2	cobalt chloride
CRT	conventional fractionated therapy
CT	threshold cycle
DAMP	damage-associated molecular pattern
DAPI	4-,6-diamidino-2-phenylindole
DMEM	Dulbecco's modified Eagle's medium
DMG	diffuse midline glioma
DMSO	dimethylsulfoxide
DNA	deoxyribonucleic acid
ECL	extracellular loop
ECM	extracellular matrix
EGFR	epidermal growth factor receptor
eIF2α	eukaryotic initiation factor 2-alpha
ELISA	enzyme-linked immunosorbent assay
EMT	epithelial-mesenchymal transition
ER	endoplasmic reticulum
ERK	extracellular signal-regulated kinase
FBS	Foetal bovine serum
FDA	Food and Drug Administration
g	gravity
G1 phase	growth 1 phase
G2 phase	growth 2 phase
GAPDH	glyceraldehyde-3-phosphate dehydrogenase
GBM	glioblastoma multiforme

GDP	guanosine diphosphate
GTP	guanosine triphosphate
GLUT1	glucose transporter type 1
GPCR	G-protein coupled receptor
GSC	glioma stem cell
Gy	Gray
h	hour
H3	histone H3
HGG	high grade glioma
HGG-AM	high grade glioma-associated microglia
HIF	hypoxia-inducible factor
HIF-1α	hypoxia-inducible factor 1-alpha
HRE	hypoxic response element
IBA1	ionised calcium-binding adapter
IFN-γ	Interferon-gamma
IgG	immunoglobulin G
IL-1β	interleukin-1 beta
IL-4	interleukin-4
IL-6	interleukin-6
IL-10	interleukin-10
IL-13	Interleukin-13
iNOS	inducible nitric oxide synthase
IR	ionising radiation
IRE1	inositol-requiring enzyme 1
JAK	Janus kinase
K27	lysine 27
KD	knockdown
LB	Luria-Bertani
LC3B	microtubule-associated protein 1A/1B-light chain 3B
LDH	lactate dehydrogenase
LPS	lipopolysaccharide
MAPK	mitogen-activated protein kinase
MAPKK	mitogen-activated protein kinase kinase

MAPKKK	mitogen-activated protein kinase kinase kinase
MASP	mannose-associated serine protease
M-CSF	macrophage-colony stimulating factor
MDSC	myeloid-derived suppressor cells
Me	methylation
MGMT	O6-methylguanine-DNA-methyltransferase
mRNA	messenger ribonucleic acid
mTOR	mammalian target of rapamycin
MTT	3-(4,5-dimethylthiazol-2-yl)-2,5-diphenyltetrazolium blue
MΦ	macrophage
NF-κB	nuclear factor-kappa B
NLGN3	neuroligin-3
NLRP1	nucleotide-binding domain, leucine-rich-containing gamily, pyrin domain-containing protein 1
NLRP3	nucleotide-binding domain, leucine-rich-containing gamily, pyrin domain-containing protein 3
OE	overexpress
OER	oxygen enhancement ratio
OPCs	oligodendrocyte-precursor cells
p62	sequestosome 1
PBMC	peripheral blood mononuclear cell
PBS	phosphate buffered saline
PD-1	programme cell death protein 1
PD-L1	programmed cell death ligand 1
PDGFRA	platelet-derived growth factor receptor subunit A
pERK	phosphorylated extracellular signal-regulated kinase
PERK	protein kinase RNA-like ER kinase
PHD	prolyl hydroxylase domain
PI3K	phosphoinositide 3-kinase
RIDD	regulated IRE-1 dependent decay
pRelA	phosphorylated RelA
qPCR	quantitative polymerase chain reaction
ROS	reactive oxygen species

RPM	revolutions per minute
RNA	ribonucleic acid
RPMI	Roswell Park Memorial Institute
RT	room temperature
S phase	synthesis phase
SD	standard deviation
Scr	scrambled
SEM	standard error of the mean
siRNA	small interfering RNA
STAT	signal transducer and activator of transcription
TCGA	The Cancer Genome Atlas
Th1	type 1 T helper cells
Thap	thapsigargin
TGF-β	transforming growth factor-beta
TIL	tumour-infiltrating lymphocyte
TM	transmembrane
TME	tumour microenvironment
TNF	tumour necrosis factor
TP53	tumour protein 53
Treg	regulatory T cells
Trp	tryptophan
Tuni	tunicamycin
UPR	unfolded protein response
VEGF	Vascular endothelial growth factor
VHL	von Hippel-Lindau
XBP1	X-box binding protein 1

Chapter 1 Introduction

1.1 Cancer

Cancer encompasses a group of diseases characterised by uncontrolled and aberrant cellular proliferation, accompanied by the capacity to invade surrounding tissues and metastasise to distinct sites. The foundational framework for understanding cancer biology was introduced by Hannahan and Weinberg in their review published in 2000, which described six core hallmarks shared by most, if not all cancer types (Hanahan and Weinberg, 2000). These include self-sufficiency in growth signals, limitless replicative potential, insensitivity to anti-growth signals, evading apoptosis, sustained angiogenesis, tissue invasion and metastasis. If any cell acquires any of these traits, it has breached the body's anti-cancer defence mechanisms, conferring enhanced proliferative, survival and invasive capabilities. In 2011, the authors expanded this framework to include two additional emerging hallmarks: dysregulated cellular metabolism and evading immune destruction, alongside two enabling characteristics: genome instability and mutation and tumour-promoting inflammation (Hanahan and Weinberg, 2011). Most recently, in 2022, Hanahan published the newest update for the hallmarks of cancer, incorporating four additional emerging hallmarks and enabling characteristics (Hanahan, 2022). These include phenotypic plasticity, senescence, non-mutational epigenetic reprogramming and polymorphic microbes. A graphical summary of these cancer hallmarks is presented in Figure 1.1. These characteristics shape the phenotype of cancer cells and serve as a conceptual foundation for the development of all therapeutic strategies.

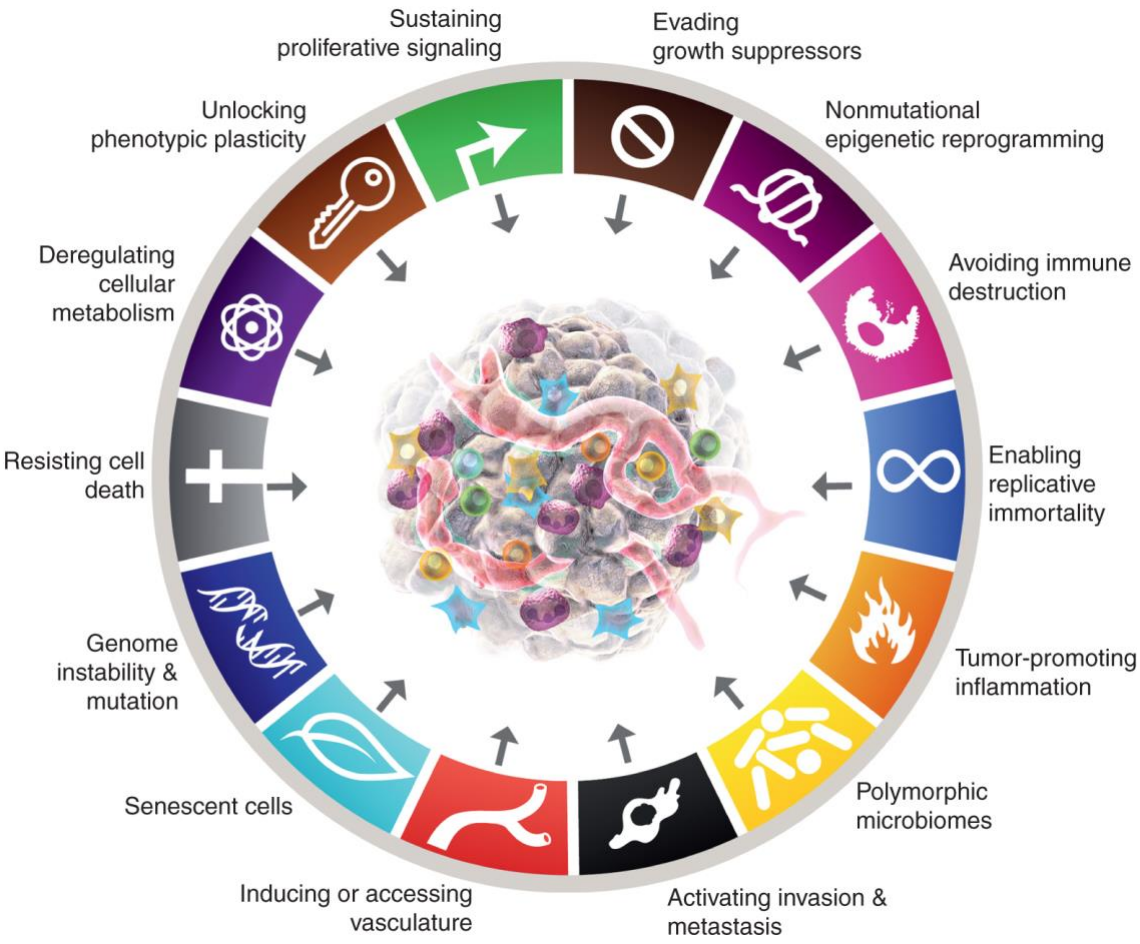

Figure 1.1 Hallmarks of Cancer

Graphical summary of the hallmarks of cancer common in most cancer cells. Adapted from Hanahan (2022).

1.2 High-Grade Glioma

Unlike most cancers, brain cancer is classified into four grades according to the World Health Organisation rather than staged, since it rarely metastasises. The grading of brain cancer is assigned to each brain tumour type based on its histology, molecular profile and median survival. These grades reflect the malignancy of tumour, with grade 1 being the least malignant and progresses slowly, while grade 4 being the most aggressive. Grades 1 and 2 are considered low-grade, and grades 3 and 4 are regarded as high-grade (Louis *et al.*, 2021). In this study, we will focus on high-grade gliomas (HGGs), particularly diffuse midline glioma (DMG) and glioblastoma (GBM), which are grade 4 gliomas, both characterised by rapid growth, poor prognosis, high recurrence rates and treatment resistance.

1.2.1 Diffuse Midline Glioma

DMG is a highly aggressive malignant glioma with poor prognosis and median age of diagnosis of 15 years old (Ostrom *et al.*, 2023). Due to its diffusive nature, the tumour's anatomic location in the brainstem and thalamus, and the critical function of this brain region, surgical resection is not always available. Radiation therapy remains the standard-of-care treatment, with addition of alkylating agent Temozolomide (TMZ) for some patients, though there is no standard chemotherapy regimen. Despite its rarity, DMG is universally regarded as fatal, with a median survival of just 11 months (Cooney *et al.*, 2017).

Studies suggest that DMGs are likely to originate from oligodendrocyte precursor cells (OPCs) which retain stem-like properties, including sustained proliferative capacity and the ability to differentiate (Filbin *et al.*, 2018; Lin *et al.*, 2018; Tomita *et al.*, 2022). Approximately 80% of DMG patients harbour the oncogenic H3K27M mutation, in which lysine 27 in is substituted by methionine in histone 3 (H3).1 or H3.3, resulting in a global loss of trimethylation (Yu *et al.*, 2021). In addition to H3K27M, DMGs frequent exhibit co-occurring genetic alterations. Mutations in the tumour protein 53 (TP53) gene are present in approximately 50% of DMG patients and have been associated with radioresistance and reduced overall survival (Mackay *et al.*, 2017; Werbrouck *et al.*, 2019). Other frequently observed genetic alterations in DMG include mutations in activin A receptor, type I (ACVR1) and amplification of platelet-derived growth factor receptor subunit A (PDGFRA) (Buczkowicz and Hawkins, 2015; Taylor *et al.*, 2014). A genetically engineered mouse model combining H3K27M expression, PDGF-A overexpression and TP53 mutation in OPC-like cells resulted in tumours recapitulating key histopathological and molecular features of human DMG (Tomita *et al.*, 2022).

1.2.2 Glioblastoma

GBM is the most malignant type of glioma and the most prevalent primary brain tumour in adults, accounting for 48.6% of all malignant central nervous system (CNS) tumours (Grochans *et al.*, 2022). GBM is most often localised in the frontal lobe of the brain, but could also be found in other sites of the brain (Ghosh *et al.*, 2017). With a median diagnosis age at 66, the incidence rate of GBM is 0.18 cases per 100,000 people in those under 18 years old and 3.27 cases per 100,000 people in adults (Ostrom *et al.*, 2023; Ostrom *et al.*, 2020). Characterised by high mitotic activity and a necrotic core, the prognosis of GBM is poor, with an overall median survival of just 15 months (Ostrom *et al.*, 2023).

GBMs are believed to originate from neural stem cells or OPCs (Alcantara Llaguno *et al.*, 2009; Liu *et al.*, 2011a). Several genetic alterations are frequently observed in GBM patients, including mutation or dysregulation of phosphate and tensin homolog (PTEN), TP53, telomerase reverse transcriptase, epidermal growth factor receptor (EGFR) and PIK3CA (Brennan *et al.*, 2013; Djuzenova *et al.*, 2015; Killela *et al.*, 2013). In addition, epigenetic silencing of O6-methylguanine-DNA-methyltransferase (MGMT) via promoter silencing has been suggested as a predictive marker for TMZ response (Wick *et al.*, 2012; Malmström *et al.*, 2012). These genetic and molecular alterations contribute to tumour growth, invasiveness and resistance to therapy, serving as important prognostic factors. Although the standard-of-care treatment for GBM generally remains consistent across patients irrespective of mutation status, patients with unmethylated MGMT promoter derive less benefit from TMZ. Despite several months of survival benefits with TMZ and radiotherapy treatment, GBM inevitably recurs after 3-9 months, making it a lethal cancer (Stupp *et al.*, 2009).

1.3 HGG tumour microenvironment

Within the tumour microenvironment (TME), various cell types interact with each other to support tumour growth, either by sabotaging healthy brain cells or altering recruitment of immune cells. The TME plays a crucial role in regulating glioma development. The tumour mass and its surrounding extracellular matrix (ECM) comprise a heterogeneous population of cells, including astrocytes, glioma stem cells (GSCs), endothelial cells, and immune cells, all of which may contribute to tumour progression and are discussed in subsequent sections. Physical feature of the TME, such as the low oxygen (hypoxic) regions found in solid tumours also impact tumour progression and treatment response.

1.3.1 Hypoxia and Cancer

Oxygen is an essential substrate for mitochondrial oxidative phosphorylation and subsequent production of adenosine triphosphate (ATP). Under conditions of reduced oxygen availability, termed hypoxia, cells initiate a range of cellular stress and adaptive responses in order to maintain the balance between oxygen supply and metabolic demand. 'Physiologically normal' oxygen levels vary significantly between tissues, with brain parenchyma typically exhibiting oxygen concentrations ranging from 2.5%-12.5% (Collingridge *et al.*, 1999). It is important to note that hypoxia is defined in a tissue/cell-specific context, occurring when local oxygen level falls below the metabolic requirements of that specific tissue.

Presence of hypoxic regions have been reported in both GBM and DMG, where hypoxia plays a key role in shaping tumour metabolism (Blandin *et al.*, 2019; Said *et al.*, 2007; Shen *et al.*, 2025; Yeom *et al.*, 2015). In a study employing EF5 binding as a marker of hypoxia, all human GBM tissues examined contained mild to moderate hypoxic regions, with severe hypoxia detected in 33% of cases (Evans *et al.*, 2008). In a larger cohort of 70 GBM tissues analysed using tissue microarrays, hypoxic regions were identified in 61% of tumours, as assessed by expression of the hypoxia-inducible target glucose transporter type 1 (GLUT1) (Dzwigonska *et al.*, 2025). Although studies directly quantifying the prevalence of hypoxia in DMG are currently lacking, the majority of HGGs, including 93% of grade 4 gliomas demonstrated positive immunohistochemical staining for HIF-1α, indicative of active hypoxic signalling (Abd Elmaogod *et al.*, 2022). These findings underscore the high prevalence of hypoxia in HGGs and highlight the importance of taking into account how low oxygen availability shapes the TME, drives tumour progression and influences therapeutic responses.

In solid tumours, oxygen is delivered via passive diffusion from nearby vasculature, leading to the formation of steep oxygen gradients, as illustrated in Figure 1.2. In gliomas, these range from mild hypoxia at 2.5%-0.5% in proximity to native functional blood vessels, to severe hypoxia or even anoxia at 0%-0.5% in more distal regions or areas near non-functional blood vessels (Evans *et al.*, 2004). Intraoperative oxygen measurements in GBM have confirmed the presence of such oxygen gradients, identifying tumour regions with moderate hypoxia (<0.5%), severe hypoxia (<0.1%) and complete anoxia (0%) (Evans *et al.*, 2004). Although direct measurements of oxygen levels in DMG are lacking, imaging studies have demonstrated substantial hypoperfusion in DMG, supporting the presence of a hypoxic TME (Yeom *et al.*, 2015).

To enhance the delivery of oxygen and nutrients to tumours, pathological angiogenesis is a key feature of cancer which facilitates tumour cell survival. Tumour vasculatures are often structurally abnormal, characterised by hyperpermeability, enlarged vessel diameter, and thickened basement membrane. The hypoxic region in glioma expresses high levels of hypoxia-inducible factor 1α (HIF-1α), its activation in turn upregulates the expression of key angiogenesis factors, such as vascular endothelial growth factor-A (VEGF-A) (Lin and Wu, 2023; Mou *et al.*, 2023). VEGF-A can also be secreted by glioma stem cells (GSCs) within extracellular vesicles, which then act on endothelial cells to promote new vessel formation, facilitating tumour growth and glioma cell dissemination (Lin and Wu, 2023; Kaur *et al.*, 2005; Mou *et al.*, 2023; Chen *et al.*, 2022; Treps *et al.*, 2017). Interestingly, GSCs have been reported to transdifferentiate into vascular endothelial cells in GBM, supporting angiogenesis through WNT5A signalling (Hu *et al.*, 2021; Soda *et al.*, 2011; Mei *et al.*, 2017).

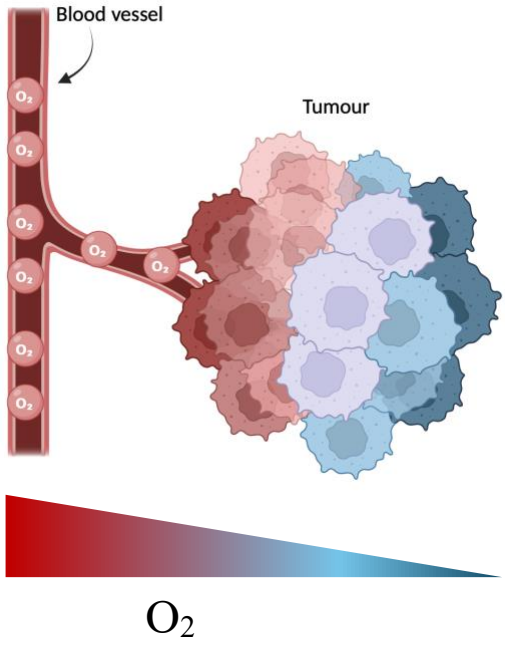

Figure 1.2 Graphical representation of oxygen delivery to tumour

Oxygen is delivered from blood vessels to tumour tissue down the concentration gradient. Cells closest to the blood vessel are exposed to higher oxygen level compared to those further away from the vessel.

1.3.1.1 HIF

One of the key regulators of the cellular response to hypoxia is HIF, a heterodimeric transcription factor complex composed of an oxygen-sensitive alpha-subunit (HIF-1α, HIF-2α, HIF-3α), and a constitutively expressed beta-subunit (HIF-1β) (Weidemann and Johnson, 2008). Under normoxic conditions, the α-subunit is rapidly degraded by prolyl hydroxylase domain (PHD) enzymes which hydroxylate specific proline residues-402 and -564 within the oxygen-dependent degradation domains NODD and CODD of HIF-1α (Chowdhury *et al.*, 2016; He *et al.*, 2021). This hydroxylation is catalysed by iron (II) and 2-oxoglutarate, promoting HIF-1α recognition by the von Hippel-Lindau (VHL) protein, which is the substrate recognition component of an E3 ubiquitin ligase complex (Chowdhury *et al.*, 2016; Cockman *et al.*, 2000; He *et al.*, 2021; Ohh *et al.*, 2000). Subsequent polyubiquitination then targets HIF-1α for proteasomal degradation.

Under hypoxic conditions, PHD activity is inhibited, HIF-1α is stabilised and translocated to the nucleus, where it dimerises with HIF-1β and binds to hypoxic response elements (HREs) in the regulatory regions of target genes (Taylor and Scholz, 2022; Weidemann and Johnson, 2008). Together with recruited co-activators such as p300 and CREB-binding protein, HIF regulates transcription of a broad range of genes involved in metabolic reprogramming, angiogenesis, cell stemness, proliferation, apoptosis and epithelial-mesenchymal transition (EMT) (Freedman *et al.*, 2002; Dengler, Galbraith and Espinosa, 2014). A graphical summary of HIF-1α signalling under normoxic and hypoxic conditions is shown in Figure 1.3.

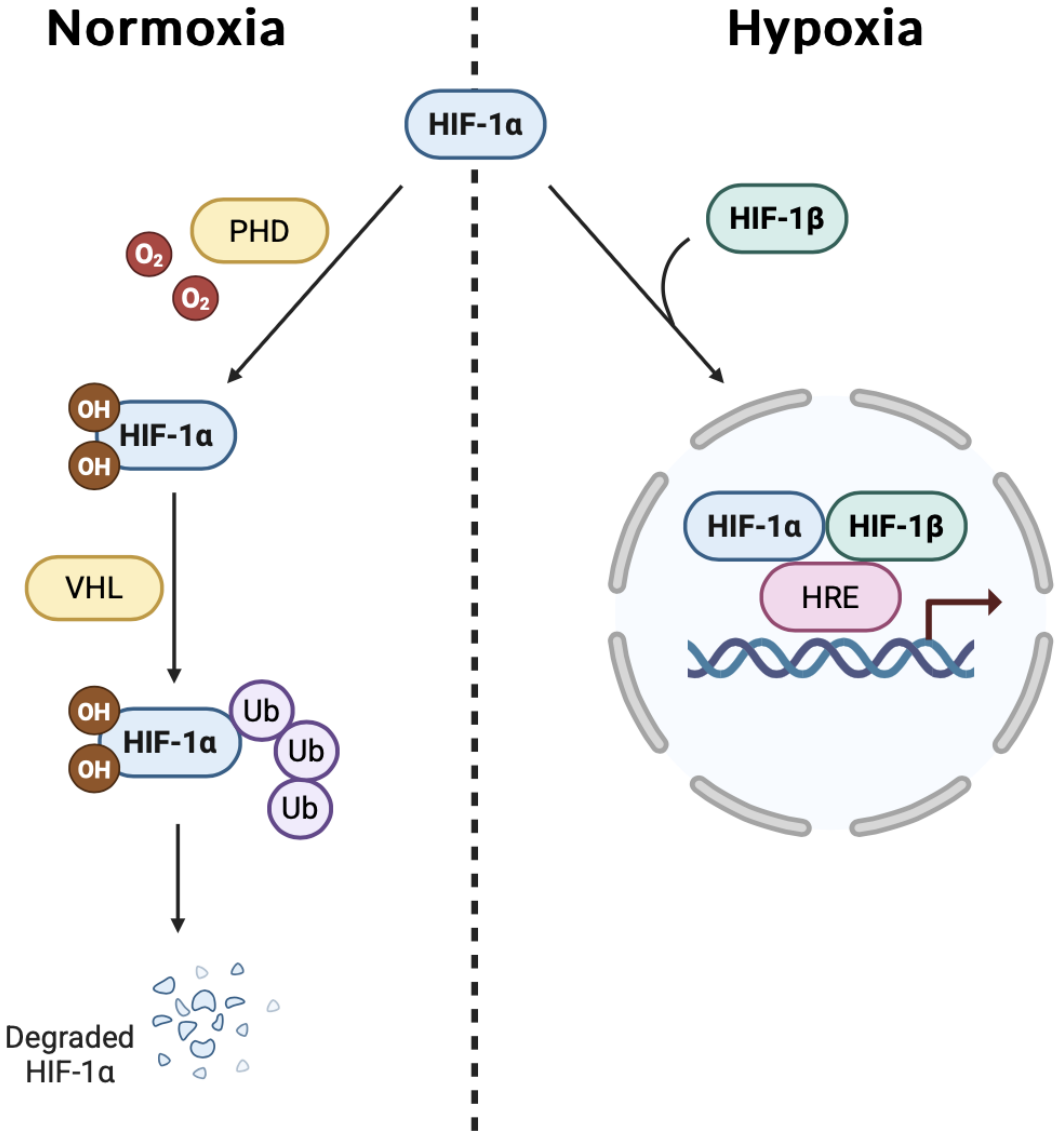

Figure 1.3 Graphical representation of HIF-1α signalling under normoxia and hypoxia

(Left) Under normoxia, HIF-1α is hydroxylated by PHD enzymes and VHL proteins promote recognition of hydroxylated HIF-1α by E3 ubiquitin ligase complex. HIF-1α is subsequently degraded. *(Right)* Under hypoxia, HIF-1α is stabilised and translocated to the nucleus, where it dimerises with HIF-1β and binds to HREs to regulate transcription of target genes.

HIF-1 is a well-established molecular marker of hypoxia and one of its downstream targets, carbonic anhydrase IX (CAIX) is expressed in GBM where it correlates with poor prognosis, and has been linked to increased necrosis in colorectal cancer models (Clara *et al.*, 2014; McIntyre *et al.*, 2012; Proescholdt *et al.*, 2012; Said *et al.*, 2007). HIF-1α has been shown to induce a mesenchymal phenotype in tumour cells through the upregulation of zinc finger E-box binding homeobox 1, thereby enhancing tumour migration and invasiveness (Joseph *et al.*, 2015; Zhang *et al.*, 2015). Moreover, HIF activity in GSCs promotes tumorigenicity by inducing transforming growth factor-beta (TGF-β) and VEGF, which support GSC maintenance, self-renewal, and survival, enhancing their tumour-initiating potential (Chen *et al.*, 2024; Li *et al.*, 2009). HIF-1α has also been implicated in the acquisition of therapy-resistance phenotypes in glioma cells by upregulating neural stem markers, which may drive resistance to conventional therapies (Bar *et al.*, 2010).

Beyond intrinsic tumour cell regulation, HIF plays an important role in shaping the immunosuppressive TME. HIF-1α has been reported to suppress cluster of differentiation 8-positve ($CD8^+$) T cell infiltration by downregulating the expression of C-X-C motif chemokine-9, -10 and -11 (Su *et al.*, 2024). Additionally, HIF-1α upregulates interleukin-1 beta (IL-1β) secretion from microglia, which has been shown to enhance glioma proliferation, invasion and migration via nuclear factor-kappa B (NF-κB)-mediated induction of heparanase, in which knockdown of heparanase reverses the pro-tumorigenic effects (Si *et al.*, 2024). Collectively, these findings highlight the multifaceted role of HIF in glioma progression, spanning metabolic, invasive, stem-like, and immunomodulatory functions.

1.3.1.2 UPR under ER stress

The endoplasmic reticulum (ER) plays a central role in post-translational protein processing, including disulphide bond formation and proper protein folding of polypeptides translated by ribosomes. Newly synthesised proteins are subject to the surveillance ER quality control system that directs properly folded proteins to their final destinations, while misfolded proteins are targeted for ER-associated degradation (ERAD) via proteasomal or autophagic pathways (Araki and Nagata, 2011; Krshnan, van de Weijer and Carvalho, 2022). Under hypoxia, typically below 1-2% O_2, the glycolytic shift induced by reduced oxygen availability results in decreased ATP production, which limits the rate of energy-intensive processes such as protein translation and folding (Liu *et al.*, 2006). This results in unfolded or misfolded proteins accumulating within the ER lumen, a condition termed as ER stress, which in turn activates the unfolded protein response (UPR), a highly conserved signalling cascade aimed at restoring ER proteostasis (Wang and Kaufman, 2016). While the UPR is primarily a cytoprotective mechanism to relieve ER stress, persistent or unresolved ER stress ultimately leads to apoptosis.

The UPR pathway is initiated by three different ER transmembrane stress sensor proteins: protein kinase ribonucleic acid (RNA)-like ER kinase (PERK), activating transcription factor 6 (ATF6) and inositol-requiring enzyme 1 (IRE1). In resting state, these protein sensors are bound to binding immunoglobulin protein (BiP), which acts as a chaperone to maintain inactive conformations of the sensors (Madden *et al.*, 2019). Upon accumulation of unfolded proteins, BiP dissociates from these ER stress sensors, allowing their activation and subsequent propagation of the UPR (Kopp *et al.*, 2019).

PERK is the first sensor activated in response to ER stress, it phosphorylates the alpha-subunit of eukaryotic initiation factor 2A (eIF2α) which transiently attenuates protein synthesis, while selectively enhancing the translation of stress-inducible genes such as activating transcription factor 4 (ATF4) and C/EBP homologous protein (CHOP), both of which promote autophagy (B'Chir *et al.*, 2013; Cao *et al.*, 2012; Harding *et al.*, 2000).

The next sensor activated by unfolded proteins is ATF6, which translocate from the ER to the Golgi apparatus and is subsequently cleaved by site-1 and site-2 proteases to its active form (Shen *et al.*, 2002; Ye *et al.*, 2000). Cleaved ATF6 translocate to the nucleus and upregulates transcription of CHOP, x-box binding protein 1 (XBP1), as well as genes involved in ER chaperone expression and Golgi biogenesis to alleviate ER stress (Bommiasamy *et al.*, 2009; Shen *et al.*, 2002; Yang *et al.*, 2020; Yoshida *et al.*, 2001). XBP1, upregulated by both ATF6 and IRE1a activation, is a critical transcriptional regulator not only of autophagy and apoptosis, but also of tumour growth, EMT, angiogenesis and therapy resistance, serving as an important regulator of tumorigenesis (Gupta *et al.*, 2016; Lyu *et al.*, 2019; Romero-Ramirez *et al.*, 2009; Wu *et al.*, 2018; Zeng *et al.*, 2013b). Elevated expression and activation of XBP1 have been reported in HGGs, where its silencing impairs tumour viability and formation (Liu *et al.*, 2016). In GBM, high XBP1 expression correlates with an immunosuppressive TME and worse patient outcomes (Oliveira *et al.*, 2024).

The third UPR sensor, IRE1, is activated when unfolded proteins binds directly to the luminal domain of the sensor, leading to receptor dimerisation and autophosphorylation (Credle et al., 2005; Zhou et al., 2006). Activated IRE1 oligomers splice XBP1 messenger ribonucleic acid (mRNA) (previously induced by ATF6) to generate active XBP1 transcription factor (sXBP1), which encodes for genes involved in ERAD, fatty acid synthesis and tumour progression (Lee *et al.*, 2008; Tam, Koong and Niwa, 2014; Tsuchiya *et al.*, 2019). IRE1a also cleaves and degrades selective microRNAs to relieve protein folding load in the ER through a process known as regulated IRE-1 dependent decay (RIDD) (Hollien and Weissman, 2006; Tam, Koong and Niwa, 2014; Upton *et al.*, 2012). However, RIDD could also promote translation of proteins responsible for mitochondrial apoptosis, inducing cell death (Upton et al., 2012). Moreover, IRE1a activation leads to stimulation of the Jun N-terminal kinase (JNK) pathway, which has a dual role in both cell survival and cell death by promoting autophagy and apoptosis (Li *et al.*, 2019; Wu *et al.*, 2021). In summary, the UPR, through PERK, ATF6 and IRE1 orchestrates complex transcriptional and translational events that balance cellular adaption and death. A graphical summary of the UPR signalling events is shown in Figure 1.4.

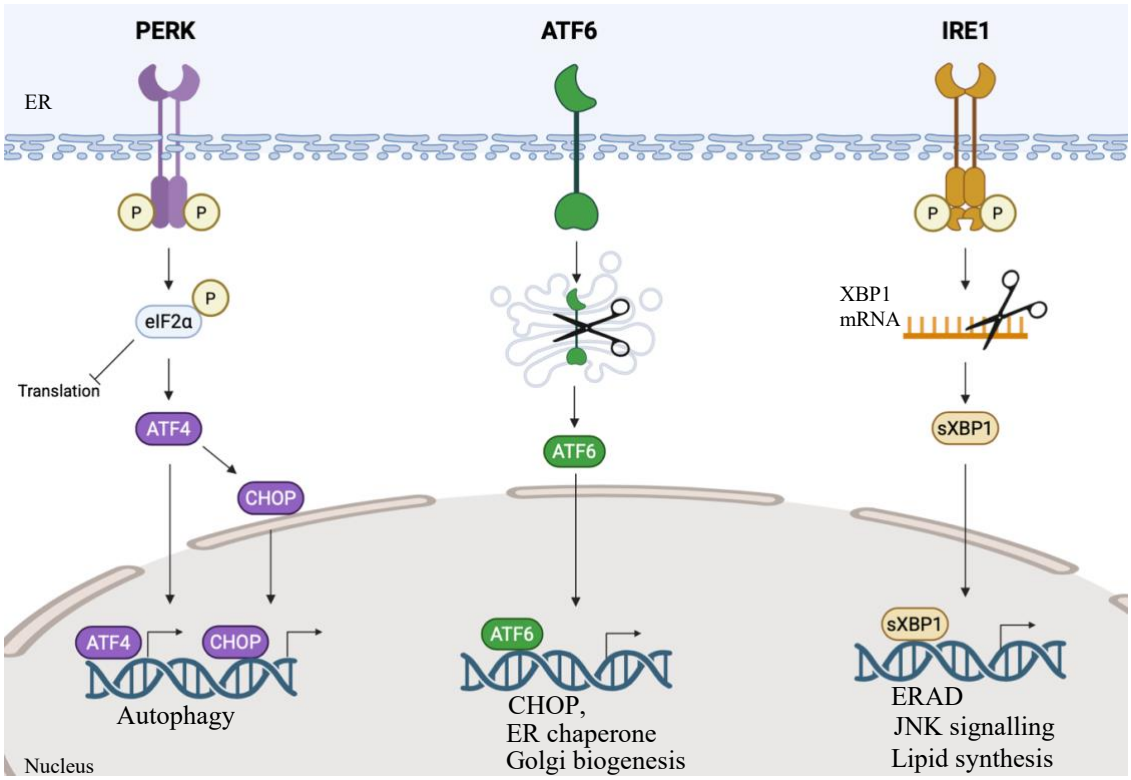

Figure 1.4 Graphical summary of UPR signalling events

PERK, ATF6 and IRE1 are UPR sensors located in the ER. Activation of PERK phosphorylates eIF2α, which transiently inhibit protein translation, but selectively enhance translation of ATF4 and CHOP which regulation transcription of genes involved in autophagy. ATF6 activation results in translocation of protein from ER to the Golgi apparatus for cleaving. Cleaved ATF6 regulates transcription of CHOP and XBP1 genes, as well as genes responsible for ER chaperones, and Golgi biogenesis. IRE1 dimerises and undergoes autophosphorylation upon binding of unfolded proteins, it splices XBP1 to generate sXBP1 which regulates transcription of genes involved in ERAD, JNK signalling and lipid synthesis.

1.3.1.3 Hypoxia contributes to radioresistance

Oxygen availability is a critical determinant of the efficacy of radiation-induced damage, with hypoxia being a well-established contributor to radioresistance, including in HGGs (Shen *et al.*, 2025; Wei *et al.*, 2023). Well-oxygenated cells can respond up to three times better to IR than hypoxic cells, the boosting ratio is known as the oxygen enhancement ratio (OER) (Hall and Giaccia, 2006). This radiosensitising effect of oxygen is only observed when oxygen is present during or immediately before irradiation. The most established mechanism underlying the OER is the oxygen fixation hypothesis. Irradiation generates highly reactive free radicals, which causes deoxyribonucleic acid (DNA) strand breaks. In the presence of molecular oxygen, DNA radicals formed by these interactions are stabilised through the formation of peroxyl adducts, thereby 'fixing' the DNA damage which makes it more permanents and difficult to repair (Bertout, Patel and Simon, 2008; Grimes and Partridge, 2015). Under hypoxic conditions, not only there is less molecular oxygen to react with free radicals, but DNA radicals are also more likely to be reduced to their original forms by intracellular compounds containing sulfhydryl groups, such as glutathione, facilitating the repair of otherwise lethal damage (Wang *et al.*, 2019).

Apart from the OER, hypoxia promotes radioresistance through additional mechanisms, one of which is HIF-1. HIF-1 regulates hundreds of genes involved in cellular metabolism, including those enhancing glycolysis and serine biosynthesis pathways which elevate intracellular antioxidant production to mitigate radiation-induced reactive oxygen species (ROS) (Li *et al.*, 2016; Zhou *et al.*, 2017). Hypoxia also activates autophagy to facilities clearance of damaged organelles and ROS, thereby protecting cells from irradiation damage (Feng *et al.*, 2016). Furthermore, components of the UPR, such

as the IRE1-XBP1 and PERK/elF2α pathways are activated under hypoxia stress and confer radioresistance. IRE1-XBP1 promotes secretion of pro-survival cytokines including interleukin-1, while PERK signalling supports activation of the NF-κB signalling, both of which enhance cell survival in response to radiation (Lyu *et al.*, 2019; Qiao *et al.*, 2017). In addition, hypoxia supports the maintenance of a quiescent cancer stem cells population which are characterised by their intrinsic resistance to DNA damage as a particularly radioresistant subpopulation, and is thought to play a key role in tumour recurrence following treatment (Bhaskara *et al.*, 2012; Menegakis *et al.*, 2021).

1.3.2 Interactions between glioma cells, neurons, GSCs and astrocytes

Apart from tumour cells, the glioma TME is composed of other types of cells, such as neurons, GSCs and astrocytes, all of which play a role in glioma progression. GBM patients often experience epileptic seizures which has led to research into the connection between tumours and the neuronal network. In addition to mechanical compression exerted by the tumour mass, growing evidence suggests neurons are affected by neurotransmitters released by gliomas. Excessive glutamate release from glioma cells have been observed in patients and tumour-bearing mice, resulting in seizures and excitotoxic cell death of neurons (Buckingham *et al.*, 2011; Marcus *et al.*, 2010; Takano *et al.*, 2001). This neuronal cell death creates space in the peritumoral region, allowing glioma cells to invade and expand. While glioma cells lack glutamate transporters, using Thiamphenicol to upregulate glutamate transporters in peritumoral cells has been shown to decrease tumour burden, prolong survival and provide neuroprotective effects (Sattler *et al.*, 2013).

Despite the neuronal toxicity caused by glioma cells, neurons, on the other hand, could also promote HGG growth. The synaptic protein neuroligin-3 (NLGN3) secreted by active neurons induces phosphoinositide 3-kinase-Akt-mammalian target of rapamycin (PI3K-Akt-mTOR) signalling in both DMG and GBM, which ultimately promotes glioma cell proliferation (Venkatesh *et al.*, 2015; Venkatesh *et al.*, 2017). It is worth noting that NLGN3 secretion is also inversely correlated with survival of HGG patients (Venkatesh *et al.*, 2015). Additionally, oligodendrocytes, another stromal cell, has also been reported to promote GBM invasion by upregulating angiopoietin-2 signalling which regulates vessel permeability and angiogenesis (Kawashima *et al.*, 2019) .

GSCs are multipotent, undifferentiated tumour-initiating cells with self-renewal capacity, and are often linked to treatment resistance due to their more efficient DNA damage repair mechanisms compared to the bulk tumour cells, driven by replication stress (Bao *et al.*, 2006). Moreover, increase in GSC population was observed in recurrent GBM after radiotherapy and chemotherapy, the authors suggested that GSC could survive treatment and contribute to glioma recurrence (Tamura *et al.*, 2013). GSC display pronounced cellular plasticity, enabling dynamic transition along a spectrum of undifferentiated, stem-like states to more differentiated phenotype in response to various intracellular signalling and external stimuli (Safa *et al.*, 2015). This plasticity is regulated by developmental signalling pathways, including Wnt/β-catenin and Notch signalling, which play key roles in maintaining stemness and regulating cell state transition in GSCs (Basak *et al.*, 2012; Yun *et al.*, 2023). Moreover, epigenetic regulations such as chromatin remodelling and DNA methylation also contribute to the flexibility of differentiation state. (Chaligne *et al.*, 2021; Liau *et al.*, 2017; Zhang *et al.*, 2019). Microenvironmental factors further shape GSC state, with hypoxic conditions promoting stem-like phenotypes and expanding the GSC population (Bar *et al.*, 2010; Chen *et al.*, 2024; Li *et al.*, 2013; Qiang *et al.*, 2012). The bidirectional and reversible nature of these differentiation state transition enables more differentiated tumour cells to reacquire stem-like properties, thereby contributing to intratumoural heterogeneity, therapeutic resistance and tumour recurrence.

Astrocytes make up of approximately 50% of the cells in the brain, and they inevitably come into contact with glioma cells in the TME. Physiologically, astrocytes regulate neurotransmitter levels and synaptic plasticity (Adermark *et al.*, 2022; Stellwagen and Malenka, 2006). In the TME, astrocytes are activated by both glioma and microglia cells via the Janus kinase-signal transducer and activator of transcription (JAK-STAT) and NF-κB pathways (Heiland *et al.*, 2019; Kim *et al.*, 2014; Chen *et al.*, 2020). Reactive astrocytes can secrete factors such as stromal-derived factor-1 and chemokine ligand 20 to simulate GBM growth and proliferation (Barbero *et al.*, 2002; Jin *et al.*, 2018). In addition, interleukin 6 (IL-6) secreted by reactive astrocytes facilitates ECM degradation by upregulating matrix metallopeptidase-2 (MMP2), and -14, facilitating glioma migration and invasion alongside fascin-1 (Yu *et al.*, 2017; Li *et al.*, 2010; Chen *et al.*, 2016). Moreover, the co-existence of astrocytes and microglia leads to upregulation of anti-inflammatory cytokines such as TGF-β and interleukin-10 (IL-10), shaping an immunosuppressive TME (Heiland *et al.*, 2019). A graphical summary of the above interactions between glioma cells and the non-immune components of the TME is shown in Figure 1.5.

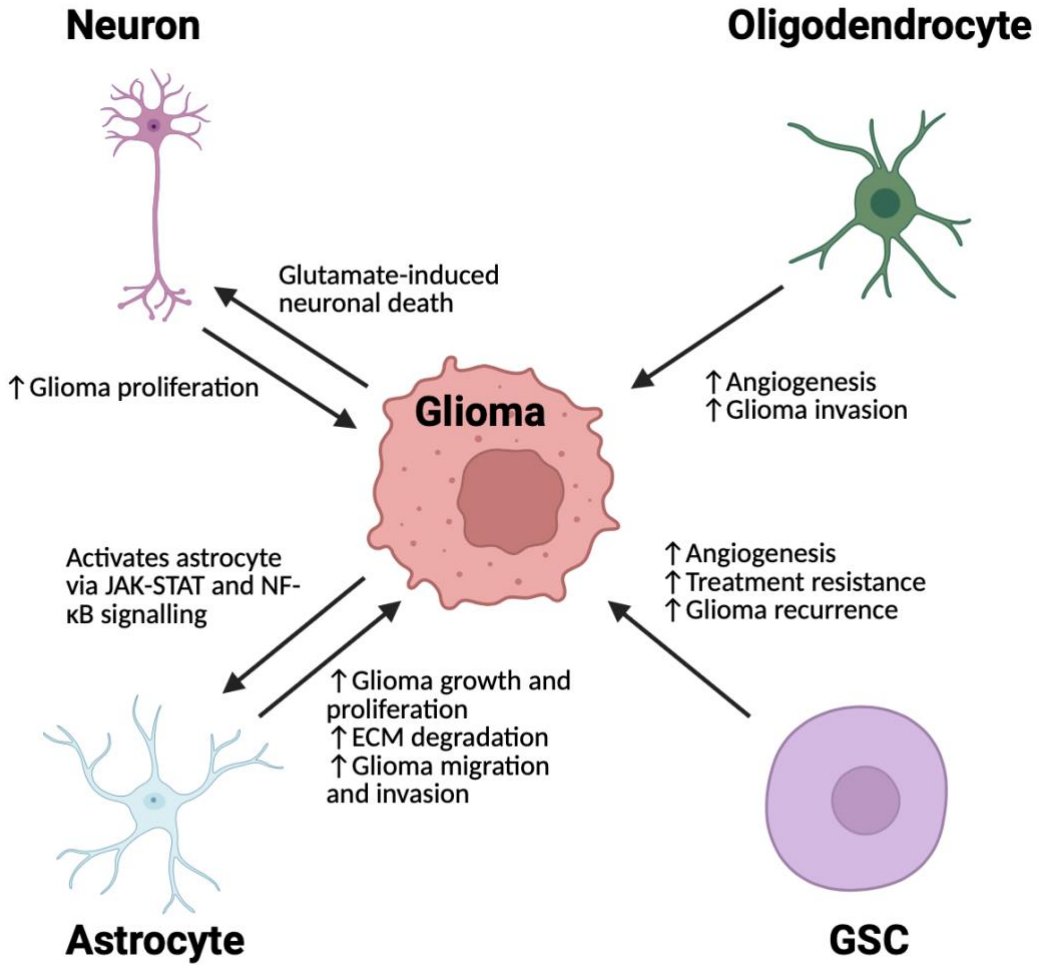

Figure 1.5 Schematic representation of interactions between glioma cell and other non-immune cells in the TME

Neuron, oligodendrocyte, astrocyte and GSC interact with glioma cell via different signalling events to promote tumorigenesis, which includes promotion of glioma proliferation, migration, invasion, angiogenesis and treatment resistance.

1.3.3 Innate immune response in HGG

The immune system plays a dual role in tumour progression. While it can help eliminate cancer cells, alternatively, cancer cells can easily evade. The innate immune system in HGG TME is composed of resident microglia and infiltrating macrophages which enter due to disruption of the blood-brain barrier (BBB) (Chen *et al.*, 2017). Macrophages primarily originate from haematopoietic stem cells in the bone marrow, while microglia originate from myeloid precursors in the yolk sac during embryonic development (Ginhoux *et al.*, 2010; Prinz and Priller, 2014). Although macrophages and microglia represent two distinct populations with different lineages, they are collectively known as tumour-associated macrophages/monocytes (TAMs). In GBM, up to 35% of TAMs are peripheral macrophages, with the remainder being microglia (Bowman *et al.*, 2016; Müller *et al.*, 2015).

The interactions between TAMs and glioma cells are bidirectional. TAMs are recruited to gliomas by chemoattractant released by glioma cells, such as C-C motif ligand 2 (CCL2), C-C motif ligand 7 (CCL7), stromal cell-derived factor 1 (also known as CXCL12), macrophage-colony stimulating factor (M-CSF) and TGF-β (Platten *et al.*, 2003; Jung *et al.*, 2018; Wang *et al.*, 2012; Ku *et al.*, 2013; Sielska *et al.*, 2013; Liu *et al.*, 2021). Additionally, TAMs also release CCL2 to recruit more monocytes, creating a positive feedback loop for constant immune cell infiltration (Chang *et al.*, 2016). Once activated, TAMs promote glioma migration and invasion through MMP2 activation, secretion of epidermal growth factor, TGF-β and IL-6 (Markovic *et al.*, 2005; Coniglio *et al.*, 2012; Wesolowska *et al.*, 2007; Zhang *et al.*, 2012). HGG proliferation can also be stimulated by TAM-derived MMP2, stress inducible protein 1 and IL-1β (da Fonseca *et al.*, 2012; Liu *et al.*, 2021; Markovic *et al.*, 2009).

The traditional model of TAM activation status is presented as a binary system of either M1 or M2. Tumour-supporting M1 is characterised by classical activation of toll-like receptor 2/4 and secretion of pro-inflammatory cytokines such as TNF-α, IL-6 and IL-1β, which support phagocytosis, as well as recruit more immune cells (Ren *et al.*, 2023). M1 macrophages are also known to release both nitric oxide and ROS to exert direct cytotoxic effects (Huang *et al.*, 2017; Liu *et al.*, 2020; Palmieri *et al.*, 2020). In contrast, tumour-suppressive M2 is alternatively activated by interleukin-4 (IL-4) and interuleukin-13 (IL-13), it is characterised by the production of anti-inflammatory cytokines such as arginase 1 (ARG1), interleukin-10 (IL-10), and TGF-β, with less cytotoxicity towards tumour cells (Ren *et al.*, 2023). Moreover, M2-like TAMs can also promote angiogenesis by transporting exosomal circRNA to endothelial cells and via TGFβ-mediated VEGF upregulation (Jiang *et al.*, 2022; Ferrari *et al.*, 2009). A graphical summary of the macrophage functions is shown in Figure 1.6.

A spectrum of TAM activation state has been revealed more recently, so in this study, we will describe TAMs as M1-like and M2-like rather than using a binary classification (Mosser and Edwards, 2008). The polarisation status of TAMs is determined by the TME. In glioma, there is a higher ratio of M2-like/M1-like TAMs, polarised by GBM-derived factors including interleukin-4, IL-10, CCL2, and M-CSF (Gabrusiewicz *et al.*, 2011; Ren *et al.*, 2023; Komohara *et al.*, 2008; Wu *et al.*, 2010). The ratio of M2-like/M1-like TAMs is correlated with the histological grade of gliomas (Komohara *et al.*, 2008). It is worth noting that although the M2-like TAM population shapes an immunosuppressive TME in HGG, M1-like TAMs are still present to exert cytotoxicity and initiate innate immune responses such as phagocytosis (Hussain *et al.*, 2006).

GBM cells have been reported to increase the phagocytotic activity of microglia, accompanied by increased glioma cell apoptosis, suggesting an anti-tumour activity of microglia in this setting (Lecoultre *et al.*, 2024). However, at the same time, phagocytosis of glioma cells has also been shown to shift macrophages from a pro-inflammatory phenotype towards an anti-inflammatory phenotype, further strengthening the immunosuppressive TME in HGG (Wu *et al.*, 2023).

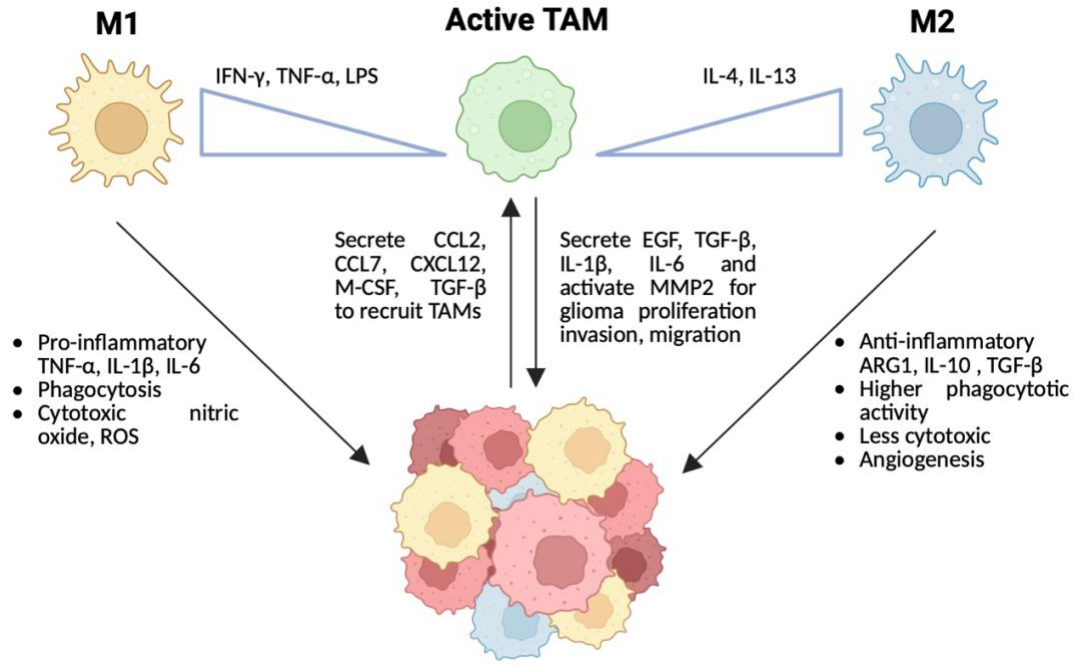

Figure 1.6 Schematic representation of macrophage functions in gliomas

Glioma cell secretes various factors such as CCL2 and CCL7 to recruit TAMs into the TME. Once activated, TAM secretes pro-tumour chemokines such as EGF and TGF-β to support glioma progression. TAM could switch to a M1-like phenotype under stimulation by IFN-γ or TNF-α, which in turn secrete pro-inflammatory TNF-α, IL-1β, nitric oxide and ROS. Alternative, TAM could adopt a M2-like phenotype under stimulation by IL-4 and IL-13, M2-like TAM secretes anti-inflammatory ARG1, IL-10 and TGF-β, as well as exhibits higher phagocytotic activity.

1.3.4 Adaptive immune response in HGG

Despite the characteristically low neoantigen burden observed in HGGs, the presence of effector T cells is positively correlated with improved survival in GBM patients, underscoring the importance of adaptive immunity in modulation glioma progression (Nejo *et al.*, 2019; Lohr *et al.*, 2011). Of note, T cell infiltration is very low in majority of the DMG patients and is generally not considered to play a predominant role in the DMG progression (Lieberman *et al.*, 2019).

Unlike cells of the innate immune system, naïve antigen-specific T cells require clonal expansion and differentiation to acquire immunologically active phenotypes. It has been proposed that tumour-associated antigens may be transported from the glioma site to the meninges via the perivascular glymphatic system, together with interstitial fluid, however this remains to be validated. (Broekman *et al.*, 2018). At the dura mater, tumour antigens either enter the cerebrospinal fluid, or be taken up by local antigen-present cells (APCs) (Broekman *et al.*, 2018). The cerebrospinal fluid and APCs then drain via dural lymphatic vessels to the deep cervical lymph nodes, where T cells can be primed by APCs (Aspelund *et al.*, 2015; Broekman *et al.*, 2018; Calzascia *et al.*, 2005; Louveau *et al.*, 2015).

Upon activation, T cells differentiate into various subtypes, such as cluster of differentiation 4-positive ($CD4^+$) T helper cells (Th), $CD8^+$ cytotoxic T cells and regulatory T cells (Tregs). $CD8^+$ T cells mediate targeted cytotoxic effects through the release of perforin and granzymes, or by engaging death receptor via expression of Fas ligand (Basu *et al.*, 2016; Hassin *et al.*, 2011). In GBM-bearing mice, increased $CD8^+$ T cell infiltration correlates positively with survival, highlighting their important anti-tumour properties (Choi *et al.*, 2017). Nevertheless, glioma cells have developed

mechanisms to evade immune surveillance, including the mass secretion of TGF-β which suppress $CD8^+$ T cell cytotoxicity (Ueda *et al.*, 2009; Crane *et al.*, 2009). Moreover, the immune checkpoint molecule, programmed death-ligand 1 (PD-L1), is often overexpressed on HGG cells and it could engage with its receptor programmed death-1 (PD-1) on $CD4^+$ and $CD8^+$ T cells (Heiland *et al.*, 2017; Berghoff *et al.*, 2015; Park *et al.*, 2016). Notably, PD-1 expression is upregulated by TGF-β , and its engagement by PD-L1 induces T cell apoptosis and functional exhaustion, ultimately hindering effects produced by anti-tumour effector T cells (Zou, Wolchok and Chen, 2016). Immune checkpoint blockade targeting the PD-1/PD-L1 axis has been shown to restore anti-tumour T cell activity, reinforcing the critical role of $CD8^+$ T cells in glioma immunosurveillance (Park *et al.*, 2018; Wainwright *et al.*, 2014).

Besides its inhibitory effects on $CD8^+$ T cells, TGF-β also promotes the expansion of Tregs, which are more abundant in GBM tumours than peripheral blood (Ueda *et al.*, 2009; Chen *et al.*, 2004; Crane *et al.*, 2012). Tregs exert immunosuppressive functions within the TME by inhibiting $CD8^+$ T cell activation, cytotoxicity and proliferation (Crane *et al.*, 2012; Chen *et al.*, 2004; van Hooren *et al.*, 2023). Collectively, these findings highlight the importance of increasing $CD8^+$: Treg ratio to potentiate effective anti-tumour responses in HGG.

1.4 Standard-of-care treatment in HGGs

Conventional fractionated radiotherapy (CRT) for DMG is typically administered over a six-week period, delivering a total dose of with 54 Gray (Gy) in 30 fractions (Park, Yea and Park, 2020). However, given that limited median survival associated with DMG, this prolonged treatment course is thought to adversely affect patient quality of life. Another approach is hypofractionated radiotherapy, which delivers higher doses per fraction over a shorter period, commonly 44.8 Gy in 16 fractions, or 39 Gy in 13 fractions (Park, Yea and Park, 2020). Both CRT and hypofractionated regimens offer transient symptom improvement or stabilisation and extend overall survival by an average of approximately three months (Gallitto *et al.*, 2019; Johung and Monje, 2017). Nevertheless, radiological evidence of local recurrence is observed in nearly all cases within 3-6 months following the completion of radiotherapy (Vanan and Eisenstat, 2015).

The standard treatment for GBM includes surgical resection if feasible, followed by a combination of radiotherapy and chemotherapy with TMZ. In GBM, CRT is typically administered over a six-week period, delivering a total dose of 60 Gy in 30 fractions, which is slightly higher than the total dose used for DMG. CRT is generally recommended for patients under the age of 65, whereas hypofractionated radiotherapy, commonly delivering 45 Gy in 15 fractions, is more often offered to elderly patients due to age-associated differences in survival benefits (Malmström *et al.*, 2012).

The conventional TMZ regimen for GBM consists of a daily dose of 200 mg per square metre of body surface area for 1 to 5 days over 28-day cycle (Stupp *et al.*, 2005). As an alkylating agent, TMZ methylates DNA, most notably at the O6 position of guanine, leading to mispairing with thymine on the complementary strand during DNA replication, rather than cytosine (Zhang, Stevens and Bradshaw, 2012). The mismatched thymine is

recognised and excised by the DNA mismatch repair system, resulting in DNA strand breaks (Zhang, Stevens and Bradshaw, 2012). Accumulation of strand breaks induces cell cycle arrest, allowing time for repair; however, unsuccessful repair ultimately leads to apoptosis (Ortiz *et al.*, 2021). Beyond its direct cytotoxic effects, TMZ also function as a radiosensitiser, enhancing the efficacy of radiotherapy in GBM (Babaloui *et al.*, 2022; Chalmers *et al.*, 2009). When administered in combination with standard radiotherapy, TMZ significantly improves survival in patients under 65 years old compared to radiotherapy alone, supporting its efficacy as adjuvant therapy (Inggas *et al.*, 2025; Stupp *et al.*, 2009).

1.4.1 Radiation-induced cytotoxicity

High-energy ionising radiation (IR) exerts its cytotoxic effects on cancer cells through both direct and indirect mechanisms. Directly, IR induces DNA damage by causing double-strand breaks, while indirectly, it ionises intracellular water molecules to generate DNA-damaging free radicals known as ROS, such as superoxide anions and hydroxyl radicals (Baskar *et al.*, 2014; Yamamori *et al.*, 2012). In response, cells initiate DNA repair mechanisms such as non-homologous end-joining, to restore genomic integrity following double-strand breaks. However, if the repair is unsuccessful or incomplete, a cascade of intracellular signalling events is activated, ultimately directing the irradiated cells towards cell death, as shown in Figure 1.7 (Kaur *et al.*, 2020; Mahaney, Meek and Lees-Miller, 2009). The mode of radiation-induced cell death depends on various factors, including cell type, radiation dose, oxygen availability, DNA repair efficiency, and the cell cycle phase at the time of exposure (Golden *et al.*, 2012; Stewart *et al.*, 2011). IR is capable of triggering multiple forms of cell death, such as apoptosis, necrosis, autophagy, proptosis, ferroptosis, and immunogenic cell death (Jiao, Cao and Liu, 2022). In the following sections, we will focus on selected forms of radiation-induced cell death of particular relevance to this project.

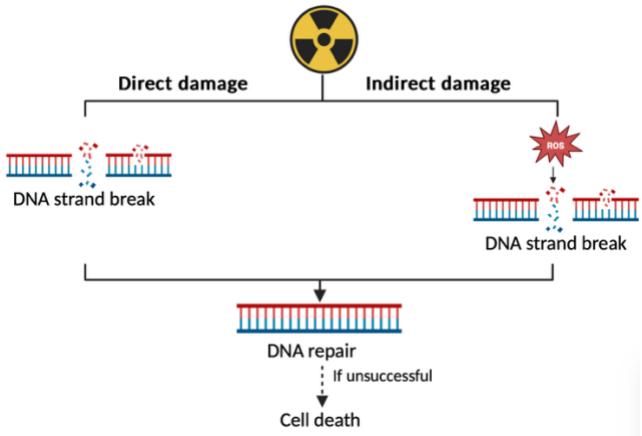

Figure 1.7 Graphical representation of radiation-induced damage

Irradiation induces cytotoxicity either directly via inducing DNA strand breaks, or indirectly via production of free radicals. Either way, if DNA is unsuccessfully repaired, irradiation ultimately leads to cell death.

1.4.1.1 Apoptosis

Apoptosis is a tightly regulated programmed cell death essential for the elimination of damaged or unwanted cells. IR primarily acts through the intrinsic (mitochondrial) apoptotic pathway, which is characterised by mitochondrial outer membrane permeabilisation and the subsequent release of cytochrome c, leading to apoptosome formation (Galluzzi *et al.*, 2018; Golden *et al.*, 2012). Triggers of intrinsic apoptosis include a variety of cellular stressors such as DNA damage, ER stress, ROS accumulation, replication stress and mitotic errors (Galluzzi *et al.*, 2018). Upon activation, proteins of the apoptosis regulator, Bcl-2 family, comprising both pro-apoptotic and anti-apoptotic proteins modulate the apoptotic response. In particular, pro-apoptotic proteins Bcl-2-associated X protein (Bax) and Bcl-2 antagonist/killer (Bak) oligomerise to form pores in the outer mitochondrial membrane, leading to the release of apoptogenic cytochrome c into the cytosol (Czabotar *et al.*, 2014; Shamas-Din *et al.*, 2013). Cytochrome c forms the apoptosome complex together with apoptotic protease-activating factor 1 (APAF1) and deoxyadenosine triphosphate, which activates caspase 9 (Cain *et al.*, 1999; Li *et al.*, 1997).

Alternatively, IR may also activate the extrinsic apoptotic pathway, in which cell surface death receptors such as Fas and tumour necrosis factor (TNF) receptor are upregulated and triggered by their respective ligands (Chakraborty *et al.*, 2003; Rübe *et al.*, 2002). This receptor-ligand interaction leads to the assembly of the death-inducing signalling complex (DISC) and subsequent activation of caspase 8 (Chakraborty *et al.*, 2003; Galluzzi *et al.*, 2018). Both intrinsic and extrinsic apoptotic pathways converge at the activation of executioner caspase, caspase 3, which orchestrates the cleavage of nuclear proteins, cytoskeletal component, and ultimately leading to cell apoptosis (Jiao,

Cao and Liu, 2022). A graphical summary of the apoptotic cascade is shown in Figure 1.8.

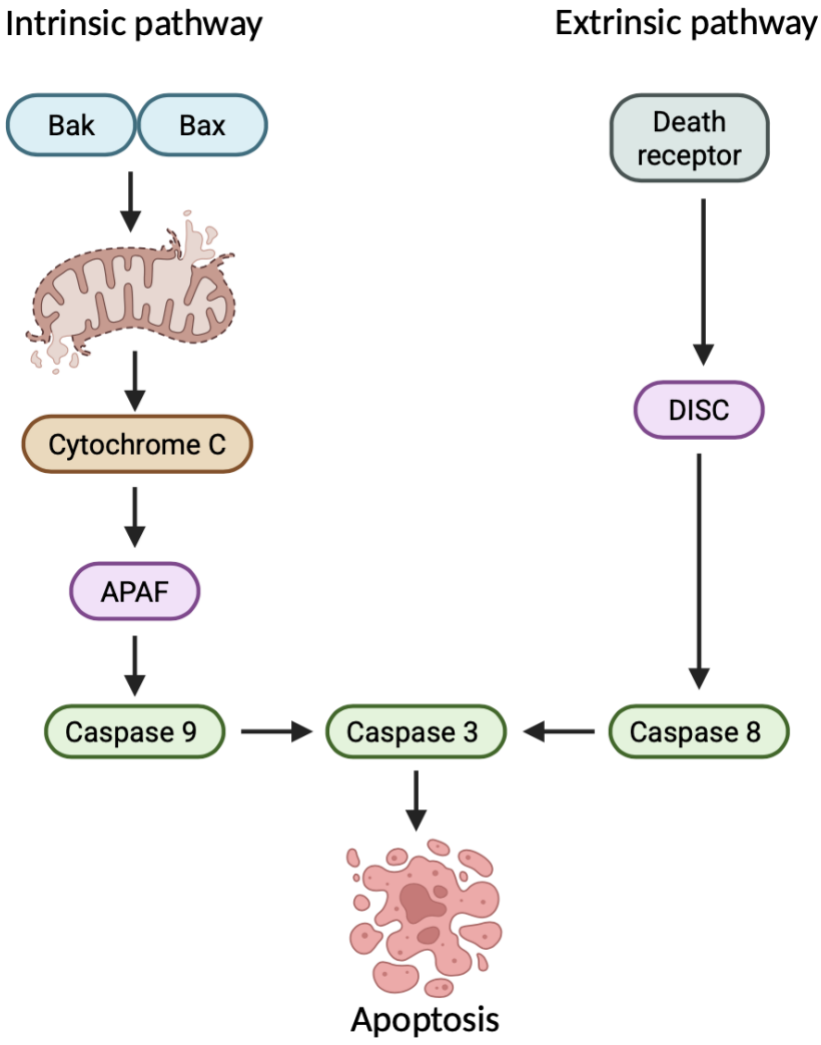

Figure 1.8 Graphical representation of the apoptotic cascade

Activation of the intrinsic apoptosis pathway results in oligomerisation of Bak and Bax which act together to permeabilise outer mitochondrial membrane. Cytochrome C is released and forms apoptosome complex with APAF, which then activates caspase 9. Alternatively, the extrinsic apoptosis pathway involves activation of death receptor, which assembles DISC and activates caspase 8. Both intrinsic and extrinsic pathways converge at caspase 3 activation which executes apoptosis.

1.4.1.2 Autophagy

Autophagy is a form of catabolic process characterised by the lysosomal degradation of intracellular organelles and macromolecules, and under certain conditions, it may contribute to regulated cell death (Jiao, Cao and Liu, 2022). At basal levels, autophagy plays a role in maintaining cell metabolic homeostasis, especially adaption to stress conditions such as hypoxia and IR, by limiting ROS accumulation and facilitating the removal of damaged organelles (Classen *et al.*, 2019; Hill *et al.*, 2023; Zhou *et al.*, 2018). However, excessive autophagy activation can shift it from a cytoprotective mechanism to a form of programmed cell death. Upon cellular stress, mammalian target of rapamycin complex 1 promotes formation of autophagosomes that encapsulates unwanted cellular components, which then subsequently fuse with lysosomes to form autophagolysosome that degrades cytoplasmic-derived contents (Golden *et al.*, 2012; Jiao, Cao and Liu, 2022). Notably, cancer cells inherently produce higher levels of ROS compared to normal cells, and radiation exacerbates this oxidative burden, often leading to increased autophagic activity as an adaptive response (Perillo *et al.*, 2020). In addition to oxidative stress, radiation-induced DNA damage can directly stimulate autophagic pathways, ultimately resulting in cell death if the damage is irreparable (Classen *et al.*, 2019; Galluzzi *et al.*, 2018).

1.4.1.3 Inflammatory responses to radiation

The therapeutic efficacy of IR extends beyond direct cytotoxicity toward tumour cells and includes significant immunomodulatory effects. Following IR, tumour cells release a range of neoantigens and damage-associated molecular patterns (DAMPs), along with ATP, which collectively stimulate APCs and initiate the activation T lymphocytes (Zanoni *et al.*, 2022; Zheng *et al.*, 2023). Moreover, major histocompatibility complex class I molecules are upregulated in irradiated cells, enhancing their recognition and clearance by cytotoxic $CD8^+$ T cells (Tailor *et al.*, 2022). Increased infiltration and activation of cytotoxic $CD8^+$ T cells following IR has been consistently observed and is correlated with improved radiation response, accompanied by an inflamed TME (Blair *et al.*, 2022; Chen *et al.*, 2018; Gupta *et al.*, 2012; Lim *et al.*, 2014; Zeng *et al.*, 2013a).

In parallel, IR upregulates the secretion several pro-inflammatory cytokines, including IL-1β, IL-6, TNF-α, which contribute to the inflammatory microenvironment (Kang *et al.*, 2021; Matsuoka *et al.*, 2016; Rübe *et al.*, 2002; Tabatabaei *et al.*, 2017). While this inflammatory response can enhance anti-tumour immunity by promoting $CD8^+$ T cells cytotoxicity, it may also facilitate tumour progression by activating oncogenic pathways such as NF-κB and by suppressing oxidative stress (Kang *et al.*, 2021; Matsuoka *et al.*, 2016). Moreover, IR promotes TAM polarisation towards a pro-inflammatory M1-like phenotype, allowing exertion of their pro-tumour effects (Genard *et al.*, 2018; Teresa Pinto *et al.*, 2016). However, it is important to note that IR also exert immunosuppressive effects in the brain by upregulating expression of anti-inflammatory genes in microglia, such as leukaemia inhibitory factor and stabilin-1 (Osman *et al.*, 2020).

1.4.2 Targeting pro-survival signalling in HGGs

Pro-survival signalling pathways, including NF-κB and mitogen-activated protein kinase (MAPK), play central roles in glioma cell survival and progression. Genetic alterations such as EGFR amplification (present in approximately 60% of GBMs) and BRAF mutations (detected in 12% of DMGs) can drive sustained activation of these pathways, highlighting them as potential therapeutic targets (Brennan *et al.*, 2013; Schüller *et al.*, 2021). A high-throughput drug screening study was conducted using a panel of patient-derived DMG cell lines and identified a subset of cells exhibiting marked sensitivity to compounds targeting the NF-κB signalling pathway (Carvalho *et al.*, 2020). Additionally, some DMG cells lines demonstrate high susceptibility to mitogen-activated protein kinase kinase (MAPKK) inhibitors, including Trametinib and Selumetinib (Carvalho *et al.*, 2020). Although Trametinib showed significant sensitivity in vitro, xenograft models and patients developed resistance to the agent due to acquired resistance of MAPKK, and sustained upregulation of the pro-survival MAPK signalling (Izquierdo *et al.*, 2022). Further details on NF-κB and MAPK are described below. Notably, both signalling pathways have been shown to contribute to cell radioresistance by upregulating transcription of pro-survival genes, and therefore represent important targets to be tackled for improving glioma radiosensitivity (Bhat *et al.*, 2013; Marampon *et al.*, 2011).

Compared to DMG, high throughput drug screening have been more extensively conducted in GBM, where both the MAPK and NF-κB pathways have similarly emerged as potential therapeutic targets (Lenin *et al.*, 2021). A Phase I clinical trial assessing the NF-κB pathway inhibitor Bortezomib was completed in HGG patients, but unfortunately failed to progress into phase II as a mono-adjuvant therapy, likely due to its limited permeability across the BBB (Phuphanich *et al.*, 2010). Taken together, both MAPK and

NF-κB signalling emerge as potential therapeutic targets in DMG and GBM to enhance radiosensitivity, underscoring the need to identify chemotherapeutical compounds capable of effectively inhibiting either of these pathways.

1.4.2.1 MAPK pathway signalling

The MAPK signalling pathway plays a crucial role in regulating diverse cellular processes, including cell proliferation, survival and apoptosis. Among its key components are extracellular signal-regulated kinase 1/2 (ERK 1/2), members of the MAPK family. Activation of the MAPK cascade can be triggered by a range of stimuli including growth factors, cytokines, and G-protein coupled receptor (GPCR) activation (Guo *et al.*, 2020). Ligand binding to cell surface receptor induces phosphorylation of intracellular tyrosine residues, leading to activation of Ras via the exchange of guanosine diphosphate (GDP) for guanosine triphosphate (GTP) (Simanshu, Nissley and McCormick, 2017). GTP-bound Ras subsequently phosphorylates and activates Raf kinases, which in turn phosphorylate and activate MAPKK (also known as MEK), culminating the activation of MAPK (also known as ERK) (Lavoie, Gagnon and Therrien, 2020). Once activated, phosphorylated ERK1/2 (pERK) dimerise and translocate to the nucleus, where it modulates the activity of various transcription factors involved in regulating cell growth and survival (Guo *et al.*, 2020). A graphic representation summarising the MAPK pathway is shown in Figure 1.9.

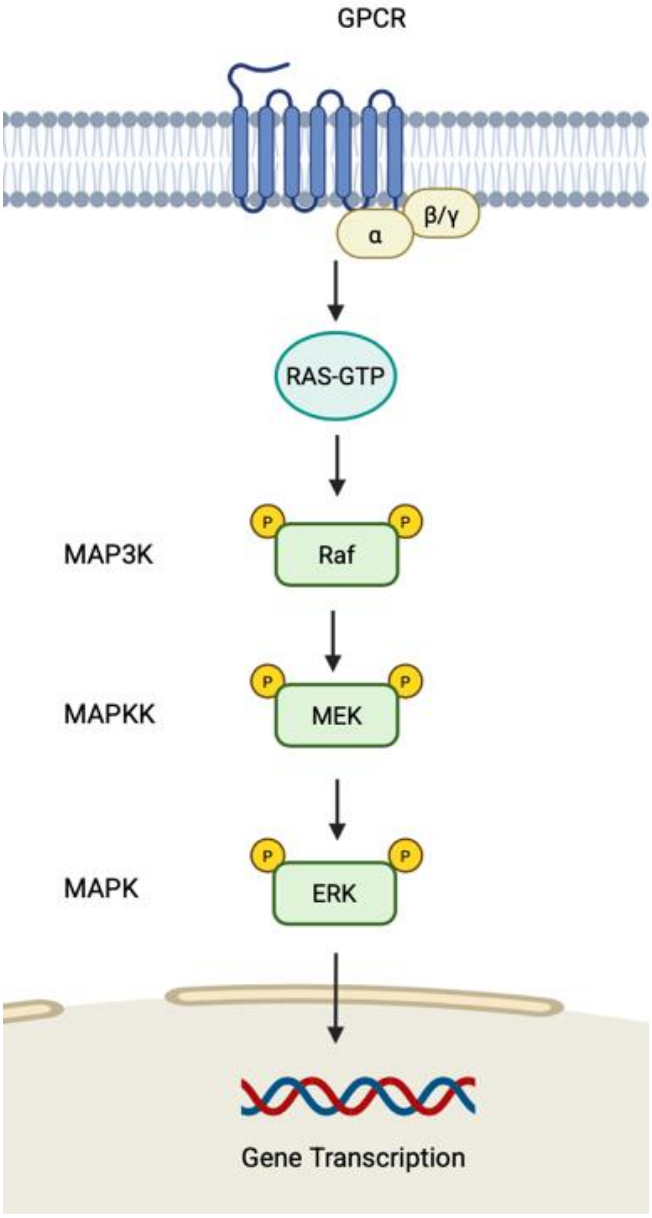

Figure 1.9 Schematic representation of the MAPK signalling pathway

Activation of the GPCR results in GTP binding to Ras, which subsequently phosphorylates Raf, MEK and ERK. pERK ultimately enters the nucleus to modulate transcription activities

1.4.2.2 Pro-survival role of NF-κB signalling

The NF-κB family comprises several transcription factors that typically function as heterodimers, most notably the p65 (RelA) and p50 complex. Under resting conditions, NF-κB dimers are retained in the cytoplasm in their inactive state through association with the inhibitory protein IκB. Upon pathway activation, the IKK complex (IκB kinase) composed of IKKα and IKKβ subunit is phosphorylated and activated (Shambharkar *et al.*, 2007). This causes IκB to be phosphorylated, leading to its ubiquitination and subsequent degradation by proteasomes (Shambharkar *et al.*, 2007). The degradation of IκB releases NF-κB dimers, allowing their free translocation into the nucleus, where they regulate transcription of various genes involved in cell survival, proliferation and inflammation. A graphical summary of the NF-κB cascade is shown in Figure 1.10, illustrating GPCR phosphorylates IκB via PI3K/Akt signalling.

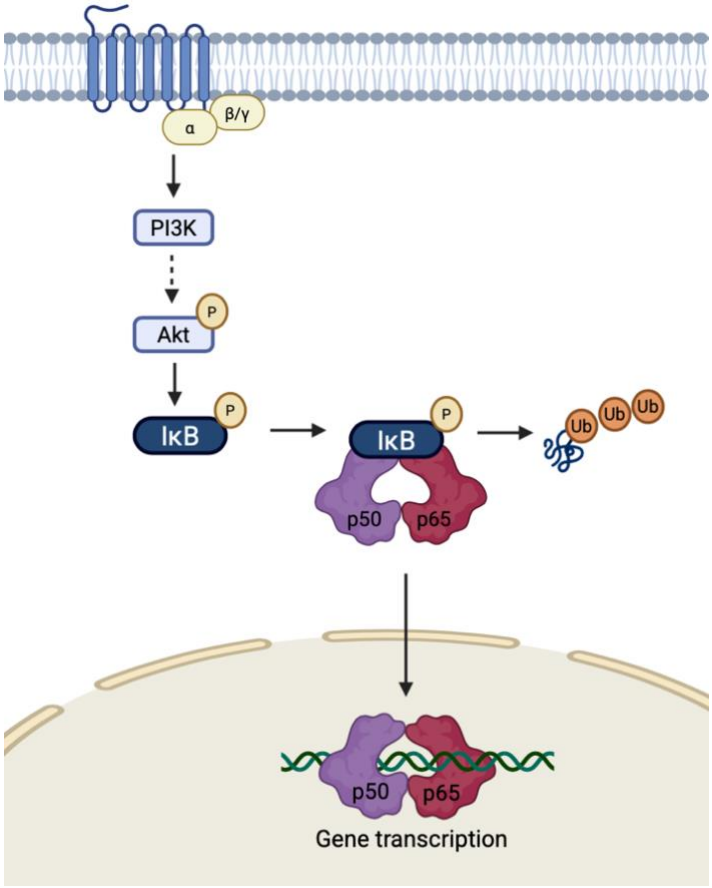

Figure 1.10 Graphical representation of the NF-κB signalling pathway

GPCR activation results in PI3K and Akt activation, which phosphorylates IκB. Activated IκB is ubiquitinated and degraded, allowing free translocation of the NF-κB dimers p50 and p65 into the nucleus to regulate transcription of pro-survival genes.

1.4.3 Current Challenges in treatment of HGGs

The effective delivery of therapies to HGG remains a significant clinical challenge due to several inherent biological barriers. One major obstacle is the limited infiltration of immune cells into the TME compared to other cancer types, which constrains the efficacy of immunotherapeutic strategies. Additionally, functional BBB acts as a selective permeability barrier, protecting the CNS from penetration of large or hydrophilic molecules, thereby restricting the intracranial delivery of many chemotherapeutical drugs. Although several clinical trials have explored novel therapeutic candidates for HGG, temozolomide (TMZ) remains the only adjuvant chemotherapeutic agent to demonstrate a survival advantage over standard radiotherapy alone in GBM (Vanan and Eisenstat, 2015; Warren, 2012). While TMZ exhibits radiosensitising properties, overall survival outcomes for GBM patients remain poor, highlighting the necessity for incorporating more potent radiosensitisers into treatment regimens (Kil *et al.*, 2008). To date, no chemotherapy or targeted therapies have been incorporated as standard of care treatment for DMG. Therefore, there is a need for the development of novel targeted therapeutic approaches that are both effective and minimally toxic to surrounding healthy brain tissue. Moreover, although HGG patients initially respond to radiotherapy, tumour inevitably recur, potentially due to the presence of radioresistant GSC and quiescent cell populations, or hypoxic TME.

1.5 The Complement System

The complement system, as a central component of innate immunity, plays an important role in a range of pathophysiological processes including immune surveillance, immune clearance, and the orchestration of inflammatory responses (Ehrnthaller et al., 2011; Ricklin et al., 2010). It comprises a variety of complement proteins that are predominantly synthesised by hepatocytes and secreted into the circulation, however local production by many immune and non-immune cell has also been documented (Lubbers *et al.*, 2017). Notably, complement proteins and their receptors are frequently overexpressed in many cancer types, where they contribute to disease progression and immune modulation in context-dependent manners (Revel *et al.*, 2020; Roumenina *et al.*, 2019). Three distinct pathways to activate the complement system are the classical pathway, the lectin pathway and the alternative pathway. Classical pathway is initiated by antigen-antibody complexes, the lectin pathway is triggered by mannose-binding lectin recognition of microbial carbohydrates, and the alternative pathway is constitutively active at low levels but can be amplified upon direct recognition of pathogen surfaces or damaged host.

All three pathways converge on the generation of complement component 3 (C3) convertase enzyme complex, which cleaves C3 into the pro-inflammatory anaphylatoxin C3a and the opsonin C3b (Revel *et al.*, 2020). C3b not only promotes phagocytosis through opsonisation but also contribute to the formation of the complement component 5 (C5) convertase, which cleaves C5 into C5a and C5b (Afashar-Kharghan, 2017). C5a is one of the most potent anaphylatoxins and though binding to its receptor complement component 5a receptor 1 (C5aR1), C5a-C5aR1 signalling initiates inflammatory responses. On the other hand, C5b initiates assembly of the terminal membrane attack

complex (MAC) through recruitment and binding of complement components C5, C7, C8 and C9 (Afashar-Kharghan, 2017). The MAC forms transmembrane pores in target cells, resulting in cell lysis, osmotic imbalance and death. Collectively, complement activation facilities pathogen clearance through inflammation, enhanced phagocytosis, and direct cell lysis. A schematic overview of the complement cascade is shown in Figure 1.11.

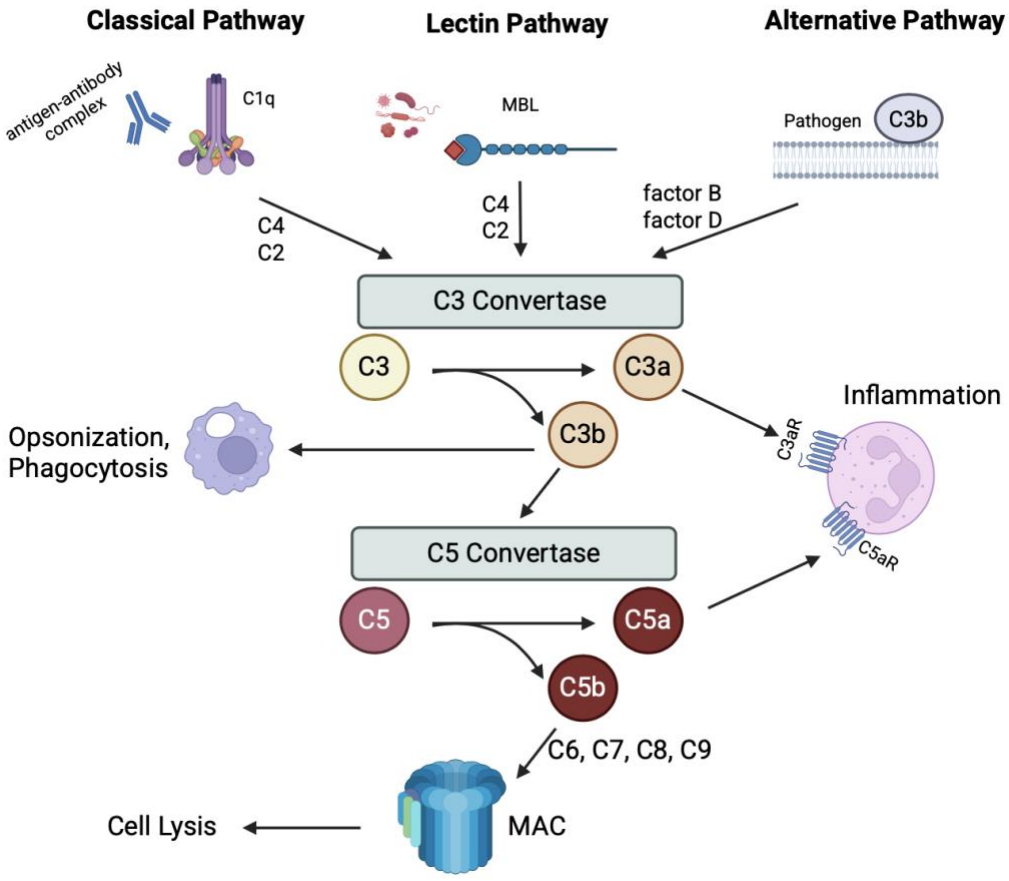

Figure 1.11 Graphical representation of the complement system

The complement system can be activated via three distinct pathways: classical, alternative and lectin. All three pathways ultimately generate the C3 convertase enzyme complex, which cleaves C3 into C3a (for inflammation) and C3b (for opsonisation). C3b could also generate the C5a convertase enzyme, which cleaves C5 into C5a (potent anaphylatoxin), and C5b (form MAC with C6, C7, C8 and C9 to perform cell lysis).

1.5.1 Complement system in the brain

Under normal physiological conditions, complement proteins in the brain are predominantly synthesised locally by microglia and astrocytes (Lian *et al.*, 2016). While circulating complement proteins are abundant in plasma, their access to the CNS is typically restricted unless the BBB integrity is compromised due to ageing, neurological disorders and cancer, in which peripheral complement proteins infiltrate the brain parenchyma (Farin *et al.*, 2006; Lian *et al.*, 2016; Watkins *et al.*, 2014).

There is a growing body of evidence emphasising the critical role of the complement system in CNS development and homeostasis. MASP, C1q, C3, and C5 have been implicated in neurogenesis during embryonic and adult stages, synaptic pruning, memory engram and the clearance of apoptotic neurons (Coulthard *et al.*, 2017; Deivasigamani *et al.*, 2023; Fraser, Pisalyaput and Tenner, 2010; Gorelik *et al.*, 2017; Rahpeymai *et al.*, 2006; Schafer *et al.*, 2012; Scott-Hewitt *et al.*, 2024; Wang *et al.*, 2012). Despite these homeostatic roles, dysregulation of the complement cascade is frequently reported in various neurological disorders. Elevated expression levels of C1q, C3, C4 and terminal complex components C5-C9 have been reported in Alzheimer's disease, amyotrophic lateral sclerosis (ALS), and GBM, suggesting that aberrant complement activation contributes to neuroinflammation and neuronal damage (Fonseca *et al.*, 2013; Mangogna *et al.*, 2019; Sta *et al.*, 2011).

1.5.2 Complement system in cancer

Within the TME, complement components such as C1a, C3a/C3a receptor (C3aR) and C5a/C5aR1 are locally expressed and have been implicated in several aspects of tumorigenesis, including tumour cell proliferation, invasion, angiogenesis, therapy resistance, monocyte recruitment, and the polarisation of TAMs towards the M2-like phenotype (Lim et al., 2020; Piao et al., 2018; Markiewski et al., 2008; Zhang et al., 2012). Some studies reported lack of association between tumour volume and complement components specific to the alternative (e.g. Factor B) and lectin (e.g. MBL) pathways, suggesting that the classical activation pathway may be predominantly responsible for complement-mediated effects in tumour progression, at least in lung cancer (Kwak et al., 2018; Markiewski et al., 2008).

The role of the complement system in cancer is likely to be context-dependent, with evidence supporting both pro- and anti-tumoral functions. On the anti-tumour side, formation of the MAC can directly mediate tumour cell lysis. However, many malignant cells evade this mechanism by overexpression of negative complement regulatory proteins, such as clusters of differentiation-59 (CD59) and -55 (CD55), which inhibit the formation of C3 or C5 convertases and prevent MAC assembly (Gelderman et al., 2002; Kesselring et al., 2014).

Conversely, high intratumoral production of complement proteins can promote tumour progression. For instance, mice implanted with high C5a-producing lymphoma xenografts exhibited accelerated tumour growth compared to those bearing low C5a-tumours (Gunn et al., 2012). The authors suggested that excessive C5a may perpetuate tumour progression, or overactivate the infiltrating immune cells, leading to an overall immunosuppressive microenvironment (Gunn et al., 2012).

C3a and C5a signalling through their respective receptors induce the secretion of inflammatory cytokines and activate canonical pro-survival signalling pathways such as MAPK, PI3K/Akt, and NF-κB, thereby enhancing tumour cell survival and progression (Cho et al., 2014; Lim et al., 2020; Revel et al., 2020; Shu et al., 2020). Supporting this, both genetic deletion and pharmacological inhibition of C3-C3aR and C5a-C5aR1 signalling have been shown to reduce tumour proliferation rate in vitro and decrease tumour burden in vivo, underscoring the pro-tumoural role of complement activation (Cho et al., 2014; Corrales et al., 2012; Markiewski et al., 2008; Nabizadeh et al., 2019; Nunez-Cruz et al., 2012). Complement activation also promote angiogenesis, EMT, migration, invasion and metastatic spread of cancer cells, which could be inhibited upon inhibition of these complement signalling (Cho et al., 2014; Corrales et al., 2012; Gu et al., 2013; Hu et al., 2016; Shu et al., 2020).

Beyond direct effects on tumour cells, tumour-derived complement components actively modulate the immune landscape of the TME. C5a has been reported to promote the recruitment and activation of myeloid-derived suppressor cells in mice bearing lung and cervical tumours, which produce ROS and reactive nitrogen species, thereby impairing cytotoxic $CD8^+$ T cell responses (Gunn et al., 2012; Markiewski et al., 2008). Inhibition of C3aR and C5aR have been shown to enhance $CD8^+$ infiltration in lung and ovarian cancer models (Markiewski *et al.*, 2008; Nunez-Cruz *et al.*, 2012). Moreover, C5a signalling facilitates the recruitment of immunosuppressive Treg cells in melanoma and lung cancer models, further strengthening the immunosuppressive TME that impairs anti-tumour immunity (Nabizadeh *et al.*, 2019; Vadrevu *et al.*, 2014). Notably, a study has shown that C3 and C5a antagonism reduced the volume of head and neck tumour only in the context of Treg depletion (Gadwa et al., 2021).

Collectively, these findings highlight the dual and context-dependent roles of the complement system in cancer biology. While complement activation can exert anti-tumour effects through direct cell lysis, its predominant impact in many solid tumours appears to be tumour-promoting. In GBM specifically, high expression of the classical and alternative complement genes is associated with reduced overall survival in patients, further highlighting the importance of targeting the complement system in HGGs (Roumenina et al., 2019).

1.5.3 Complement activation and radiation

Multiple studies have reported upregulation of complement proteins including C1s, C3, C3aR1, C5, C5aR1, factor B and MASP in various cancer models following radiotherapy (Beach *et al.*, 2023; Elvington *et al.*, 2014; Lee *et al.*, 2025; Surace *et al.*, 2015). This induction is thought to be triggered by immunoglobulin M binding to necrotic cells following irradiation, which in turn activates the complement system. Specifically in the brain, C1q and C3 expression were found to be elevated in the normal hippocampus tissue after irradiation, and they were co-localising with microglia (Markarian et al., 2021). However, whether complement activation promotes or impairs the tumour response to radiotherapy remains an open controversy. Some studies suggest that C3 and C5 signalling are essential for the therapeutic efficacy of radiotherapy, while others report enhanced tumour control when these signalling are inhibited (Beach *et al.*, 2023; Elvington *et al.*, 2014; Gadwa *et al.*, 2021; Rosberg *et al.*, 2024; Sodji *et al.*, 2022; Surace *et al.*, 2015; Yuan *et al.*, 2023).

Using genetically complement-deficient tumour-bearing mice, Surace et al. demonstrated that C3a and C5a signalling are crucial for radiotherapy efficacy. Studies showed that these anaphylatoxins promote the maturation of tumour-associated dendritic cells, and enhance interferon-gamma (IFN-γ) production to sustain cytotoxic $CD8^+$ T cell responses following irradiation (Gupta et al., 2012; Strainic et al., 2013; Surace et al., 2015). A separate study also reported that pharmacological inhibition of C3aR (using SB290157) and C5aR1 (using PMX205) did not enhance tumour response to radiotherapy, and instead increased tumour growth in the absence of irradiation (Gadwa et al., 2021). The authors proposed that targeting the C3a/C5a signalling axis drives the phenotypic switch of $CD4^+$ T cells into Tregs and therefore suppressing anti-tumour immunity.

However, the combination of C3a and C5a receptor blockade together with Treg depletion significantly reduced head and neck tumour growth, suggesting a synergistic role of complement signalling and Treg cell suppression in shaping the TME (Gadwa et al., 2021).

In contrast, a study previously showed that blocking C3 in lymphoma models with the recombinant protein CR2-crry significantly enhanced the efficacy of radiotherapy in a neutrophil-dependent manner (Elvington et al., 2014). Similarly, Sodji et al. reported that the C3aR antagonist SB290157, when used in combination with irradiation, slowed tumour progression and prolonged survival in pancreatic cancer xenograft models, an effect linked to increased infiltration of natural killer cells, and independent of $CD8^+$ T cells (Sodji et al., 2022). Further supporting this, improved survival in hypoxic GBM models was observed when SB290157 was administered alongside radiotherapy, compared to mice treated with radiotherapy alone (Rosberg *et al.*, 2024). This study suggests that complement inhibition may be capable of sensitising radioresistant tumour cells, augmenting cytotoxicity in radioresistant GBM. However, as discussed in our review, interpretation of these findings must be considered cautiously, as SB290157 has reported off-target effects in which in addition to antagonising C3aR, in which it also partially agonises C5aR2 (Lee *et al.*, 2025; Li *et al.*, 2020a).

Conflicting results in the literature regarding whether complement inhibition enhances or diminishes the response to radiotherapy may reflect variations in study designs, including tumour type, treatment regimens, radiation dose, or the cellular sources of complement proteins within the specific TME (Lee *et al.*, 2025). The impact of complement activation on radiotherapy outcomes therefore appears to be context-dependent. Moreover, genetic depletion of complement components may not fully

recapitulate the effects of pharmacological inhibition, which acts within a defined therapeutic window. Knockout models can have broader systemic implications and may trigger compensatory mechanisms, for instance, thrombin-mediated generation of C5 convertase in the absence of C3, a mechanism not observed with pharmacologic blockade (Huber-Lang et al., 2006). In addition, some knockout mouse models display reduced baseline tumour growth compared to wildtype controls even without therapeutic intervention, which further complicates interpretation of results upon addition of radiotherapy in these models (Cho et al., 2014; Corrales et al., 2012; Kwak et al., 2018; Markiewski et al., 2008; Nabizadeh et al., 2019; Nunez-Cruz et al., 2012).

1.5.4 C5aR1

C5a is a 74-amino acid anaphylatoxin generated by proteolytic cleavage of C5, and it primarily exerts its biological effects through binding to the G-protein coupled receptor (GPCR) C5aR1, also known as CD88. C5aR1 comprises an extracellular ligand-binding domain, three extracellular loops (ECLs) and seven transmembrane (TM) helices which transduce intracellular signals via coupling with heterotrimeric Gα proteins (Robertson *et al.*, 2018; Yang *et al.*, 2024). Structural studies have demonstrated that C5a engages with C5aR1 via three physically distinct domains on the receptor. Site 1 is located within the N-terminal region of the extracellular domain, Site 2 involves TM2, TM3 and TM5-7 which interact with the C-terminal region of C5a, and Site 3 is situated at ECL2 (DeMartino *et al.*, 1994; Feng *et al.*, 2023; Siciliano *et al.*, 1994). Figure 1.12 illustrates the structure of the C5a-C5aR1 complex created by Feng *et al.,* 2023.

Upon ligand engagement, C5aR1 undergoes conformational changes that facilitate recruitment of distinct G-protein subtypes and β-arrestin, initiating downstream signalling cascades (Feng *et al.*, 2023; Yang *et al.*, 2024). While C5a-C5aR1 interactions mediate a wide range of immune responses, as a GPCR, C5aR1 also activates canonical pro-survival pathways such as NF-κB and MAPK, making C5a-C5aR1 signalling a potential candidate for targeting cancer cell survival (Beach *et al.*, 2023; Li *et al.*, 2020b; Schraufstatter *et al.*, 2009; Song *et al.*, 2018). It is worth noting that C5a can also bind to another receptor, C5a receptor 2 (C5aR2). Although C5aR2 can recruit β-arrestin, it lacks the capability to couple G-protein functionally, and is therefore considered functionally distinct, with a limited role in classical GPCR-mediated signalling (Scole *et al.*, 2009).

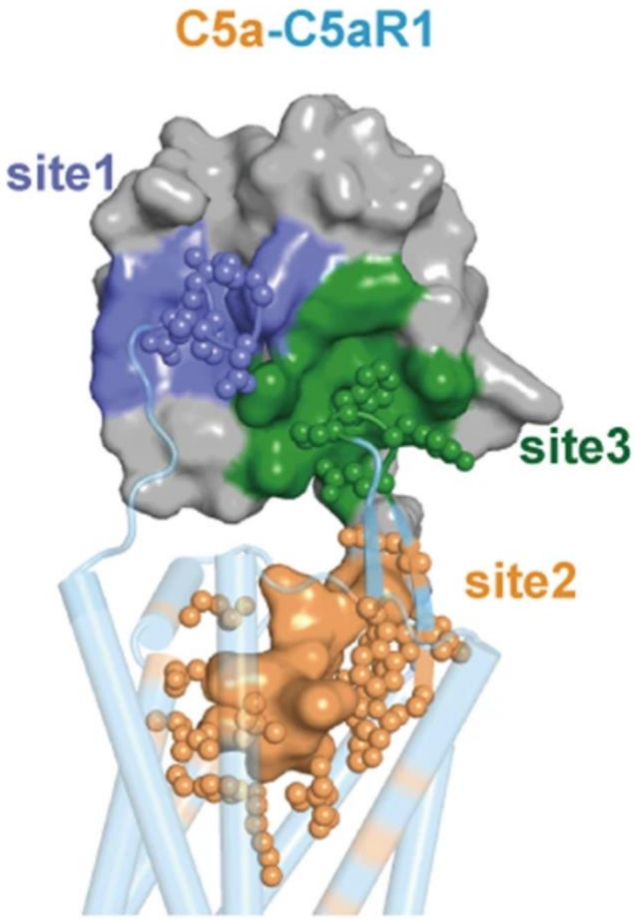

Figure 1.12 Graphical representation of the C5a-C5aR1 complex structure

The top part represents C5a surface, while the bottom cylindrical helices represent C5aR1, with three binding sites labelled. Adapted from Feng *et al.*, 2023.

1.5.4.1 C5a-C5aR1 in HGG tumorigenesis

C5 has been implicated in glioma malignancy by contributing to multiple aspects of tumorigenesis (Meng *et al.*, 2019). In GBM, a high ratio of $CD4^+$ tumour-infiltrating lymphocytes to $CD8^+$ lymphocytes is associated with worse prognosis (Han *et al.*, 2014). $CD4^+$ T cells can differentiate into various subtypes, two of which are pro-tumour Tregs and anti-tumour Th1 cells. Notably, C5a has been shown to regulate $CD4^+$ T cell polarisation in a concentration-dependent manner, where low levels of C5a promote Th1 differentiation, and high levels favour Treg induction (Gunn *et al.*, 2012). These findings highlight the critical role of C5a in shaping the immune landscape of the glioma TME.

One of the key contributors to treatment resistance and relapse in HGG is the presence of GSCs (Muthukrishnan *et al.*, 2022). Upon exposure to TME stimuli, GSCs can transition into a mesenchymal-like state, which is associated with tumour growth, invasion, vascularisation, and therapy resistance (Cheng *et al.*, 2013; Lau *et al.*, 2015; Lim *et al.*, 2020; Muthukrishnan *et al.*, 2022). This GSC-to-mesenchymal switch could be enhanced by standard GBM treatments such as radiation and TMZ (Cheng *et al.*, 2013; Lau *et al.*, 2015; Muthukrishnan *et al.*, 2022). A study reported that mesenchymal stemlike cells promote GBM invasion by releasing C5a, which activates the MAPK through C5aR1 (Lim *et al.*, 2020). Additionally, C5a supports mesenchymal stem cell migration and protects them from oxidative stress while sustaining MAPK signalling, contributing to therapy resistance (Schraufstatter *et al.*, 2009).

Moreover, C5 produced by TAMs engages with C5aR1 on glioma cells, leading to upregulation of DNA damage repair proteins after TMZ treatment, and thereby promoting resistance to chemotherapy (Li *et al.*, 2021). Furthermore, our group has also recently reported that hypoxic conditions increase C5aR1 expression in GBM cells,

further implicating the C5a-C5aR1 axis in HGG adaption and survival under cellular stress (Suwa *et al.*, 2025). To date, no studies have reported the role of C5a in the context of DMG specifically. However, together, these findings highlight the importance of C5a-C5aR1 signalling in promoting immune evasion, mesenchymal transition, and therapy resistance in GBM. Inhibition of C5a-C5aR1 signalling inhibition therefore represents a potential promising strategy to enhance the efficacy of current HGG therapies and to overcome resistance mechanisms.

1.5.4.2 PMX205

PMX205 is an orally bioavailable cyclic hexapeptide which functions as competitive antagonist of C5aR1. It has completed Phase 1b clinical trials for the treatment of ALS, though full trial results have not yet been published (trial number: ACTRN12622000927729). PMX205 binds to an orthosteric site on the extracellular domain of C5aR1, overlapping with the ligand-binding region of C5a itself, thereby preventing receptor activation (Pandey *et al.*, 2020). In human macrophages, PMX205 exhibits a half-life of approximately 0.9 hours (h) at a concentration of 1 μM, and retains about 40% inhibitory activity against C5a-induced signalling after 24 hours (Li *et al.*, 2020b). Importantly, the ability of PMX205 to cross the BBB makes it ideal for HGG treatment, or other CNS malignancies (Kumar *et al.*, 2020).

In Alzheimer's disease models, PMX205 has been shown to suppress expression of microglial activation markers, and rescue cognitive impairment with neuroprotective effects (Gomez-Arboledas *et al.*, 2022). These therapeutic effects were believed to be attributed, at least in part, to the ability of PMX205 in modulating microglial phenotype by inhibiting C5a-C5aR1-mediated pro-inflammatory microglial gene expression (Schartz *et al.*, 2023). In addition to its neurological applications, PMX205 has demonstrated efficacy in cancer settings. Our group previously reported that PMX205, when used in combination with radiotherapy enhances tumour-specific apoptosis in colorectal cancer, while mitigating normal intestinal tissue toxicity (Beach *et al.*, 2023). These effects of PMX205 are thought to result from attenuation of canonical C5a/C5aR1 signalling, which downregulates key apoptotic modulators such as NF-κB and MAPK, thereby sensitising tumour cells to radiation-induced cell death.

1.5.4.3 Avacopan

Another C5aR1 antagonist of significant interest is Avacopan, an orally bioavailable and highly selective small molecule that targets C5aR1 (Bekker *et al.*, 2016). Avacopan is approved by the U.S. Food and Drug Administration (FDA) as an adjuvant therapy for antineutrophil cytoplasmic antibody-associated vasculitis, and has demonstrated potent anti-inflammation activity through suppression of C5a-induced cluster of differentiation 11b (CD11b) expression on neutrophils (Bekker *et al.*, 2016). Avacopan exhibits a relatively prolonged half-life of 64 hours in blood following a single dose and maintains its full C5aR1 inhibitory efficacy for at least 24 hours (Bekker *et al.*, 2016; Li *et al.*, 2020b). Comparative analysis revealed that Avacopan demonstrates higher potency than PMX205, particularly in its ability to inhibit C5aR1-mediated MAPK signalling, and has a significantly longer half-life than five other C5aR1 antagonists assessed (Li *et al.*, 2020b). Our group has also previously reported higher efficacy of Avacopan targeting C5aR1 compared to PMX205, especially under severe hypoxia where there was reported upregulation of intracellular C5aR1 that serves a crucial pro-survival role (Suwa *et al.*, 2025).

However, an important limitation of Avacopan is its reduced efficacy in murine C5aR1, due to species-specific differences in C5aR1 structure (Liu *et al.*, 2018; Waters *et al.*, 2005). Avacopan exhibits high affinity for human C5aR1 but binds poorly to the murine homolog, limiting its translational application in preclinical non-humanised mouse studies. This differential bindings is linked to variation at TM5, particularly the substitution of tryptophan (Trp213) in human C5aR1 with leucine in mouse and rat orthologs, which compromises the activity of allosteric small-molecule antagonists, including Avacopan (Liu *et al.*, 2018; Waters *et al.*, 2005).

Structurally, PMX205 and Avacopan interact with distinct binding domains on C5aR1. PMX205 binds to the orthosteric site of C5aR1 located at ECL2, allowing it to function as an effective peptide antagonists in both human and murine C5aR1 (Liu *et al.*, 2018). In contrast, Avacopan binds to an allosteric pocket which is an extra-helical region formed by residues spanning TM3, TM4 and TM5, without interacting with the extracellular N-terminal domain where C5a predominantly binds (Liu *et al.*, 2018). By binding to this allosteric site, Avacopan stabilises C5aR1 in an inactive conformation, allosterically suppressing the receptor's capacity to undergo the conformational changes required for G-protein coupling and signal transduction. The mechanism of Avacopan is distinct from the competitive inhibition exhibited by PMX205, as summarised in Figure 1.13, and these different modes of action potentially influence their respective pharmacodynamics and efficacy.

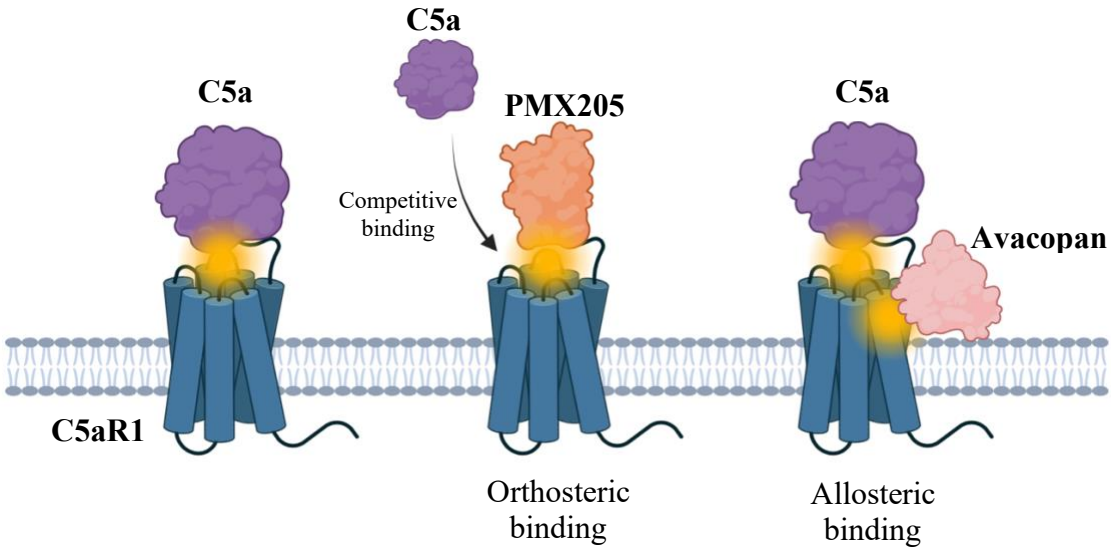

Figure 1.13 Graphical representation of C5, PMX205 and Avacopan binding to C5aR1

(Left) Binding of C5a ligand to C5aR1, the yellow area represents the binding site. (Middle) PMX205 binds to the same orthosteric sit as C5a. *(Right)* Avacopan binds to an allosteric site of C5aR1.

Aim

Emerging evidence suggests that the complement system, particularly the C5-C5aR1 signalling axis, contributes to tumorigenesis by promoting tumour invasion and therapy resistance in GBM (Li *et al.*, 2021; Lim *et al.*, 2020; Meng *et al.*, 2019). Previous work from our group demonstrated that pharmacological inhibition of C5aR1 with PMX205 enhanced the efficacy of radiotherapy in colorectal cancer, even within an immunosuppressive TME (Beach *et al.*, 2023). Given the immunosuppressive nature of HGG, we hypothesised that targeting C5aR1 could enhance radiosensitivity in DMG and GBM, potentially through attenuation of canonical pro-survival signalling pathways downstream of C5aR1 activation. To better reflect the radioresistant glioma milieu, hypoxic conditions were incorporated into our experimental models to assess the efficacy of C5aR1 inhibition under mor physiologically relevant conditions. Additionally, the abundance of C5aR1-expressing microglia within the HGG microenvironment prompted us to investigate the dynamic interactions between microglia and glioma cells, and to elucidate the broader impact of C5-C5aR1 blockade within the HGG TME.

Chapter 2 Materials and Methods

2.1 Materials

2.1.1 General laboratory and cell culture materials

Cell culture media were supplied by Sigma-Aldrich and Applied Biological Materials. All cell culture plasticware were supplied by Costar and Sarstedt. Additional reagents used are described in Table 2.1.

Table 2.1 Chemicals and cell culture reagents

Name	Supplier
Ampicillin	Thermo Scientific
Bovine serum albumin (BSA)	Sigma-Aldrich
Bromophenol blue	Sigma-Aldrich
Crystal violet	Sigma-Aldrich
Dimethyl sulfoxide (DMSO)	Sigma-Aldrich
Dulbecco's Modified Eagle's medium (DMEM)	Sigma-Aldrich
DMEM + GlutaMAX™ supplement	Gibco
Ethanol	Sigma-Aldrich
Foetal bovine serum (FBS)	Sigma-Aldrich
Glycine	Sigma-Aldrich
Human Serum	Sigma-Aldrich
Licor buffer (blocking buffer)	LI-COR
Luria-Bertani (LB) agar	Thermo Scientific
LB broth	Thermo Scientific
Lipofecatmine ™ 3000	Invitrogen
Lipofectamine® RNAiMAX	Invitrogen
Methanol	Sigma-Aldrich
Nuclease-free water	Invitrogen
Paraformaldehyde solution (PFA)	Thermo Scientific
Penicillin-Streptomycin	Thermo Scientific
Phosphate-buffered saline (PBS)	Invitrogen
PriGrow III medium	Applied Biological Materials
Prolong gold antifade reagents with DAPI	Invitrogen

Propan-2-ol (isopropanol)	Fisher Scientific
Propidium iodide	Invitrogen
PureLink RNAse A	Invitrogen
Roswell Park Memorial Institute (RPMI) 1640 Medium	Gibco
Sodium dodecyl sulfate (SDS)	Sigam-Aldrich
SYBR® green PCR master mix	Applied Biosystems
Thiazolyl blue tetrazolium bromide	Sigma-Aldrich
Tris base	Sigma-Aldrich
Tris hydrochloride (Tris-HCl)	Sigma-Aldrich
Tris-buffered saline (TBS)	Thermo Scientific
Tris-glycine buffer	BioRad
Trypan blue 0.4%	Invitrogen
Trypsin-EDTA	Sigma-Aldrich
Tween 20	Sigma-Aldrich
UltraPure™ Phenol:Chloroform:Isoamyl Alcohol	Thermo Scientific
Urea	Sigma-Aldrich
X-vivo 10 medium	Lonza
β-Mercaptoethanol	Sigma-Aldrich

2.1.2 Antibodies

Table 2.2 Antibodies used for Western blotting

Name	Species	Dilution	Supplier	Cat number
β-Actin	Mouse	1:1000	Cell Signaling	3700
APOE	Rabbit	1:1000	Invitrogen	701241
HIF-1α	Mouse	1:1000	BD Biosciences	610959
Histone H3	Rabbit	1:2000	Cell Signaling	9715
LC3B	Rabbit	1:1000	Cell Signaling	3868
NF-κB p65 (total RelA)	Rabbit	1:1000	Cell Signaling	8242
p44/42 MAPK (total ERK)	Mouse	1:1000	Cell Signaling	4696
p62	Mouse	1:1000	Cell Signaling	88588
Phospho-p44/42 MAPK (Thr202/Tyr204) (pERK)	Rabbit	1:500	Cell Signaling	9101
P-NF-kappaB p65 (S536) (pRelA)	Rabbit	1:500	Cell Signaling	3033

Table 2.3 Antibodies used for flow cytometry

Name	Species	Dilution	Supplier	Cat number
CD88	Mouse	1:20	BD Biosciences	742315
IgG1, k Isotype Control	Mouse	1:20	BD Biosciences	610959

Table 2.4 Secondary antibodies used for Western blotting

Name	Dilution	Supplier	Cat number
IRDye® 680RD Goat anti-Rabbit IgG	1:10000	LI-COR	926-68071
IRDye® 800CW Donkey anti-Mouse IgG	1:10000	LI-COR	926-32212

2.1.3 Primers

Table 2.5 Human primers used for quantitative polymerase chain reaction (qPCR)

Target gene	Forward sequence	Reverse sequence
18S	GTGGAGCGATTTGTCTGGTT	ACGCTGAGCCAGTCAGTGTA
ACTB	ACATCCGCAAAGACCTCTAC G	TTGCTGATCCACATCTGCTGG
APOE	CAGCAGACCGAGTGGCAGAG	TCCATCAGCGCCCTCAGTTC
ARG1	TTCTCAAAGGGACAGCCACG AG	AGCAAAGGGCAGGTCCCCATA
ATF4	GGAGATAGGAAGCCAGACTA CA	GGCTCATACAGATGCCACTATC
ATF6	CAGACAGTACCAACGCTTAT GCC	GCAGAACTCCAGGTGCTTGAAG
C5	CTCCTCAGGCCATGTTCATT	TCTTTTGGCTGGCTTCAAGT
C5aR1	TCCTTCAATTATACCACCCCT GA	ACGCAGCGTGTTAGAAGTTTTAT
CAIX	CTTGGAAGAAATCGCTGAGG	TGGAAGTAGCGGCTGAAGTC

CCL2	TGAAGCTCGCACTCTCGCCT	TGGGGCATTGATTGATTGCATCTGGC
CD11b	TTCCTTGTGGTTCCTCAGTG	GACATAAGGTCAAGGCTGTT
CD163	GGAGTTGCCCTTTCTACCCC	TTGGGACTGGTTTCCTGAGC
CD206	GCCCGGAGTCAGATCACACA	AGTGGCTCAACCCGATATGACAG
CD40	TATGGTTCGTCTGCCTCTGC	ACCAGTTTCTGTCCTGGCTG
CD80	GCTGCCTGACCTACTGCTTT	GCAAATGGAGGTGGGACCTT
CD86	AGCACAGACACACGGATGAG	AGAGGAGCAGCACCAGAGAG
CHOP	GGGAGCTGGAAGCCTGGTA	CCCCCATTTTCATCTGAAGACA
IBA1	AGAGGTGTCCAGTGGCTCCG	GGGGGCCTGTTGGCTTTTCC
IL1β	CCAGGGACAGGATATGGAGCA	TTCAACACGCAGGACAGGTACAG
IL4	CCTTCTGCAGGGCTGCGACT	TCCTTCACAGGACAGGAATTCAAGC
IL6	TGTGCCTGCAGCTTCGTCAG	CAAGCCAGAGCTGTGCACATCA
IL10	GAGATGCCTTCAGCAGAGTGAAGA	AGGCTTGGCAACCCAGGTAAC
iNOS	CCCCGTGTTTCACCAGGAG	GGCAAAGAGCACAGCTTTGACCA
TGFβ	ATTCCTGGCGATACCTCAGC	CCCTCAATTTCCCCTCCACG
TNF	TGTAGCCCATGTTGTACAAACCC	GCCCTTGAAGAGGACCTGGA
XBP1	TGCTGAGTCCGCAGCAGGTG	GCTGGCAGGCTCTGGGGAAG

Table 2.6 Mouse primers used for qPCR

Target gene	Forward sequence	Reverse sequence
18S	GTGGAGCGATTTGTCTGGTT	ACGCTGAGCCAGTCAGTGTA
ACTB	CCACTGTCGAGTCGCGTCCA	TCATCCATGGCGAACTGGTGG
ARG1	ACATTGGCTTGCGAGACGTA	TCGGCCTTTTCTTCCTTCCC
C5	TACCAATGCCAACCTGGTGAA AGG	TCTGCAGAACCTCTTTGCCCA TGA
C5aR1	ACATGGACCCCATAGATAAC	ACCACCGAGTAGATGATAAG
CCL2	AGCTCTCTCTTCCTCCACCA	GGGCGTTAACTGCATCTGG
CD11b	GTCCTTTGGGAACCTCCGAC	ACCAAAGTGTCCAAGCCCAT
CD163	GGCTAGACGAAGTCATCTGCA C	CTTCGTTGGTCAGCCTCAGAG A
CD206	GCCCACACCTGCTCCACAAG	TCGCGCGTTGTCCATGGTTT
CD40	ACCAGCAAGGATTGCGAGGCA T	GGATGACAGACGGTATCAGTG G
CD80	CACCTGGGAAAAACCCCCA	GCCCGAAGGTAAGGCTGTT
CD86	CTGCTGTGCTTGTGTGTGTG	CTCCACGGAAACAGCATCTGA
GLUT 1	AAACATGGAACCACCGCTAC	GAGAAGCCCATAAGCACAGC
IBA1	TCTGCCGTCCAAACTTGAAGCC	CTCTTCAGCTCTAGGTGGGTC T
IL1β	GCAGGCAGTATCACTCATTGTG G	GAGTCACAGAGGATGGGCTCT TC

IL4	ATCATCGGCATTTTGAACGAGG TC	ACCTTGGAAGCCCTACAGACG A
IL6	CTCTGGGAAATCGTGGAAAT	CCAGTTTGGTAGCATCCATC
IL10	CAGTACAGCCGGGAAGACAA	TGGCAACCCAAGTAACCCTTA
iNOS	GAGCCACAGTCCTCTTTGCT	CCATGCAGACAACCTTGGTG
TGFb	TGATACGCCTGAGTGGCTGTCT	CACAAGAGCAGTGAGCGCTG AA
TNF	ATGGCCTCCCTCTCATCAGT	CTTGGTGGTTTGCTACGACG

2.1.4 Ribonucleic acid (RNA) interference

All small interfering RNA (siRNA) were purchased from Dharmacon. A list of siRNA used for transfection is detailed in Table 2.7.

Table 2.7 siRNA used for transfection

Target gene	Cat number
ATF4	L-005125-00
ATF6	L-009917-00
C5aR1 (human)	L-005442-00
C5aR1 (mouse)	L-043176-00
Non-targeting control (scramble)	D-001810-10
XBP1	L-009552-00

2.2 Methods

2.2.1 Cell culture

Human DMG cell line SF8628 and mouse microglia cells IMG were kindly given by Dr Kristoffer Petersson (Oxford, UK). Human GBM cells LN229, A172, H4 and U-118 MG were kindly given by Prof Vincenzo D'Angiolella (Oxford, UK). Mouse microglia-like cells hSV40 and mouse microglia BV2 were kindly provided by Dr Katarzyna Leszczynska and Prof Bozena Kaminska (Nencki Institute of Experimental Biology, Poland).

All cells except hSV40 and BV2 were cultured in DMEM supplemented with 10% heat-inactivated FBS treated at 55 degrees Celsius (^{0}C) for 30 minutes and 1% 10000 U/mL Penicillin-Streptomycin. Cells were incubated in a standard humidified incubator at 37^{0}C and 5% CO_2. hSV40 cells were cultured in PriGrow III medium supplemented with 10% heat-inactivated FBS and 1% Penicillin-Streptomycin. BV2 cells were cultured in DMEM supplemented with GlutaMAX, 2% heat-inactivated FBS and 1% Penicillin-Streptomycin.

Regular passaging of cells involved removal of culture medium, washing with PBS, followed by addition of 0.25% trypsin-EDTA. Trypsin was then immediately removed, and cells were incubated at 37^{0}C for 5 minutes before the inactivation of trypsin by adding pre-warmed fresh media. Cell density was determined using the Countess automated cell counter (Invitrogen) by mixing 10 µL cell suspension with 10 µL trypan blue. The desired cell numbers were seeded in fresh media for all experiments.

All cells were routinely tested for mycoplasma contamination using the MycoAlert® mycoplasma detection kit (Lonza, #LT-703). In brief, culture medium of

cells at 70% confluence was collected and spun down. 100 µL of the cell supernatant was transferred to a 96-well plate, together with positive control, MycoAlert® assay control set (Lonza, #LT-518). 100 µL of the MycoAlert® reagent was added to the cell supernatant and luminescence was measured on the POLARstar plate reader (BMG Labtech) after 5 minutes incubation, this measurement was referred as reading A. 100 µL MycoAlert® substrate was then added to the above mixture which lysed viable mycoplasma, and mycoplasmic enzymes would react with the substrate to catalyse ATP production. Luminescence was measured again after 10 minutes incubation, which was referred as reading B. Value of reading B divided by value of reading A was calculated to determine the ratio, and a ratio of >1.2 indicated presence of mycoplasma.

2.2.1.1 Spheroids

LN229 cells at 70% confluency were trypsinised and resuspended in fresh media. After determination of cell density, 3000 – 7000 cells were seeded in ultra-low attachment U-bottom plates (Grenier Bio-One) and grown until at least 350 µm in diameter, which was confirmed with a GelCount Colony Counter (Oxford Optronix).

2.2.1.2 Peripheral mononuclear blood cell (PBMC)-derived MΦ

Blood was collected from healthy donors and was processed by Qingyang Zhang from our lab. Blood sample was centrifuged in SepMate™ tubes (STEMCELL Technologies) together with Ficoll (Cytiva) at 1200 gravity (g) for 10 minutes at room temperature (RT). PBMCs were collected from the top compartment of the SepMate™

tubes (STEMCELL Technologies) and washed in PBS supplemented with 2% FBS, followed by centrifugation at 900 g for 8 minutes at RT. Cell pellet was washed twice in PBS with FBS, then resuspended in RPMI medium supplemented with 10% FBS. With 15 mL tube flat on the surface, PBMCs were overlaid on top of Percoll Plus (46% Percoll (Sigma-Aldrich) + 5.4% FBS). After spinning at 950 g for 30 minutes at RT (acceleration=5), monocyte fraction was carefully collected and differentiated into MΦ by culturing in X-VIVO media supplemented with 2% human serum for four days.

2.2.1.3 Cryopreservation of cell lines

Cells at 70% confluency were trypsinised, resuspended in 5 mL fresh media and cell density was counted. After centrifuging at 250 g for 5 minutes at RT, supernatant was removed and cell pellet was resuspended in fresh media containing 10% FBS, 10% DMSO and 1% Penicillin-Streptomycin. Approximately 1 million cells were placed in each 1.5 mL cryovial (Corning), stored at -80^{0}C in a Mr. Frosty (Nalgene) containing isopropanol for 24 hours before being transferred to liquid nitrogen for long-term storage.

When cells were recovered from liquid nitrogen, they were thawed quickly in a 37^{0}C water bath and transferred to 5 mL pre-warmed fresh media. Cell suspension was centrifuged at 400 g for 5 minutes at RT, supernatant was discarded and cell pellet was resuspended in 5 mL fresh media and transferred to a 25 cm^2 flask.

2.2.2 Drug treatments

HIF inducer $CoCl_2$ (Sigma-Aldrich, #15862) was used at concentration of 200 μM for 16 or 24 hours as indicated. UPR inducers Tunicamycin (Tuni) (Sigma-Aldrich, #T7765) and Thapsigargin (Thap) (Thermo Scientific, #T7458) were used at concentrations of 10μg/mL and 3 μM respectively for 16 or 24 hours. C5aR1 inhibitor PMX205 (Tocris, #5196) was used at a concentration of 12 μM, unless specified otherwise for the indicated time periods. Avacopan (Cayman Chemical, #CAY36639) was used at a concentration of 2 μM in LN229, A172, H4 and hSV40 cells, 4 μM in SF8628 cells for indicated time periods. Lipopolysaccharide (LPS) (InvivoGen, #tlrl-eklps) was used at a concentration of 100 ng/mL for 24 hours.

Human C5a proteins was purchased from Quidel (#A420) and recombinant C5a proteins were kindly given by Dr. Jimmy Xi (Standford University, US), used at the indicated concentrations for 2 hours in serum-free media, unless specified otherwise. Recombinant IL-1β (Sino Biologicals, #10139-HNAE) was used at 1 ng/mL or 10 ng/mL for 16 hours unless specified otherwise.

2.2.3 small interfering RNA (siRNA) transfection

Cells at 70% confluency were plated in a 6-well plate and incubated overnight. On the day of transfection, using the Lipofectamine® RNAiMAX kit, two solutions were prepared according to the manufacturer's protocol:

Tube 1: 9 µL Lipofectamine® RNAiMAX + 150 µL serum-free media for each well

Tube 2: 9 µL siRNA (30µM) + 150 µL serum-free media per well

Diluted siRNA was mixed with diluted lipofecatime in 1:1 ratio and incubated at room temperature (RT) for 5 minutes before added to the cells. Cells were transfected and incubated for 72 hours in total, with addition of 1 mL fresh media the day after transfection.

2.2.4 DNA Transfection

C5AR1_OHu107216C_pcDNA3.1(+)-C-eGFP (pcDNA3.1/C5aR1-GFP), RelA _OHu26911D_pcDNA3.1+C-(K)-DYK and empty vector plasmids were purchased from GenScript. Cells at 70% confluency were plated at a density of 7 x 10^5 in a 6cm dish the day before transfection. On the day of transection, Lipofectamine 3000 was used according to manufacturer's instructions, and cells were cultured in serum-free media for one night, before having plasmid-containing media replaced with fresh FBS-supplemented media. Transfected cells were harvested, irradiated, or exposed to hypoxia or irradiation treatment 48 hours post-transfection.

2.2.5 Exposure to γ-irradiation

All irradiations were carried out using Gamma Service GSR D1 irradiator installed with Cs-137 sources. Samples were placed on the first shelf and exposure times for desired dose (1-9 Gy) were calculated according to calibration.

2.2.6 Hypoxia treatment

Anoxia treatment was carried out using a Bactron II anaerobic chamber. Theoretically, no oxygen is supplied to the chamber, but a complete absence of oxygen is not guaranteed at all times due to potential leaks, oxygen level for experiments carried out in the Bactron were referred to as <0.1% O_2 in this study. Except for clonogenic studies where plastic 6-well plates were used, cells for all anoxic experiments were seeded on glass dishes (DWK Life Sciences) to minimise introduction of oxygen into chamber due to the oxygen-absorbing properties of plastics. Experiments at 1% O_2 were carried out in the Don Whitley M35 chamber, with oxygen levels routinely calibrated. For all hypoxia experiments, cells were harvested inside the chamber with equilibrated solutions, unless specified.

For treatments involving irradiation, cells were transferred directly from the hypoxia chamber into sealed, airtight irradiation boxes, remaining under hypoxia throughout the irradiation process. Irradiation boxes were kept in anaerobic pass box of the hypoxia chamber the night before to remove oxygen. Once irradiated, cells were returned back to 21% incubator.

2.3 Protein Analysis

2.3.1 Protein preparation

Cells at 70% confluency were seeded at density of 5 x 10^5 in each 6 cm dish. After treatment, culture media was collected, and cells were washed in PBS. 500 µL trypsin-EDTA was added into each dish and incubated at 37^0C for 5 minutes. Trypsin solution was pipetted up and down to flush the well and added to the culture media collected. Alternatively, cell scraper (Sarstedt) was used to detach cells mechanically. A quick pop-spin at RT was performed to centrifuge the cell suspension. Supernatant was carefully removed and cell pellets were lysed in 20 µL UTB buffer (9M Urea, 75mM Tris-HCl pH 7.5, 0.1M β-mercaptoethanol). Samples were then sonicated for 20 seconds and centrifuged at 10,000 revolutions per minute (rpm) for 10 minutes at 4^0C. Supernatants were transferred to new tubes and 2 µL of the samples was used for protein quantification on the NanoDrop™ spectrophotometer (Thermo Fisher). UTB buffer used as blank when calibrating the spectrophotometer, protein absorbance was read at 300 nm.

2.3.2 SDS-PAGE

4-15% Mini-PROTEAN® TGX™ Precast Protein Gels were purchased from BioRad. The appropriate volumes of samples corresponding to typically 50 µg proteins were mixed with 5µL sample buffer (3.3% SDS, 6M Urea, 17mM Tris-HCl, 0.07M β-mercaptoethanol, 0.01% Bromophenol Blue) and heated to 95^0C for 5 minutes. To allow analysis of protein molecular weight, 2-7 µL protein ladder (Precision Plus Protein™ Kaleidoscope™, BioRad, #1610375) was loaded to one/two of the lanes, followed by

loading of protein samples. Gels were electrophoresed at 110V for one hour in Tris-Glycine running buffer (24mM Tris base, 192mM glycine, 0.1% SDS).

2.3.3 Western Blotting

Using Trans-Blot Turbo Transfer System (BioRad, #1704150), proteins were transferred onto nitrocellulose membranes (BioRad, #1610112) in transfer buffer (1x tris-glycine buffer, 20% methanol). Membranes were then blocked in Licor Intercept® buffer diluted 1:1 in TBS for one hour at RT. Membranes were probed with primary antibodies overnight at 4^0C on rocking platform. A full list of primary antibodies used can be found in Table 2.2. On the following day, membranes were washed in TBST (TBS + 0.1% tween 20) three times, five minutes each before being probed with secondary antibodies for one hour at RT whilst shaking. The membranes were then washed again three times in TBST before being visualised on Odyssey® Classic Imager (LI-COR).

2.4 DNA Plasmids

2.4.1 Preparation of LB-agar plates

Luria-Bertaani (LB)-agar plates were kindly provided by Prof. Ester Hammond (University of Oxford, UK). 35 grams of LB-agar (Thermo Scientific) was dissolved in 1 litre of deionised water. After sterilisation by autoclaving and cooling down, 100 μg/mL ampicillin was added. 25 mL of LB-agar was added to each 10 cm Petri dish next to a Bunsen burner, then set at RT and stored at 4^0C until needed.

2.4.2 Bacteria Transformation

DH5α competent cells purchased from Invitrogen were used to transform bacteria for plasmid production. DH5α cells were thawed on ice for 30 minutes before addition of 10 μg DNA, the mixture was then incubated on ice for 20 minutes, followed by heat-shock at 42^0C for 45 seconds. Immediately after heat-shocking, transformation reactions were incubated on ice for two minutes, then incubated for one hour at 37^0C in a shaking incubator. Transformation reactions were then spread on LB-agar plate and incubated at 37^0C overnight.

2.4.3 Bacteria expansion

Bacteria colonies grown on LB-agar plate were collected using a sterile inoculation loop (Corning), and expanded in a 2 litre flask containing 300 mL of LB broth at 37^0C for three days. LB-agar plate was sealed with parafilm and stored at 4^0C for future use.

2.4.4 Medium-scale preparation (Midi-prep) for plasmid DNA

Midi-prep of DNA was performed using the Plasmid Midi kit (Qiagen, #12143) as per manufacturer's instructions.

2.4.5 Determination of DNA concentration and purity

On the NanoDrop™ spectrophotometer, optical density at 260nm was measured to quantify the concentration of DNA. Nuclease-free water was used as blank. The ratio of absorbance at 260 nm:280 nm determined the purity of DNA, with a ratio of ≥1.8 indicating the DNA was free from protein contamination and therefore pure.

2.5 qPCR

2.5.1 RNA extraction and purification

For monolayer culture, subconfluent cells were plated. Following treatment, culture media was removed and cells were washed in PBS. 1 mL TRI reagent™ was added to the cells and pipetted up and down to flush the well, while introducing air bubbles to help shear DNA. Samples were either used immediately or stored at 4^0C until extraction. For spheroids, diameter of each spheroid was confirmed with GelCount Colony Counter just before harvesting. A total of 72 individual spheroids were collected, sorted according to their sizes and split into four size groups. Within each size group, six to seven spheroids were randomly selected, collected and harvested together using 1 mL TRI reagent™, this represented one biological replicate. All biological replicates within each size group were tested with no statistically significant differences in their sizes.

To harvest RNA, 200 µL chloroform was added per 1 mL cell suspension and shaken vigorously for 30 seconds, before 3 minutes incubation at RT. After that, samples were centrifuged at 12,000 g for 15 minutes at 4^0C, and the clear aqueous phase liquid was transferred to new tubes without disturbing the white intermediate or pink organic layer. 500 µL isopropanol was added prior to centrifugation at 12,000 rpm for 10 minutes at 4^0C. Then, supernatants were removed, pellets were resuspended in 1mL 75% ethanol and vortexed for a few seconds. Samples were centrifuged at 12,000 rpm for 5 minutes at 4^0C, supernatant was removed, and ethanol was added again to repeat the washing process. After centrifugation, any remaining ethanol was removed, pellets were left to air dry for 10-15 minutes, before being resuspended in 20 µL nuclease-free water and stored at -80^0C.

2.5.2 Determination of RNA concentration and purity

On the NanoDrop™ spectrophotometer, optical density at 260nm was measured to quantify the concentration of RNA. Nuclease-free water was used as blank. The ratio of absorbance at 260 nm:280 nm determined the purity of RNA, with a ratio of ≥1.6 indicating the RNA was free from protein contamination and therefore pure.

2.5.3 cDNA Synthesis

The appropriate volumes of samples corresponding to 1-2 µg RNA were added nuclease-free water to create final volumes of 10 µL solution. Verso cDNA Synthesis Kit (Thermo Scientific, #AB1453A) was used to reverse transcribe cDNA from total RNA. Samples were mixed with 10 µL cDNA reaction mix and heated up in a themocycler: 60 minutes at 42^0C for cDNA synthesis, 2 minutes at 95^0C for inactivation and cooled down at 4^0C. cDNA was diluted by adding 20-80 µL nuclease water and stored at 4^0C.

2.5.4 qPCR reaction

A reaction mix consisting of SYBR® Green PCR master mix, 10 µM primers and nuclease-free water was prepared according to Table 2.8. SYBR® Green PCR master mix contains 2x SYBR® Green 1x dye, AmpliTaq Gold™ DNA polymerase, deoxynucleoside triphosphate, with deoxyuridine triphosphate, passive reference 1 (ROX) and optimised buffer.

Table 2.8 Components of the reaction mix for qPCR

Reagent	Volume/well
Forward primer (10 µM)	1.25 µL
Reverse primer (10 µM)	1.25 µL
Nuclease-free water	1.25 µL
2x SYBR® Green PCR master mix	6.25 µL

In each well of a 96-well reaction plate, 10 µL of master mix and 2.5 µL diluted cDNA were added. qPCR reaction was carried out in StepOnePlus™ Real-Time PCR System (Applied Biosystems) with the following condition: 20 seconds at 50^0C, 15 minutes at 95^0C, followed by 40 cycles of 15 seconds at 95^0C, 30 seconds at 50^0C, 30 seconds at 72^0C, then a melt curve stage of 1 minute at 60^0C, 30 seconds at 95^0C and 15 seconds at 60^0C.

mRNA expression was analysed by normalising mRNA fold change to housekeep gene and calculated using the $2^{-\Delta\Delta Ct}$ method. Each biological repeat contains three technical replicates per sample.

2.6 Flow cytometry

For detection of C5aR1 proteins, $1x10^6$ cells were plated in 10 cm dishes and after incubation overnight, they were exposed to irradiation or hypoxia treatment. At the time of harvest, cells were washed in PBS and detached using a cell scraper. After a quick spin, cell pellets were fixed in 1 mL of 4% PFA for 10 minutes under normoxic or hypoxic condition. PFA was quickly removed by spinning and cells were washed in PBS twice. When measuring for intracellular proteins, cell membrane was permeabilised by incubating with 1 mL 100% methanol for 10 minutes on ice, before washing in PBS twice. Cells were then blocked in 200 µL 0.5% BSA for 10 minutes at room temperature. 0 CD88 and IgG1 antibody was added in 1:20 dilution and incubated for 30 minutes on ice in the dark. Samples were then analysed via flow cytometry. CD88-specific mean fluorescence intensity was calculated by subtracting geometric mean fluorescence intensity of IgG from CD88.

For cell cycle analysis, cells were trypsinised, washed in PBS and fixed in 1 mL 70% ethanol for 30 minutes on ice. After three PBS washes, with centrifugation at 250 g for 5 minutes at 4^0C, supernatant was carefully removed. 100 µg/mL PureLink RNase A was added directly to cell pellet, following by 50 µg/mL propidium iodide solution in PBS. After 10 minutes incubation at RT, cell cycle was analysed on flow cytometry.

All flow cytometry was performed using the Cytoflex (Beckman Coulter Inc.) Live cells were gated based on morphology forward scatter (FSC-H) vs forward scatter (SSC-H) and doublet cells were excluded using FSC-A vs FSC-H. Cells were selected using viability dye, at least 10000 events were recorded per condition using initial gating and data was analysed on FlowJo software (version 10.10.0, BD Biosciences).

2.7 Proliferation Assay

Subconfluent cells were seeded in 6-well plates at the indicated density. For siRNA treatment, cells were seeded after transfection. For drug treatment, PMX205, Avacopan or vehicle were added after seeding. Cells were trypsinised and counted using a haemocytometer every two days for the indicated time period, unless specified otherwise. Drugs were replenished after each trypsinisation.

2.8 Apoptosis Assay

Subconfluent cells were seeded and treated according to each specific experiment condition. Culture media containing dead cells was collected and cells were washed in PBS. Trypsin-EDTA was added into each well and incubated at 37^0C for 5 mins to detach cells, or alternatively, cell scraper was used. Cell suspension was added to the previously collected culture media and centrifuged at 250 g for 5 minutes. Supernatant was carefully removed, 200 µL of the cell pellets were transferred to new tubes and washed in 1mL PBS. Following that, cells were fixed in 200 µL 4% PFA solution for 10 minutes. Cells used in hypoxia experiments were taken out of the hypoxic chamber after fixation. Fixed cells were centrifuged at 250 g for 5 minutes, followed by PBS wall. 7 µL of cell pellet was mixed with 7 µL Prolong Gold Antifade Reagents with DAPI and mounted on slides, which were left to dry overnight in the dark at 4^0C. Slides were imaged under Eclipse Nikon Ni-E microscope using DAPI camera at 40x magnification with oil. Morphologies of at least 100 cells per condition were analysed using Image J software (version 1.54) to obtain an average percentage of apoptotic cells per biological replicate.

2.9 Cell Survival Assay – Clonogenics

100-15000 cells were plated per well on a 6-well plate depending on the cell line and radiation dose. Following treatment, cells were left to incubate undisturbed for 7-14 days. The cells were then gently washed in PBS and stained with 1mL crystal violet solution (2.5 g/L, 20% methanol). Plates were washed in water bath twice before being left to dry overnight. Stained colonies consisting of more than 50 cells were manually counted under CNW 325 010X colony counter (Gallenkamp) and survival fraction was calculated using the formula below:

$$Survival\ Fraction = \frac{No.of\ colonies\ formed}{No.of\ cells\ seeded \times plating\ efficiency\ of\ control} \times 100\%$$

Survival fractions for each radiation dose were plotted, the formula for the line of best fit was derived, with α representing the linear component and β representing the quadratic component. Survival curves were then plotted and extrapolated using the following linear quadratic model:

$$Survival\ Fraction = \exp((-\alpha \times \text{dose}) - (\beta \times dose^2))$$

2.10 Cell Viability Assay – MTT Assay

Cells at 70% confluency were seeded at density of 3000 – 8000 per well of a 96-well plate depending on cell line and treatment. 5mg/mL thiazolyl blue tetrazolium bromide (MTT reagent) was prepared by dissolving MTT powder in sterile PBS, followed by sonication and passing through a 0.22 μM filter (Santa Cruz Biotechnology). At the end of treatment timepoint, 10 μL of MTT reagent was added per 100 μL media and cells were incubated for 2 hours at 37^0C protected from light. Then, media containing MTT reagent were aspirated and replaced with 100 μL DMSO to solubilise crystals. Plates were incubated for 5 mins before absorbance values at 570 nm were measured on POLARstar plate reader.

2.11 Enzyme-linked immunosorbent assay (ELISA)

hSV40 cells at 70% confluency were seeded in 15 cm dishes at a density of 2 x 10^6 per dish. Just before treatment with 2 μM Avacopan, supplemented media was replaced with fresh serum-free media. Cells were irradiated 24 hours after addition of Avacopan, and culture media was collected 24 hours post-irradiation. Media was centrifuged at 250 g for 5 minutes at RT, supernatant was passed through a 0.22 μM filter to remove cells. Media was transferred to centrifugal concentrator tubes inserted with 3000 Dalton molecular cutoff filter which was pre-activated with deionised water (Merck, #UFC900308). After centrifugation at 3400 g for 45 minutes at RT, concentrated media was collected and used for ELISA immediately.

ELISA was carried out using the human IL-1β uncoated ELISA kit (Thermo Scientific, #88-7261-22) according to manufacturer's instruction. In brief, 96-well ELISA plate was coated with 100 μL capture anti-IL1β antibody (diluted in PBS) and incubated overnight at 4^0C. Next day, wells were washed in wash buffer (1x PBS, 0.05% Tween-20) three times with at least one minute soaking time, plate was blotted on absorbent paper to ensure removal of any residual buffer. 200 μL ELISA/ELISPOT diluent (in deionised water) was added to each well for one hour at RT for blocking. After washing with wash buffer twice, 100 μL of samples and standards were added to each well, and there were two technical replicates for each condition. For standards, 150 pg/mL IL-1β protein was reconstituted in deionised water, and two-fold serial dilutions were performed for a total of 7 concentrations, ELISA/ELISPOT diluent was added to one set of wells for blanking. Plate was sealed and incubated for two nights at 4^0C. After five washes with the wash buffer, 100 μL detection antibody was added to the wells and incubated for one hour at RT. Wells were washed again for five times, followed by

incubation with 100 μL Avidin-HRP concentrate (diluted in ELISA/ELISPOT diluent) for 30 minutes at RT. After seven washes with the wash buffer, 100 μL TMB solution was added to each well for 15 minutes incubation at RT, and lastly, 100 μL 1 M phosphoric acid was added as stop solution. Absorbance values at 450 nm were measured on POLARstar plate reader, and protein concentration of the unconcentrated sample was determined using the standard curve generated from measurements of the standards.

2.12 Analysis and Schematics

All statistical analysis and graphs were performed and plotted on Prism software (Version 10.4.2, GraphPad). A p value of ≤ 0.05 was considered statistically significant. Clonogenic survival curves were plotted on Microsoft Excel (Version 2408). Protein bands from Western blotting were quantified on LiCor Odyssey software. All schematics were created on biorender.com.

Chapter 3 C5aR1 inhibition under hypoxic stress

3.1 Introduction

Hypoxia is a key feature of the TME across many cancer types, including in HGG, where it is associated with tumour progression, therapeutic resistance and poor patient outcomes (Blandin *et al.*, 2019; Said *et al.*, 2007; Yeom *et al.*, 2015). Hypoxic stress alters multiple cellular programmes that promote adaptation and survival, often by engaging stress response pathways and pro-survival signalling cascades. Our group has previously demonstrated that expression of C5aR1 is regulated by ER stress in other cancer context (Suwa *et al.*, 2025). We therefore investigated whether hypoxia also modulates C5aR1 expression in HGG, and whether the changes in expression differ between GBM and DMG. Importantly, C5aR1, as a GPCR, is known to activate pro-survival pathways such as NF-κB and MAPK signalling (Beach *et al.*, 2023; Li *et al.*, 2020b; Schraufstatter *et al.*, 2009; Song *et al.*, 2018). We sought to determine whether C5a-C5aR1 signalling is required for glioma cell survival under hypoxic stress, and if genetic silencing and pharmacological inhibition of C5aR1 could compromise this adaptive advantage.

3.2 Results

3.2.1 Elevated C5aR1 expression in HGGs

First, we confirmed whether C5aR1 is expressed in HGGs. Analysis of The Cancer Genome Atlas (TCGA) database shows that there is higher C5aR1 expression in GBM compared to normal brain tissue, and it is associated with reduced overall patient survival (Figure 3.1A-B). Publicly available transcriptomic data on DMG is limited, however, RNA sequence data on a cohort of 221 paediatric HGG patients from our collaborator Prof Chris Jones (Institute of Cancer Research, UK) is available. As illustrated in Figure 3.1C, all paediatric high-grade tumours express elevated C5aR1 mRNA levels compared to healthy controls. Among all, H3.3K27M tumours express the highest level of C5aR1, which is the mutation found in majority of DMG cases. These findings support C5aR1 as a potential therapeutic target in both DMG and GBM, as targeting C5aR1 potentially have less direct impact on surrounding healthy tissues.

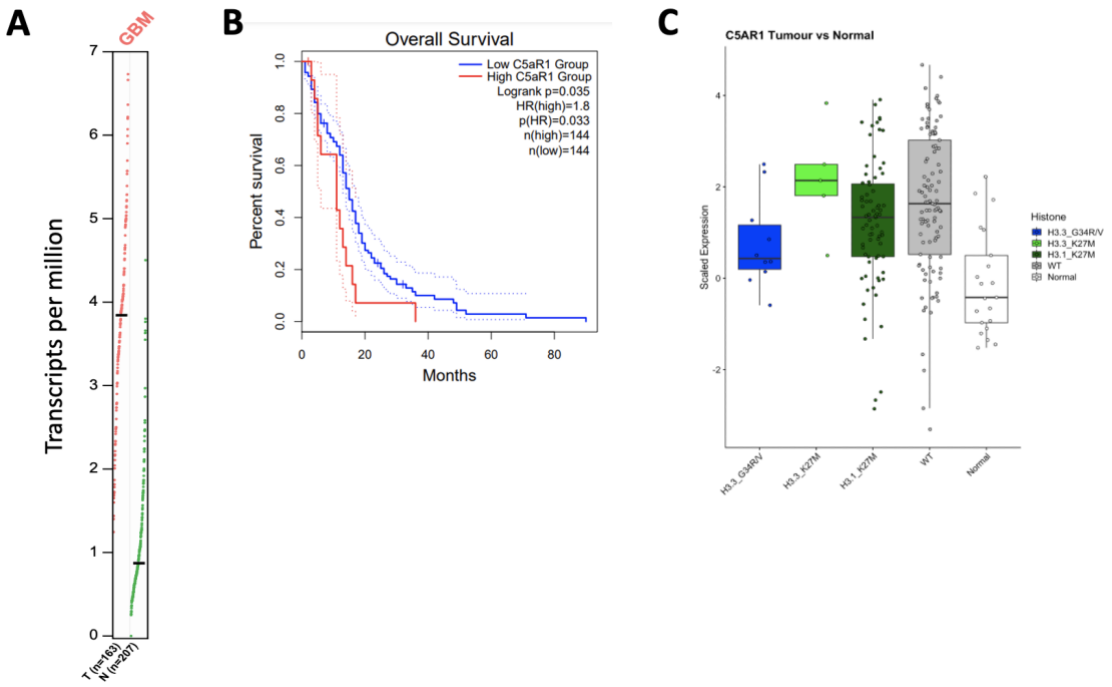

Figure 3.1 Elevated C5aR1 expression in HGGs

(A) Number of C5aR1 transcripts in GBM patient samples vs normal tissue. T=GBM tumour sample (n=163), n=normal tissue (n=207). Data obtained from TCGA database. (B) Survival curves of GBM patients with high and low C5aR1 expression. Data obtained from TCGA database. (C) C5aR1 mRNA expression of paediatric high-grade gliomas (H3.3_G34RV, H3.3_K27M, H3.1_K27M, WT) and normal tissue.

3.2.2 Upregulation of C5aR1 under severe hypoxia

We then questioned whether the upregulation of C5aR1 in HGG is driven by hypoxic conditions. Given that hypoxia can broadly promote and suppress transcription of a wide range of genes, we assessed the mRNA expression of C5aR1 and C5 (the gene encoding its ligand) following 16 hours exposure to three oxygen concentrations: 21% (normoxia), 1% (mild hypoxia) and <0.1% (severe hypoxia). The effectiveness of hypoxia treatment was validated by increased expression of CAIX, a downstream target of HIF-1α (Figure 3.2A, D). In both SF8628 and LN229 cell lines, exposure to <0.1% oxygen resulted in a 6 to 8-fold increase in C5aR1 mRNA expression, whereas no significant changes were observed under 1% (Figure 3.2B, E). However, severe hypoxia resulted in a significant reduction of C5 mRNA level only in SF8628, but not in LN229 cells (Figure 3.2C, F).

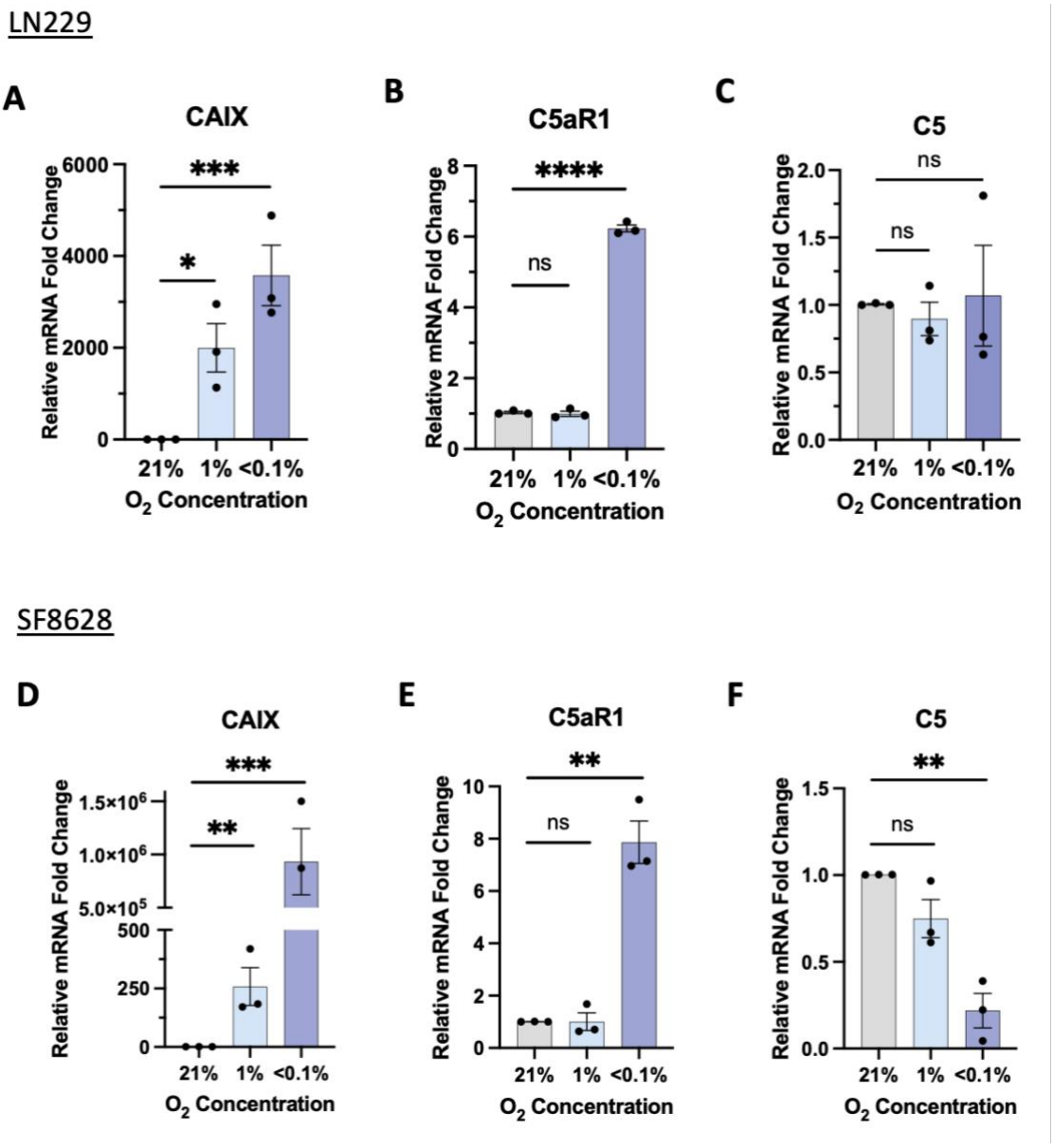

Figure 3.2 Upregulation of C5aR1 under severe hypoxia

mRNA expression of CAIX, C5aR1 and C5 were assessed by qPCR in **(A-C)** LN229 and **(D-F)** SF8628 cells following 16 h exposure to 21%, 1% or <0.1% O_2. All mRNA levels were normalised to 18S and expressed as fold change relative to the level of expression at 21%. Data presented as mean ± SEM of biological replicates. n=3. Statistical analysis was performed on unnormalised values using one-way ANOVA with Dunnett's test. *p≤0.05, *p≤0.01, ***p≤0.001.

To confirm whether the observed upregulation of C5aR1 mRNA under severe hypoxia is also reflected at the protein level, flow cytometry analyses were conducted. Although GPCRs are predominantly localised to the cell membrane, C5aR1 could also be expressed intracellularly (Ding *et al.*, 2020; Suwa *et al.*, 2025) . Therefore, our samples were permeabilised with methanol to enable detection of both cell surface and intracellular C5aR1 proteins. By permeabilising cell membrane, we were able to assess both cell surface and total (cell surface + intracellular) C5aR1 levels. In LN229 cells, exposure to severe hypoxic conditions (<0.1% O_2) led to an increase in total C5aR1 protein expression, consistent with the qPCR result (Figure 3.3A). Notably, this increase was restricted to intracellular C5aR1, as no upregulation of cell surface C5aR1 was detected. In contrast, SF8628 cells showed no significant changes in either cell surface or total C5aR1 protein levels, diverging from the earlier qPCR result (Figure 3.3B). This discrepancy suggests a potential post-transcriptional regulatory mechanism influencing C5aR1 expression in this cell line. To rule out the possibility that the mRNA-protein discrepancy being caused by delayed protein translation or accumulation, hypoxia exposure was extended to 24 hours. However, SF8628 continued to show no significant changes in C5aR1 protein expression (Figure 3.3C).

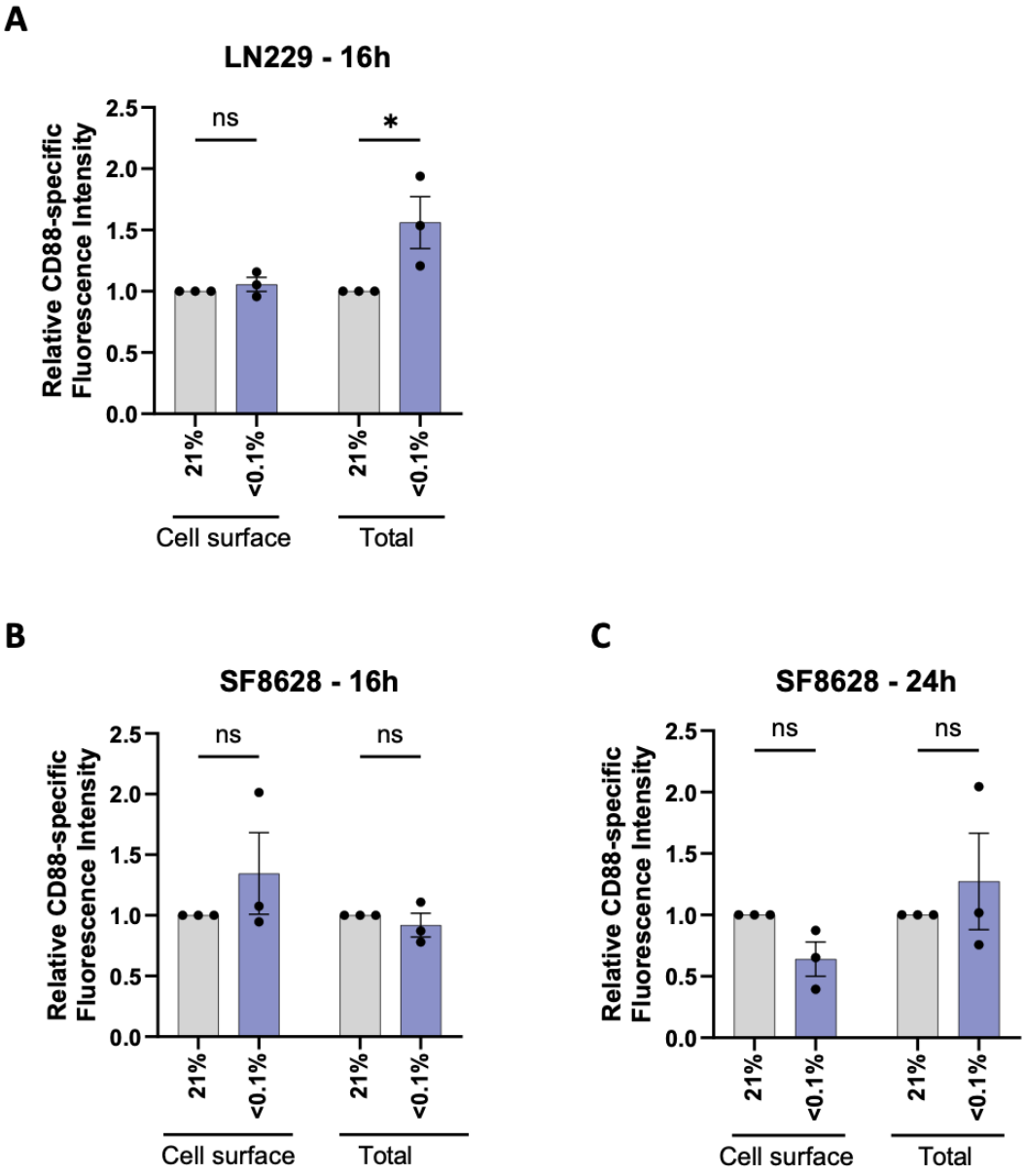

Figure 3.3 Hypoxia upregulates intracellular C5aR1 protein in LN229, but not SF8628

Cell surface and total protein expression of C5aR1 were assessed in **(A)** LN229 and **(B-C)** SF8628 cells via flow cytometry following 16 or 24 h exposure to 21% or <0.1% O_2. CD88-specific fluorescence intensity expressed as fold change relative to the fluorescence intensity at 21%. Data presented as mean ± SEM of biological replicates. n=3. Statistical analysis used two-way ANOVA with Šidák's test. *$p \leq 0.05$.

Our group has previously reported hypoxia-induced C5aR1 occurring in a UPR-dependent manner in colorectal cancer (Suwa *et al.*, 2025). Here, we decided to investigate the mechanisms underlying the upregulation of C5aR1 in HGG under severe hypoxia. Two major pathways we explored were HIFs and UPR activation, both with well-established role in regulating gene transcription under hypoxia. To dissect the potential contribution of these pathways individually, we used specific chemical inducers to activate each pathway independently. HIF signalling was induced by the addition of cobalt (II) chloride ($CoCl_2$), a pan-HIF activator, as evidenced by the upregulation of CAIX (Figure 3.4A). To activate UPR, we used Tunicamycin (Tuni) and Thapsigargin (Thap) which are ER stressors that trigger the UPR pathways via different mechanisms. Expression of two UPR downstream target genes, CHOP and XBP1, were used as controls to confirm pathway activation by Tuni and Thap and ensure coverage of all three UPR branches (Figure 3.4B-C).

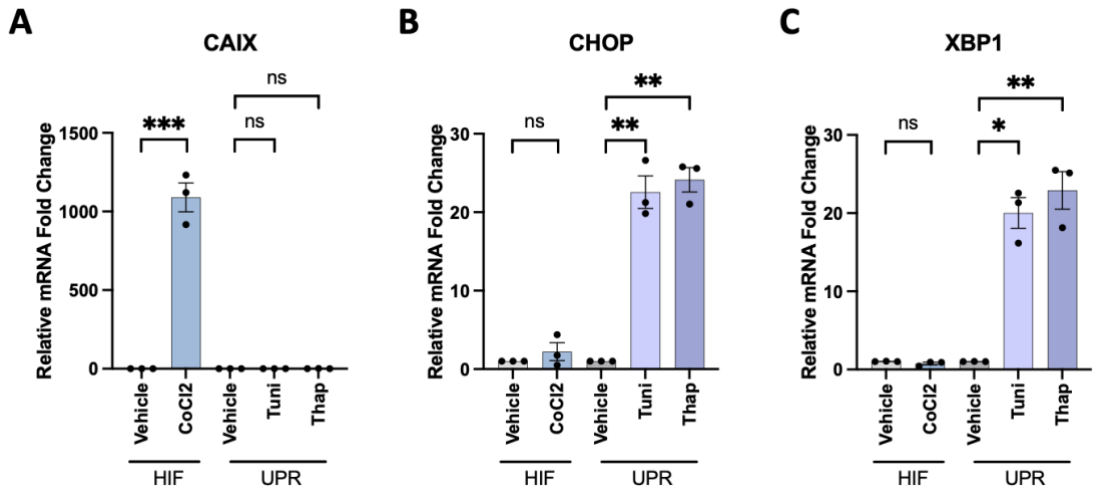

Figure 3.4 Validation of HIF and UPR inducers

mRNA expression of **(A)** CAIX, **(B)** CHOP and **(C)** XBP1 were assessed by qPCR in LN229 cells following 16 h treatment with vehicle (water or DMSO), $CoCl_2$, Tuni or Thap. All mRNA levels were normalised to 18S and expressed as fold change relative to the level of expression of vehicle-treated cells. Data presented as mean ± SEM of biological replicates. n=3. Statistical analysis was performed on unnormalised values using one-way ANOVA with Šidák's test. *p≤0.05, **p≤0.01, ***p≤0.001.

Given the differential regulation of C5aR1 protein levels observed between LN229 and SF8628 cells, we first focused on further characterising the underlying mechanisms in the GBM cell line LN229. Both mRNA and protein expression levels of C5aR1 were studied following stimulation with HIF and UPR inducers. Our data demonstrate that HIF activation alone did not alter C5aR1 mRNA or protein expression in LN229 cells, in line with the lack of induction at 1% O_2 which is the level at which HIF would be most active (Figure 3.5A-C). In contrast, activation of the UPR resulted in C5aR1 upregulation. Both Tuni and Thap treatment led to a significant increase in C5aR1 mRNA and protein levels, consistent with our previous study (Suwa *et al.*, 2025). Notably, as previously observed under severe hypoxia, this C5aR1 protein induction was limited to the intracellular level and no increase in cell surface C5aR1 expression was detected following UPR activation.

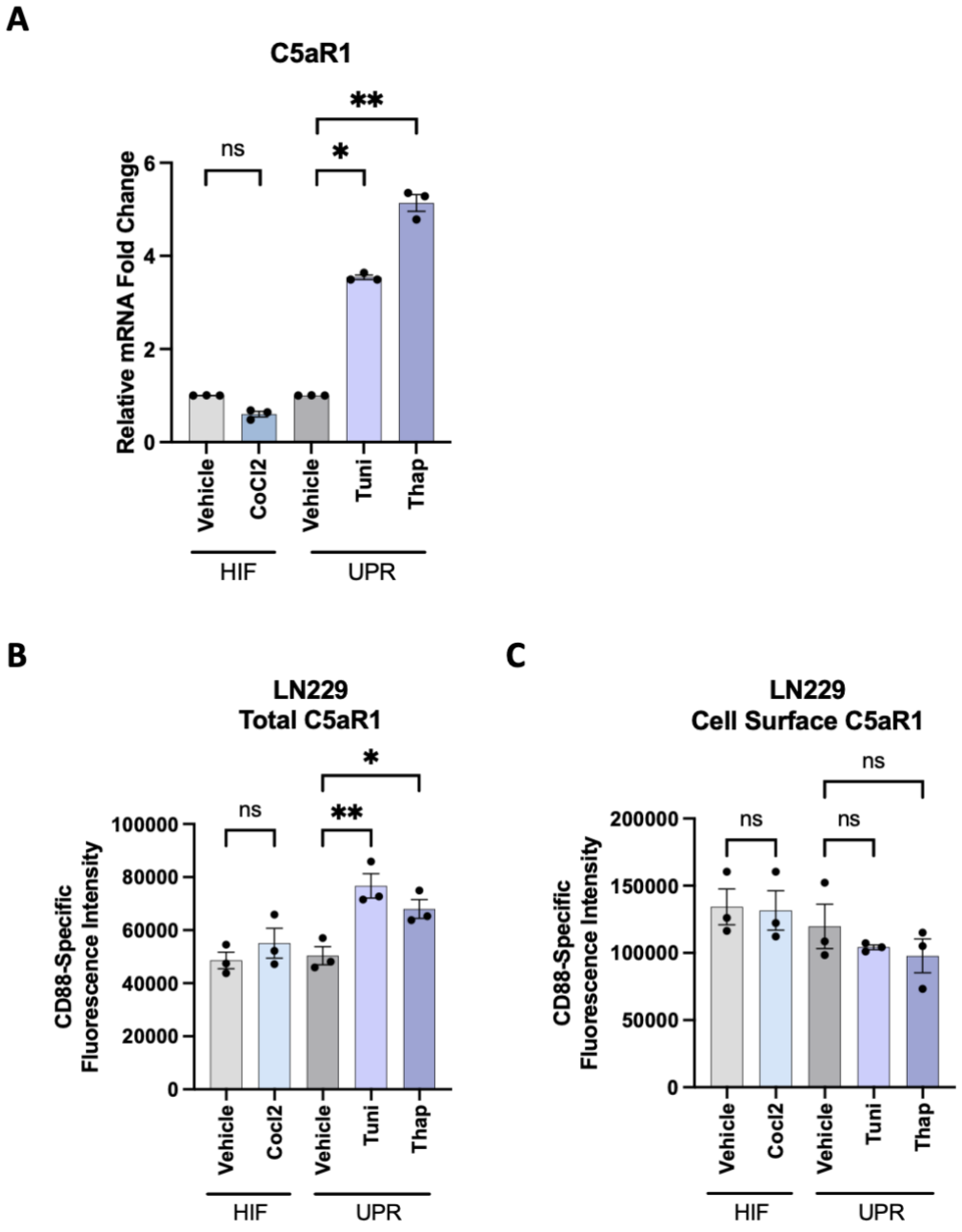

Figure 3.5 Hypoxia-induced C5aR1 upregulation is UPR-dependent

LN229 cells were treated with vehicle (water, DMSO), CoCl2, Tuni or Thap.

(A) mRNA expression of C5aR1 was assessed by qPCR in LN229 cells following 16 h treatment. All mRNA levels were normalised to 18S and expressed as fold change relative to the level of expression of vehicle-treated cells. Data presented as mean ± SEM of biological replicates. n=3. Statistical analysis was performed on unnormalised values using one-way ANOVA with Šidák's test. *p≤0.05, **p≤0.01.

(B) Protein expression of C5aR1 were assessed via flow cytometry following 24 h treatment with HIF and UPR inducers. Data presented as mean ± SEM of biological replicates. n=3. Statistical analysis used one-way ANOVA with Šidák's test. *p≤0.05, **p≤0.01.

To further confirm the involvement of UPR activation in upregulating C5aR1, we examined the effects of silencing XBP1, ATF4 and ATF6, which are major downstream transcription factors representing the three branches of the UPR pathway. Our previous study showed that knockdown of any single UPR component was insufficient to suppress C5aR1 upregulation under hypoxia (Suwa *et al.*, 2025). Therefore, to achieve comprehensive inhibition of the UPR activation, we concurrently silenced XBP1, ATF4 and ATF6 in LN229 cells by using triple knockdown (KD) si-Mixture (Figure 3.6A-C). Under the lack of UPR activation, C5aR1 upregulation in response to severe hypoxia was abrogated, indicating that complementary activity of all three UPR pathway is required to induce C5aR1 upregulation under severe hypoxia (Figure 3.6D).

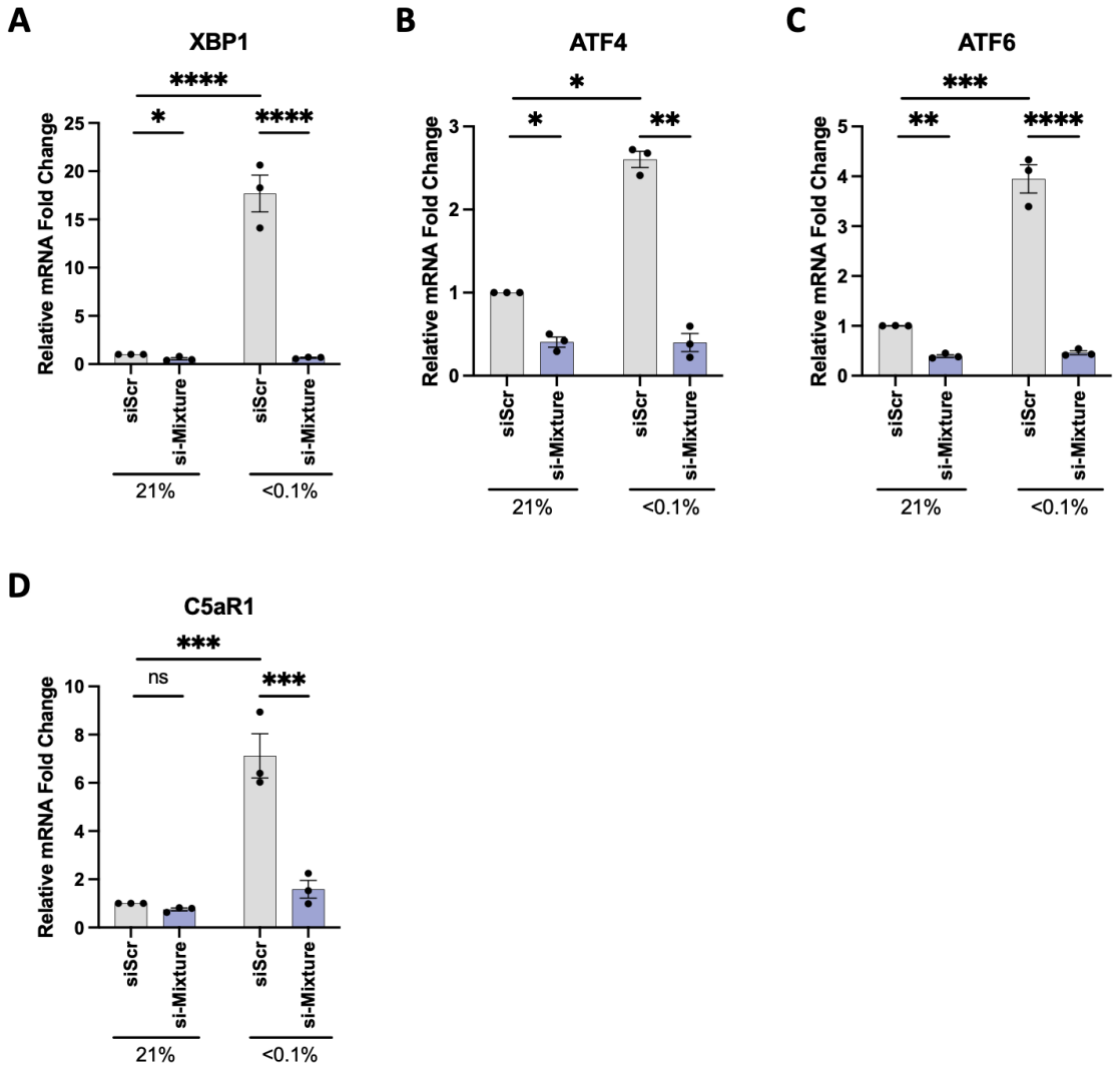

Figure 3.6 Triple knockdown of XBP1, ATF4 and ATF6 abrogates C5aR1 induction under severe hypoxia

LN229 cells were transfected with siScr or si-Mixture (XBP1, ATF4, ATF6) siRNA and exposed to 21% or <0.1% O_2 for 16 h. mRNA expression of **(A)** XBP1, **(B)** ATF4, **(C)** ATF6 and **(D)** C5aR1 were assessed by qPCR. All mRNA levels were normalised to 18S and expressed as fold change relative to the level of expression of 21% siScr. Data presented as mean ± SEM of biological replicates. n=3. Statistical analysis was performed on unnormalised values using two-way ANOVA with Fisher's LSD test. *p≤0.05, **p≤0.01, ***p≤0.001, ****p≤0.0001.

Having established that UPR activation induces C5aR1 expression in LN229 cells, we next tested whether a similar mechanism operates in the DMG cell line SF8628, which previously showed increased mRNA expression, but no protein expression changes in C5aR1 under hypoxia. SF8628 cells were initially treated with HIF and UPR inducers for 16 hours. Although successful activation of HIF and UPR pathways were confirmed, as shown in Figure 3.7A-C, C5aR1 mRNA levels remained unchanged compared to vehicle-treated controls (Figure 3.8A). To minimize the possibility of delayed C5aR1 transcription, the duration of treatment was extended to 24 hours. Under this condition, a modest increase in C5aR1 mRNA was observed; however, this change did not reach statistical significance due to considerable variability between replicates (Figure 3.8B). Therefore, we acknowledge that UPR-induced C5aR1 upregulation differ between our GBM and DMG models.

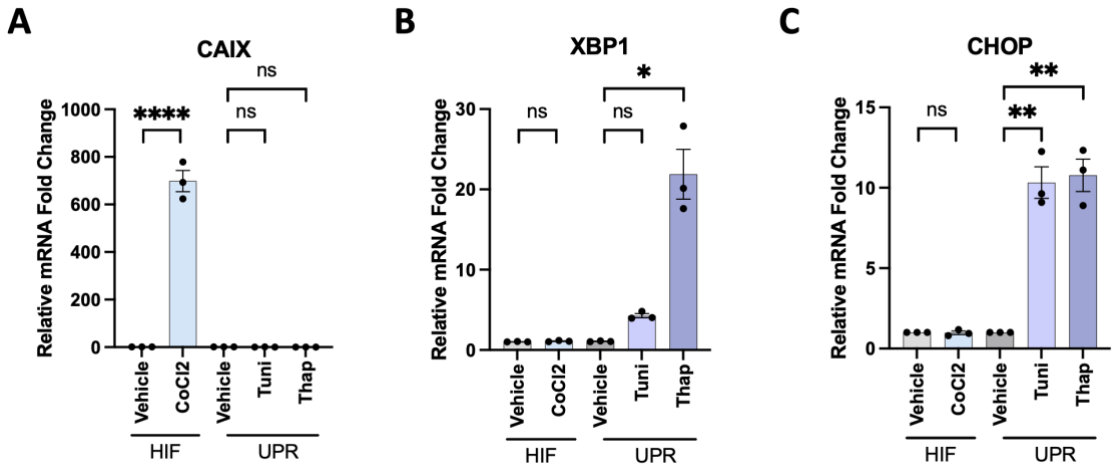

Figure 3.7 Induction of HIF and UPR in SF8628

mRNA expression of **(A)** CAIX, **(B)** CHOP and **(C)** XBP1 were assessed by qPCR in SF8628 cells following 16 h treatment with vehicle (water or DMSO), $CoCl_2$, Tuni or Thap. All mRNA levels were normalised to 18S and expressed as fold change relative to the level of expression of vehicle-treated cells. Data presented as mean ± SEM of biological replicates. n=3. Statistical analysis was performed on unnormalised values using one-way ANOVA with Šidák's test. *p≤0.05, **p≤0.01, ****p≤0.0001.

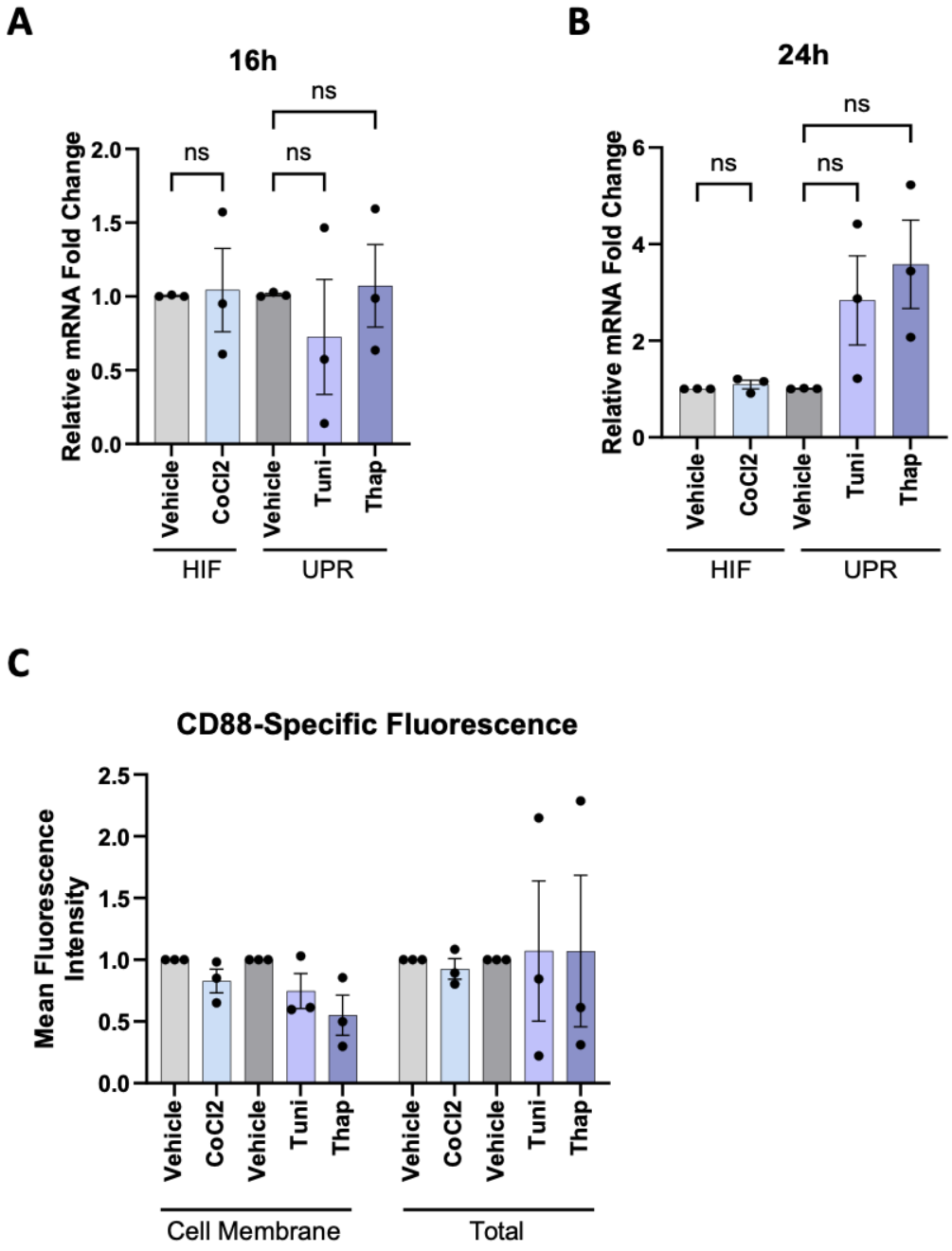

Figure 3.8 UPR activation does not upregulate C5aR1 in SF8628

(A-B) mRNA expression of C5aR1 were assessed by qPCR in SF8628 cells following 16 h and 24 h treatment with vehicle (water or DMSO), $CoCl_2$, Tuni or Thap. All mRNA levels were normalised to 18S and expressed as fold change relative to the level of expression of vehicle-treated cells. Data presented as mean ± SEM of biological replicates. n=3. Statistical analysis was performed on unnormalised values using one-way ANOVA with Šidák's test.

(C) Protein expression of C5aR1 were assessed via flow cytometry following 24 h treatment with HIF and UPR inducers. Fluorescence Intensities normalised to the intensity of vehicle-treated cells. Data presented as mean ± SEM of biological replicates. n=3.

Given the differential UPR responses observed between SF8628 and LN229 affecting their corresponding effects on C5aR1 expression, we further examined this relationship across a panel of HGG (SF8628, LN229, H4, A172, U118-MG) and microglia cell lines (hSV40, BV2, IMG). Cells were treated with the same concentration of Thap for the same duration of time, and mRNA expression levels of C5aR1 and the UPR marker XBP1 were measured. Across the panel, we observed a strong positive correlation between Thap-induced XBP1 induction and the corresponding upregulation of C5aR1 mRNA expression ($R^2 = 0.8069$) (Figure 3.9). These results further supported our earlier findings, suggesting the magnitude of UPR activation is one of the key determinants of C5aR1 transcriptional upregulation in HGG cells.

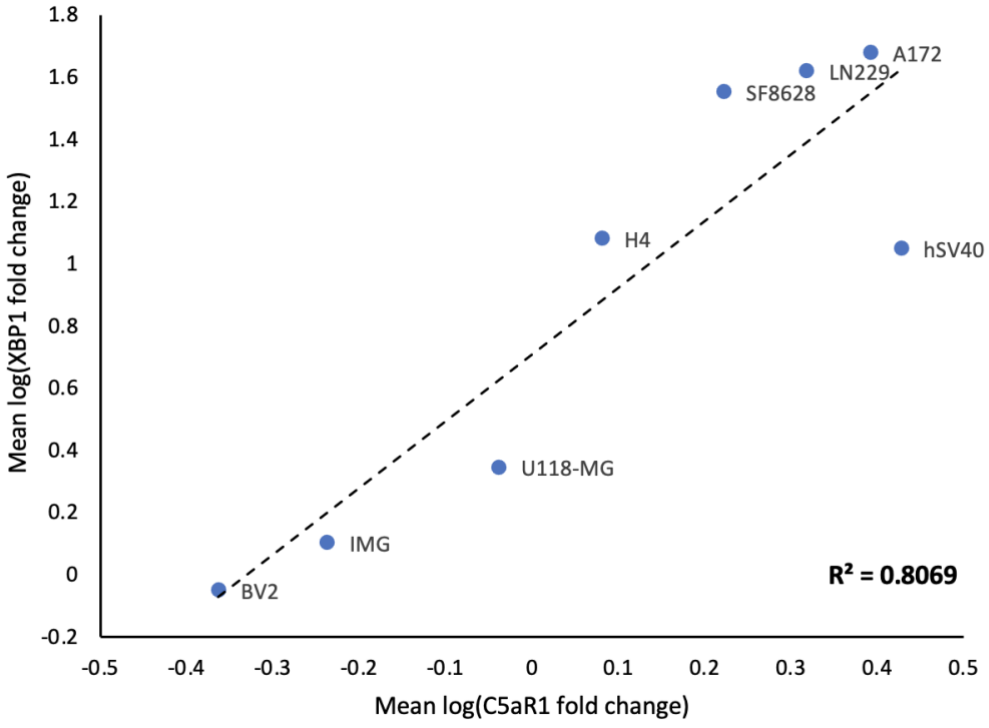

Figure 3.9 Strong correlation between UPR activation and C5aR1 mRNA upregulation

SF8628, LN229, A172, U-118 MG, H4, hSV40, IMG and BV2 cells were treated with Thap for 16 h. mRNA expression of C5aR1 and XBP1 were assessed by qPCR. All mRNA levels were normalised to 18S and expressed as fold change relative to the level of expression in vehicle-treated cell. Each data point represents the mean of biological replicates. n=3.

In addition to glioma cells, we also assessed C5aR1 and C5 expression in microglia models under mild (1%) and severe (<0.1%) hypoxic conditions as microglia constitutes up to 30% of tumour mass. The induction of hypoxia was validated after 6 hours by increased expression of HIF-target genes, CAIX and GLUT1. (Figure 3.10A-C). In hSV40 microglia-like cells, no statistical differences in C5aR1 expression were detected under hypoxia, although a trend towards upregulation was observed after 16 hours of exposure (Figure 3.10D). In contrast, C5aR1 expression was markedly suppressed in IMG cells under severe hypoxia, and in BV2 cells under both mild and severe hypoxia (Figure 3.10E-F). This hypoxia-induced changes in C5aR1 expression differ across microglia models. Interestingly, there was a trend of increased C5 mRNA expression in hSV40 cells after 16 hours of mild hypoxia treatment, though it did not reach statistical significance due to variability between replicates (Figure 3.10G). No such changes were observed in either IMG or BV2 cells, where C5 expression remained stable across all oxygen concentrations (Figure 3.10H-I).

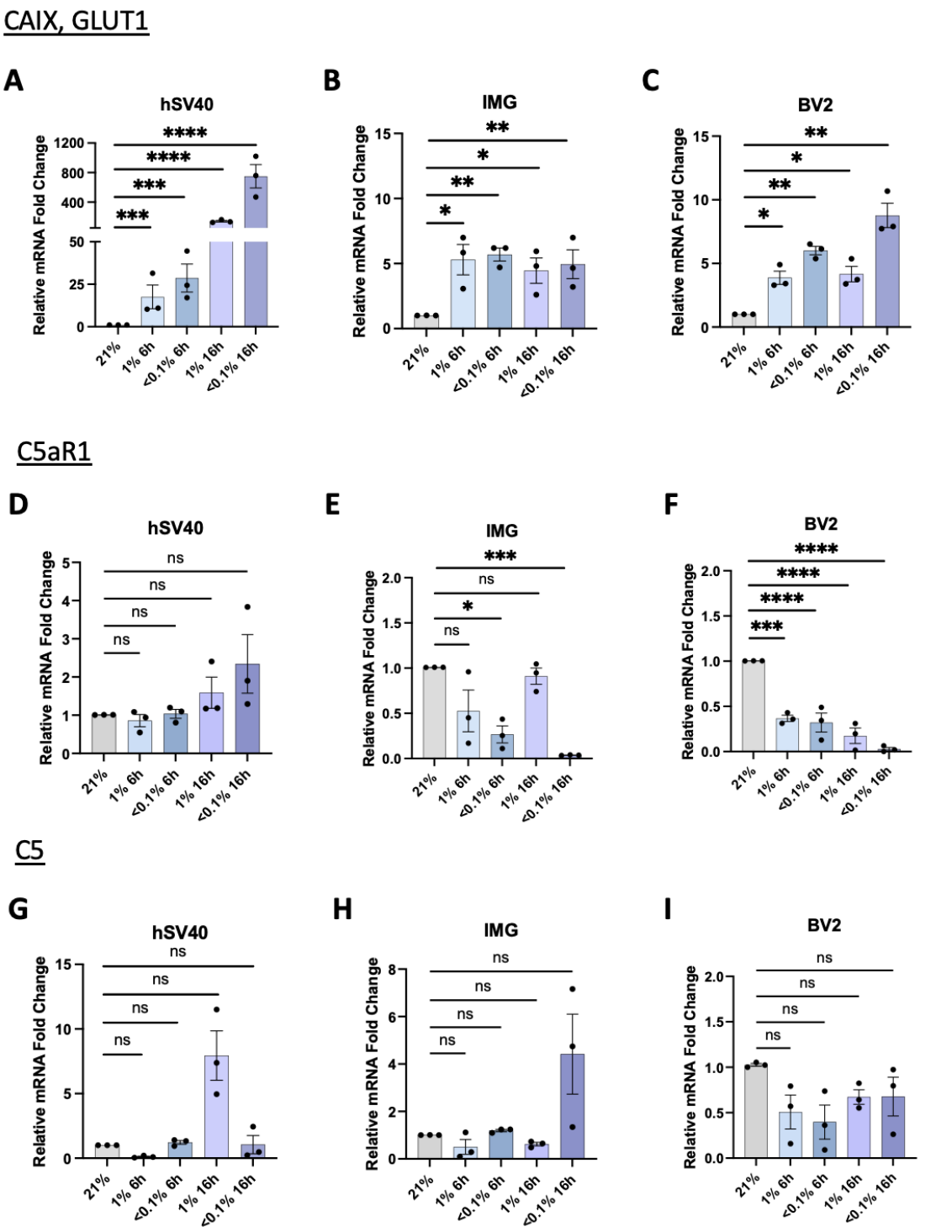

Figure 3.10 Hypoxia suppresses C5aR1 expression in IMG and BV2 microglia only

mRNA expression of **(A)** CAIX, **(B-C)** GLUT1, **(D-F)** C5aR1 and **(G-I)** C5 were assessed by qPCR in hSV40, IMG and BV2 cells following 6 h and16 h exposure to of 21%, 1% or <0.1% O_2. All mRNA levels were normalised to 18S and expressed as fold change relative to the level of expression at 21%. Data presented as mean ± SEM of biological replicates. n=3. Statistical analysis was performed on unnormalised values using one-way ANOVA with Dunnett's test. *p≤0.05, **p≤0.01, ***p≤0.001, ****p≤0.0001.

3.2.3 The pro-survival role of C5aR1

We next investigated the functional role of C5aR1 in the context of severe hypoxia, specifically whether its expression was critical for cancer cell survival. Firstly, we utilised siRNA to silence C5aR1, achieving approximately 70% reduction in mRNA expression in both SF8628 and LN229 cells (Figure 3.11A-B). Under normoxic conditions, C5aR1 knockdown (KD) led to a modest increase in apoptosis in LN229 cells. Silencing C5aR1 under hypoxia further amplified apoptotic cell death compared to scramble (Scr) controls in both SF8628 and LN229 cell lines, suggesting a more prominent anti-apoptotic role of C5aR1 under hypoxic stress (Figure 3.11C-D).

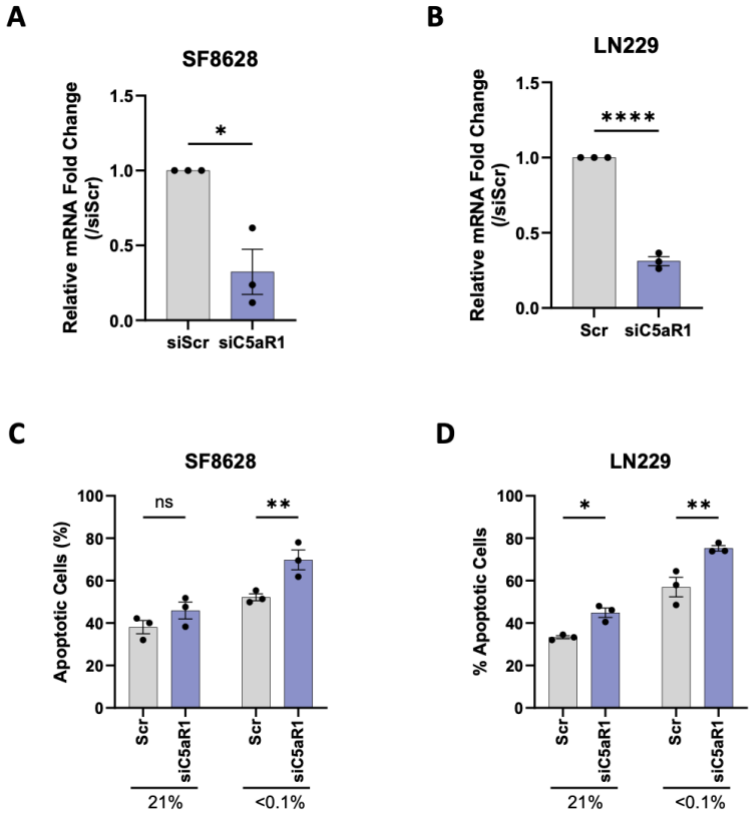

Figure 3.11 Silencing C5aR1 results in higher apoptotic count under hypoxia

Cells were transfected with Scr or C5aR1 siRNA. mRNA expression of C5aR1 in **(A)** SF8628 and **(B)** LN229 cells were assessed by qPCR. mRNA levels were normalised to GAPDH and 18S respectively. Data presented as mean ± SEM of biological replicates. n=3. Statistical analysis was performed on unnormalised values using unpaired t-test. **(C-D)** Following siRNA treatment, SF8628 and LN229 cells were exposed to 21% or <0.1% O_2 for 16 h. At least 100 cells per condition were analysed via apoptosis assay. Data presented as mean ± SEM of biological replicates. n=3. Statistical analysis used two-way ANOVA with Šidák's test. *p≤0.05, **p≤0.01, ****p≤0.0001.

We then evaluated the role of C5aR1 on cell survival under hypoxia using clonogenic assays. Silencing C5aR1 under normoxic conditions already led to a pronounced reduction in cell survival, in both SF8628 and LN229 cells. As a result, subsequent exposure of C5aR1 KD cells to hypoxic stress did not further decrease survival, likely due to an already compromised baseline viability (Figure 3.12A-B). To further study cell survival, we generated C5aR1-overexpressing (OE) cells via DNA plasmid transfection, validated by a marked increase in C5aR1 mRNA expression (Figure 3.12C). Under hypoxia, C5aR1 OE cells exhibited a significantly higher survival fraction compared to cells treated with empty vector (EV) controls (Figure 3.12D). Collectively, these finding support a critical role for C5aR1 in supporting cell survival in both HGG models, irrespective of oxygen availability.

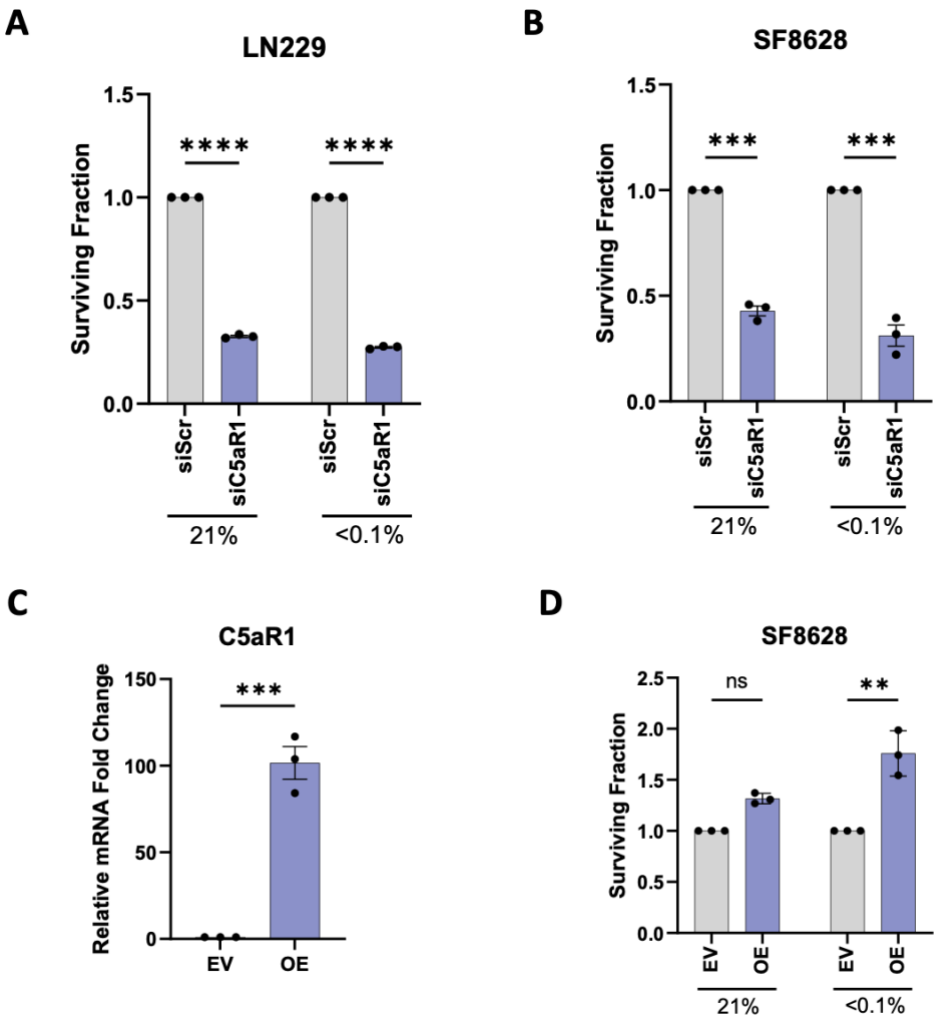

Figure 3.12 C5aR1 plays a crucial pro-survival role in HGGs

(A-B) SF8628 and LN229 cells were transfected with Scr or C5aR1 siRNA before exposure to 21% or <0.1% O_2 for 16h. Cell survival was assessed via clonogenic assay. Data presented as mean ± SEM of biological replicates. n=3. Statistical analysis used two-way ANOVA with Šidák's test.
(C) mRNA expression of C5aR1 in SF8628 cells treated with empty vector or C5aR1 overexpression plasmids were assessed by qPCR. mRNA levels were normalised to 18S. Data presented as mean ± SEM of biological replicates. n=3. Statistical analysis used unpaired t-test. **(D)** SF8628 cells were treated with empty vector or C5aR1 overexpression plasmids, then exposed to 21% or <0.1% O2 for 16h. Cell survival was assessed via clonogenic assay. Data presented as mean ± SEM of biological replicates. n=3. Statistical analysis was performed on unnormalised values using two-way ANOVA with Šidák's test. **p≤0.01, ***p≤0.001, ****p≤0.0001.

To investigate the mechanism by which C5aR1 promotes HGG survival, we examined whether it was mediated through its canonical signalling. As a GPCR, C5aR1 engagement with its ligand C5a initiates intracellular signalling cascades, especially pro-survival signalling pathways. We first focused on the NF-κB pathway, an established downstream effector of C5aR1 activation (Beach *et al.*, 2023; Song *et al.*, 2018). To assess NF-κB activity in HGG cells, we added recombinant human C5a and measured expression of phosphorylated RelA (pRelA) at Ser536 as a readout of NF-κB activation. Upon C5a stimulation, we observed a trend toward increased pRelA expression but consistent total RelA expression, indicating activation of NF-κB signalling as a result of C5a-C5aR1 signalling (Figure 3.13).

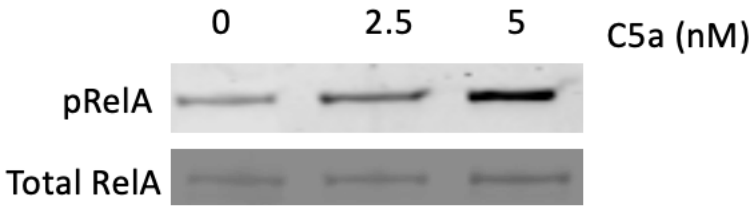

Figure 3.13 C5a-C5aR1 signalling activates NF-κB pathway

Recombinant C5a proteins at the described concentrations were added to SF8628 cells for 2 h. Western blotting was carried out with the antibodies indicated. Total RelA was used as loading control. n=3

Functionally, adding human-derived C5a proteins for 2 hours increased survival of LN229 cells, and the addition of C5aR1 antagonists, PMX205 and Avacopan abrogated the pro-survival benefits of C5a-C5aR1 signalling (Figure 3.14). This finding further supports our hypothesis that C5aR1 interaction with its ligand is important in HGG survival. Of note, the anti-survival effects of C5aR1 antagonists were only observed in the presence of recombinant C5a proteins, and not without stimulation of receptor signalling.

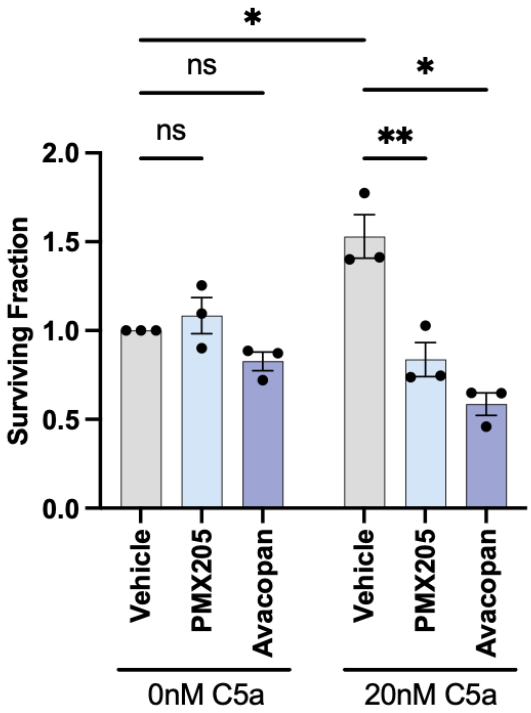

Figure 3.14 C5aR1 antagonists abrogates C5a-induced pro-survival effects

LN229 cells were treated with 0 or 20 nM recombinant C5a proteins, together with vehicle, PMX205 or Avacopan for 2 h. Cell survival was assessed via clonogenic assay. Data presented as mean ± SEM of biological replicates. n=3. Statistical analysis used two-way ANOVA with Tukey's test. *p≤0.05, **p≤0.01.

To further validate the role of NF-κB signalling in the pro-survival phenotype mediated by C5aR1, we examined whether overexpression of RelA could compensate for the loss of C5aR1 activity induced by C5aR1 antagonists. As expected, overexpression of RelA via plasmid transfection led to marked increase of both pRelA and total RelA protein expression (Figure 3.15A). However, treatment with the C5aR1 antagonists PMX205 and Avacopan slightly attenuated this increase in RelA OE cells, indicating that C5aR1 inhibition interferes with the full activation of NF-κB signalling. Functionally, inhibition of C5aR1 in RelA OE cells led to a modest increase in apoptosis (15-20%) compared to vehicle-treated controls, although this did not reach statistical significance (Figure 3.15B). While RelA OE alone significantly enhanced cell survival, consistent with its anti-apoptotic role, treatment with C5aR1 antagonists at baseline (0 Gy) had a modest reduction in this pro-survival effects exerted by RelA (Figure 3.16A). Given the established role of RelA in promoting cell survival under cellular stress, we were also intrigued by how the antagonists would react when combined with irradiation in RelA OE cells. As shown in Figure 3.16B, Avacopan significantly reduced cell survival under irradiation at 4 Gy, particularly in RelA OE cells, with PMX205 also exerting an anti-survival effect. Under irradiation, survival fractions of RelA OE cells treated with C5aR1 antagonists were not significant different compared to those treated with EV. If SF8628 cells were fully dependent on NF-κB signalling, RelA OE cells treated with C5aR1 antagonists would be expected to show higher survival than EV-treated cells. Collectively these data suggest that C5aR1 inhibition partially reverses the pro-survival effects of RelA overexpression under irradiation.

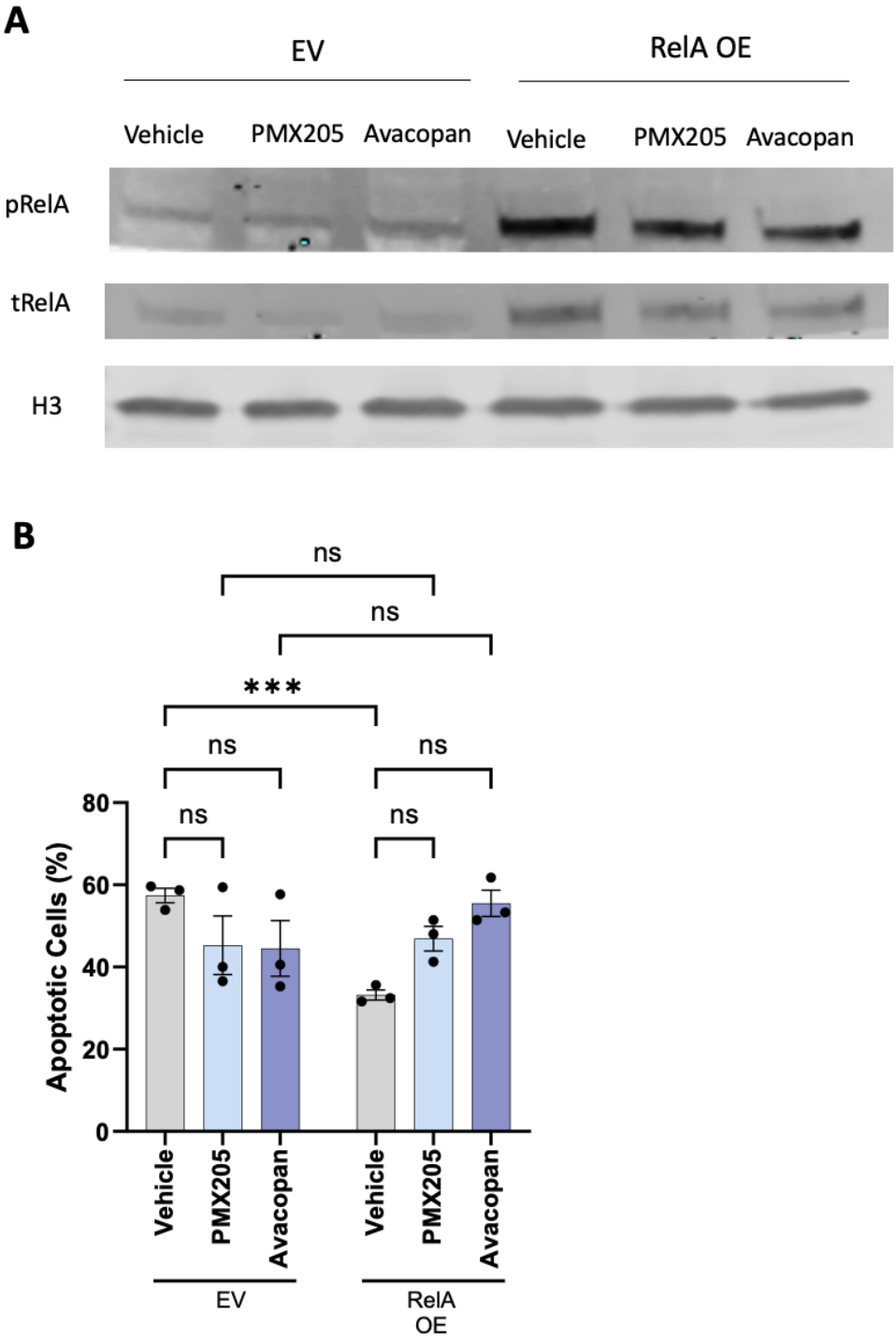

Figure 3.15 C5aR1 inhibition reduce RelA levels under RelA overexpression

SF8628 cells were transfected with EV or RelA OE plasmids for 24 hours before the addition of vehicle, PMX205 or Avacopan for 48 h treatment.
(A) Western blotting was carried out with the antibodies indicated. H3 was used as loading control. n=3
(B) At least 100 cells per condition were analysed via apoptosis assay. Data presented as mean ± SEM of biological replicates. n=3. Statistical analysis used two-way ANOVA with Tukey's test. ***p≤0.001.

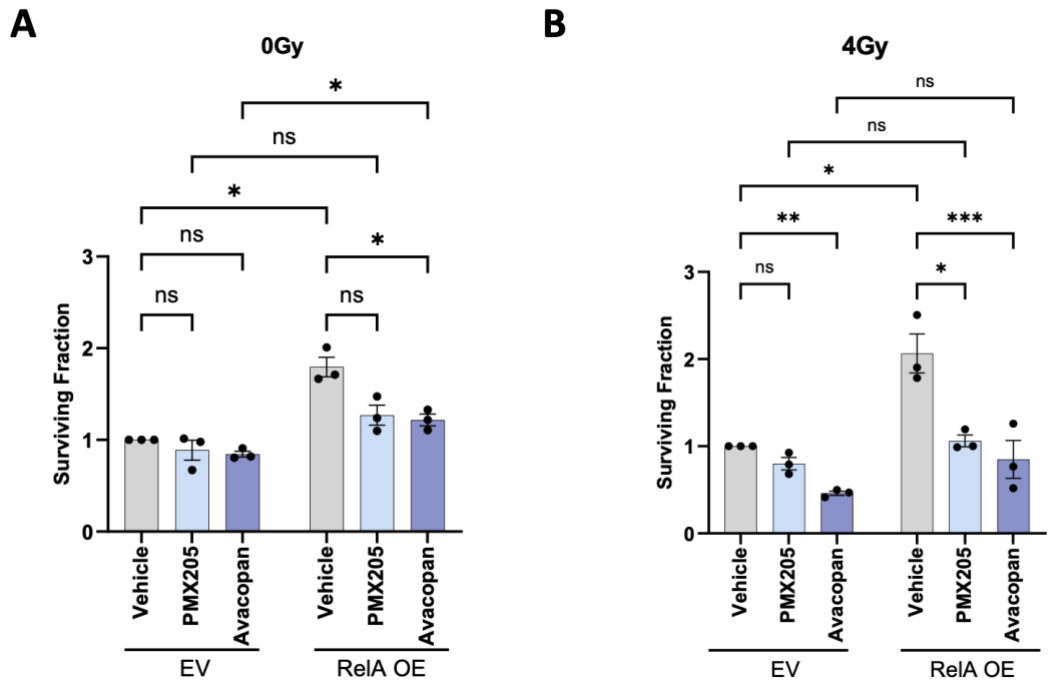

Figure 3.16 C5aR1 inhibition partially reverses the pro-survival effects of RelA overexpression under irradiation

SF8628 cells were transfected with EV or RelA OE plasmids for 24 hours before the addition of vehicle (DMSO), PMX205 or Avacopan for 48 h treatment. Cells were then irradiated at **(A)** 0 Gy or **(B)** 4 Gy. Cell survival was assessed via clonogenic assay. Data on both graphs were derived from the same experiment. Data presented as mean ± SEM of biological replicates. n=3. Statistical analysis used two-way ANOVA with Tukey's test. *p≤0.05, **p≤0.01, ***p≤0.001.

In addition to NF-κB, we also assessed another pro-survival signalling pathway, MAPK, by examining levels of phosphorylated ERK (pERK) at site Thr202/Tyr204. The MAPK pathway is also a downstream target of GPCR, and 12% of DMG patients carry the BRAF mutation that results in sustained MAPK signalling (Schüller *et al.*, 2021). To assess the involvement of MAPK signalling upon C5aR1 activation, we treated cells with the MEK inhibitor Selumetinib alone, or in combination with the C5aR1 antagonist Avacopan to test if dual targeting could further suppress MAPK activity. As shown in Figure 3.17A, Selumetinib consistently reduced pERK expression regardless of radiation dose, whereas Avacopan reduced pERK levels only under irradiated conditions, possibly reflecting increased reliance of C5aR1 signalling under cellular stress. Interestingly, we previously did not detect the direct induction of pERK with recombinant C5a, perhaps due to timing of sample collection, but here we observed reduced MAPK activation following C5aR1 inhibition with Avacopan. Next, we measured the viability of cells treated with Selumetinib and Avacopan via MTT assay. MTT assay measures the activity of mitochondrial dehydrogenases in living cells, which reduce MTT reagent into purple formazan crystals. Crystals are subsequently solubilised, and the absorbance is directly proportionate to the number of viable cells. As shown in Figure 3.17B, combination treatment with Selumetinib and Avacopan did not elicit additional suppression of pERK, or further reduce cellular viability compared to Avacopan or Selumetinib alone at both 0 and 9 Gy, suggesting that the two inhibitors act via overlapping signalling pathways. These findings support that C5aR1 engages with MAPK signalling. The lack of additive effects with dual inhibition in our viability assay implies that C5aR1 contributes to cell survival at least partially through MAPK signalling, and potentially in parallel with NF-κB signalling.

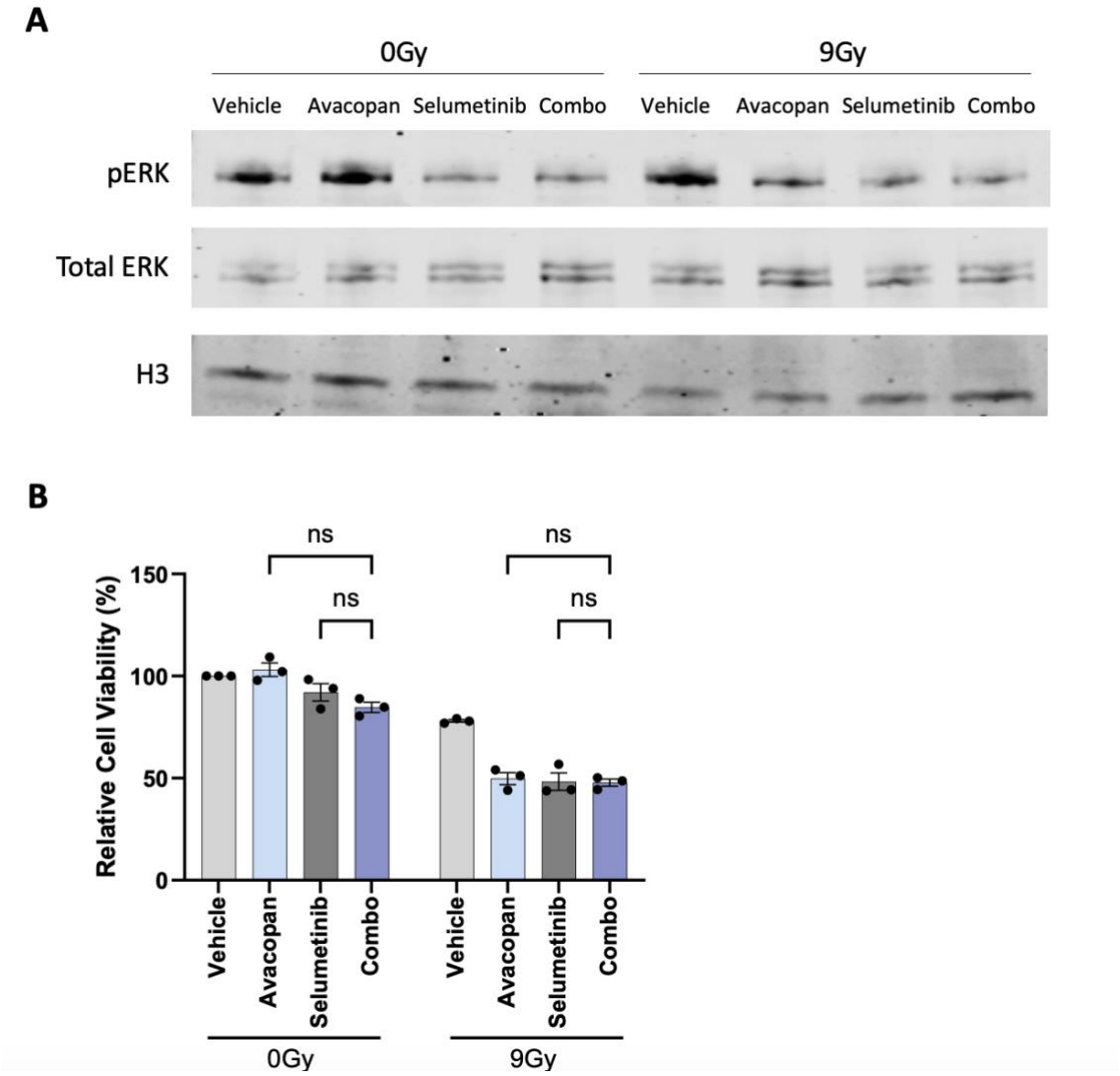

Figure 3.17 Involvement of MAPK signalling with C5aR1 activation

SF8628 cells were treated with vehicle (DMSO), 4 μM Avacopan (48 h), 0.125 μM Selumetinib (24 h) or combo (Avacopan + Selumetinib) before 0 or 9 Gy irradiation. Samples harvested 24 h post-irradiation.

(A) Western blotting was carried out with the antibodies indicated. H3 was used as loading control. n=3
(B) Cell viability was assessed using MTT assay and normalised to the 0 Gy vehicle control. Data presented as mean ± SEM of biological replicates. n=3. Statistical analysis used two-way ANOVA with Šidák's test.

3.2.4 C5aR1 signalling under hypoxia

Having characterised the role of C5a-C5aR1 signalling under normoxic conditions, we continued to investigate its role under hypoxic stress. Previous studies have reported that HIF-1α can either enhance or suppress NF-κB or MAPK signalling depending on cellular context and the duration of hypoxic exposure (Kučera *et al.*, 2017; Walmsley *et al.*, 2005). To investigate this in HGG, LN229 and SF8628 cells were subjected to severe hypoxia for 16 hours upon genetic silencing of C5aR1. Successful hypoxic induction was confirmed by marked elevation of HIF-1α levels. When we compared the effect of hypoxia treatment alone, level of pRelA in SF8628 cells was reduced under hypoxia, suggesting suppression of NF-κB activity (Figure 3.18A). We anticipated the expression of pRelA and pERK would decrease with C5aR1 KD, however, this was not always observed as the changes in these proteins were inconsistent among biological replicates (quantification of bands shown in Appendix A, Figure A.1). Therefore, we could not draw definite conclusion on the impact of C5aR1 silencing on signalling modulations under these experimental conditions.

In LN229 cells, hypoxia treatment appeared to reduce pERK levels slightly, indicating modest diminished MAPK signalling (Figure 3.18B). While C5aR1 KD had limited effect on NF-κB activation under either normoxia or hypoxia, it evidently attenuated MAPK signalling, as shown by a significant decrease in pERK expression at both oxygen conditions. Collectively, these results suggest that C5aR1-mediated MAPK signalling is preserved under hypoxia, whereas NF-κB signalling may be suppressed by the hypoxic environment itself. Importantly, the impact of C5aR1 silencing in LN229 cells under hypoxia appears comparable to its effects under normoxia. However, we do

acknowledge that there were differences in cell signalling changes observed between the two cell lines.

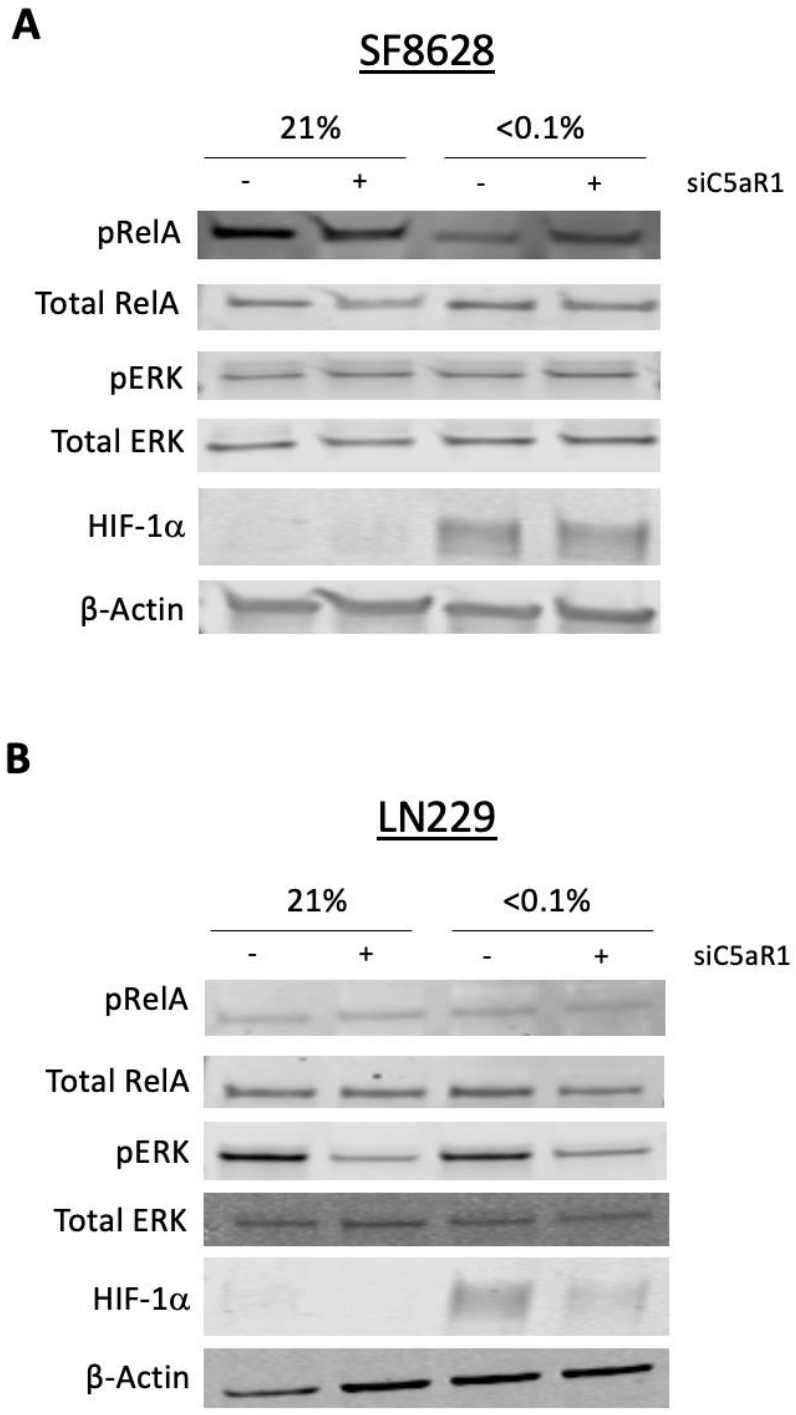

Figure 3.18 Silencing C5aR1 attenuated MAPK signalling in LN229 cells at both normoxia and hypoxia

(A) SF8628 and **(B)** LN229 cells were transfected with siScr or siC5aR1 for 72 hours before 16 h of exposure to 21% or <0.1% O_2. Western blotting was carried out with the antibodies indicated. β-actin was used as loading control. n=3.

We next evaluated the effects of the pharmacological C5aR1 antagonist, Avacopan, on pro-survival signalling under hypoxic stress. Hypoxia alone led to a reduction in pRelA levels in both cell lines, suggesting that NF-κB activity was suppressed under hypoxic conditions (Figure 3.19A-B). Although we previously observed attenuation of NF-κB signalling with Avacopan treatment in RelA OE cells under irradiation, Avacopan treatment did not alter the pRelA expression compared to vehicle controls under both normoxia and hypoxia in this case. This indicates limited involvement of C5aR1 in modulating NF-κB signalling under hypoxia, likely due to an already attenuated signalling state. A similar pattern was observed with MAPK signalling, where hypoxia alone also reduced pERK expression in SF8628 cells, but not in LN229 cells. Notably, Avacopan did not appear to alter either NF-κB or MAPK signalling in SF8628 cells under normoxic or hypoxic conditions, contrasting with earlier results when RelA was overexpressed (Figure 3.19A). In contrast, Avacopan consistently attenuated MAPK signalling in LN229 cells under both normoxia and hypoxia, as reflected by the reduction in pERK levels (Figure 3.19B). C5aR1-mediated MAPK signalling remains functionally active in these cells despite hypoxic stress. These data suggest cell line-specific difference in signalling dynamics, where NF-κB may be more susceptible to hypoxic suppression, and MAPK signalling through C5aR1 was preserved in LN229 but not in SF8628 cells. Avacopan appears to exert different modulatory effects on cell signalling between the two cell lines.

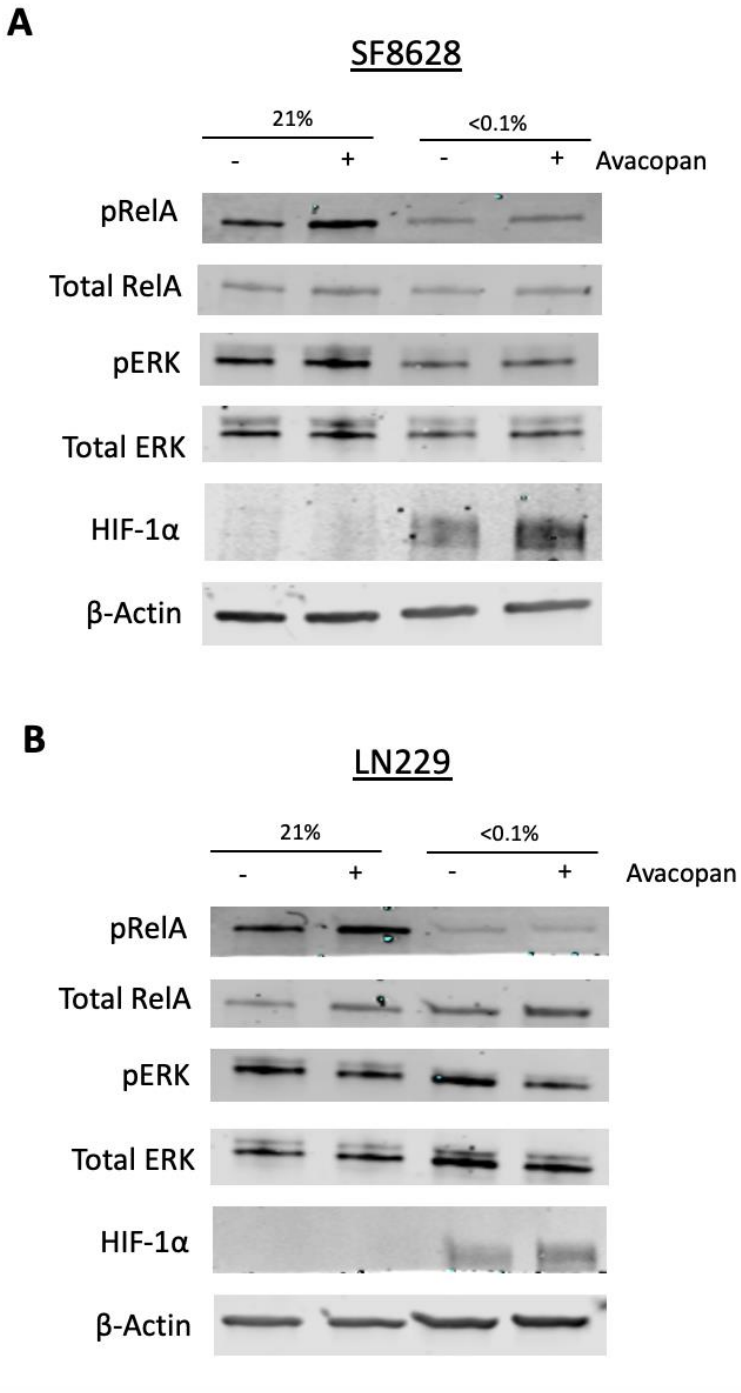

Figure 3.19 Avacopan attenuated MAPK signalling under hypoxia in LN229

Vehicle (DMSO) or Avacopan was added to **(A)** SF8628 cells (48 h) and **(B)** LN229 cells (24 h) before 16 h of exposure to 21% or <0.1% O_2. Western blotting was carried out with the antibodies indicated. β-actin was used as loading control. n=3.

Severe hypoxia is known to impair cell viability, and consistent with this, we observed a significant increase in apoptotic cell death under hypoxic conditions compared to normoxia (Figure 3.20A-B). In SF8628 cells, Avacopan treatment did not further elevate apoptosis under both oxygen concentrations, aligning with the absence of Avacopan-mediated modulation of pro-survival signaling in this cell line (Figure 3.20A). In contrast, Avacopan induced a modest, but statistically significant increase in apoptosis in LN229 cells, with a more pronounced effect under hypoxic stress compared to normoxia (Figure 3.20B). These findings suggest that the pro-apoptotic effects of Avacopan may be downstream effects of MAPK signalling and are potentiated in hypoxic conditions, at least in GBM-derived LN229 cells.

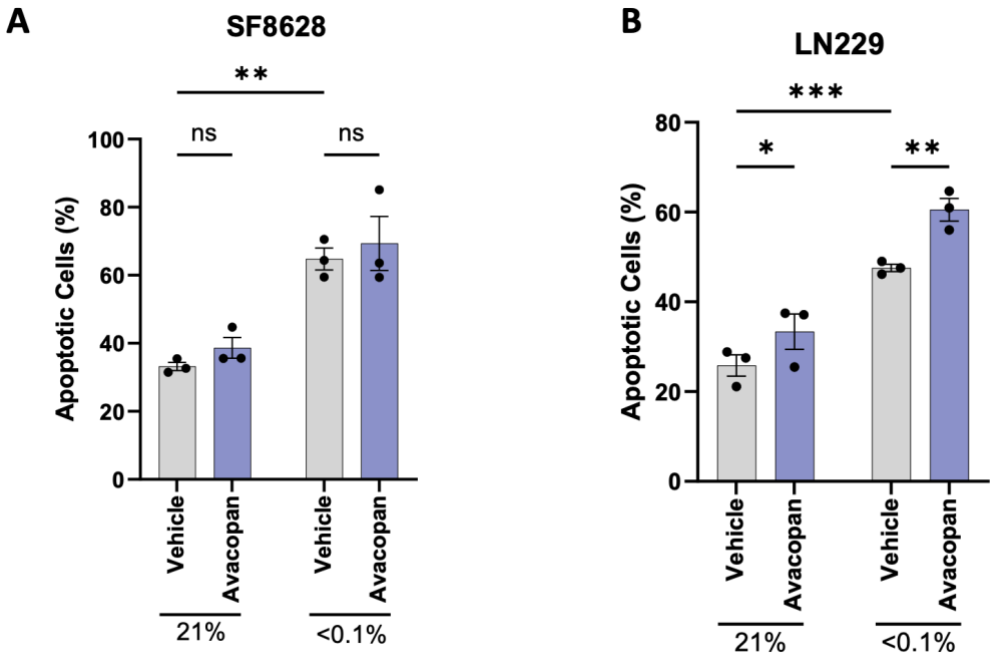

Figure 3.20 Avacopan promotes apoptosis in LN229

Vehicle (DMSO) or Avacopan was added to **(A)** SF8628 cell (48 h) and **(B)** LN229 cells (24 h) before being exposed to 21% or <0.1% O_2 for 16 h. At least 100 cells were analysed per condition via apoptosis assay. Data presented as mean ± SEM of biological replicates. n=3. Statistical analysis used two-way ANOVA with Fisher's LSD test. *p≤0.05, **p≤0.01, ***p≤0.001.

Another well-documented cellular response to hypoxic stress is autophagy which could lead to cell death depending on context and duration. To test whether C5aR1 inhibition influences autophagy under hypoxia, we assessed key autophagic markers in HGG cells. We first analysed the expression of microtubule-associated protein 1A/1B-light chain 3B (LC3B) which undergoes post-translational modification during autophagy. The cytosolic form, LC3B-I (top band), is converted to its lapidated form LC3B-II (bottom band) upon autophagosome formation. Western blotting revealed that exposure to <0.1% oxygen for 16 hours led to increased LC3B-II expression in LN229 cells, suggesting autophagy induction (Figure 3.21A). Notably, Avacopan treatment did not result in any significant changes in LC3B expression in these cells. However, to our surprise, in SF8628 cells, hypoxia unexpectedly led to a decrease in both isoforms, which may suggest impaired autophagosome formation, or cell line-specific regulatory mechanisms (Figure 3.21B).

To further validate these observations, we also assessed the levels of sequestosome 1 (p62/SQSTM1), a selective autophagy substrate that binds to LC3 and is degraded during autophagic flux. In both cell lines, hypoxia led to a decrease in p62 reduction, suggesting active autophagic degradation. Interestingly, the reduction in p62 in SF8628 cells occurred despite the decrease in LC3B-II, suggesting possible differences in autophagy dynamic. Importantly, Avacopan treatment, under hypoxia, only resulted in a very modest reduction of p62 in SF8628 cells, and had no effect in LN229 cells under either normoxic or hypoxic conditions. These data suggest that Avacopan exerts minimal influence on autophagy and that any cytotoxic effects, particularly in LN229 cells under hypoxia, are likely driven predominantly by promotion of apoptosis (or other forms of cell death). Collectively, these findings suggest that C5aR1 inhibition via Avacopan

selectively enhances apoptotic pathways without broadly affecting autophagy, at least in LN229 cells, within the experimental conditions and time frame assessed.

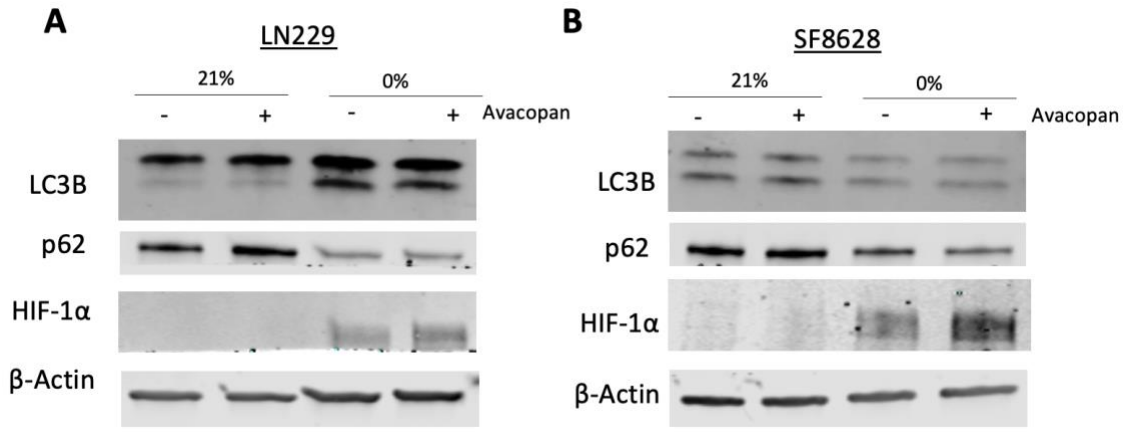

Figure 3.21 Avacopan has minimal impact on autophagy

Vehicle (DMSO) or Avacopan was added to **(A)** LN229 cells (24 h) and **(B)** SF8628 cells (48 h) before being exposed to 21% or <0.1% O_2 for 16 h. Western blotting was carried out with the antibodies indicated. β-actin was used as loading control. Experiment shown here is part of the same experiment shown in Figure 3.19. n=3.

Aligning with the lack of changes in pro-survival signalling or cell death, Avacopan also had no significant impact on cell survival in SF8628 cells (Figure 3.22A). In contrast, in LN229 cells, Avacopan treatment under hypoxic conditions led to a modest, but statistically significant reduction in cell survival, while no effect was observed under normoxia (Figure 3.22B). All these results suggest that the cytotoxic effects of Avacopan are more pronounced in the GBM cell line compared to DMG-derived SF8628, possibly reflecting the differences in canonical C5aR1 signalling dynamics. Nonetheless, the overall impact of Avacopan on cell viability remains relatively modest when compared to C5aR1 gene knockdown, highlighting the stronger and more consistent anti-survival effect of genetic silencing over pharmacological inhibition under hypoxic stress.

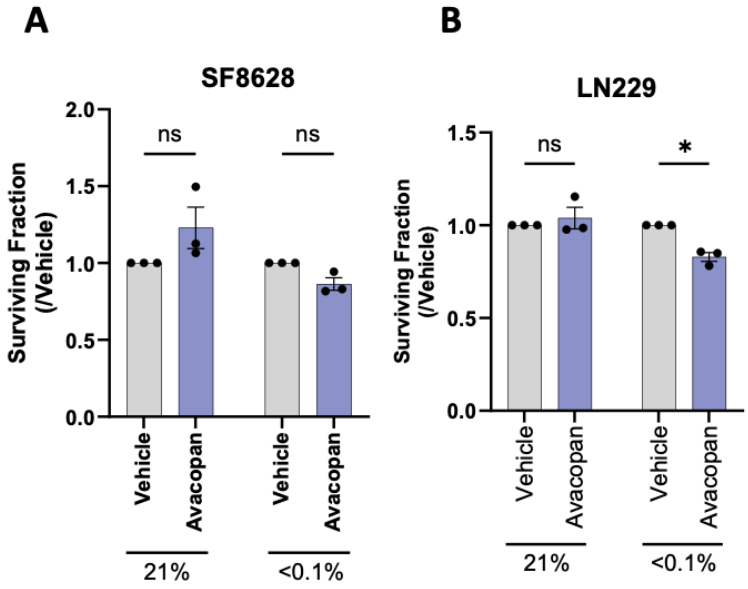

Figure 3.22 Modest reduction in LN229 cell survival under hypoxia following Avacopan treatment

Vehicle (DMSO) or Avacopan was added to **(A)** SF8628 cell (48 h) and **(B)** LN229 cells (24 h) before exposure to 21% or <0.1% O_2 for 16 h. Cell survival was assessed via clonogenic assay. Data presented as mean ± SEM of biological replicates. n=3. Statistical analysis used two-way ANOVA with Šidák's test. *p≤0.05.

3.3 Discussion

Our initial observation that severe hypoxia (<0.1%) selectively induced C5aR1 protein expression in LN229 cells, but not SF8628 cells prompted a more detailed investigation into the regulatory mechanisms driving this differential response. Despite induction of C5aR1 mRNA expression under hypoxia, this transcriptional induction was not consistently reflected at the protein level across all cell lines, suggesting the presence of post-transcriptional control mechanism. These may include protein translational inefficiencies or post-translational regulations such as proteasomal degradation, contributing to the observed cell line-specific differences in C5aR1 protein abundance. Using chemical inducers of HIF and UPR pathways, we found that C5aR1 induction in LN229 under hypoxic stress is driven by UPR, rather than HIF signalling. The magnitude of UPR-mediated C5aR1 induction varied significantly between cell lines, with LN229 cells exhibiting significant upregulation, while SF8628 cells showed only modest transcriptional changes and negligible protein-level induction. Regarding using chemical inducers to active HIF signalling, it should be noted that $CoCl_2$ induces multiple HIF isoforms and lacks specificity for HIF-1α (Fang *et al.*, 2016). Triple knockdown of UPR downstream effectors further supported the involvement of all three UPR branches in C5aR1 upregulation under hypoxia. Moreover, we observed a strong correlation between XBP1 and C5aR1 mRNA induction across multiple HGG and microglia cell lines, and a positive correlation between C5aR1 and UPR signatures in patient samples available on the TCGA database (Suwa *et al.*, 2025).

Mechanistically, recombinant C5a stimulation increased pRelA expression, implicating NF-κB activation as a downstream consequence of C5aR1 signalling. Although MAPK pathway activation was more difficult to detect following recombinant

C5a addition, this may reflect technical limitations such as transient activation windows or delayed sample collection. Nevertheless, our experiments using RelA OE and dual inhibition with Selumetinib and Avacopan suggested that C5aR1 activation engages both NF-κB and MAPK signalling axes, in line with other reports (Beach *et al.*, 2023; Li *et al.*, 2020b; Schraufstatter *et al.*, 2009). In SF8628 cells, dependence on MAPK signalling appeared greater than on the NF-κB pathway, despite the absence of reported mutation in BRAF, RAS or MEK that would typically drive constitutive MAPK activation.

Under severe hypoxia, NF-κB signalling was diminished in both cell lines, indicating direct repression by hypoxic stress and consequently, further inhibition via C5aR1 blockade did not further suppress this pathway. This is different to another study that reported NF-κB pathway activation under hypoxia within 30 minutes, which is much earlier than our sample collection after 16 hours of hypoxic culture (Culver *et al.*, 2010). In contrast, MAPK signalling was more consistently attenuated via C5aR1 gene silencing and pharmacological inhibition, particularly in LN229 cells, underscoring a predominant reliance on the MAPK survival signalling under hypoxic conditions. Our functional assays further support a pro-survival role for C5aR1 in HGGs, aligning with previous report that highlights complement proteins as drivers of GBM aggressiveness (Roumenina *et al.*, 2019). Although C5aR1 knockdown had no significant effects on apoptosis under normoxia, it resulted in a significant reduction in cell survival, suggesting involvement of non-apoptotic death mechanisms such as necrosis, which requires further investigation. The use of pharmacological C5aR1 antagonist, Avacopan induced modest, but statistically significant apoptosis in LN229 cells under hypoxia, while SF8628 cells remained unresponsive. Clonogenic assays followed this trend, with mild reduction in LN229 survival after Avacopan treatment, but no significant effect in SF8628. The lack of response in SF8628 maybe be attributed by the lack of C5aR1 upregulation and

reduced levels of C5 ligand in this cell line under hypoxia. These findings underscore the context-specific nature of C5aR1 signalling, and suggest that therapeutic efficacy of C5aR1 inhibition may vary across HGG subtypes.

Collectively, our data suggest that hypoxia-induced C5aR1 upregulation, mediated via the UPR, promotes glioma cell survival through activation of pro-survival signalling pathways. While genetic silencing of C5aR1 exerts more pronounced anti-survival effects than pharmacological inhibition, antagonist such as Avacopan retain some therapeutic potential under hypoxia, particularly in GBM. The differential response to C5aR1 inhibition highlights the complexity of C5aR1 signalling in HGG and emphasises the need for context-dependent therapeutic approaches. Future studies could further explore combination strategies that pair C5aR1 inhibition with UPR-enhancing agents or stress modulators to maximise tumour-selective cytotoxicity.

Chapter 4 C5aR1 inhibition and radiotherapy

4.1 Introduction

Radiotherapy is the standard-of-care treatment for HGG, however, the overall survival remains relatively low, with no improvement in 5-year survival rate since the approval of TMZ + radiotherapy used in GBM (Frosina, 2023). Radioresistance remains as key challenge in HGG, contributing to tumour recurrence after initial therapy, affecting >90% of GBM and almost 100% of DMG patients (Navarria *et al.*, 2016; Vanan and Eisenstat, 2015). One of the major barriers to radiotherapy efficacy is the highly immunosuppressive nature of the TME, characterised by limited T cell infiltration. Our previous studies demonstrated that C5aR1 plays a key role in promoting colorectal cancer cell survival under irradiation, even in the context of a depleted immune milieu (Beach *et al.*, 2023). Mechanistically, this radiosensitising effect was attributed to NF-κB signalling, a well-established driver of radioresistance in cancer cells (Bhat *et al.*, 2013). Given the immunosuppressive nature of HGGs, we hypothesised that C5aR1 may function as a regulator of radioresistance in glioma as well, due to its role in modulating canonical pro-survival signalling.

Given that hypoxic regions have been reported in HGGs, and hypoxia has been widely implicated in promoting radioresistance, it is essential to investigate how oxygen availability influences cellular responses to irradiation in HGG. We first assessed the impact of C5aR1 inhibition in combination with irradiation under normoxic conditions by evaluating changes in pro-survival signalling and potential subsequent effects in apoptosis, cell proliferation and survival. This allowed us to isolate irradiation-specific changes before introducing the added variable of hypoxic stress. We then examined the

role of C5aR1 under combined hypoxia and irradiation to evaluate its potential contribution to hypoxia-driven radioresistance and its suitability as a therapeutic target in oxygen-deprived tumour regions.

4.2 Results

4.2.1 C5aR1 expression under irradiation

Firstly, we focused on the effect of radiation alone, under normoxic conditions. To assess C5aR1 expression under both non-irradiated and irradiated conditions, a single radiation dose of 9 Gy was selected based on our prior studies conducted in colorectal cancer models. C5aR1 mRNA expression was measured at two time points – 4 hours and 24 hours post-irradiation, to capture potential temporary changes in expression. Across all HGG cell lines tested, no statistically significant changes in C5aR1 mRNA levels were observed at either time point following irradiation, except for the GBM cell line H4 (Figure 4.1A-D). Although there was a transient downregulation of C5aR1 expression in H4 cells 4 hours post-irradiation, followed by a rebound, there was no statistical difference between 0 Gy control and 24 hours post-irradiation (Figure 4.1D). In addition, we also tested the mRNA expression of C5, the ligand for C5aR1. Similar to C5aR1, C5 expression remained largely unaltered upon radiation across the tested HGG cell lines, except for a transient downregulation observed in SF8628 cells 4 hours post-irradiation (Figure 4.1E-F).

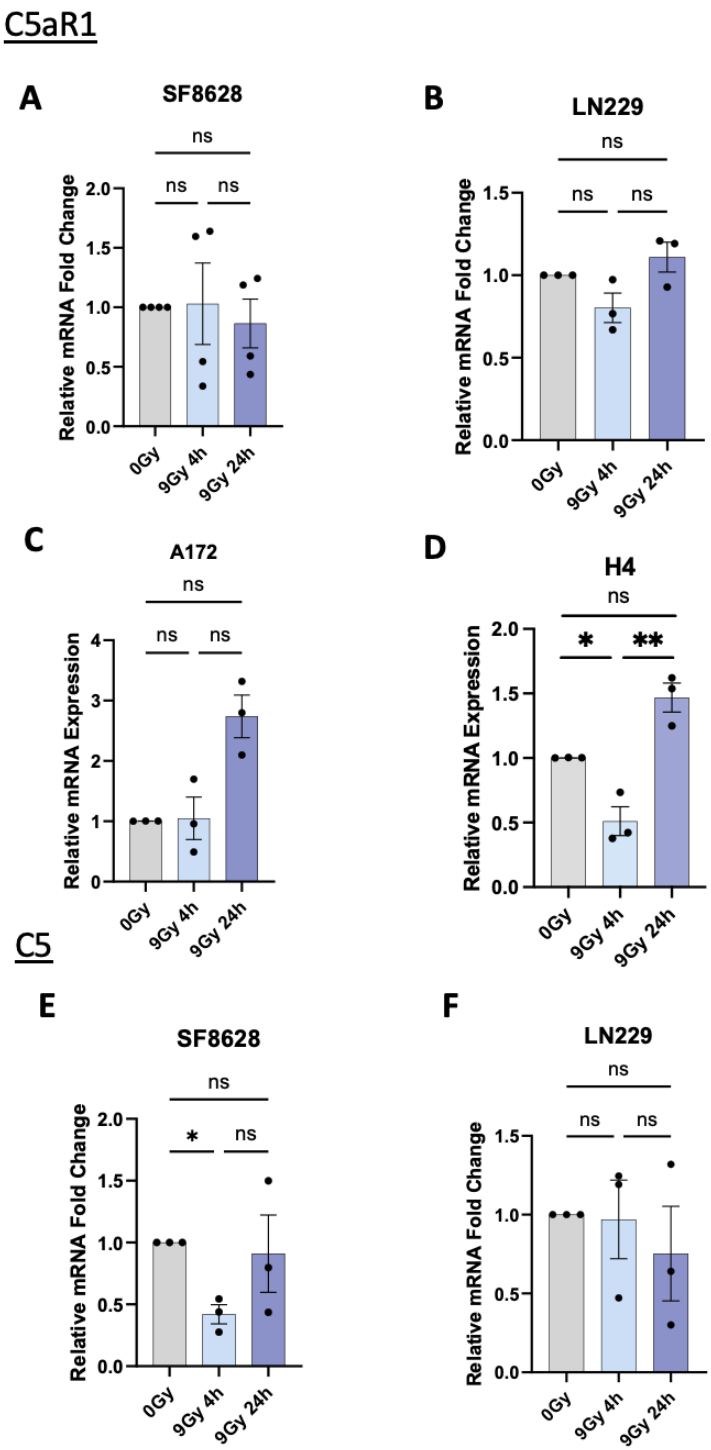

Figure 4.1 C5aR1 mRNA expression remains unchanged 24 h following irradiation

mRNA expression of **(A-D)** C5aR1 and **(E-F)** C5 were assessed by qPCR in SF8628, LN229, A172 and H4 cells at 4 h and 24 h following 0 or 9 Gy irradiation. All mRNA levels were normalised to GAPDH and expressed as fold change relative to the level of expression at 0 Gy. Data presented as mean ± SEM of biological replicates. n=3. Statistical analysis was performed on unnormalised values using one-way ANOVA with Tukey's test. *p≤0.05, **p≤0.01.

To validate C5aR1 expression at the protein level, flow cytometry was performed on SF8628 and LN229 cell lines. Consistent with the mRNA expression data in Figure 4.1A, irradiation did not result in significant changes in C5aR1 protein levels in SF8628 (Figure 4.2A). However, LN229 cells demonstrated a slight increase in both cell surface and total C5aR1 protein expression upon IR (Figure 4.2B). Additionally, we also directly compared C5aR1 protein levels between SF8628 and LN229 cells which revealed no statistically significant differences regardless of radiation dose (Figure 4.2C).

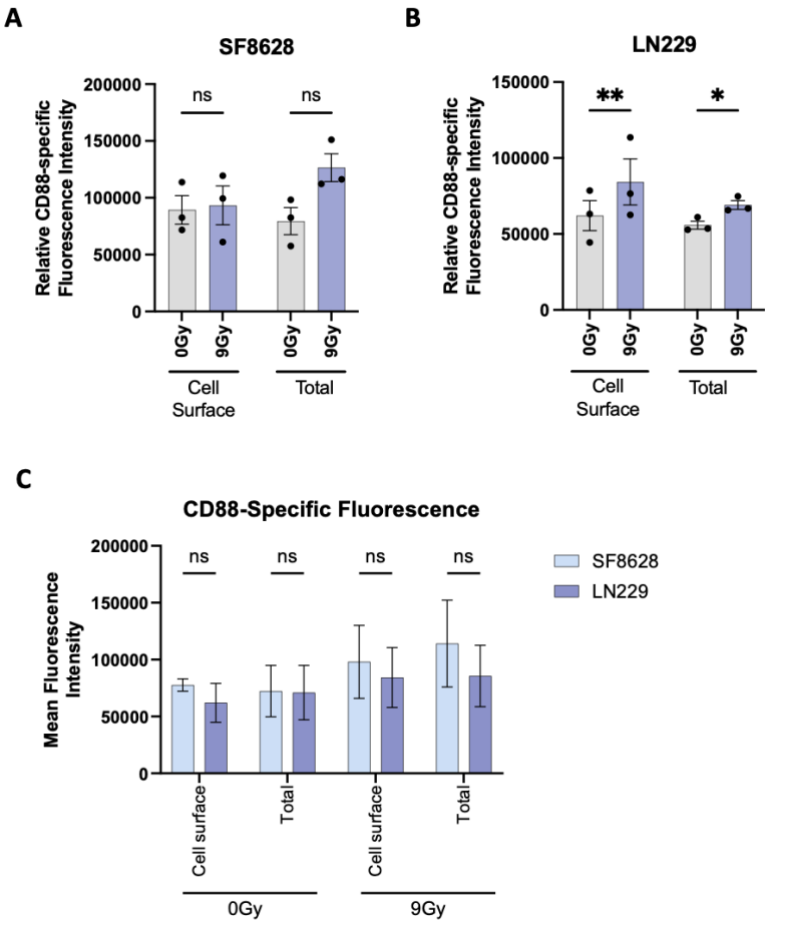

Figure 4.2 Modest upregulation of C5aR1 protein expression in LN229 post-irradiation

Cell surface and total (intracellular + surface) protein expression of C5aR1 was assessed in SF8628 and LN229 cells via flow cytometry 24 h after 0 or 9 Gy irradiation.

(A-B) Data presented as mean ± SEM of biological replicates. n=3. Statistical analysis used two-way ANOVA with Fisher's LSD test. *p≤0.05, **p≤0.01.
(C) Data presented as mean ± SEM of biological replicates. n=3. Statistical analysis used two-way ANOVA with Šidák's test.

4.2.2 Genetic silencing of C5aR1 under irradiation

To assess whether C5aR1 may regulate NF-κB and MAPK signalling following irradiation, we began with genetic silencing of C5aR1 to assess its role under irradiation stress, prior to examining the effects of pharmacological antagonists. Figure 4.3A-B shows that knockdown of C5aR1 in both SF8628 and LN229 cells resulted in a significant reduction in pRelA and pERK levels, regardless of radiation dose, suggesting attenuation of both NF-κB and MAPK signalling pathways. Interestingly, in our previous C5aR1 KD experiments conducted under normoxic conditions (21% O_2), no significant changes in NF-κB signalling were observed in either cell lines, and MAPK signalling remained unchanged in SF8628. These discrepancies may be caused by differences in the timing of sample collection. Moreover, although C5aR1 KD resulted in reduced levels of pRelA in SF8628 cells, decrease in total RelA expression was also observed consistently. This complicates the interpretation of NF-κB signalling activity, as it is unclear whether the reduction of pRelA reflects true pathway attenuation or is simply a consequence of diminished total protein levels. It is difficult to conclude whether C5aR1 KD suppresses NF-κB pathway activation in SF8628 cells. Nonetheless, our data suggest that under irradiation, C5aR1 plays a role in the activation of both NF-κB and MAPK signalling pathways, at least in LN229 cells.

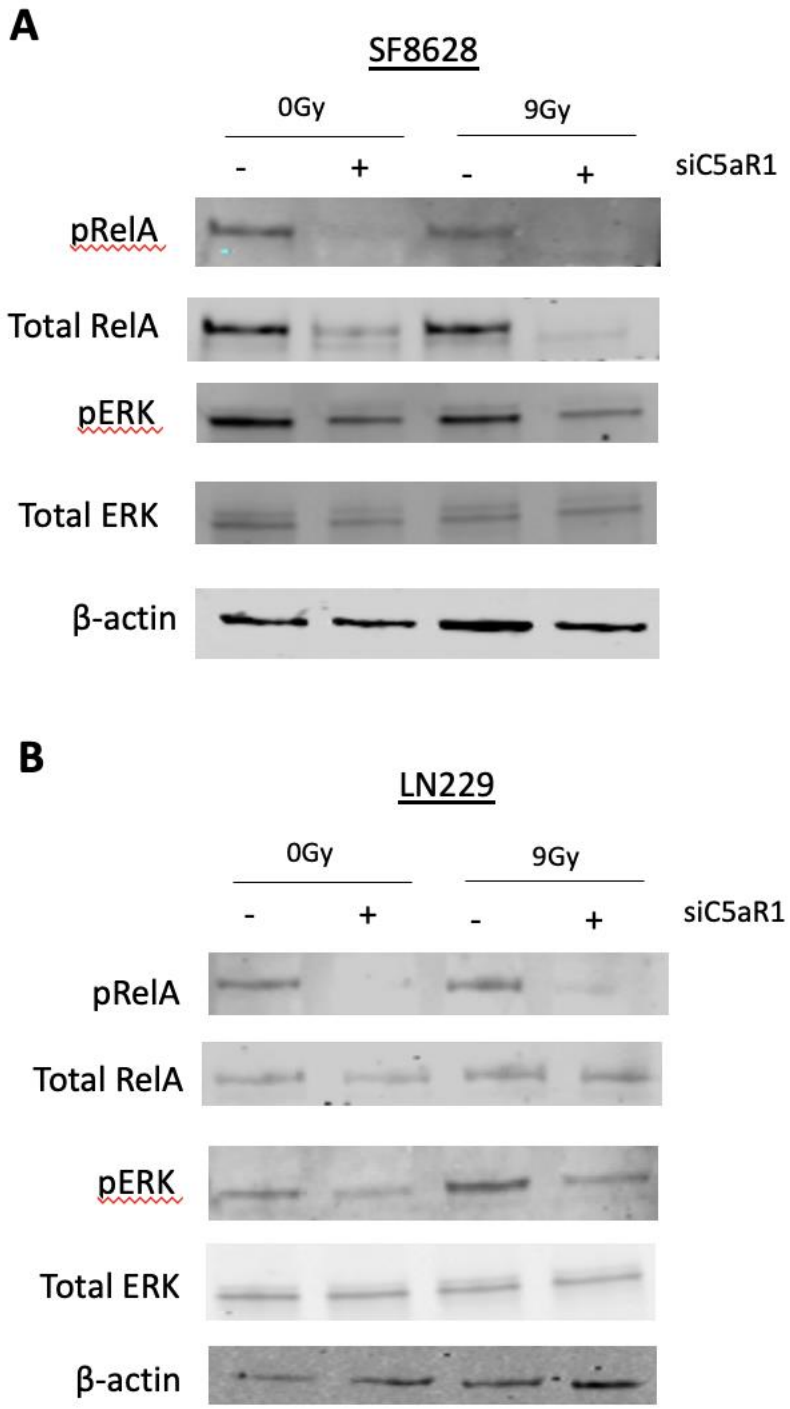

Figure 4.3 Silencing C5aR1 attenuates both NF-κB and MAPK signalling with or without irradiation

(A) SF8628 and **(B)** LN229 cells were transfected with Scr or C5aR1 siRNA before 0 or 9 Gy irradiation. Samples were harvested 24 h post-irradiation. Western blotting was carried out with the antibodies indicated. β-actin was used as loading control. n=3

We continued to investigate the functional consequences of C5aR1 gene silencing in radiation treatment by assessing its impact on cell proliferation and apoptosis. C5aR1 KD in LN229 cells led to a reduction in cell proliferation even in the absence of irradiation (0 Gy), likely reflecting the suppression of NF-κB and MAPK signalling which are both known to promote cell proliferation (Figure 4.4A) (Huang *et al.*, 2015; Zhang *et al.*, 2017). Importantly, the anti-proliferative effect of C5aR1 inhibition was more significant under irradiated conditions, with much slower cell growth in siC5aR1 cells at 9 Gy, compared to siScr controls at 9 Gy. In fact, there was almost no cell growth observed in the siC5aR1 + 9 Gy treated cells. In addition to reduced proliferation, the combination of C5aR1 silencing and irradiation also resulted in higher apoptotic counts than irradiation alone in both SF8628 and LN229 cells (Figure 4.4B-C). Irradiation alone already resulted in significantly more apoptosis events but combining it with C5aR1 KD enhances apoptosis even further, highlighting the importance of C5aR1 in protecting cells from radiation damage.

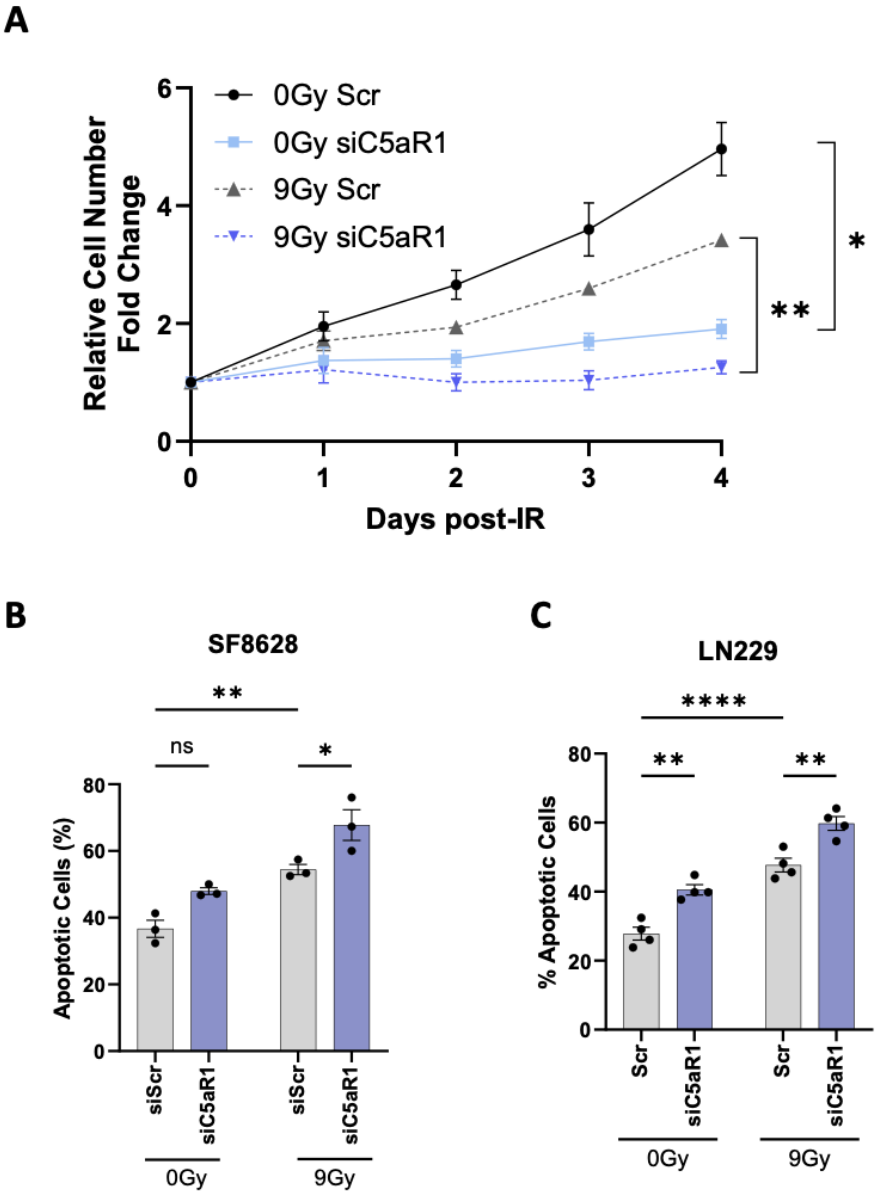

Figure 4.4 C5aR1 inhibition exerts greater anti-proliferation and anti-apoptosis effects under irradiation

SF8628 and LN229 cells were transfected with Scr or C5aR1 siRNA before 0 or 9 Gy irradiation.
(A) LN229 cells were counted after irradiation, and represented as fold change in relative to the cell number on day 0. Data presented as mean ± SEM of biological replicates. n=3 Statistical analysis used two-way ANOVA with Tukey's test for cell number on the final day of counting.
(B-C) At least 100 cells were analysed per condition via apoptosis assay 24 h post-irradiation. Data presented as mean ± SEM of biological replicates. n=3 and n=4 respectively. Statistical analysis used two-way ANOVA with Fisher's LSD test. *p≤0.05, **p≤0.01, ****p≤0.0001.

Irradiation is well known to exert anti-survival effects in a dose-dependent manner. In our study, we found that C5aR1 inhibition functions as a potential radiosensitiser in HGGs. In both SF8628 and LN229 cells, C5aR1 KD significantly reduced the surviving fractions of cells compared to siScr controls at matched radiation dose (Figure 4.5A-B). Conversely, C5aR1 overexpression conferred a radioprotective effect, in which it enhanced cell survival, with the effect being more prominent under irradiated conditions (Figure 4.5C). To isolate the effects of C5aR1 gene silencing under irradiation, survival fractions at each radiation dose were normalised to the respective 0 Gy control for each siRNA treatment. Of note, a radiation dose of 4 Gy was selected for clonogenic assays instead of 9 Gy which was used for most other experiments, due to the practical limitations associated with colony formation at higher radiation doses in this cell line. Taken together, these findings support the potential of C5aR1 inhibition in enhancing radiosensitivity in HGGs.

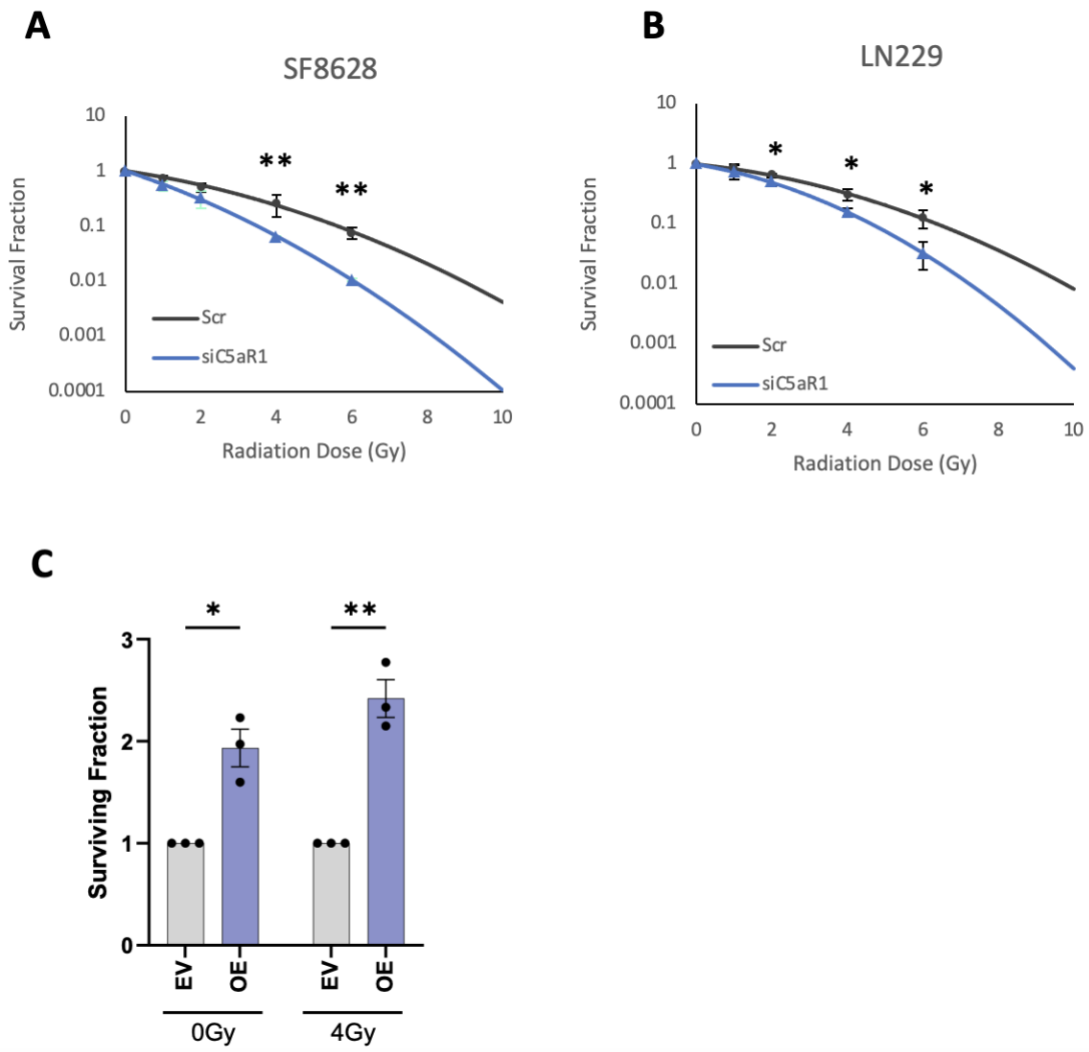

Figure 4.5 C5aR1 knockdown enhances cell radiosensitivity

(A-B) SF8628 and LN229 cells were transfected with Scr or C5aR1 siRNA, then irradiated at 0 or 9 Gy. Cell survival was assessed via clonogenic assay. Data point presented as mean ± SEM of biological replicates, with extrapolated line of best fit. n=3. Statistical analysis used two-way ANOVA with Šidák's test. *p≤0.05, **p≤0.01.

(C) SF8628 cells were transfected with empty vector or C5aR1 overexpressing plasmids. Cell survival was assessed via clonogenic assay. Data presented as mean ± SEM of biological replicates. n=3. Statistical analysis used two-way ANOVA with Šidák's test. *p≤0.05, **p≤0.01.

4.2.3 Pharmacological C5aR1 inhibition under irradiation

Our previous work in colorectal cancer models showed that PMX205 exerts its effects more effectively when administered prior to irradiation, acting as a priming agent that enhances susceptibility to radiation damage (Beach et al., 2023). Building upon these findings, we optimised the timing of PMX205 pre-treatment in HGG cells, ranging from 1 to 72 hours before irradiation (Appendix A, Figure A.2). The most pronounced effects were observed when PMX205 was administered 72 hours prior to irradiation. Despite its role as a C5aR1 antagonist, PMX205 had no significant impact on NF-κB signalling in both SF8628 and LN229 cells in this setting (Figure 4.6A-B). In contrast, PMX205 resulted in a marked reduction in pERK levels, both in the presence and absence of irradiation in LN229 cells, suggesting attenuation of MAPK signalling. Unexpectedly, no consistent changes in MAPK signalling were observed in SF8628 cells (quantification of bands are shown in Appendix A, Figure A.3). Although we cannot exclude the possibility of missed changes in pRelA levels due to timing of sample collection, our current data suggest that the primary mode of action of PMX205 involves attenuation of the MAPK signalling pathway, rather than NF-κB modulation, at least in LN229 cells.

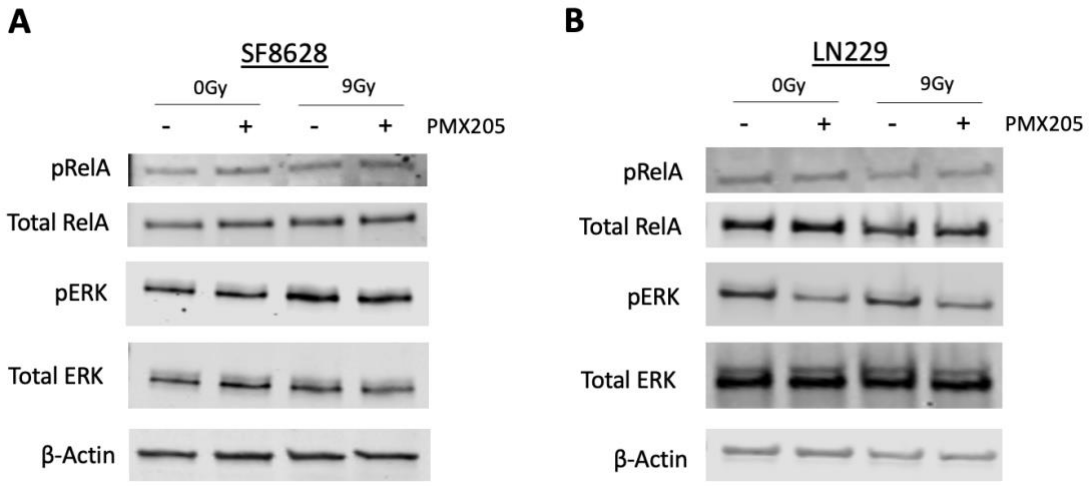

Figure 4.6 PMX205 attenuates MAPK signalling with or without irradiation

Vehicle (water) or PMX205 was added to **(A)** SF8628 and **(B)** LN229 cells for 72 h before 0 or 9 Gy irradiation. Samples were harvested 24 h post-irradiation. Western blotting was carried out with the antibodies indicated. β-actin was used as loading control. n=3

Functionally, given that PMX205 did not alter pro-survival signalling in SF8628 cells, we also did not observe any significant apoptotic changes with PMX205 treatment in SF8628 cells, as expected (Figure 4.7A). In LN229 cells, PMX205 treatment resulted in only a modest increase in apoptotic count, which appeared to be independent of irradiation dose, mirroring the attenuation of MAPK signalling previously observed with PMX205 treatment (Figure 4.7B). A similar trend was observed when cell survival was assessed via clonogenic assays: PMX205 treatment resulted in a slight reduction in surviving fraction of LN229 cells at both 0 and 9 Gy, while no significant effects were observed in SF8628 cells (Figure 4.8A-B). Collectively, these findings suggest that PMX205 exerts modest anti-survival effects in HGGs, with limited capacity to enhance radiation-induced cytotoxicity even after prolonged treatment duration.

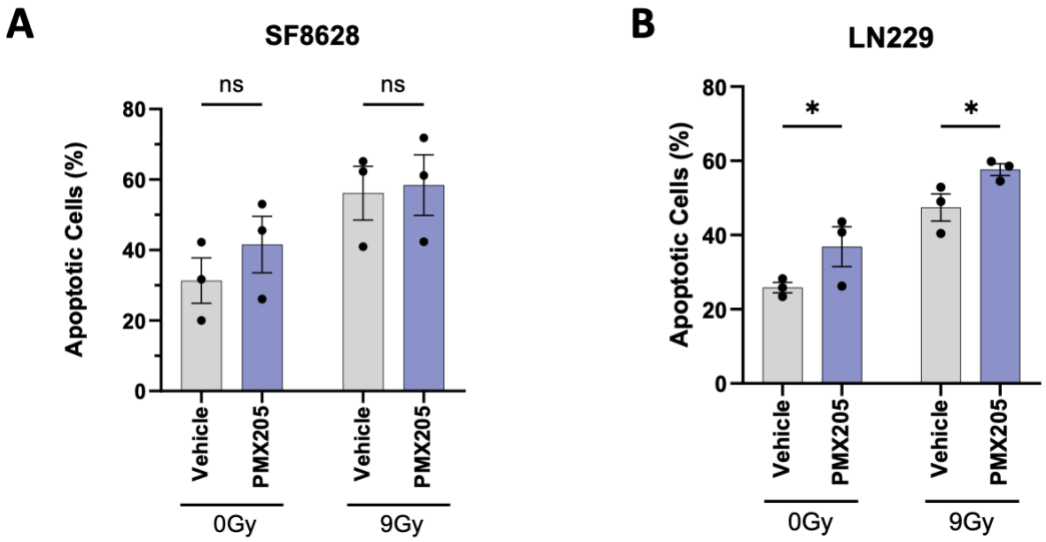

Figure 4.7 Modest pro-apoptotic effects of PMX205 in LN229

Vehicle (water) or PMX205 was added to **(A)** SF8628 and **(B)** LN229 cells for 72 h before irradiation at 0 or 9 Gy. At least 100 cells were analysed per condition via apoptosis assay 24 h post-irradiation. Data presented as mean ± SEM of biological replicates. n=3. Statistical analysis used two-way ANOVA with Fisher's LSD test. *p≤0.05.

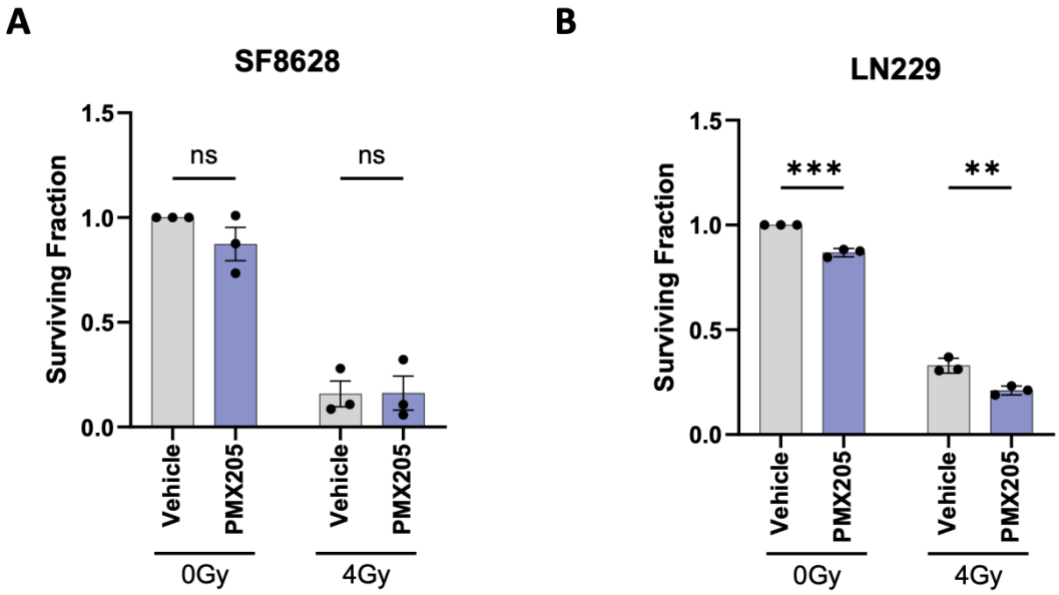

Figure 4.8 PMX205 improves radiosensitivity of LN229

Vehicle (water) or PMX205 was added to **(A)** SF8628 and **(B)** LN229 cells for 72 h before irradiation at 0 or 4 Gy. Cell survival was assessed via clonogenic assay. Data presented as mean ± SEM of biological replicates. n=3. Statistical analysis used two-way ANOVA with Šidák's test. **p≤0.01. ***p≤0.001.

Due to the limited functional effects observed with PMX205 in combination with irradiation, particularly in DMG cells, we extended our investigation to another selective C5aR1 antagonist, Avacopan, under radiation stress. Again, we used pRelA and pERK expression as downstream readouts of C5aR1 inhibition. While PMX205 had no significant effects on NF-κB signalling, Avacopan exhibited context-dependent modulation on this pathway. In SF8628 cells, Avacopan treatment led to an increase in pRelA level at 0 Gy; however, upon irradiation, it resulted in a slight reduction in pRelA level, and a marked suppression of pERK compared to vehicle controls, suggesting that Avacopan attenuated pro-survival signalling only when combined with irradiation in this cell line (Figure 4.9A).

In LN229 cells, Avacopan consistently reduced pERK expression regardless of irradiation dose, indicating significant attenuation of MAPK signalling (Figure 4.9B). Although a decrease in pRelA was also observed under both non-irradiated and irradiated conditions in some instances, this effect was not reproducible, implying that in both HGG cells lines, Avacopan primarily modulates the MAPK signalling pathway. Quantification of bands are shown in Appendix A, Figure A.4. Of note, a higher concentration of Avacopan and an extended pre-treatment duration were required to detect changes in pro-survival signalling in SF8628 cells compared to LN229 cells. Yet, changes in MAPK signalling were more prominent in LN229 cells, further highlight the potential of cell line-specific differences in drug sensitivity or C5aR1 signalling dynamics.

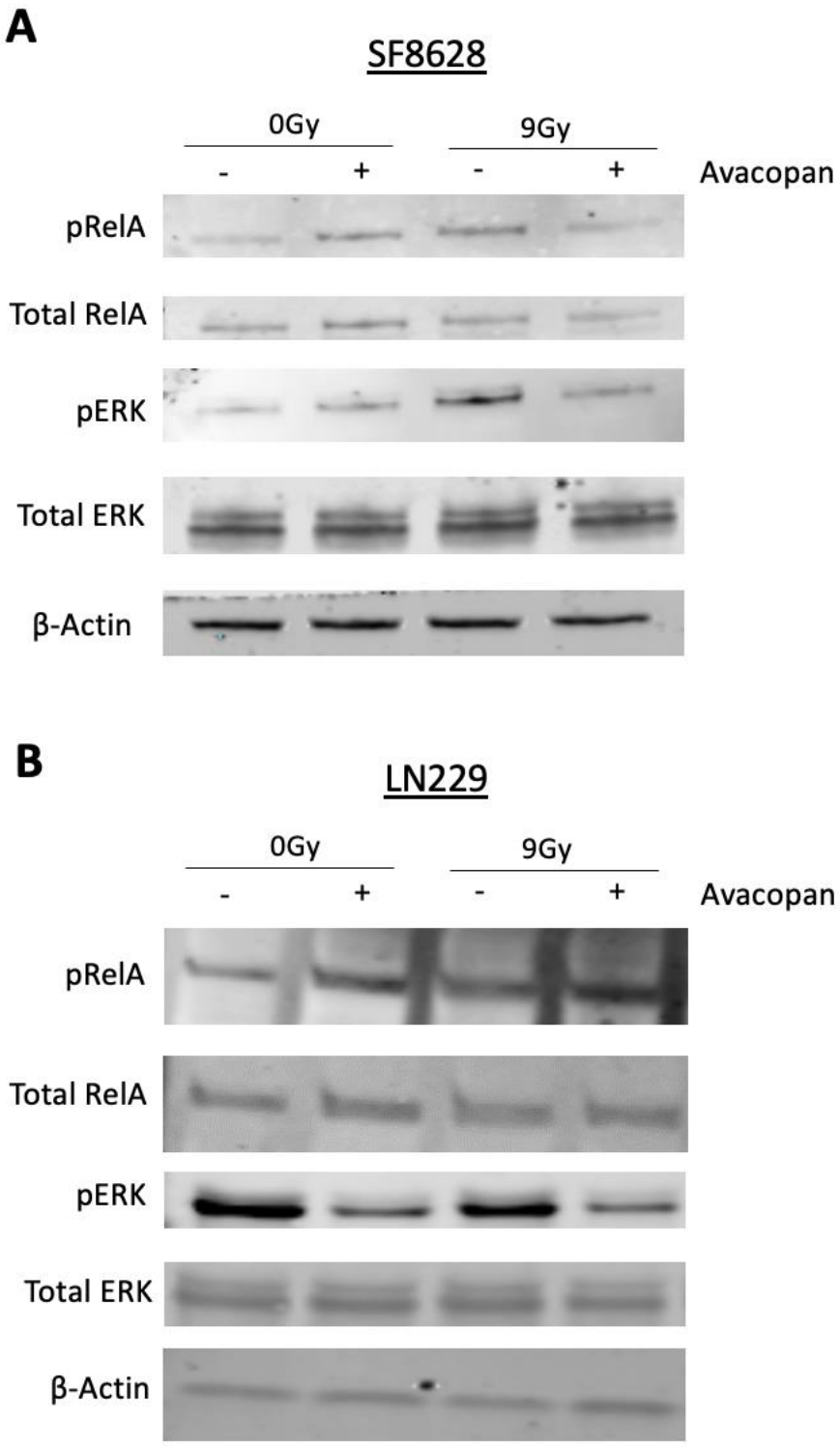

Figure 4.9 Avacopan attenuates both NF-κB and MAPK in a context-dependent manner

Vehicle (DMSO) or Avacopan was added to **(A)** SF8628 (48 h) and **(B)** LN229 (24 h) before irradiation at 0 or 9 Gy. Samples were harvested 24 h post-IR. Western blotting was carried out with the antibodies indicated. β-actin was used as loading control. n=3

MAPK signalling plays a key role in cell cycle progression through regulating cyclin D1 expression (Lavoie *et al.*, 1996). Interestingly, despite the observed attenuation of MAPK signalling following Avacopan treatment, no changes in cell cycle distribution were observed in both DMG and GBM cell lines (Figure 4.10A-B). To quantify cell cycle phases, cells were stained with propidium iodide (PI), which binds to DNA. Subsequent flow cytometry analysis enables assessment of DNA content across G1, S and G2 phases. As expected, exposure to 9 Gy irradiation induced cell cycle arrest, as shown by marked increased in the G2 population. However, Avacopan treatment did not lead to significant shifts in the population of cells within G1, S, or G2 phases when compared to vehicle-treated cells, irrespective of irradiation dose.

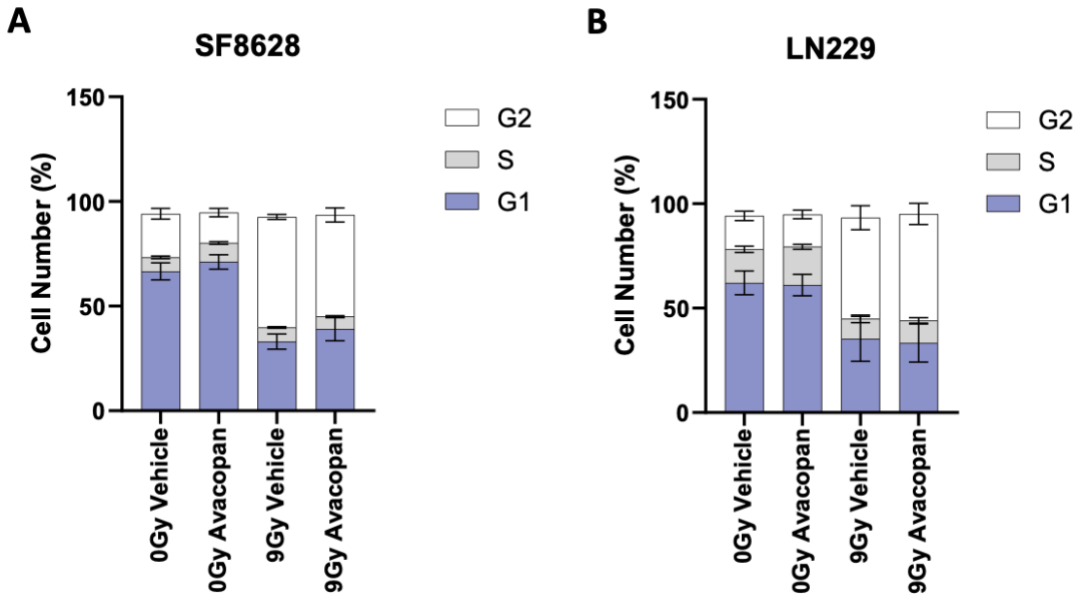

Figure 4.10 Avacopan does not alter the cell cycle

Vehicle (DMSO) or Avacopan was added to (**A)** SF8628 cells (48 h) and (**B)** LN229 cells (24 h) before irradiation at 0 or 9 Gy. Cell cycle was analysed via flow cytometry 16 h post-irradiation. Data presented as mean ± SEM of biological replicates. Statistical analysis used one-way ANOVA with Tukey's test. n=3.

To assess whether Avacopan modulates cell proliferation similarly to C5aR1 KD, we performed 7-8 days growth analyses combined with or without irradiation. At baseline (0 Gy), Avacopan treatment unexpectedly exhibited a trend towards increased proliferation, particularly between day 6-8 of measurement in both SF8628 and LN229 cells (Figure 4.11A-B). However, this effect did not reach statistical significance. Irradiation alone resulted in a pronounced suppression of cell growth, reflected by a plateaued proliferation curve. Under irradiated conditions, repeated dosing with Avacopan resulted in a modest, yet statistically significant reduction in cell proliferation on the final day of measurement, suggesting that its effects may be potentiated by radiation stress. Avacopan treatment therefore recapitulated the anti-proliferative trend observed with C5aR1 gene silencing.

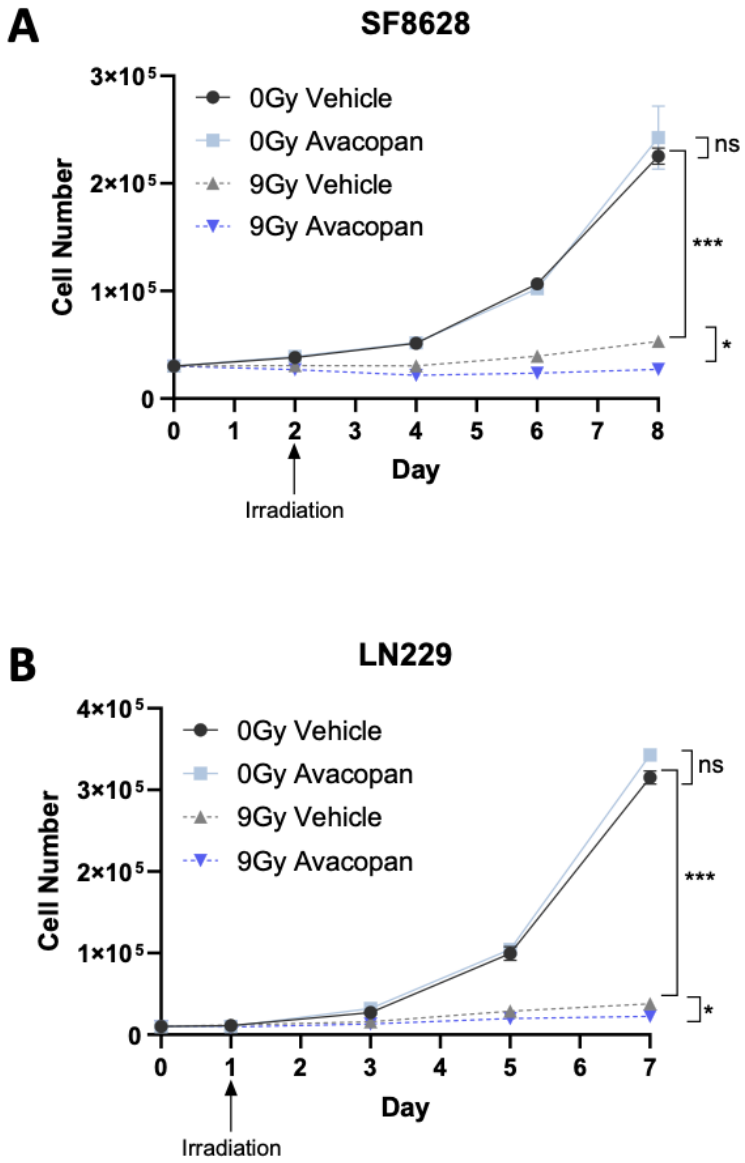

Figure 4.11 Modest reduction in cell proliferation with Avacopan treatment under irradiation

Vehicle (DMSO) or Avacopan was added to **(A)** SF8628 (48 h) and **(B)** LN229 cells (24 h) on day 0, with subsequent dosing coinciding with each cell counting time point. Cells were irradiated at 0 or 9 Gy on day 2 for SF8628 cells, and on day 1 for LN229 cells. Cell number was counted on the following dates. Data presented as mean ± SEM of biological replicates. n=3. Statistical analysis used two-way ANOVA with Tukey's test. *p≤0.05, ***p≤0.001.

We continued to evaluate the functional effects of Avacopan in HGG models by performing apoptosis assays under irradiated and non-irradiated conditions. As expected, irradiation alone significantly increased apoptotic count by around 25%. Notably, the combination of irradiation with Avacopan treatment resulted in a further increase in apoptotic count across all cell lines tested (Figure 4.12A-D). Although the increases in apoptosis were modest, they were significant. Importantly, this pro-apoptotic effect of Avacopan was only observed under irradiated conditions, as treatment under 0 Gy did not elicit significant changes in cell death. These findings indicate that Avacopan did not act as a direct cytotoxic agent but rather potentiated radiation-induced apoptosis.

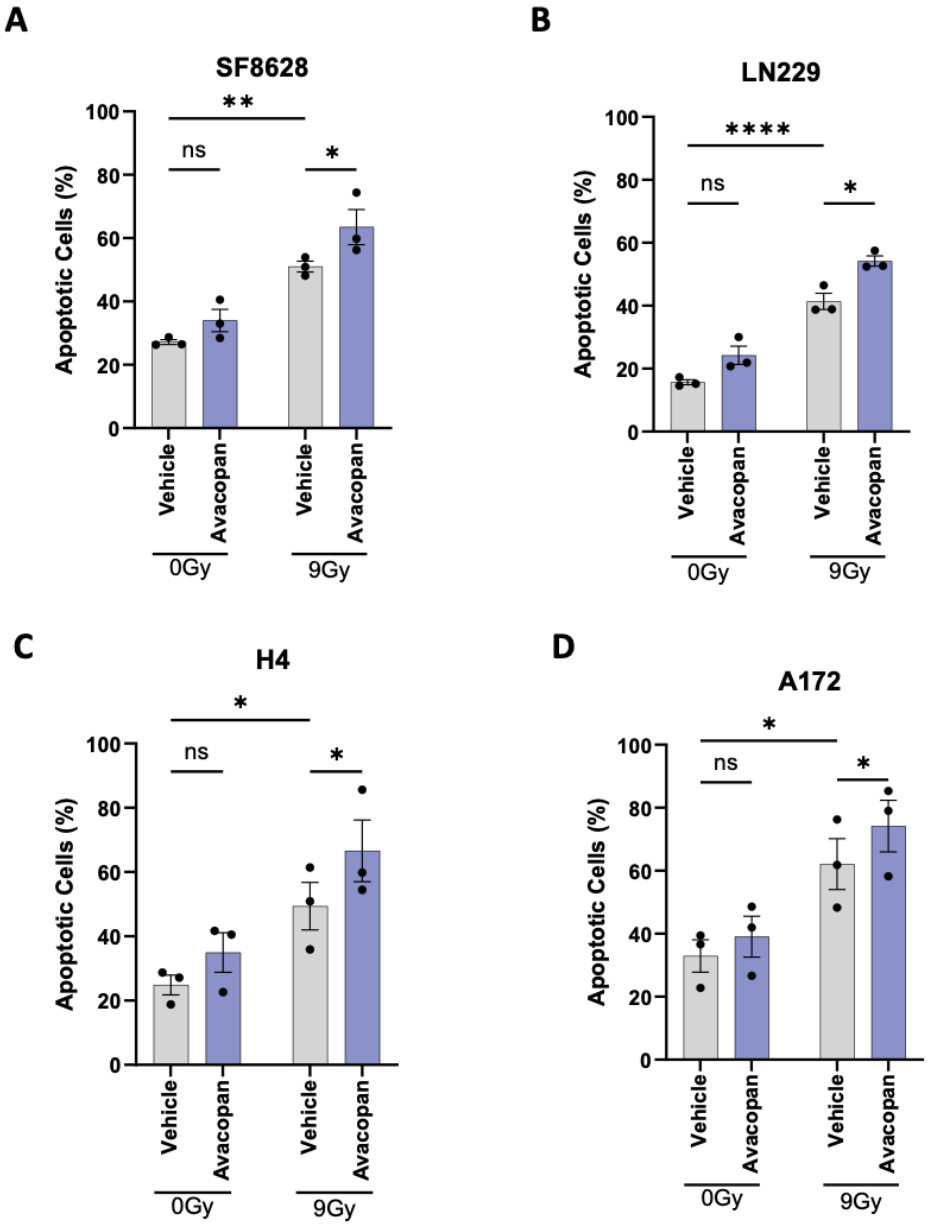

Figure 4.12 Pro-apoptotic effect of Avacopan was only evident under irradiation

Vehicle (DMSO) or Avacopan was added to **(A)** SF8628 cells (48h), **(B-D)** LN229, H4 and A172 cells (24 h) before irradiation at 0 or 9 Gy. At least 100 cells were analysed per condition via apoptosis assay 24 h post-irradiation. Data presented as mean ± SEM of biological replicates. n=3. Statistical analysis used two-way ANOVA with Fisher's LSD test. *p≤0.05, **p≤0.01, ****p≤0.0001.

Next, we investigated the anti-survival of Avacopan using two approaches. First, a dose-response MTT cell viability assay was performed across a range of Avacopan concentrations. In Figure 4.13A-B, data for each condition were normalised to the corresponding 0 μM control within each radiation dose group (e.g. 0 Gy 0 μM vs 0 Gy 4 μM; 4 Gy 0 μM vs 4 Gy 4 μM) to isolate drug-specific effects. Under non-irradiated conditions, Avacopan treatment up to 8 μM did not significantly impact cell viability in either SF8628 or LN229 cells (Figure 4.13A-B). In contrast, under irradiation, Avacopan significantly decreased cell viability in a dose-dependent manner from 1-2 μM onwards, indicating that its anti-survival effect is potentiated by radiation, and is otherwise negligible in non-stressed condition, at least for doses below 8 μM.

To evaluate the sustained effects of Avacopan treatment, clonogenic survival assays were also performed using fixed concentrations tailored to each cell line. In alignment with earlier viability data, Avacopan alone did not significantly affect cell survival under non-irradiated conditions in SF8628 and LN229 cells (Figure 4.14A-B). However, when combined with irradiation, Avacopan treatment resulted in a significant reduction in cell survival in both cell lines. A comparable trend was also observed in another GBM cel line H4, which similarly exhibited reduced in survival when Avacopan was combined with irradiation treatment (Figure 4.14C). These findings all support the role of Avacopan as a radiosensitiser in HGGs, enhancing cellular susceptibility to radiation-induced cytotoxicity.

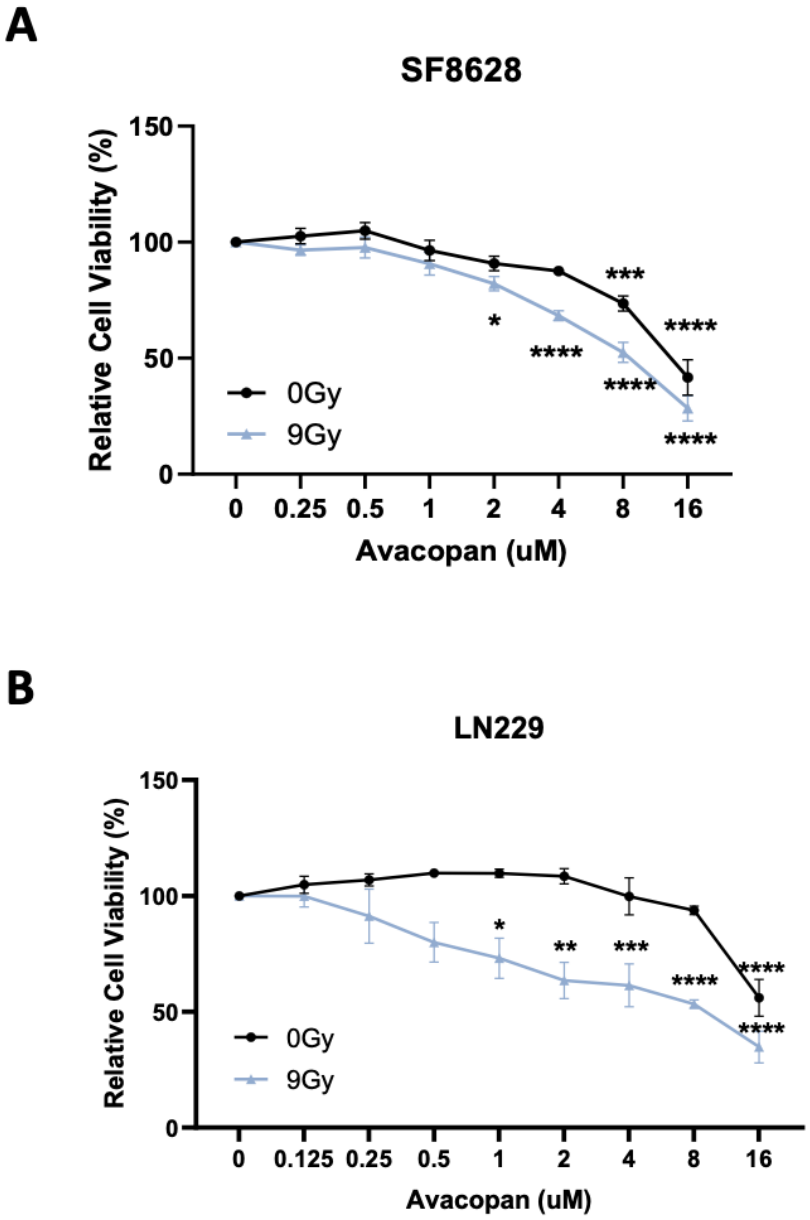

Figure 4.13 Avacopan reduces cell viability at a lower concentration under irradiation

0-16 uM Avacopan was added to **(A)** SF8628 and **(B)** LN229 cells for 24 h before 0 or 9 Gy irradiation. Cell viability was assessed using MTT assay 24 h post-irradiation and normalised to the corresponding 0 uM control for each radiation condition. Data presented as mean ± SEM of biological replicates. n=3. Statistical analysis between each condition and the corresponding 0 uM control was performed using two-way ANOVA with Šidák's test. *p≤0.05, **p≤0.01, ***p≤0.001, ****p≤0.0001.

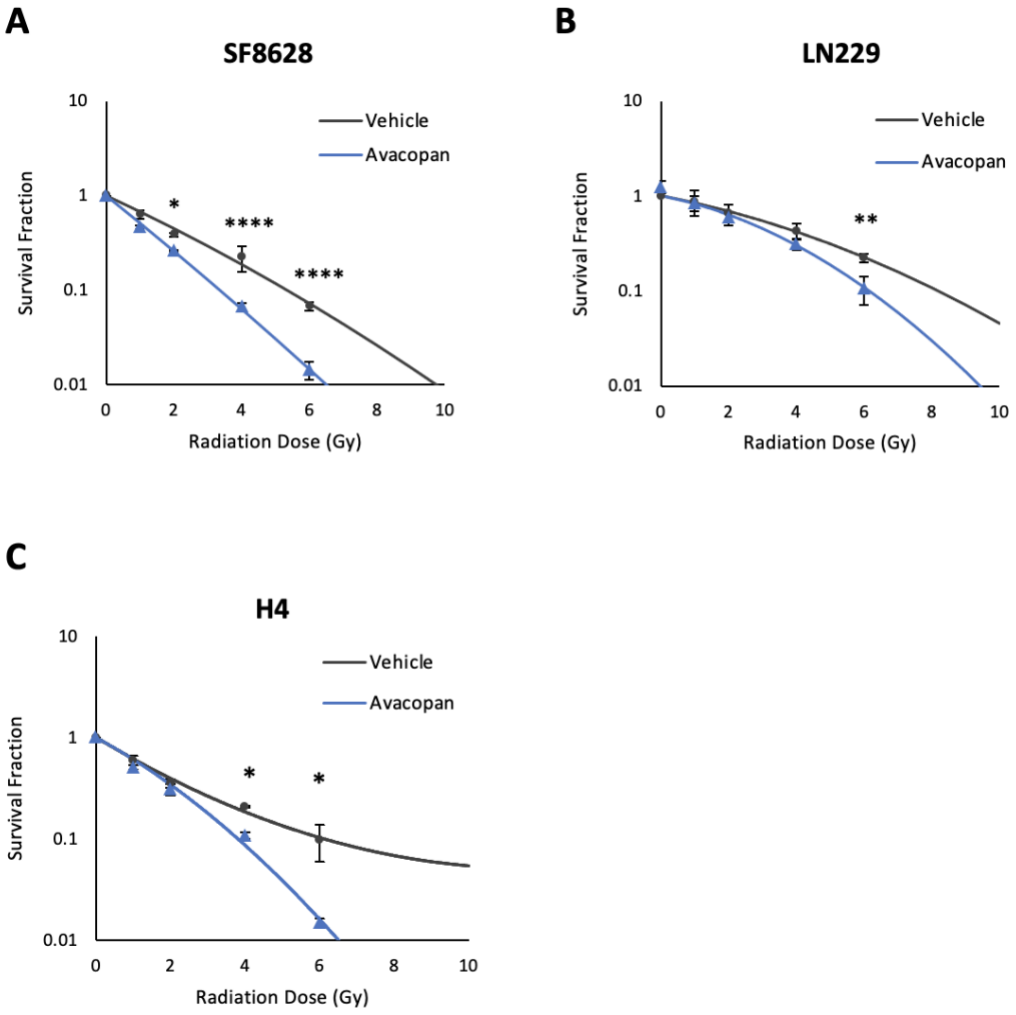

Figure 4.14 Avacopan improves radiation sensitivity of HGGs

Vehicle (DMSO) or Avacopan was added to **(A)** SF8628 cells (48 h), **(B)** LN229 and **(C)** H4 (24 h) before 0-6 Gy irradiation. Cell survival was assessed via clonogenic assay. Data point presented as mean ± SEM of biological replicates, with extrapolated line of best fit. n=3. Statistical analysis used two-way ANOVA with Šidák's test. *p≤0.05, **p≤0.01, ***p≤0.001, ****p≤0.0001.

4.2.4 Hypoxia and Radioresistance

Having established the potential role of C5aR1 in modulating radiosensitivity of HGG cells, we next aimed to assess if this impact persists under hypoxic stress. Due to limited oxygen availability to react with free radicals to exert indirect damage, hypoxia is a well-established contributor to cell radioresistance. Given the hypoxic nature of HGGs, we first confirmed that both SF8628 and LN229 cells were less sensitive to radiation following exposure to <0.1% O_2 for 16 hours prior to irradiation (Figure 4.15A-B) (Evans *et al.*, 2004; Yeom *et al.*, 2015). To maintain hypoxic conditions during irradiation, cells were transferred directly from the hypoxia chamber into sealed, airtight irradiation boxes, remaining under hypoxia throughout the irradiation process (as described in methods section 2.2.6). Following irradiation, cells were returned to normoxic (21% O_2) conditions for colony formation, due to the technical challenges associated with sustaining long-term cell growth under hypoxia. Nevertheless, the calculated OER was approximately 2.8 for SF8628 cells and 2.2 for LN229 cells, meaning these cells were at least two times more resistant to irradiation under severe hypoxia.

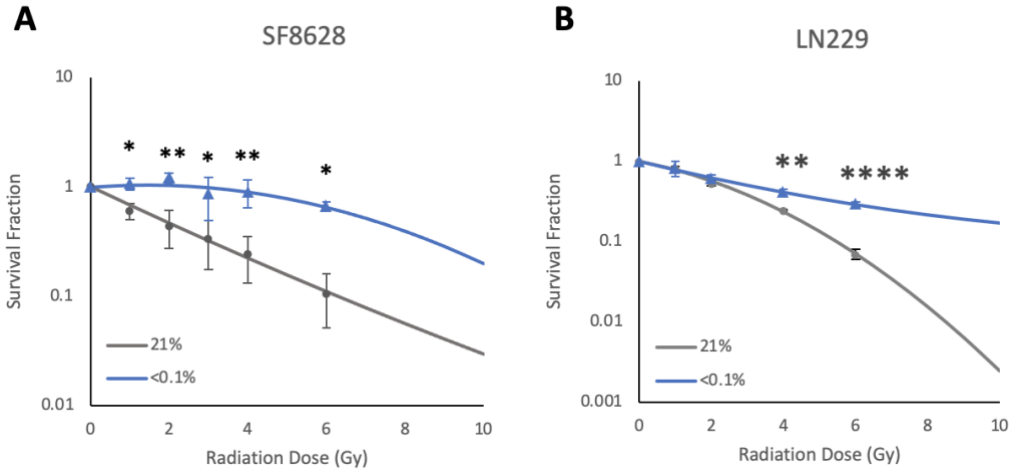

Figure 4.15 Hypoxia contributes to radioresistance in HGGs

(A) SF8628 and **(B)** LN229 cells were exposed to 21% or <0.1% O_2 for 16 h, followed by 0 or 9 Gy irradiation. Cell survival was assessed via clonogenic assay. Data presented as mean ± SEM of biological replicates, with extrapolated line of best fit. n=3. Statistical analysis of each radiation dose between two oxygen levels used two-way ANOVA with Šidák's test. *p≤0.05, **p≤0.01, ****p≤0.0001.

Since we previously observed an induction of C5aR1 expression under severe hypoxia, as shown in Figure 3.2, we therefore next assessed whether irradiation in a hypoxic environment would further modulate C5aR1 levels. SF8628 and LN229 cells were irradiated under <0.1% O_2 and C5aR1 mRNA levels were measured 24 hours later. Surprisingly, no significant changes in C5aR1 expression were observed in either cell line under hypoxia + irradiation compared to hypoxia alone, though we might have missed any transient changes post-irradiation due to timing of sample collection or re-oxygenation (Figure 4.16A-B). The combination of hypoxic and irradiation stress did not appear to synergistically influence C5aR1 levels. Although LN229 showed a trend towards increased C5aR1 expression following irradiation at both 0 Gy and 9 Gy, the difference did not reach statistical significance due to biological variability across replicates.

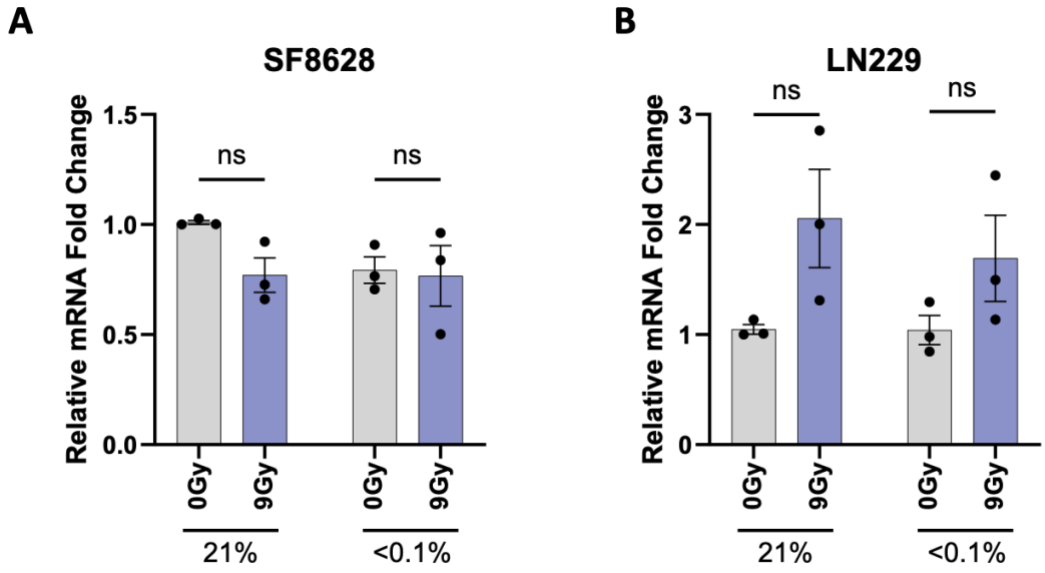

Figure 4.16 C5aR1 expression remains unchanged following irradiation under hypoxic conditions

(A) SF8628 and **(B)** LN229 cells were exposed to 21% or <0.1% O_2 for 16 h, then irradiated at 0 or 9 Gy. mRNA expression of C5aR1 were assessed via qPCR 24 h post-irradiation. All mRNA levels were normalised to 18S and expressed as fold change relative to the level of expression of 21% 0 Gy. Data presented as mean ± SEM of biological replicates. n=3. Statistical analysis was performed on unnormalised values using two-way ANOVA with Šidák's test.

Building on our investigation of C5aR1 expression changes, we next sought to determine whether C5aR1 remains functionally important for modulating glioma cell responses to irradiation under hypoxia. In both SF8628 and LN229 cells, C5aR1 knockdown resulted in a modest reduction in pRelA levels following 9 Gy irradiation at under <0.1% O_2, compared to siScr controls (Figure 4.17A-B). However, this decrease in pRelA was accompanied by a concurrent reduction in total RelA expression, complicating interpretation of NF-κB pathway activity, as it remains unclear whether reduced pRelA levels was truly attenuation of NF-κB signalling or simply diminished protein abundance. A similar trend was observed for MAPK signalling in SF8628 cells, where C5aR1 KD reduced both pERK and total ERK levels under hypoxia, making it difficult to draw definitive conclusions regarding pathway modulations in this cell line (Figure 4.17A).

In contrast, LN229 cells exhibited a more consistent, definitive response. C5aR1 KD robustly attenuated MAPK signalling, as indicated by a significant reduction in pERK levels across both normoxic and hypoxic conditions, and independent of irradiation dose or oxygen level (Figure 4.17B). Notably, in siScr-treated controls, pERK levels were elevated under hypoxia and further increased following irradiation. However, C5aR1 silencing successfully restored pERK to levels comparable to normoxic siC5aR1-treated cells. These findings suggest that C5aR1 maintains its ability to regulate MAPK signalling under combined hypoxic and radiation stress, at least within LN229 cells.

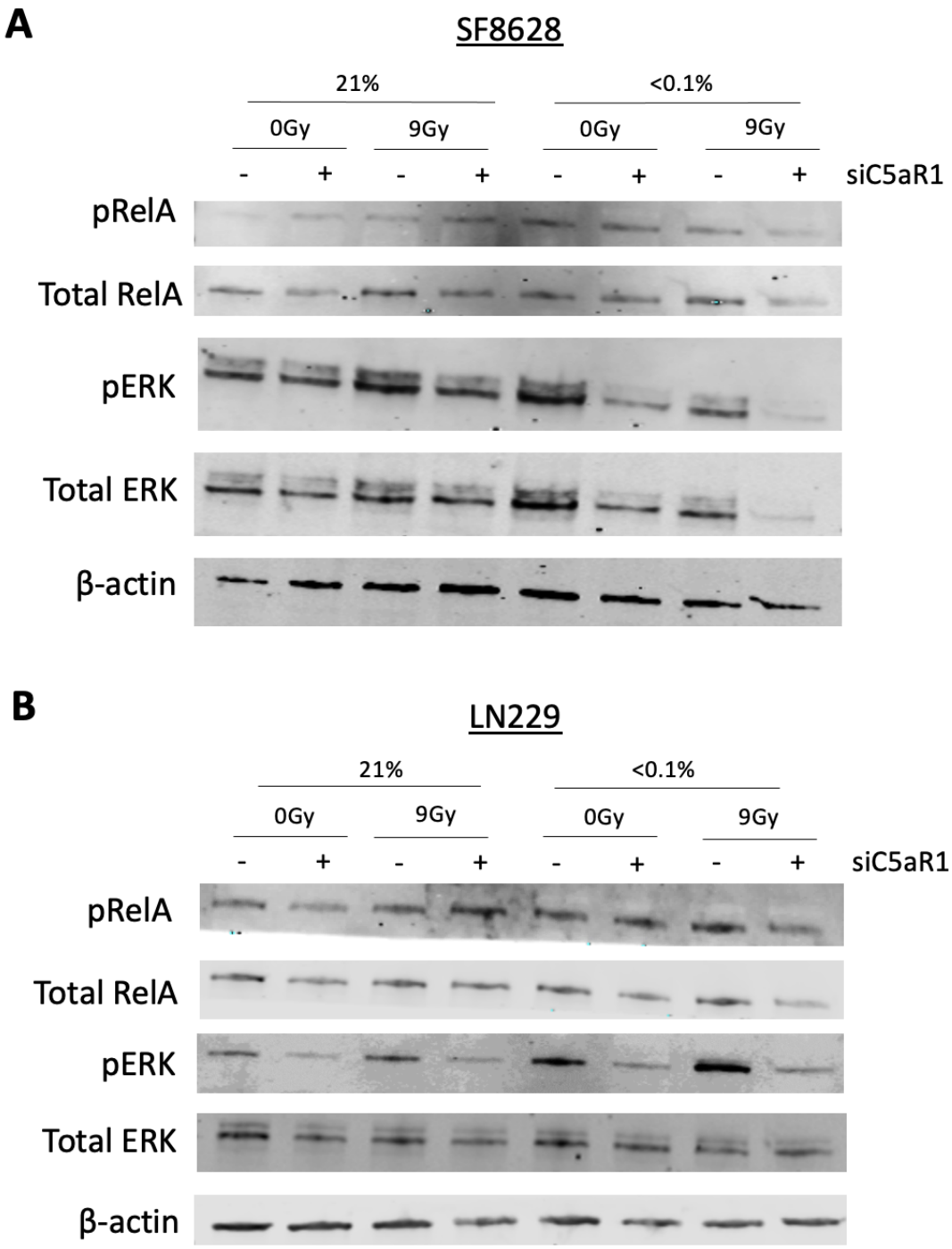

Figure 4.17 C5aR1 modulates MAPK signalling in LN229 under combined hypoxic and radiation stress

(A) SF8628 and **(B)** LN229 cells were transfected with Scr or C5aR1 siRNA before exposure to 21% or <0.1% O2 for 16 h. Following hypoxia exposure, cells were irradiated at 0 or 9 Gy. Samples were harvested 24 h post-irradiation. Western blotting was carried out with the antibodies indicated. β-actin was used as loading control. n=3

Functionally, 4 Gy irradiation alone had a diminished anti-survival effect on both cell lines under hypoxic conditions compared to normoxia, consistent with the known role of hypoxia in promoting radioresistance as demonstrated in Figure 4.15. To allow direct comparison of treatment effects between 0 Gy and 4 Gy within each oxygen level, all data at 21% O_2 were normalized to the 21% 0 Gy Scr control, and all data at <0.1% O_2 were normalised to the <0.1% 0 Gy siScr control. This approach enabled clearer interpretation by isolating relative changes within each oxygen level, minimising confounding effects of baseline differences between normoxic and hypoxic conditions. Relative to these controls, Figure 4.18A-B shows that C5aR1 KD significantly reduced cell survival across both non-irradiated and irradiated conditions at both oxygen levels. These survival effects were consistent with prior findings under normoxia (Figure 4.5) and were maintained following hypoxic treatment. Together, these results demonstrate that C5aR1 supports glioma cell survival in both normoxic and hypoxic environments, and that its silencing enhances radiosensitivity even under conditions typically associated with resistance.

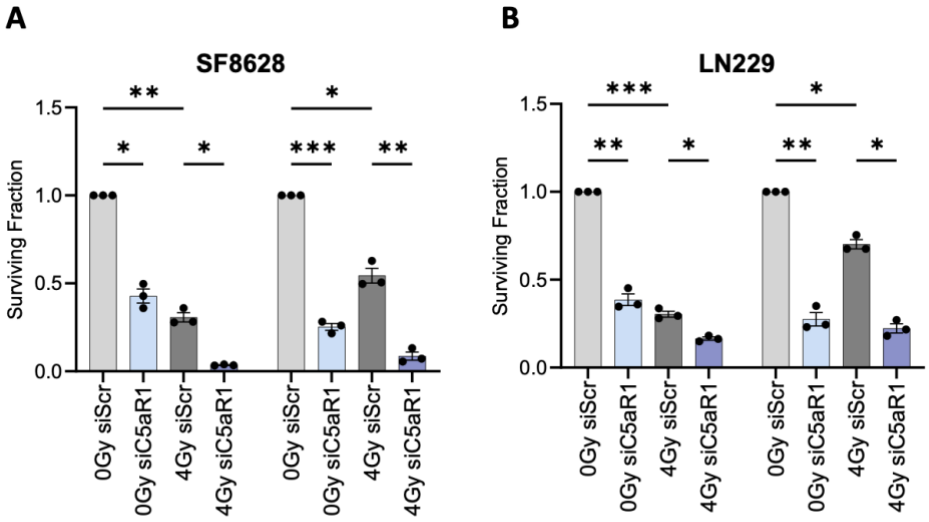

Figure 4.18 Radiosensitising effects of C5aR1 silencing retains under hypoxia

(A) SF8628 and **(B)** LN229 cells were transfected with Scr or C5aR1 siRNA before exposure to 21% or <0.1% O2 for 16 h. Cells were then irradiated at 0 or 4 Gy. Cell survival was assessed via clonogenic assay. Data presented as mean ± SEM of biological replicates. n=3. Statistical analysis used two-way ANOVA with Tukey's test. *p≤0.05, **p≤0.01, ***p≤0.001.

We next explored whether pharmacological inhibition of C5aR1 could similarly enhance radiosensitivity and offer a more clinically translatable therapeutic strategy compared to genetic knockdown. In SF8628 cells, treatment with PMX205 did not affect pRelA expression under normoxia, same as what we previously observed in Figure 4.6. At hypoxic conditions, PMX205 treatment resulted in a modest reduction in pRelA levels, at both 0 Gy and 9 Gy (Figure 4.19A). However, no comparable decrease was observed in LN229 cells, suggesting that PMX205-mediated attenuation of NF-κB signalling may be cell line-specific in the context of hypoxia and irradiation (Figure 4.19B). In contrast, PMX205 treatment resulted in a more pronounced reduction in pERK levels in LN229 cells when combined with irradiation, especially under hypoxic conditions, resembling the MAPK suppression effect seen with C5aR1 KD under hypoxia (Figure 4.17B). While this observation supports the potential of PMX205 attenuating MAPK signalling under stress conditions, the concurrent reductions in total ERK levels complicates interpretation of PMX205-indued modulation of pro-survival signalling pathways in these cells.

To determine whether the observed modulations of pro-survival pathways translate into functional outcomes, we assessed the impact of PMX205 on the survival of HGG cells under both hypoxia and irradiation. Despite modest reduction in pRelA levels, PMX205 treatment had no significant impact on the survival of SF8628 cells under all condition tested (Figure 4.20A). Similarly, despite potential attenuation of MAPK signalling in LN229 cells, PMX205 treatment only resulted in a modest reduction in cell survival at 0 Gy, under hypoxia only (Figure 4.20B). We also prolonged the pre-treatment duration of PMX205, but a similar trend was observed with no significant reduction in cell survival (data not included). These findings suggest that the anti-survival effects of PMX205 are limited and are insufficient to enhance radiosensitivity in our HGG models.

Overall, PMX205 appears to have limited efficacy as a radiosensitiser in the context of hypoxia.

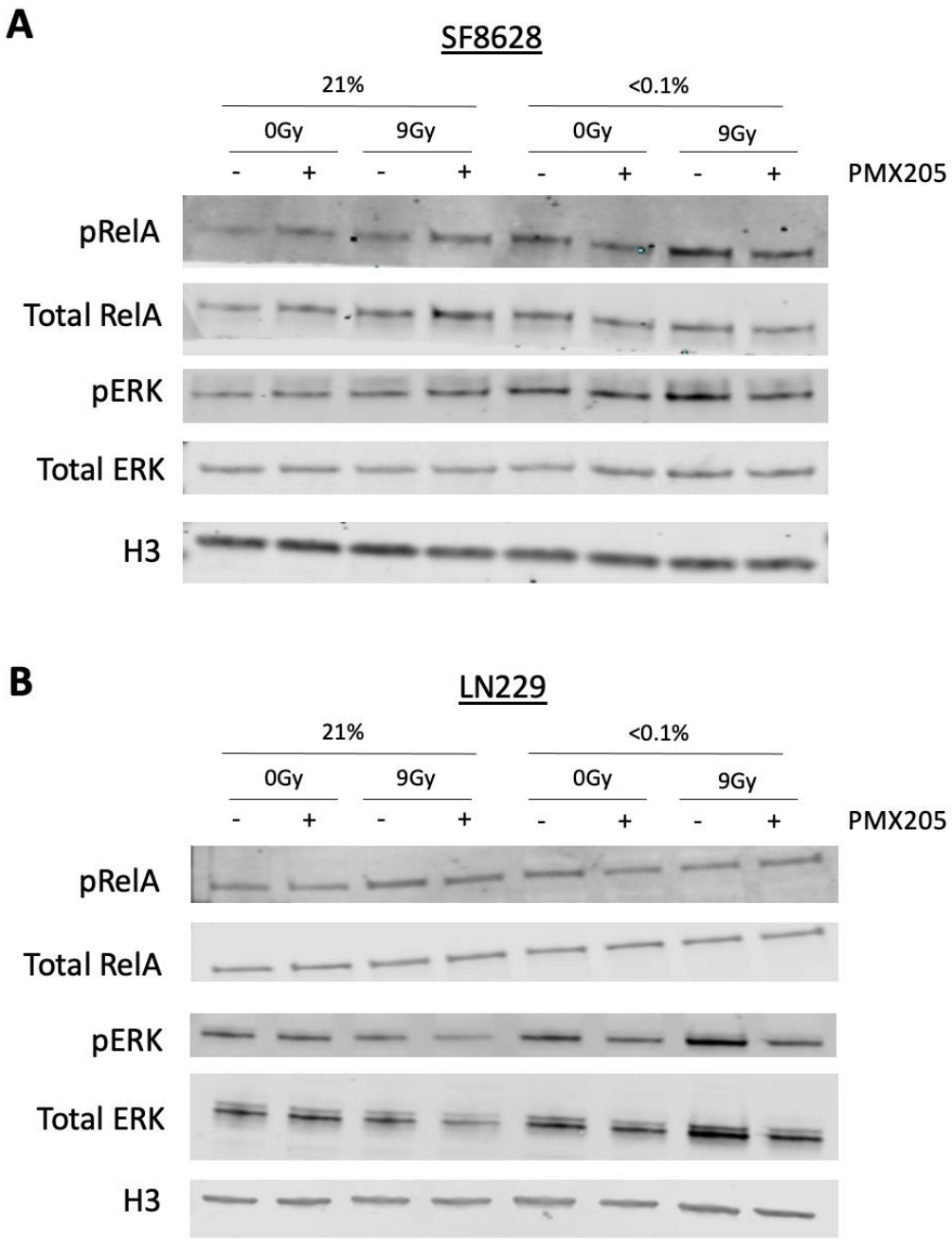

Figure 4.19 Modest changes in pro-survival signalling with PMX205 when combined with irradiation, under hypoxia

Vehicle (water) or PMX205 was added to **(A)** SF8628 and **(B)** LN229 cells for 32 h before exposure to 21% or <0.1% O2 for 16 h. Cells were then irradiated at 0 or 9 Gy and samples were harvested 24 h post-irradiation. Western blotting was carried out with the antibodies indicated. H3 was used as loading controls. n=3.

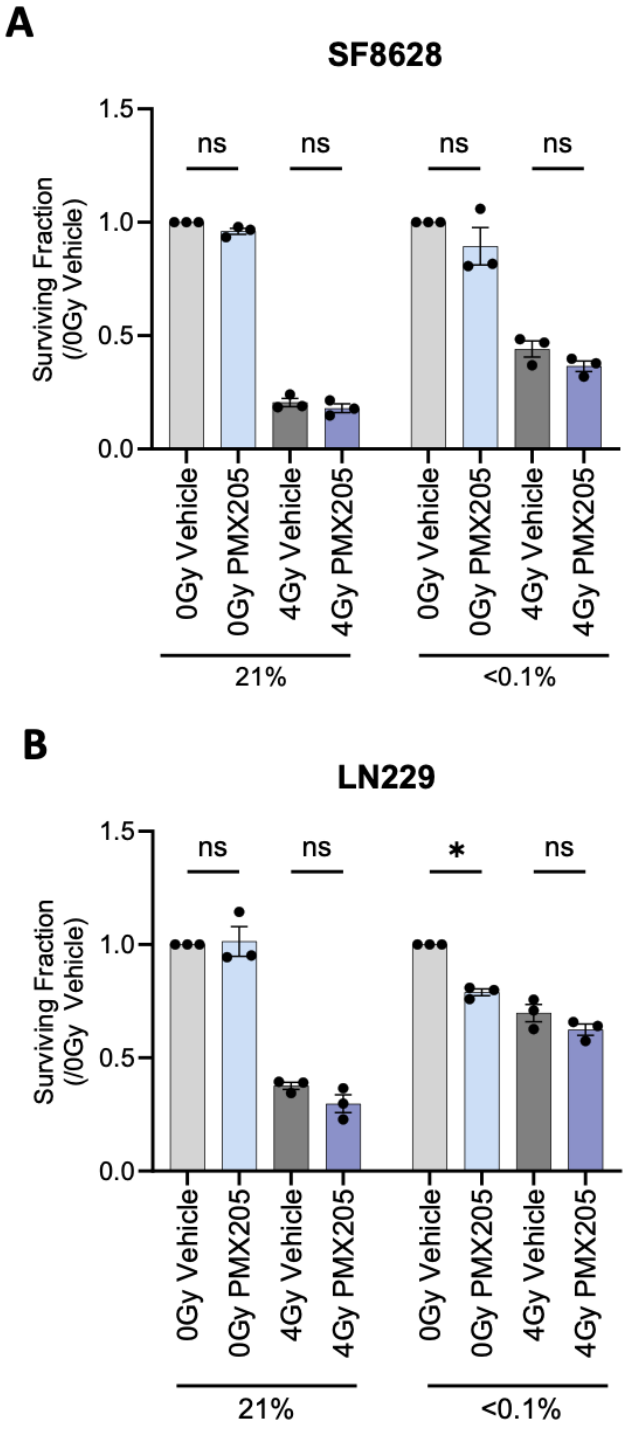

Figure 4.20 Limited anti-survival effects of PMX205 under hypoxia and irradiation

Vehicle (water) or PMX205 was added to **(A)** SF8628 and **(B)** LN229 cells for 32 h before exposure to 21% or <0.1% O2 for 16 h. Cells were then irradiated at 0 or 4 Gy and incubated at 21% post-irradiation. Cell survival was assessed via clonogenic assay. Data presented as mean ± SEM of biological replicates. n=3. Statistical analysis used two-way ANOVA with Tukey's test. *p≤0.05.

Given the limited radiosensitising effects observed with PMX205, we turned our attention to Avacopan, to evaluate whether a different pharmacological inhibition strategy could more effectively impair HGG cell survival under both hypoxic and irradiation stress. Although modest reductions in both pRelA and pERK expression were observed in SF8628 cells following Avacopan treatment under hypoxic and irradiation, there were again concurrent changes at the total protein levels (Figure 4.21A). To our surprise, no major changes in pro-survival signalling were detected in LN229 cells, which was different to what we previously observed, at least with irradiation under normoxia, this difference was potentially caused by different treatment duration and sampling time collection (Figure 4.21B).

Functionally, in SF8628 cells, dual treatment with Avacopan and irradiation reduced cell survival under both normoxic and hypoxic conditions, compared to vehicle-treated irradiated controls (Figure 4.22A). No anti-survival effects were observed without irradiation, consistent with what we previously observed (Figure 4.14). A similar trend was observed in the GBM cell lines LN229 (even with the lack of pro-survival signalling changes observed) and H4, where the radiosensitising effects of Avacopan under normoxia were sustained in hypoxic conditions, despite its association with increased radioresistance (Figure 4.22B-C). Collectively, these data indicate that Avacopan can enhance radiation-induced cytotoxicity in glioma cells even under hypoxic stress in two-dimensional (2D) culture, supporting its potential as a radiosensitising agent across multiple HGG models.

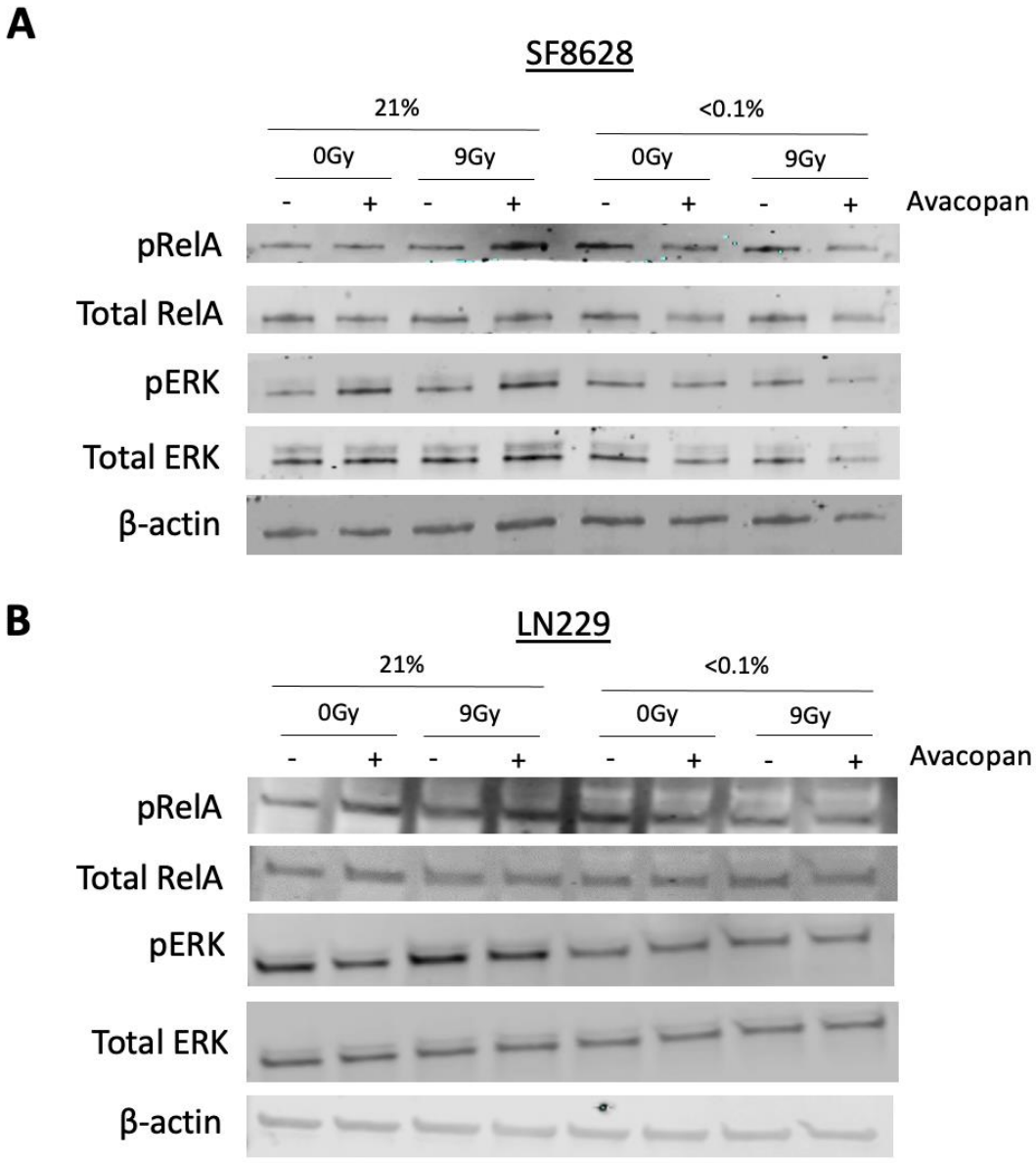

Figure 4.21 Avacopan did not modulate pro-survival signalling in LN229 cells under hypoxia irradiation

Vehicle (DMSO) or Avacopan was added to **(A)** SF8628 cells (4 μM, 32 h) and **(B)** LN229 cells (2 μM, 8 h) before exposure to 21% or <0.1% O2 for 16 h. Following hypoxia exposure, cells were irradiated at 0 or 9 Gy. Samples were harvested 24 h post-irradiation. Western blotting was carried out with the antibodies indicated. β-actin was used as loading control. n=3.

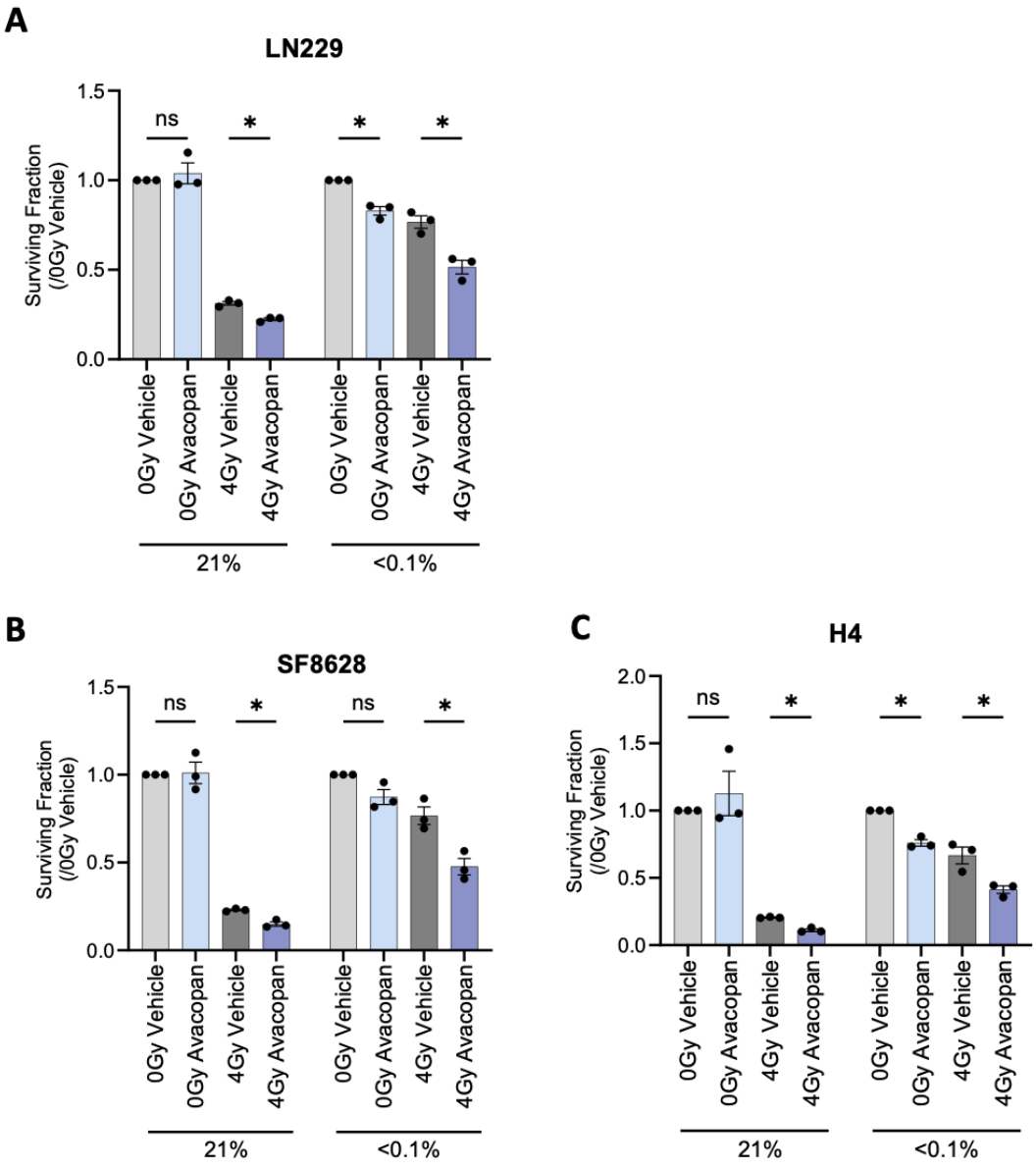

Figure 4.22 Avacopan enhances radiation-induced cytotoxicity under both normoxic and hypoxic conditions

Vehicle (DMSO) or Avacopan was added to **(A)** SF8628 cells (32 h), **(B)** LN229 and **(C)** H4 cells (8 h) before exposure to 21% or <0.1% O2 for 16 h. Cells were then irradiated at 0 or 4 Gy and incubated at 21%. Cell survival was assessed via clonogenic assay. Data presented as mean ± SEM of biological replicates. n=3. Statistical analysis used two-way ANOVA with Tukey's test. *p≤0.05.

To better mimic the TME in vitro, we attempted to culture HGG cells as three-dimensional (3D) spheroids, of which the GBM cell line LN229 was successful. Spheroids are known to develop hypoxic cores due to diffusion limitations of 3D structures. Before assessing radiation responses of these spheroids, we first validated the presence of hypoxic regions within spheroids cultured in a normoxic (21% O_2) incubator. LN229 spheroids of varying diameters were harvested and their sizes were measured just before collection. Spheroids were then categorised into four size groups, with monolayer cultures (0 μm) serving as controls. qPCR analysis confirmed that the longer the spheroid diameter, the higher the hypoxia-associated genes CAIX and XBP1, confirming validity of our spheroids as hypoxic models (Figure 4.23A-B). In parallel, C5aR1 mRNA levels similarly increased with spheroid size, most notably in spheroids exceeding 500 μm in diameter (Figure 4.23C). The pattern of C5aR1 upregulation closely mirrored that of XBP1, consistent with our earlier findings that C5aR1 transcription is induced via UPR activation under hypoxic stress.

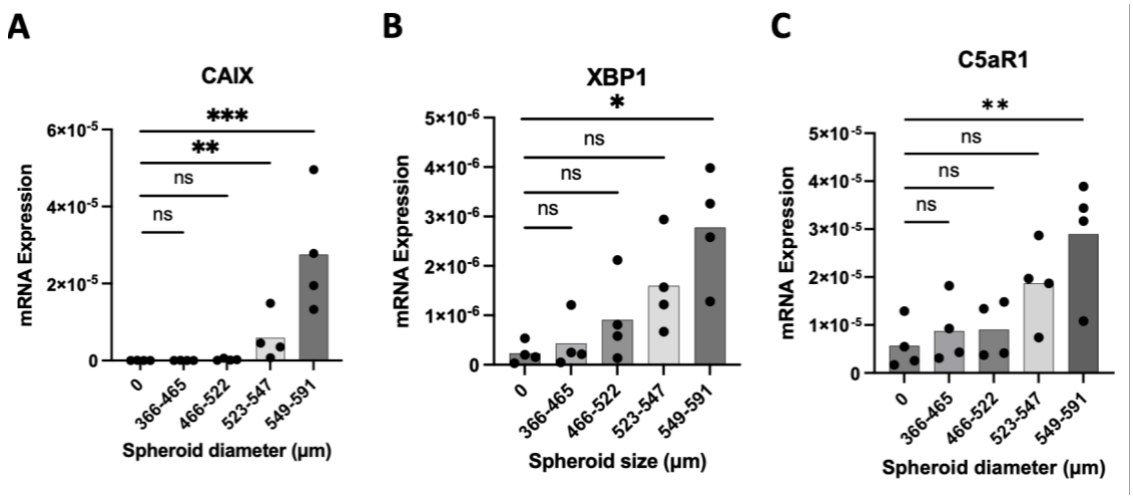

Figure 4.23 Hypoxic signatures and C5aR1 increase as spheroid size increases

mRNA expression of **(A)** CAIX and **(B)** XBP1 **and (B)** C5aR1 were assessed by qPCR in LN229 spheroids of different sizes and monolayer cells. Each biological repeat contains 6-7 spheroids harvested together. All mRNA levels were normalised to 18S. Data presented as mean ± SEM of biological replicates. n=4. analysis used one-way ANOVA with Dunnett's test. *p≤0.05, **p≤0.01, ***p≤0.001.

Unexpectedly, under non-irradiated conditions, treatment with a single dose of C5aR1 antagonists PMX205 or Avacopan promoted spheroid growth, despite the use of concentrations higher than those applied in 2D monolayer cultures to account for limited drug penetration in 3D structures (Figure 4.24A-B). Initially, the antagonists had minimal impact on spheroid size for the first few days. However, from approximately day 8 onward, spheroids treated with either PMX205 or Avacopan began to exhibit increased growth rates compared to vehicle-treated controls. By the end of the 18-day observation period, spheroid diameters in the PMX205- and Avacopan-treated groups were significant larger than vehicle controls, indicating these antagonists enhance tumour cell proliferation in 3D culture systems in the absence of radiation.

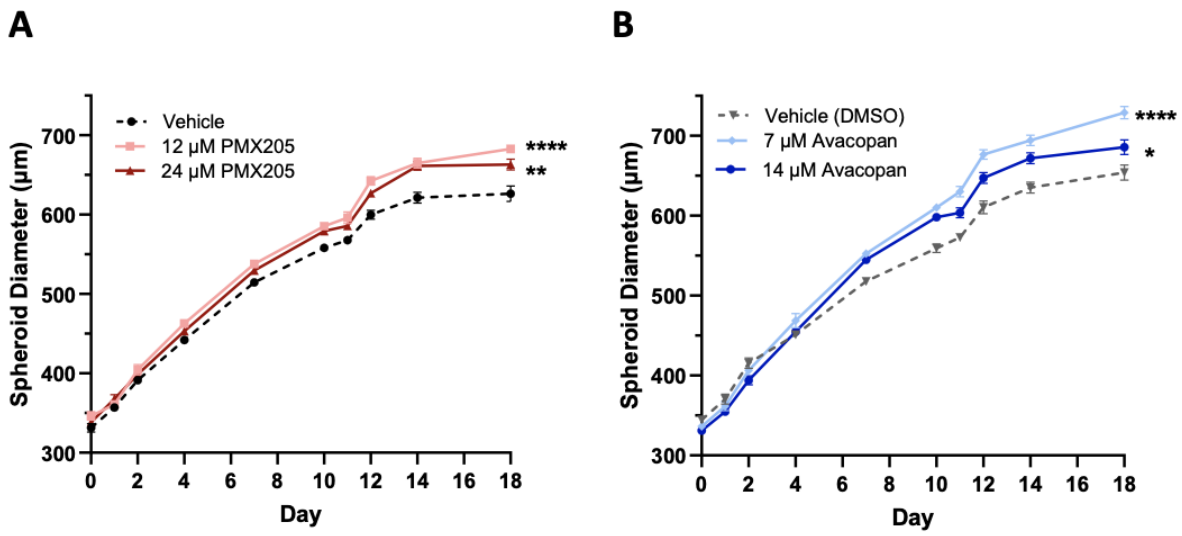

Figure 4.24 PMX205 and Avacopan promote spheroid growth

LN229 spheroids were treated with a single dose of vehicle (water or DMSO), **(A)** PMX205, or **(B)** Avacopan at the indicated concentrations. Diameter of spheroids were measured for 18 days after drug administration. Data presented as mean ± SEM of biological replicates. n=12. Analysis of diameter on day 18 used one-way ANOVA with Dunnett's test. *p≤0.05, **p≤0.01, ****p≤0.0001.

Given the unexpected growth effects of C5aR1 antagonists in non-irradiated spheroids, we next determined whether these inhibitors could sensitise spheroids to irradiation. LN229 spheroids were irradiated at 8 Gy, a dose previously established in our colorectal cancer studies to model combined hypoxic and irradiation stress in 3D culture. As shown in Figure 4.25A-B, irradiation alone markedly inhibited spheroid growth and addition of C5aR1 antagonists failed to enhance the anti-growth effect under irradiation in the same manner as observed in 2D culture. Instead, 12 μM PMX205 sustained spheroid growth even in the irradiated settings, mirroring its effects under non-irradiation conditions (Figure 4.25C). A similar pattern was observed with 7 μM Avacopan, which also promoted spheroid expansion following irradiation (Figure 4.25D). These findings indicate that, in contrast to their effects in 2D monolayer cultures, both PMX205 and Avacopan are insufficient to radiosensentise 3D spheroid models of LN229, and may even confer a survival advantage under irradiation depending on the doses of antagonists.

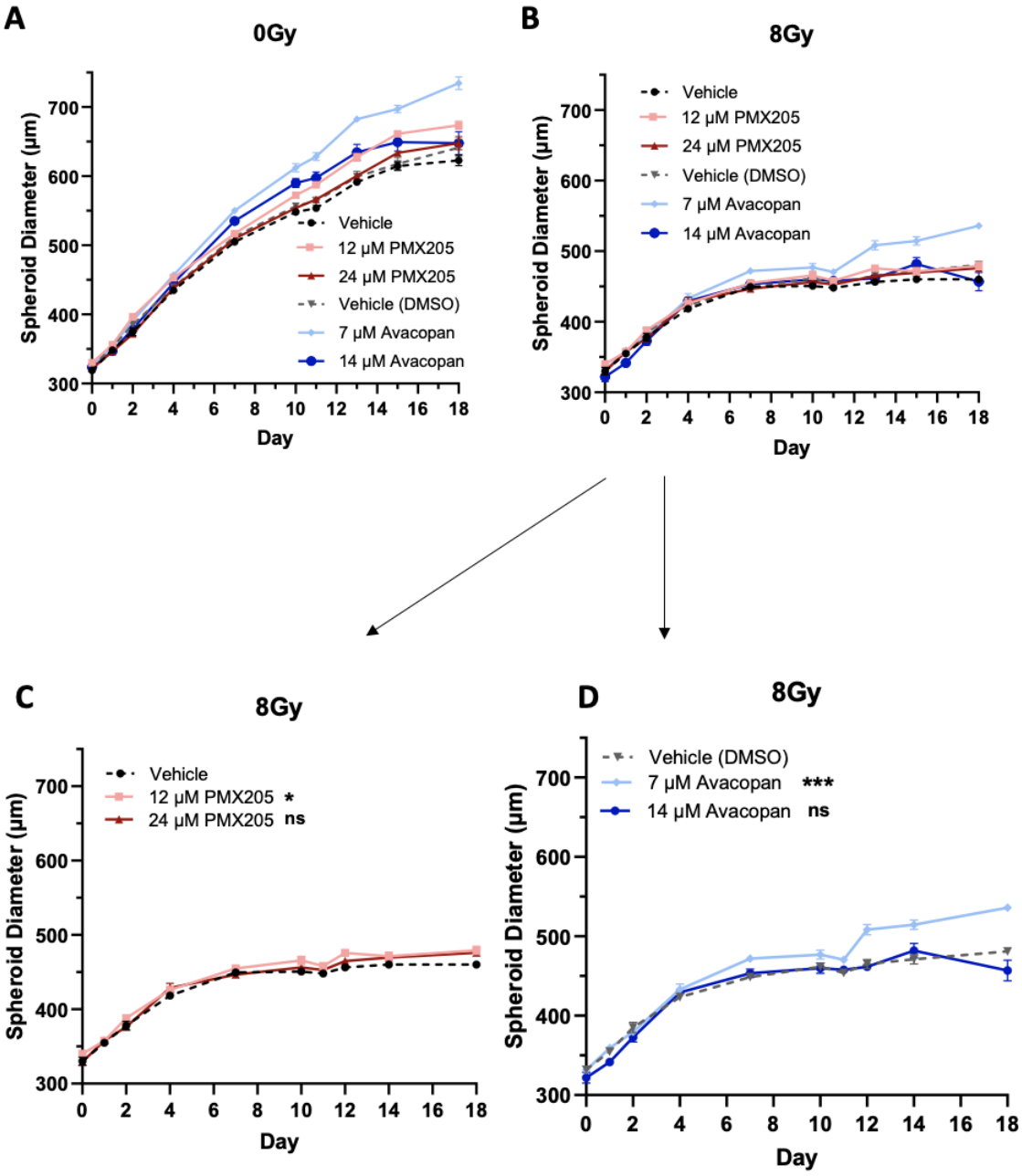

Figure 4.25 PMX205 and Avacopan are insufficient to radiosensitise LN229 spheroids in 3D settings

LN229 spheroids were treated with vehicle (water or DMSO), PMX205, or Avacopan at the indicated concentrations on day 1. Cells were irradiated at **(A)** 0 or **(B)** 8 Gy on day 2. Diameter of spheroids were measured for 18 days after drug administration. **(C-D)** part of the same experiment as (B). Data presented as mean ± SEM of biological replicates. n=12. Analysis of diameter on day 18 used one-way ANOVA with Dunnett's test. *p≤0.05, ***p≤0.001.

4.3 Discussion

In this chapter, we demonstrated that C5aR1 is a critical regulator of pro-survival signalling and radiation sensitivity in HGG. Through both genetic and pharmacological inhibition approaches, we showed that targeting C5aR1 could impair key survival pathways and enhances the vulnerability of glioma cells to radiation-induced cytotoxicity, even under the challenging conditions of severe hypoxia, at least in 2D monolayer culture. Unlike hypoxic stress, irradiation did not significantly modulate the expression of C5aR1 or C5 at the 24-hour time point. Although a statistically significant increase in C5aR1 protein levels was observed post-irradiation in LN229 cells, the changes were less than 50%, suggesting it may lack biological relevance and instead reflect low variability in the biological repeats.

The timing of sample collection remains a challenge when assessing changes in pro-survival signalling pathways. For instance, while NF-κB activation was not consistently altered 72 hours post-siC5aR1 transfection under normoxic conditions, we consistently observe a reduction in pRelA level at 0 Gy, 96 hours following siC5aR1 transfection. These findings highlight the transient and context-depending nature of NF-κB signalling. In addition, while clonogenic assays provided important insights into the impact of C5aR1 inhibition on radiosensitivity, extrapolation of survival curves beyond available data points was necessary due to limitations in colony formation at higher radiation doses (>6 Gy). This introduces a degree of uncertainty in the predicted survival at higher doses, and highlights a technical limitation of the assay in these HGG models.

Among the two pharmacological C5aR1 inhibitors tested, Avacopan exhibited a more pronounced radiosensitising effect than PMX205 in 2D monolayer cultures.

However, the observed attenuation of NF-κB signalling was modest and restricted with SF8628 cells, with no detectable effects in LN229 cells under conditions of irradiation in hypoxia. This could potentially be due to missed changes in pRelA level due to timing of sample collection, but if it is true that there were no changes in NF-κB signalling activation with Avacopan treatment, it contrasts with the robust suppression observed with siRNA-mediated knockdown. Avacopan may exhibit lower efficacy in inhibiting C5aR1 compared to genetic knockdown, a finding that aligns with expectations. Nevertheless, it was encouraging that both genetic and Avacoapn-induced C5aR1 inhibition enhanced radiosensitivity of HGGs under hypoxic stress in 2D culture, which are conditions that more closely resemble the hypoxic TME. Importantly, the radiosensitising effects of C5aR1 inhibition were preserved even within the hypoxic microenvironment which is typically associated with therapeutic resistance. This sustained impact implies that C5aR1 may mediate survival through hypoxia-compatible signalling mechanisms, such as MAPK activation or UPR-linked stress adaptation, which remain targetable despite oxygen deprivation.

Unfortunately, these promising effects did not translate into our 3D spheroid model. In LN229 spheroids, both PMX205 and Avacopan not only failed to enhance radiation response, but unexpectedly promoted spheroid growth, even under irradiation. These results raise concerns regarding the translational potential of C5aR1 inhibition as a radiosensitising agent in HGGs, and highlight the need for further investigation using more physiologically relevant models. Overall, while C5aR1 remains a mechanistically interesting target, its role as a therapeutic radiosensitiser may be limited by context-specific factors such as 3D architecture and drug penetration in HGG cells.

Chapter 5 Microglia and glioma

5.1 Introduction

Microglia and macrophages in HGG, collectively known as TAMs constitute up to 30% of tumour mass, forming a major component to the glioma TME and modulating tumour behaviours (Bowman *et al.*, 2016; Müller *et al.*, 2015). Both glioma and microglia cell populations are known to express C5aR1 and engagement with C5aR1 have been reported to upregulate release of pro-inflammatory TNF-α and IL-6 in microglia, which play dual roles in supporting phagocytosis to inhibit tumour growth, while also promoting therapy resistance (An *et al.*, 2018; Ren *et al.*, 2023; Wei *et al.*, 2021; Zhang *et al.*, 2024).

TAMs promote HGG progression by supporting glioma proliferation, migration and invasion through secretion of factors such MMP, TGF-β, IL-1β and IL-6 (Liu *et al.*, 2021; Markovic *et al.*, 2005; Wesolowska *et al.*, 2007; Zhang *et al.*, 2012). A previous study reported that GBM releases TGF-β to activate resting microglia into a specific subtype termed as HGG-associated microglia (HGG-AM) (Liu *et al.*, 2021). These HGG-AM cells are characterised by elevated expression of apolipoprotein E (APOE), a protein linked to pro-inflammatory activity through its interaction with the nucleotide-binding domain, leucine-rich-containing gamily, pyrin domain-containing-1 (NLRP1) inflammasome. Activated pro-inflammatory HGG-AM then secrete IL-1β, which feeds back into GBM to stimulate GBM proliferation and growth. A schematic adapted description of this study is shown in Figure 5.1. Given the abundance of TAM, the high expression of C5aR1 in these cells, and their role in shaping tumour growth and treatment resistance, this chapter focuses on understanding the impact of targeting C5aR1 in microglia and how this might impact treatment response of HGG.

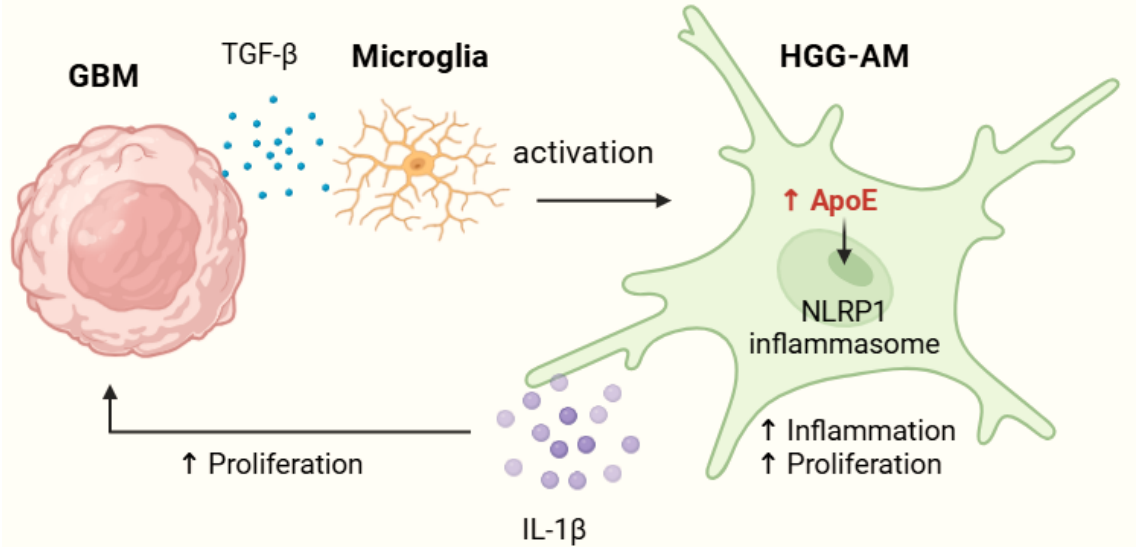

Figure 5.1 Schematic representation of reported GBM-microglia interaction

Adapted from Ling et al., (2023). GBM activates resting microglia into pro-inflammatory HGG-AM, which in turn stimulates proliferation of GBM, forming a positive feedback loop. Figure created on biorender.com.

5.2 Results

5.2.1 Microglia supports HGG viability

Before investigating the direct effects of C5aR1 inhibition on microglia, we first investigated the importance of microglia and macrophages in supporting HGG. Indirect co-culture experiments were performed using conditioned media (CM) to assess if microglia secrete any chemokines that favour glioma survival. CM was collected from hSV40 microglia-like cells and MΦ differentiated from peripheral blood mononuclear cells (PBMCs) derived from healthy patients. As illustrated in Figure 5.2A, both microglia and MΦ were subjected to 0 or 9 Gy irradiation, then the resulting CM was collected and transferred to SF8628 and LN229 glioma cells for 24 hour, followed by assessment of cell viability. In comparison to unconditioned media, CM collected from both irradiated and non-irradiated microglia and MΦ significantly enhanced glioma cell viability, independent of irradiation dose (Figure 5.2B-E). These data suggest that microglia and macrophages contribute to a microenvironment favourable for HGG survival by releasing certain soluble factors.

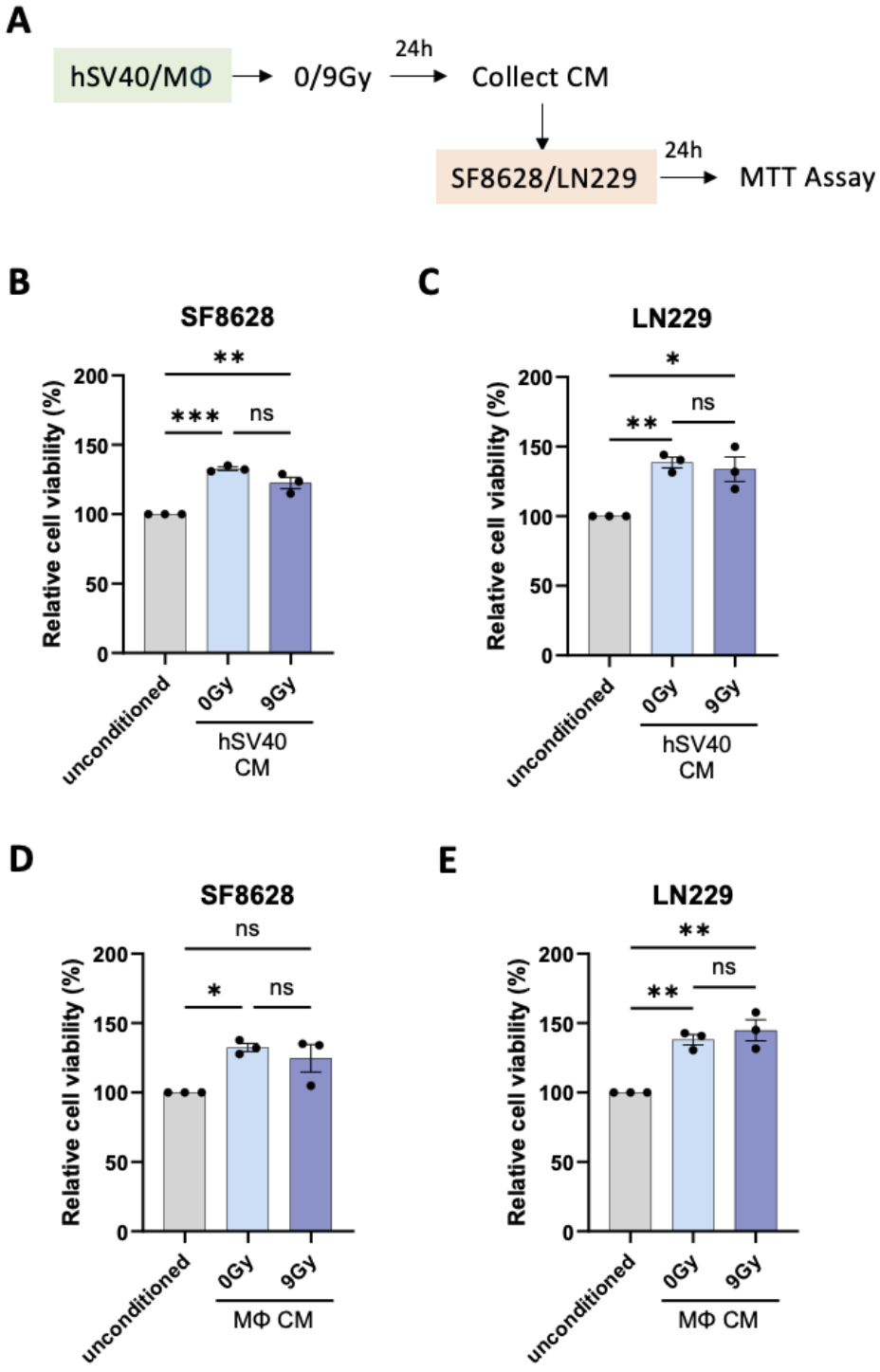

Figure 5.2 Microglia promotes HGG viability

(A) Graphical representation of the experiment. hSV40 and MΦ were irradiated at 0 or 9 Gy. CM was collected 24 h post-irradiation and transferred to SF8628 and LN229 cells. **(B-E)** Cell viability was assessed via MTT assays. Viability was normalised to the level at unconditioned media. Data presented as mean ± SEM of biological replicates. n=3. Statistical analysis used one-way ANOVA with Tukey's test. *p≤0.05, **p≤0.01, ***p≤0.001.

Next, we investigated how treating microglia with C5aR1 inhibitors might affect the viability of HGG cells, given that if PMX205 or Avacopan is administered in vivo, microglia will inevitably also receive inhibitor treatment. Graphical representation of the experiment workflow is illustrated in Figure 5.3A. Under non-irradiated conditions, CM collected from microglia-like cells treated with PMX205 or Avacopan did not result in significant changes in HGG viability compared to vehicle controls. However, when combined with 9 Gy irradiation, C5aR1 inhibition in hSV40 reduced the viability of both SF8628 and LN229 glioma cells to a level comparable to cells treated with unconditioned media (Figure 5.3B-E). A comparable trend was also observed in the same experiment setup utilising our MΦ model (Figure 5.4A-D). These findings support the hypothesis that, in both microglia and macrophages, alterations in the profile of soluble factors following C5aR1 inhibition under irradiation conditions modulate the microenvironment in a manner that influences HGG survival. Potential microglia-derived components contributing to this effect will be discussed later.

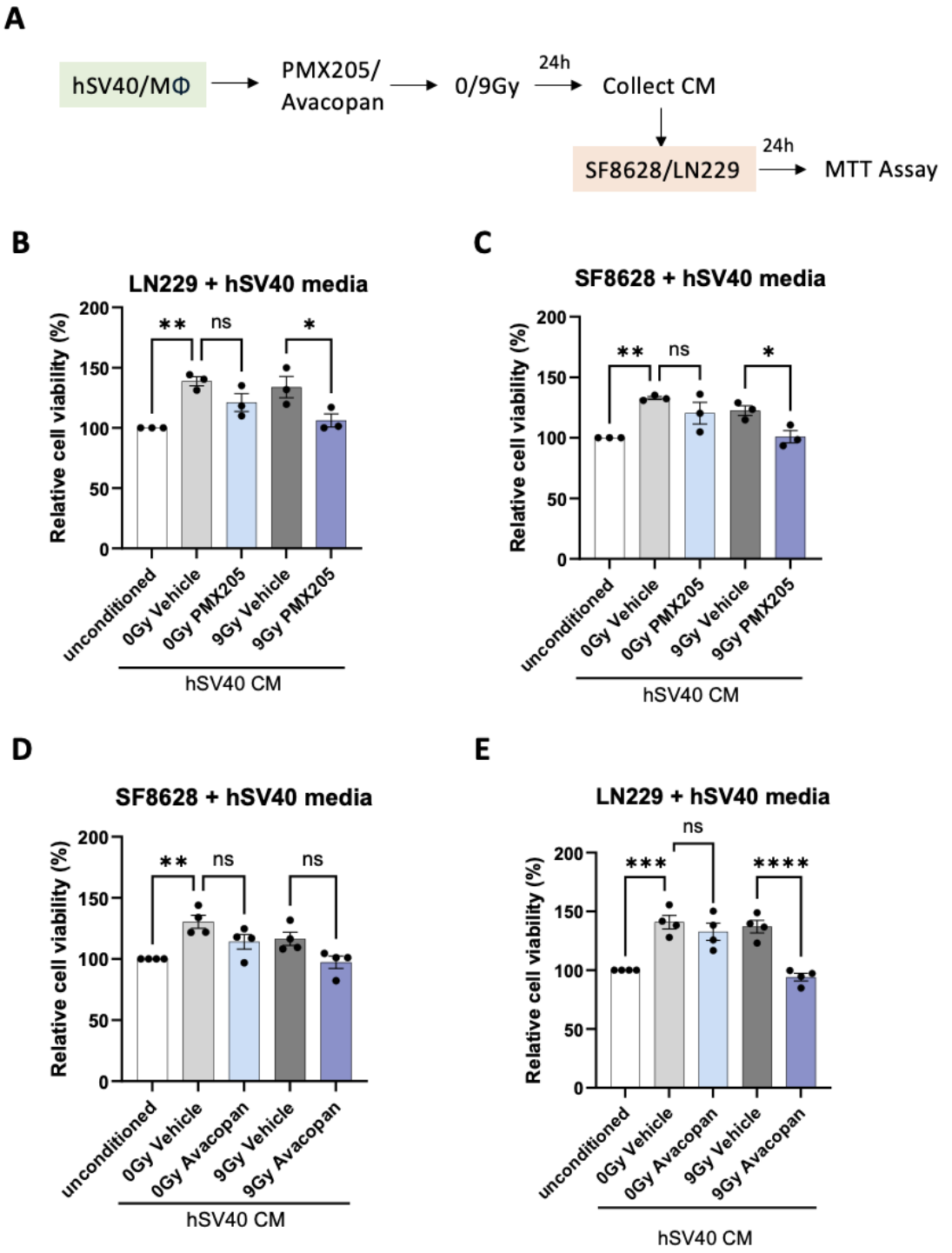

Figure 5.3 C5aR1 inhibition in irradiated microglia reduces viability of HGGs

(A) Graphical representation of the experiment. Part of the same experiment as Figure 5.1. hSV40 cells were treated with vehicle (water or DSMO), **(B-C)** PMX205 (48 h) or **(D-E)** Avacopan (24 h) before 0 or 9 Gy irradiation. CM was collected 24 h post-irradiation and transferred to SF8628 and LN229 cells. Cell viability was assessed 24 h later via MTT assays. Data presented as mean ± SEM of biological replicates. n=3. Statistical analysis used one-way ANOVA with Šidák's test. *p≤0.05, **p≤0.01, ***p≤0.001, ****p≤0.0001.

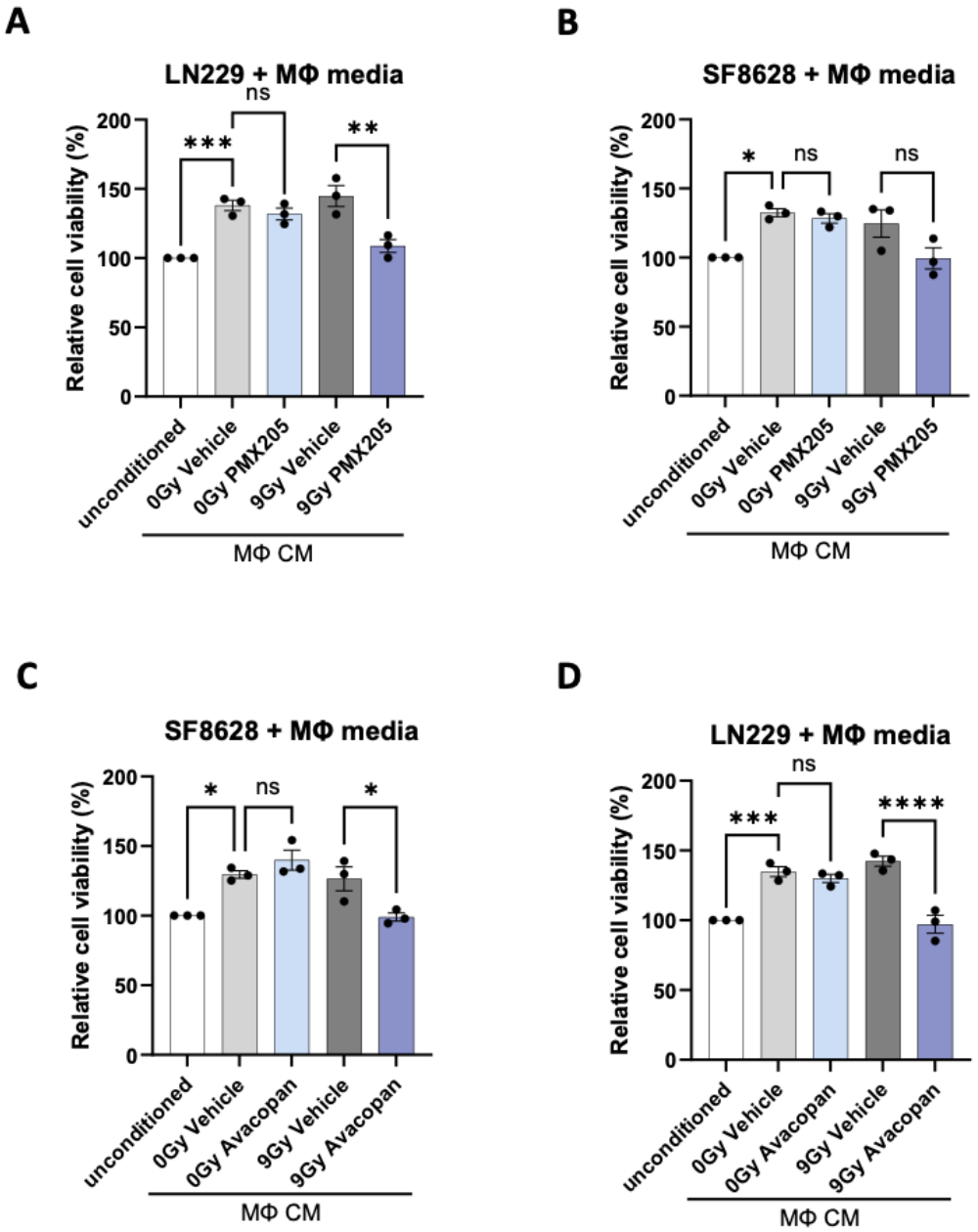

Figure 5.4 C5aR1 inhibition in irradiated macrophages reduces HGG cell viability

Part of the same experiment as Figure 5.2. MΦ were treated with vehicle (water or DMSO), **(A-B)** PMX205 (48 h) or **(C-D)** Avacopan (24 h) before 0 or 9 Gy irradiation. CM was collected 24 h post-IR and transferred to SF8628 and LN229 cells. Cell viability was assessed 24 h later via MTT assays. Data presented as mean ± SEM of biological replicates. n=3. Statistical analysis used one-way ANOVA with Šidák's test. *p≤0.05, **p≤0.01, ***p≤0.001, ****p≤0.0001.

Next, we confirmed that C5aR1 inhibition resulted in the anticipated attenuation of NF-κB and MAPK signalling in our microglia model. As shown in Figure 5.5, treatment with the C5aR1 antagonists PMX205 and Avacopan effectively abrogated C5a-induced upregulation of pRelA and pERK proteins, validating receptor engagement and inhibition of downstream signalling. We then further assessed whether C5aR1 pharmacological inhibition impacted the viability or survival of microglia cells, in the same manner as observed in HGGs. In IMG cells, PMX205 did not reduce microglial cell survival under either irradiated or non-irradiated conditions following 48 or 72 h pre-treatment (Figure 5.6A). Interestingly, PMX205 slightly enhanced microglial survival under irradiation following 72 h pre-treatment, a response opposite from the reduction in survival previously observed in GBM, shown in Figure 4.8. Due to inability of hSV40 cells to form colonies, MTT assays were used to assess the effects of Avacopan on cell viability, in an alternative microglia-like model. In hSV40 cells, Avacopan at doses equivalent to those effective in glioma cells (2 μM 24 h and 4 μM 48 h) did not significantly alter cell viability either at baseline or under irradiated conditions (Figure 5.5B-C). A slight reduction in cell viability was observed with 7 μM Avacopan, although this concentration exceeded that which was used in our glioma models. These findings suggest that the anti-survival effects of C5aR1 antagonists observed in HGG cells are not recapitulated in our microglia-like cells, indicating a differential cellular response to C5aR1 targeting.

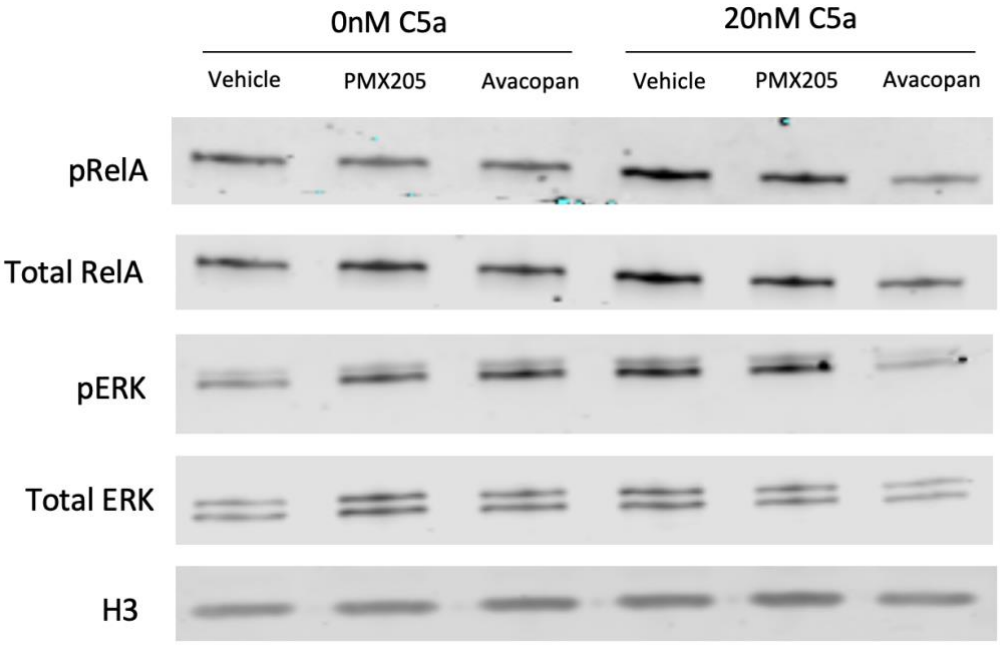

Figure 5.5 Attenuation of C5a-induced signalling changes by C5aR1 inhibitors in microglia-like cells

Recombinant C5a, PMX205 (12 μM) and Avacopan (2 μM) were added to hSV40 cells for 2 h. Western blotting was carried out using the indicated antibodies. H3 was used as loading control. n=2.

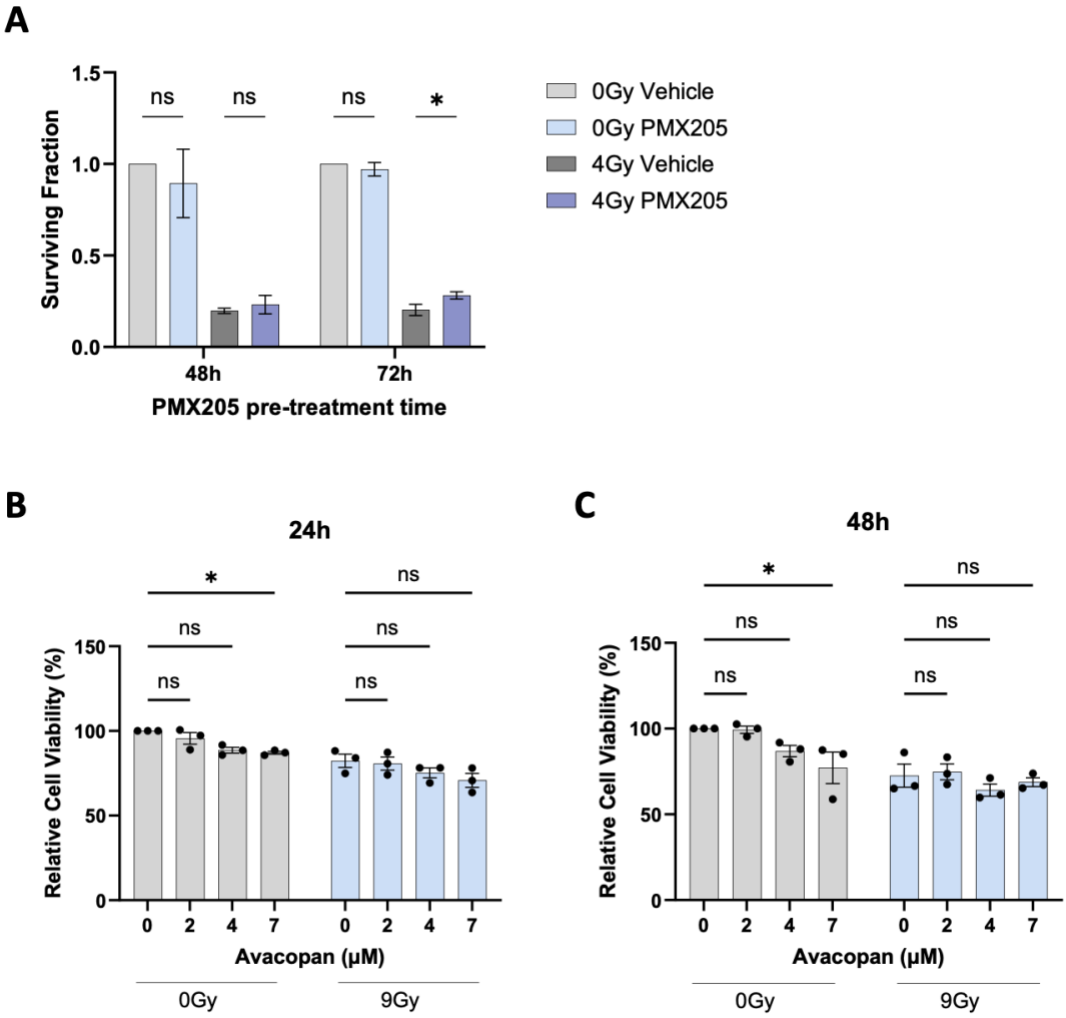

Figure 5.6 C5aR1 antagonists at glioma-effective doses did not affect microglial survival or viability

(A) Vehicle (water) or PMX205 was added to IMG cells for 48 or 72 h before 0 or 4 Gy irradiation. Cell survival was assessed via clonogenic assay. Data presented as mean ± SEM of biological replicates. n=3. Statistical analysis used two-way ANOVA with Tukey's test. *p≤0.05.

(B) 0-7 μM Avacopan was added to hSV40 cells for 24 or 48 h before 0 or 9 Gy irradiation. Cell viability was assessed using MTT assay 24 h post-irradiation and normalised to the corresponding 0 Gy 0 μM vehicle control. Data presented as mean ± SEM of biological replicates. n=3. Statistical analysis used two-way ANOVA with Tukey's test. *p≤0.05.

5.2.2 Inflammatory profile of microglia with C5aR1 inhibition

Having established that C5aR1 antagonists do not significantly affect microglia survival and viability, we next investigated how C5aR1 antagonism modulates the inflammatory phenotype of microglia, and the potential released soluble mediators contributing to altered HGG viability. Microglial activation and polarisation are characterised by the expression of specific markers and the secretion of cytokines associated with either pro- or anti-inflammatory states (Jurga, Paleczna and Kuter, 2020). To assess how C5aR1 antagonists influence the inflammatory profile of microglia, we performed qPCR for a panel of inflammation-related genes specific to microglia (Figure 5.7). Lipopolysaccharide (LPS) was used as control due to its established role in promoting a pro-inflammatory phenotype (Appendix B, Figure B.1).

At baseline (0 Gy), PMX205 treatment significantly altered the expression of only one marker, cluster of differentiation 163 (CD163), which codes for a receptor typically associated with an anti-inflammatory M2-like polarisation. In the context of irradiation, 9 Gy alone resulted in changes of several inflammatory markers in IMG cells, although most did not reach statistical significance when analysed using two-way ANOVA with Fisher's LSD test. Of which, only CD163 expression was significantly downregulated, while both IL1β (pro-inflammatory) and CD206 (anti-inflammatory) were significantly upregulated following irradiation (Figure 5.5B-D). Notably, PMX205 treatment in irradiated microglia suppressed the expression of both IL1β and CD206 compared to vehicle controls, suggesting that PMX205 modulates specific inflammatory responses in IMG cells post-irradiation. Given that among those genes that were altered, both pro- and anti-inflammatory markers were affected by the combination of PMX205 and irradiation,

no clear pattern emerged to indicate whether PMX205 promotes a specific microglial polarisation state.

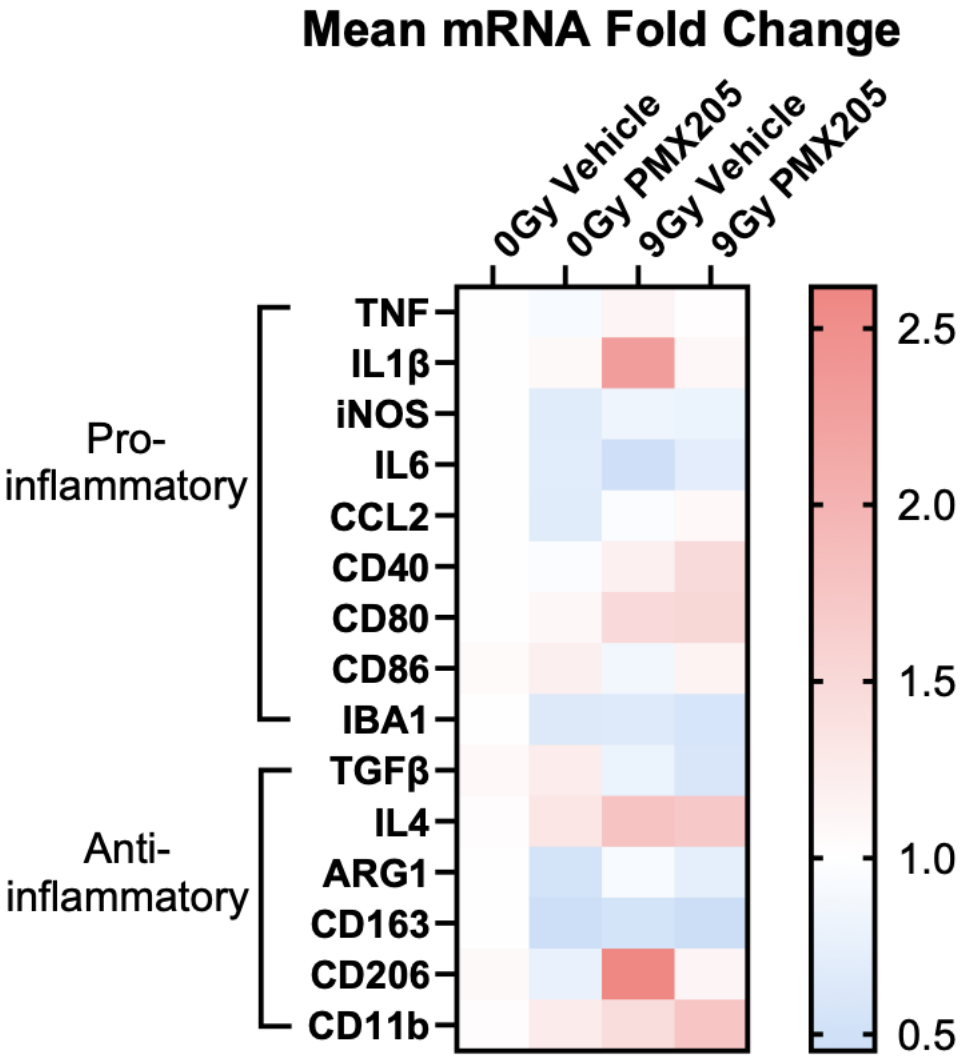

Figure 5.7 PMX205 does not polarise microglia into pro- or anti-inflammatory phenotype

IMG cells were treated with vehicle (water) or PMX205 for 72 h before 0 or 9 Gy irradiation. mRNA expression of the indicated genes were assessed by qPCR 24 h post-irradiation. All mRNA levels were normalised to ACTB and expressed as fold change relative to the expression of 0 Gy Vehicle. Data present as mean of biological replicates. n=3.

Next, we investigated how the other C5aR1 antagonist Avacopan influences inflammatory gene expression in hSV40 microglia-like cells. A similar panel of inflammatory markers used in the IMG cell experiment was applied here, with LPS included as a control (Appendix B, Figure B.2). Under non-irradiation conditions, Avacopan treatment significantly downregulated only two markers: IL6 (pro-inflammatory) and CD163 (anti-inflammatory) when analysed via two-way ANOVA with Fisher's LSD test (Figure 5.8).

As shown in Figure 5.8, exposure to 9 Gy irradiation induced a pronounced pro-inflammatory response, significantly upregulating nearly all pro-inflammatory genes tested, except for CCL2 and ionised calcium binding adapter protein (IBA1). Conversely, most anti-inflammatory markers were downregulated post-irradiation except for TGFβ and IL10 which were significantly upregulated, potentially due to compensatory feedback mechanisms. These results showed that irradiation alone polarises hSV40 microglia-like cells toward a pro-inflammatory phenotype, though more inflammatory markers could be used to support this.

Under irradiated conditions, Avacopan treatment effectively suppressed the radiation-induced upregulation of all tested pro-inflammatory genes. Of which, the most prominent downregulated pro-inflammatory genes observed were TNF, IL1β, cluster of differentiation 80 (CD80) and cluster of differentiation 86 (CD86). CD80 and CD86 together are surface markers typically used to characterise the pro-inflammatory M1-like phenotype. Despite this reduction of pro-inflammatory gene expression under irradiation, Avacopan did not conversely upregulate any anti-inflammatory markers relative to vehicle-treated controls, and most remained downregulated when compared to baseline. In fact, anti-inflammatory TGFβ, IL10 and CD163 were further downregulated following

Avacopan treatment at 9 Gy, suggesting that microglia were not polarised toward an M2-like anti-inflammatory phenotype. Taken together, these findings indicate that while Avacopan suppresses the radiation-induced pro-inflammatory shift in microglia, it may not actively promote a compensatory anti-inflammatory phenotype.

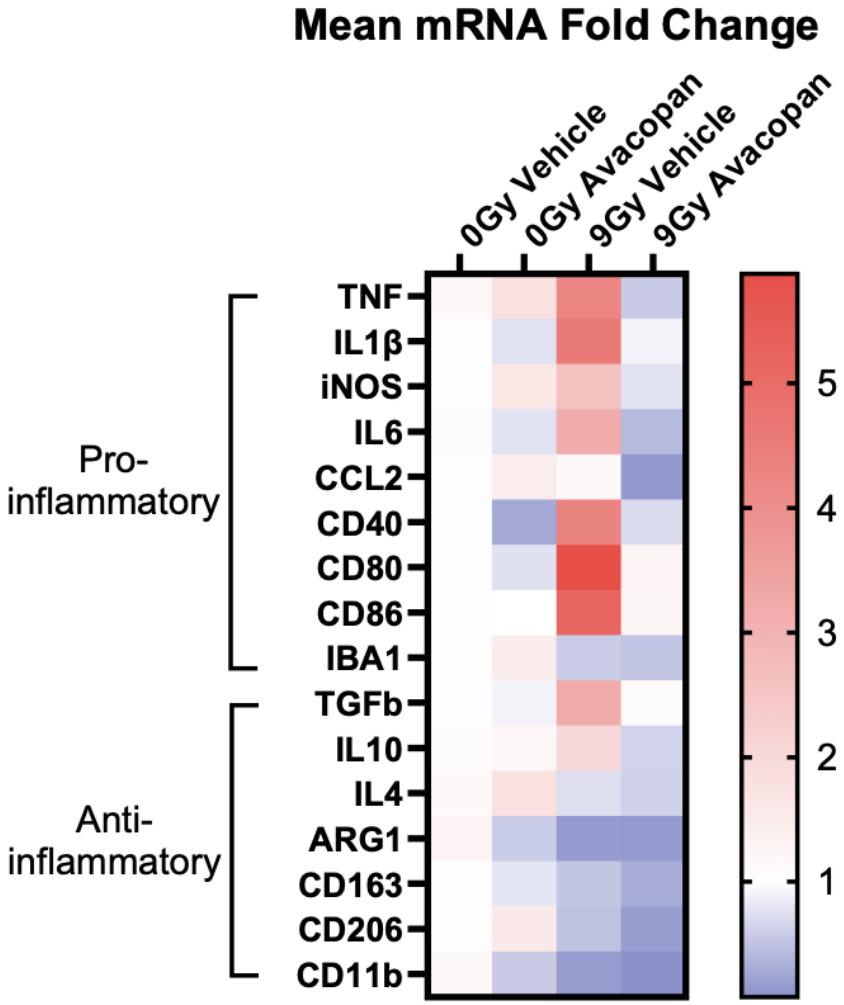

Figure 5.8 Avacopan suppresses the pro-inflammatory microglia phenotype induced by radiation

hSV40 cells were treated with vehicle (DMSO) or 2 μM Avacopan for 24 h before 0 or 9 Gy irradiation. mRNA expression of the indicated genes were assessed by qPCR 24 h post-irradiation. All mRNA levels were normalised to ACTB and expressed as fold change relative to the expression of 0 Gy Vehicle. Data presented as mean of biological replicates. n=3.

To further validate the effects of C5aR1 inhibition in microglial inflammatory phenotype, we utilised siRNA to silence C5aR1 in hSV40 cells. qPCR analysis confirmed an approximately 30% reduction in C5aR1 mRNA expression, which although modest, was statistically significant compared to Scr controls (Figure 5.9A). At baseline, C5aR1 KD did not significantly alter the expression of most pro-inflammatory genes, as assessed by two-way ANOVA, consistent with the effects observed following Avacopan treatment (Figure 5.9B). A general trend towards upregulation of anti-inflammatory genes was observed upon C5aR1 silencing, but only interleukin 4 (IL4) reached statistical significance.

Following irradiation, all pro-inflammatory genes assessed were markedly upregulated. Notably, siC5aR1 treatment successfully attenuated this radiation-induced upregulation, with the most pronounced changes observed with IL1β. The changes in pro-inflammatory markers suggest a shift toward a less pro-inflammatory phenotype, mirroring the trend observed with Avacopan treatment. In contrast, there was a trend in downregulation of anti-inflammatory markers upon irradiation treatment, opposing the pro-inflammatory response. However, none of these changes reached statistical significance due to variability between biological replicates. Following irradiation, C5aR1 KD appeared to restore the expression of most anti-inflammatory genes to baseline levels, with the exception of CD163, though these effects also did not reach statistical significance. Collectively, our siC5aR1 data recapitulate the trend observed with Avacopan treatment, in which C5aR1 inhibition alone does not substantially alter inflammatory gene expression at 0 Gy. Irradiation alone drives microglial polarisation toward an M1-like pro-inflammatory state, and C5aR1 inhibition mitigates this radiation-induces pro-inflammatory shift without inducing a fully anti-inflammatory phenotype.

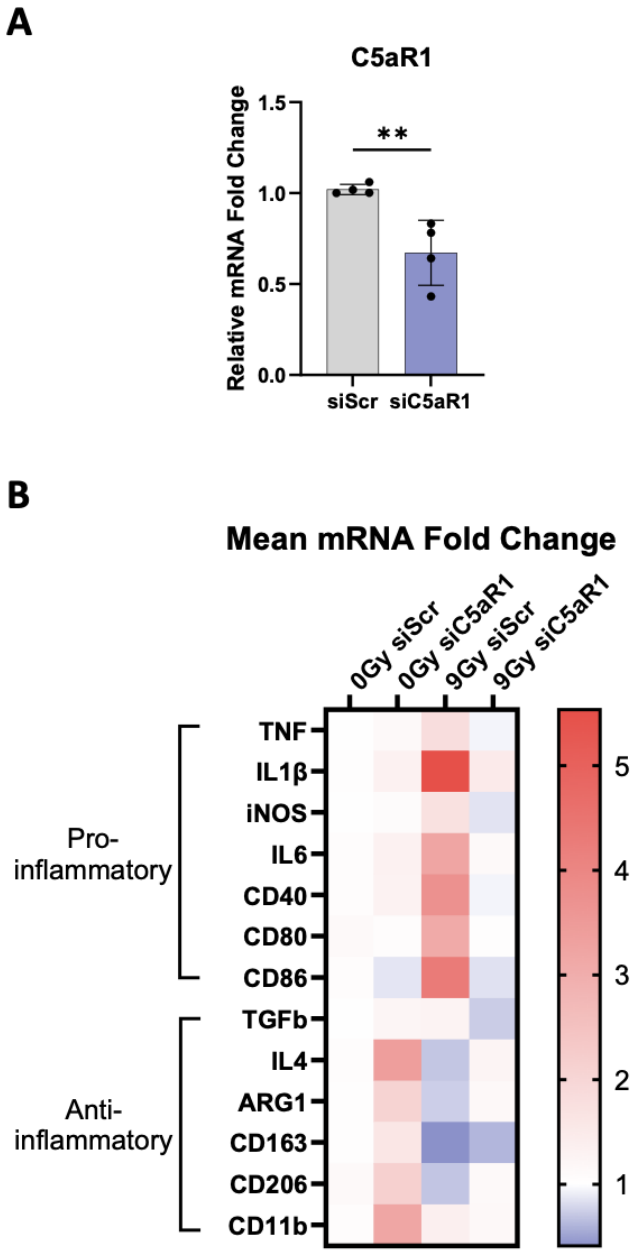

Figure 5.9 Silencing C5aR1 mitigates radiation-induces pro-inflammatory shift in microglia-like cells

hSV40 cells were transfected with Scr or C5aR1 siRNA.

(A) mRNA expression of the C5aR1 was assessed by qPCR. All mRNA levels were normalised to β-actin and expressed as fold change relative to the expression of siScr-treated cells. Data presented as mean of biological replicates. n=4. Statistical analysis was performed on unnormalised values using unpaired t-test. **p≤0.01

(B) Following transfection, cells were irradiated at 0 or 9 Gy. mRNA expression of the indicated genes were assessed by qPCR 24 h post-irradiation. All mRNA levels were normalised to ACTB and expressed as fold change relative to the expression of 0 Gy Vehicle. Data presented as mean of biological replicates. n=3.

The significant upregulation of pro-inflammatory markers in microglia upon irradiation mirrored the trend observed in HGG-AM, which have been reported to exhibit a pro-inflammatory phenotype (Liu *et al.*, 2021). Based on these findings, we then examined whether C5aR1 inhibition modulates APOE expression in our hSV40 cells, as APOE has been identified by Liu *et al*. as a key driver of pro-inflammatory cytokine secretion in microglia. As shown in Figure 5.10A, irradiation significantly increased APOE gene expression, a response not previously reported in existing literature. Notably, Avacopan treatment under irradiation effectively brought the APOE expression down to levels comparable to untreated controls. LPS was included as a positive control which showed marked APOE upregulation (Figure 5.10B). To confirm that these transcriptional changes were reflected at the protein level, western blot analysis performed by Dr. Lolita Singh from our group revealed a similar pattern of intracellular APOE protein expression, consistent with the qPCR results (Figure 5.10C). These results therefore suggest that Avacopan suppresses radiation-induced intracellular APOE upregulation in microglia, potentially limiting the establishment of a pro-inflammatory, glioma-supportive microglial phenotype under irradiation.

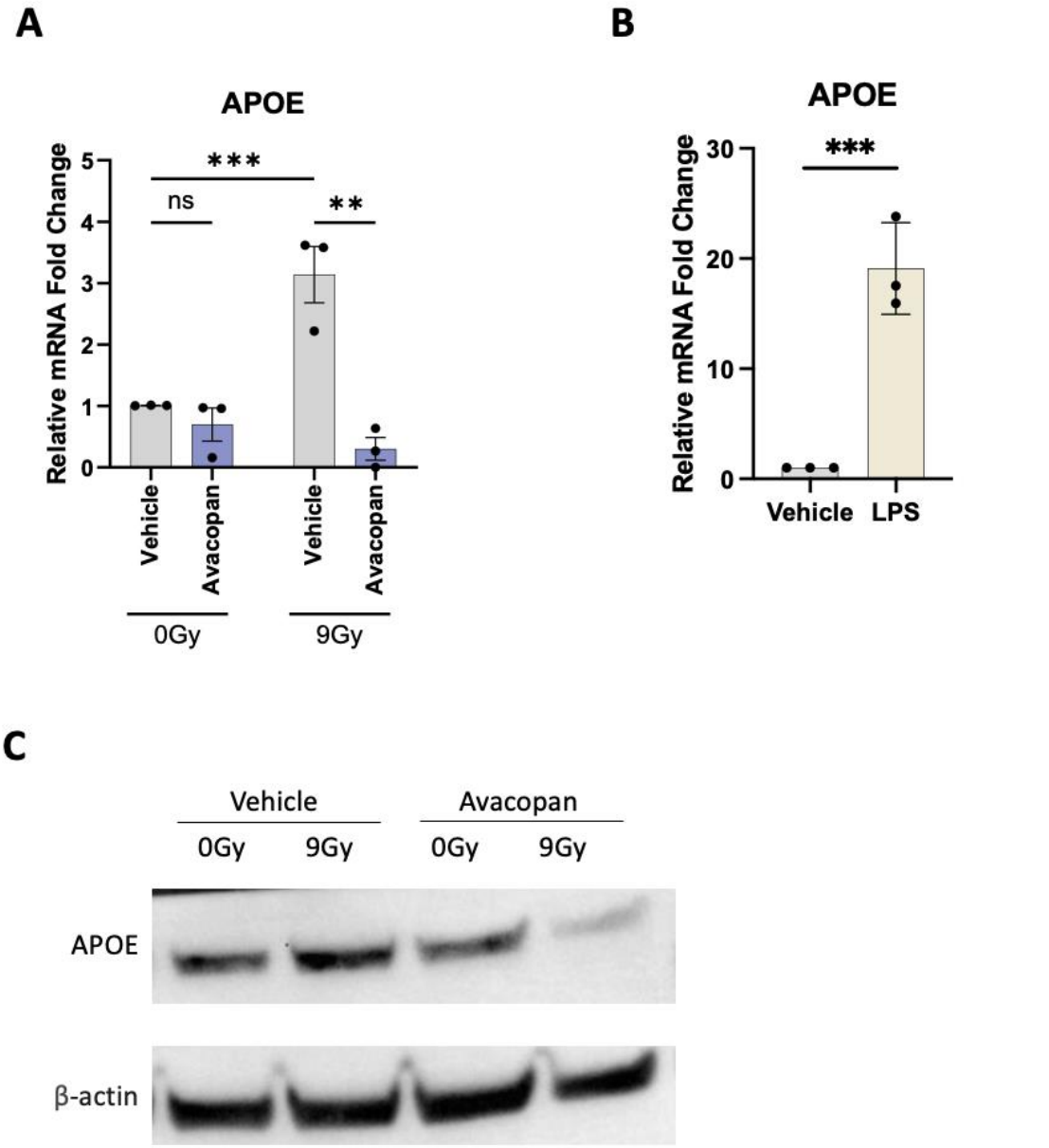

Figure 5.10 Avacopan suppresses radiation-induced APOE upregulation

hSV40 cells were treated with **(A)** vehicle (DMSO) or Avacopan for 24 h before 0 or 9 Gy irradiation. Cells were harvested 24 h post-IR. **(B)** hSV40 cells were treated with LPS. mRNA expression of APOE was assessed by qPCR. All mRNA levels were normalised to 18S. Data presented as mean ± SEM of biological replicates. n=3. Statistical analysis on unnormalised values were performed using one-way ANOVA with Fisher's LSD test and unpaired t-test respectively. **p≤0.01, ***p≤0.001.
(C) 24 h post-irradiation, western blotting was carried out using the indicated antibodies. β-actin was used as loading control. n=2.

The qPCR heatmaps in Figure 5.7-5.9 prompted further investigation into which secreted cytokines may mediate the pro-viability effects of microglia on glioma cells observed in Figure 5.3. Among the candidates, IL-1β emerged as a key focus, given its significant downregulation upon C5aR1 inhibition under irradiation in both cell lines, and its previously reported role in promoting GBM proliferation (Liu *et al.*, 2021). Therefore, we further evaluated the regulation of IL-1β in our microglial model. To determine whether these transcriptional changes translate into altered cytokine secretion, we quantified IL-1β protein levels in the culture media using enzyme-linked immunosorbent assay (ELISA). As shown in Figure 5.11A, the ELISA results corroborated the qPCR data, in which irradiation alone led to a significant increase in IL-1β secretion, while Avacopan treatment suppressed this radiation-induced elevation. Treatment with LPS served as a positive control (Figure 5.11B). These findings further validated the role of C5aR1 inhibition in mediating radiation-induced IL-1β release from microglia and suggest that Avacopan attenuates this cytokine response.

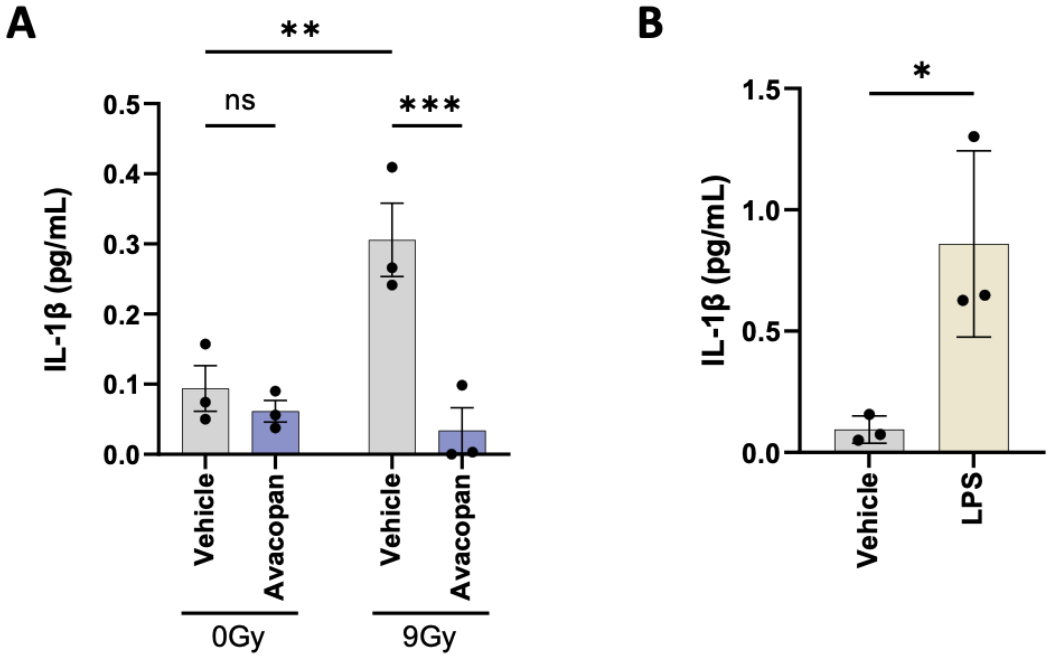

Figure 5.11 Avacopan suppresses radiation-induced secretion of IL-1β

(A) hSV40 cells was treated with vehicle (DMSO) or Avacopan for 24 h before 0 or 9 Gy irradiation. Media collected 24 h post-irradiation. **(B)** hSV40 cells were treated with LPS for 24 h. IL-1β level was detected via ELISA. Data presented as mean ± SEM of biological replicates. n=3. Statistical analysis used two-way ANOVA with Fisher's LSD test and unpaired t-test respectively. *p≤0.05, **p≤0.01, ***p≤0.001.

5.2.3 IL-1β regulates proliferation and radiosensitivity of gliomas

Following confirmation of IL-1β secretion from microglia, we next sought to directly test its functional role in promoting glioma growth. Upon inflammasome activation, pro-IL-1β is cleaved into its biologically active form mainly by caspase-1 and active IL-1β is subsequently secreted (Thornberry *et al.*, 1992). To mimic this signalling, we supplemented the culture media of HGG cells with recombinant cleaved IL-1β, thereby identifying its direct effects on glioma cells. As shown in Figure 5.12A-B, the addition of recombinant IL-1β significantly enhanced proliferation of both LN229 and SF8628 glioma cells after repeated dosing, consistent with the pro-proliferative role of IL-1β previously reported by Liu et al., (2021), though a higher concentration was needed to observe significant effects in LN229 cells. These results confirm that IL-1β is a soluble factor capable of directly stimulating glioma growth, thereby linking microglial cytokine secretion to glioma progression.

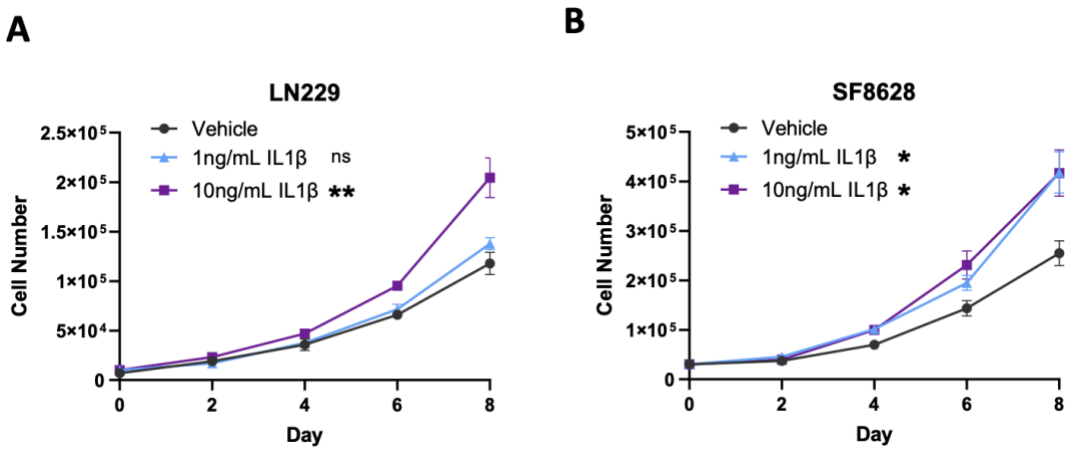

Figure 5.12 IL-1β promotes glioma proliferation

(A) LN229 and **(B)** SF8628 cells were treated with 0-10 nM recombinant IL-1β and cell number was counted cell every two days from day 0-8. Data presented as mean ± SEM of biological replicates. n=3. Statistical analysis of cell number on day 8 was performed using one-way ANOVA with Dunnett's test. *p≤0.05, **p≤0.01.

Having established the role of IL-1β in glioma proliferation, we next investigated whether this cytokine also modulates glioma radiosensitivity. We first focused on just the general effects on CM collected from microglia-like cells under different treatment conditions, before investigating specific microglia-derived factors. A schematic overview of the experimental design is shown in Figure 5.13A. hSV40 microglia-like cells were treated with Avacopan, followed by exposure to 0 or 9 Gy irradiation. The resulting CM was then transferred to HGG cells, a setup similar to that described in Figure 5.3A. Clonogenic assays were performed to assess glioma cell survival.

As demonstrated in Figure 5.13B-C, CM collected from hSV40 cells significantly enhanced glioma cell survival compared to unconditioned media, consistent with our earlier findings that microglia-derived factors support HGG viability. However, unlike the reduction in glioma viability previously observed with CM from Avacopan + irradiation treated microglia (Figure 5.3B-C), no significant changes in long-term clonogenic survival were detected with Avacopan treatment in this experiment, irrespective of irradiation dose.

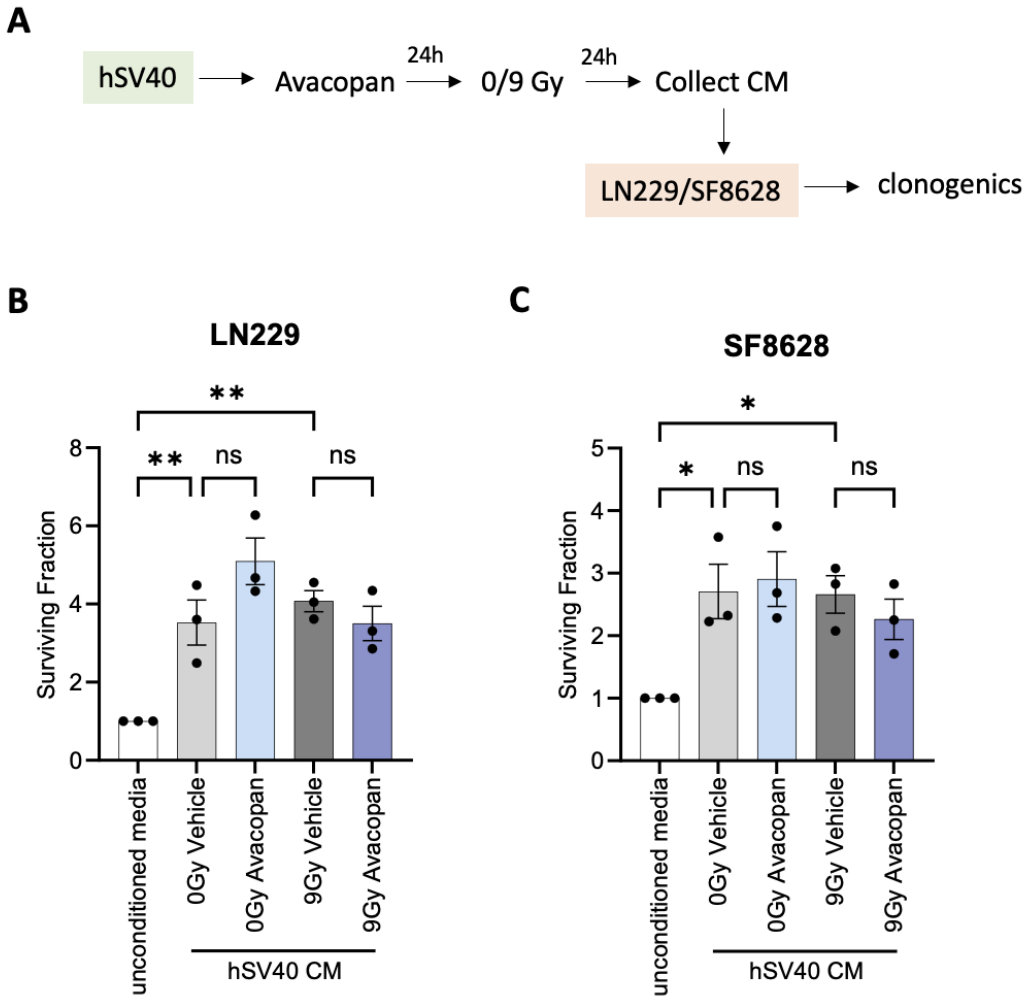

Figure 5.13 Avacopan treatment in microglia-like cells does not affect glioma cell survival

(A) Graphical representation of the experiment. hSV40 cells were treated with vehicle (DMSO) or Avacopan before 0 or 9 Gy irradiation. CM was collected 24 h post-irradiation and transferred to **(B)** LN229 and **(C)** SF8628 cells. Cell survival was analysed via clonogenic assays. Data presented as mean ± SEM of biological replicates. n=3. Statistical analysis used one-way ANOVA with Šidák's test. *p≤0.05, **p≤0.01.

Although we did not observe any changes in glioma survival at baseline (0 Gy) when microglia-like cells were treated with Avacopan, we proceeded to investigate whether microglia could affect radiosensitivity of glioma cells. A similar set up to our previous experiment was designed, but HGG cells were exposed to irradiation after receiving CM, and assays were performed to assess glioma cell survival under irradiation. A schematic overview of the experimental design is shown in Figure 5.14A. This design simulates the HGG microenvironment, where therapeutic radiation inevitably impacts both glioma and adjacent microglial cells. Our set up enabled us to test if soluble factors released from irradiated microglia affects radiosensitivity of nearby glioma cell, making them more sensitive or resistant to irradiation. Of note, 4 Gy was selected for microglia to match the radiation dose applied to glioma cells in clonogenic assays, while 9 Gy was included to remain consistent with prior experiments (e.g. viability assays, qPCR).

As shown in Figure 5.14B-C, CM from Avacopan treatment had no significant impact on LN229 or SF8628 survival when microglia were not irradiated (0 Gy). However, CM collected from Avacopan-treated microglia that were irradiated at either 4 or 9 Gy significantly reduced the glioma survival fraction following irradiation. These findings suggest that C5aR1 inhibition in irradiated microglia alters the secretome in a manner that sensitises glioma cells to radiation-induced cytotoxicity.

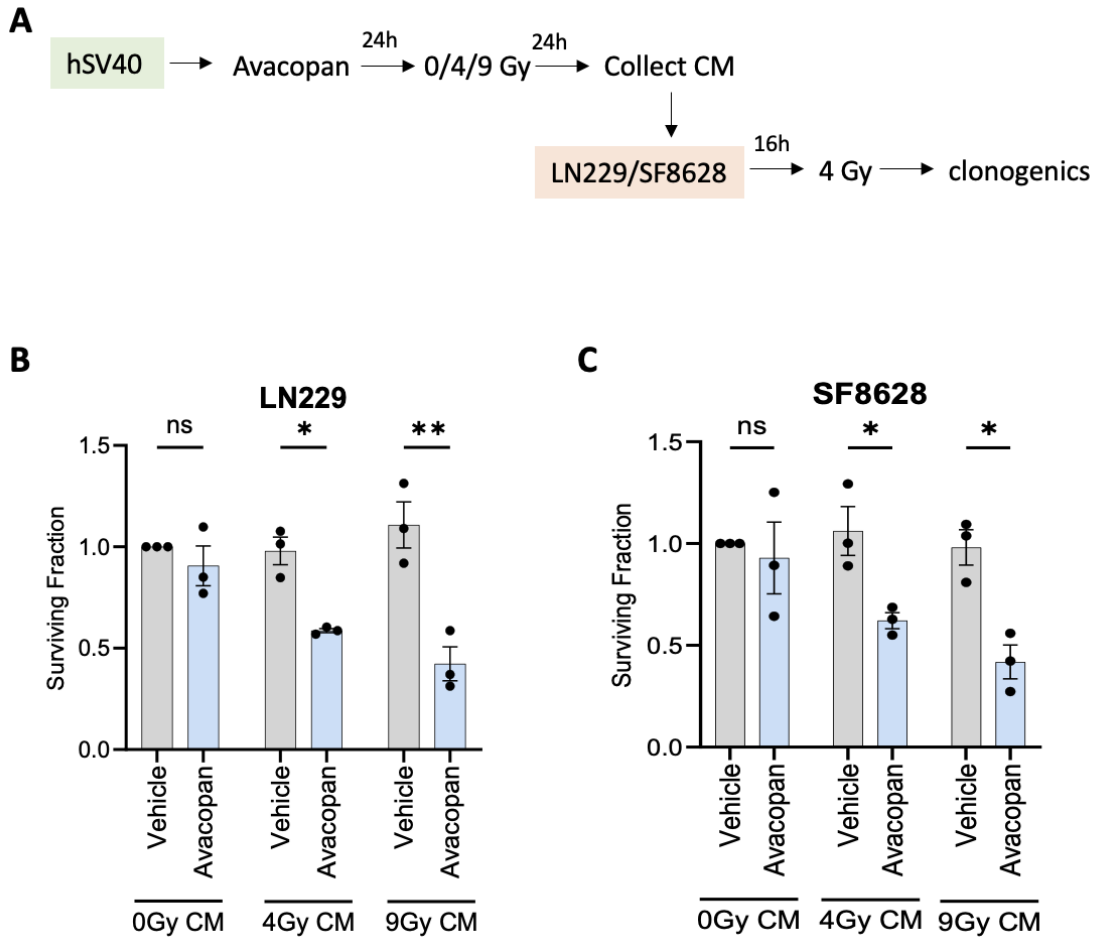

Figure 5.14 Avacopan treatment in microglia-like cells improves radiosensitivity of HGG cells

(A) Graphical representation of the experiment. hSV40 cells were treated with vehicle (DMSO) or Avacopan before 0 or 9 Gy irradiation. CM was collected 24 h post-irradiation and transferred to **(B)** LN229 and **(C)** SF8628 cells. Glioma cells were irradiated at 4 Gy and cell survival was analysed via clonogenic assays. Data presented as mean ± SEM of biological replicates. n=3. Statistical analysis used two-way ANOVA with Šidák's test. *p≤0.05, **p≤0.01.

To investigate the effect of IL-1β in contributing to the observed changes in glioma radiosensitivity, we supplemented the microglia-derived CM with recombinant IL-1β. A schematic of the experimental design is shown in Figure 5.15A. CM was collected from hSV40 microglia-like cells treated with Avacopan and irradiation (the condition which was previously shown to have reduced IL-1β levels). We then added recombinant IL-1β to this CM prior to transfer to SF8628 and LN229 cells, which were subsequently irradiated at 4 Gy.

As shown in Figure 5.15B-C, supplementation with IL-1β significantly restored survival of glioma cells cultured in irradiated CM, reversing the radiosensitising effects conferred by Avacopan treatment under irradiation. Interestingly, adding recombinant IL-1β alone did not affect glioma cell survival across a dose range of 0 – 6 Gy in both cell lines (Figure 5.16). Collectively, our findings demonstrate a key role for microglia-derived IL-1β, and potentially in conjunction with other microglia-derived factors in promoting glioma radioresistance. Targeting C5aR1 in microglia may enhance the therapeutic efficacy of radiotherapy in HGGs.

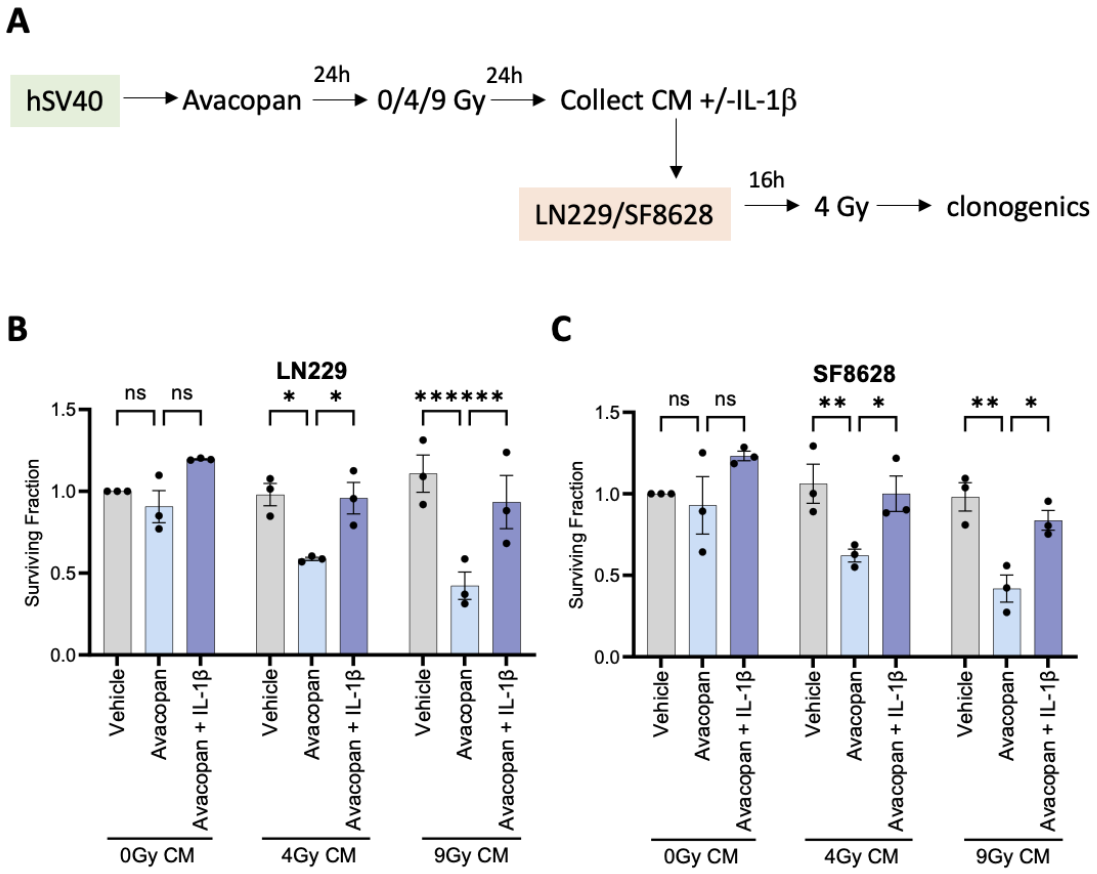

Figure 5.15 Reduction in IL-1β secreted by Avacopan-treated microglia post-irradiation is responsible for the radiosensitising effects exerted on HGGs

(A) Graphical representation of the experiment. hSV40 cells were treated with vehicle (DMSO) or Avacopan before 0 or 9 Gy irradiation. CM was collected 24 h post-irradiation, with or without addition of recombinant IL-1β and transferred to **(B)** LN229 (10 ng/mL IL-1β) and **(C)** SF8628 cells (1 ng/mL IL-1β). Glioma cells were irradiated at 4 Gy and cell survival was analysed via clonogenic assays. Data presented as mean ± SEM of biological replicates. n=3. Statistical analysis used two-way ANOVA with Tukey's test. *p≤0.05, **p≤0.01, ***p≤0.001.

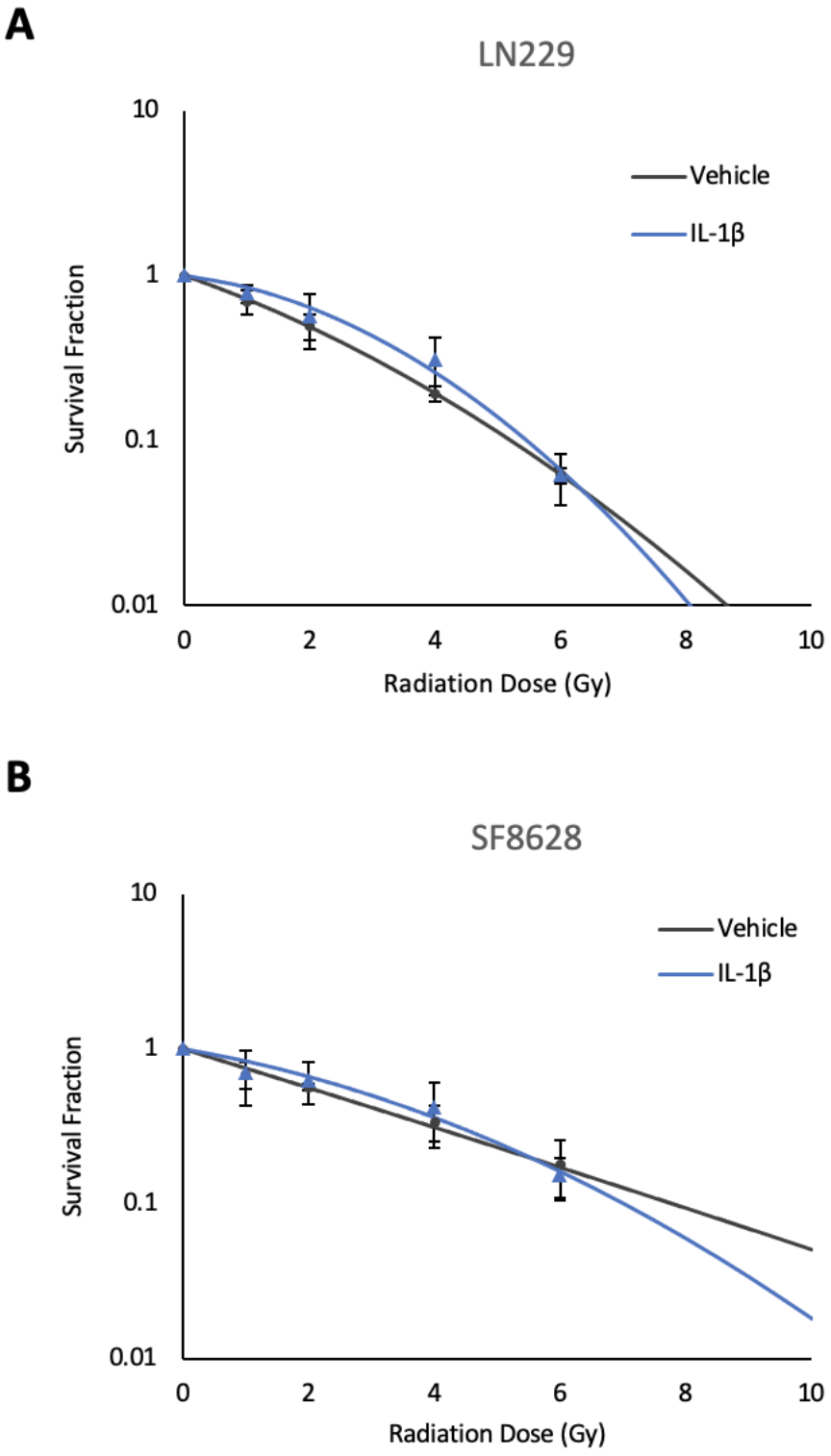

Figure 5.16 Recombinant IL-1β alone does not modulate glioma radiosensitivity

Vehicle (water) or recombinant IL-1β was added to **(A)** LN229 cells (10 ng/mL) and **(B)** SF8628 cells (1 ng/mL) for 16 h before 0-6 Gy irradiation. Cell survival was assessed via clonogenic assay. Data presented as mean ± SEM of biological replicates, with extrapolated line of best fit. n=3.

5.3 Discussion

In this chapter, we investigated the bidirectional communication between microglia and glioma cells, with a particular focus on the role of C5aR1 modulating microglial function and glioma response to radiation. We first demonstrated that irradiated microglia and MΦ significantly promote glioma viability, highlighting their pro-tumorigenic role. It was surprising that CM from irradiated cells retained the pro-viability effect despite the expected presence of DAMPs and PAMPs resulted from irradiation. Importantly, when microglia were pre-treated with Avacopan prior to irradiation, the CM significantly sensitised glioma cells to radiation-induced cytotoxicity. However, we cannot rule out the possibility that the radiosensitising effect observed was due to residual Avacopan in the CM, rather than the soluble factors released by microglia.

Using a panel of inflammatory markers, we observed that irradiation alone induced a predominantly pro-inflammatory transcriptional response in both microglia models. This is in line with previous findings describing radiation-induced pro-inflammatory phenotypes of microglia (Han *et al.*, 2016; Karimi Roshan *et al.*, 2024; Li *et al.*, 2015; Voshart *et al.*, 2024; Xue *et al.*, 2014). Interestingly, Avacopan effectively suppressed several of these pro-inflammatory genes following irradiation without concurrently promoting markers of a classic anti-inflammatory M2-like phenotype. These results suggest that C5aR1 inhibition may broadly dampen the M1-like activation of microglia post-irradiation, rather than redirecting them towards an alternative polarisation state. While qPCR provided valuable insights into transcriptional changes, future studies quantifying cytokine secretion of protein-level expression of inflammatory mediators will be necessary to fully characterise microglial inflammatory profile. Notably, the radiation-induced pro-inflammatory signature was more prominent in hSV40 compared to IMG

cells, indicating potential differences in radiosensitivity between microglial models, or it could be caused by quicker recovery time from irradiation in IMG cells. With its rapid doubling rate, we could have analysed the inflammatory markers of IMG at an earlier timepoint to capture potential transient changes of inflammation gene transcription.

Among the several cytokines affected by C5aR1 inhibition under irradiation, IL-1β emerged as one of the key players in modulating microglia-glioma interactions. We showed that recombinant IL-1β not only enhanced glioma proliferation but also reversed the radiosensitising effects of Avacopan-treated microglia on glioma cells. This reinforces the role of IL-1β as a critical mediator of microglia-induced glioma radioresistance, and that modulating microglial IL-1β secretion via C5aR1 inhibition could potentially enhance radiosensitivity in HGGs. However, given that recombinant IL-1β does not modulate radiosensitivity of glioma cells, the observed radiosensitising effect could be a result parallel, or in combination with other microglia-derived factors in the CM.

Mechanistically, we found that irradiation upregulated APOE expression in microglia cells, which was suppressed by Avacopan treatment. While APOE can be secreted or remain intracellular, our study focused on its potential role in activating intracellular inflammasome, and only cell lysates were analysed by western blotting using pan-APOE antibody, not specific APOE isoforms. Further studies into the direct link between APOE and IL-1β would be beneficial to investigate if C5aR1 beaks the crosstalk between APOE and IL-1β, as well as inflammasome activation.

Taken together, our findings reveal a complex, but potentially targetable interaction between glioma cells and microglia that is regulated by C5aR1 signalling. C5aR1 inhibition in microglia suppresses IL-1β secretion and other inflammatory mediators to mitigate their tumour-promoting role under irradiation. A schematic summary is shown in Figure 5.17. These effects underscore the therapeutic potential of targeting C5aR1 to disrupt the glioma–microglia crosstalk and enhance radiosensitivity in HGGs.

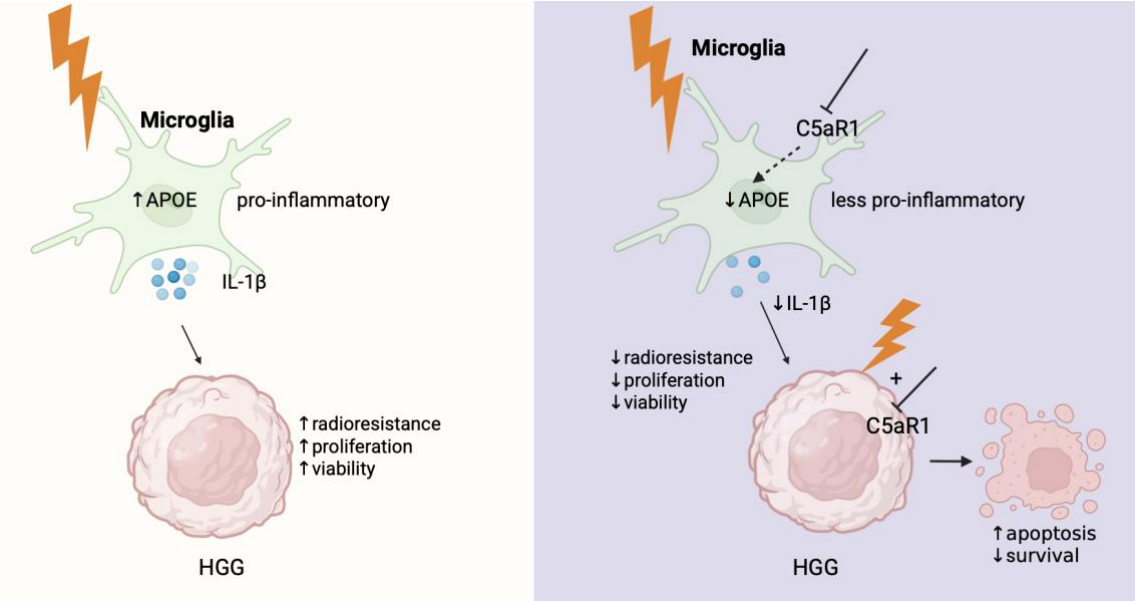

Figure 5.17 Schematic summary of microglia-glioma interactions under irradiation and C5aR1 inhibition

Illustration of the bidirectional communication between microglia and glioma cells. *(Left)* Upon irradiation, microglia upregulate APOE expression, leading to a shift toward a pro-inflammatory state and increased secretion of IL-1β. IL-1β acts on HGG cells to enhance their proliferation, viability, and resistance to radiation. *(Right)* Inhibition of C5aR1 in microglia attenuates radiation-induced IL-1β production, thereby enhancing the radiosensitivity of glioma cells. When combined with the direct radiosensitising effects of C5aR1 antagonists on HGGs, this dual mechanism contributes to an overall increase in glioma cell sensitivity to radiation.

Chapter 6 General Discussion

With the poor outcomes of HGG patients, novel therapeutic agents are needed to improve efficacy of standard of care treatments such as radiotherapy. The HGG TME is relatively hypoxic, and we found that intracellular C5aR1 expression was upregulated under severe hypoxia in our GBM model, but not in DMG. Both genetic silencing and pharmacological inhibition of C5aR1 demonstrated that C5aR1 is crucial for glioma cell survival under both normoxic and hypoxic condition. We then showed that targeting C5aR1 could potentiate radiation-induced cytotoxicity, thereby improving the radiosensitivity of HGGs. Interestingly, the anti-survival effects exerted by C5aR1 inhibitors were not observed in microglia. Instead, C5aR1 inhibition modulated the microglial inflammatory profile under irradiation, which in turned affected glioma radiosensitivity thorough secreting microglia-derived factors.

While our findings demonstrate that C5aR1 mRNA expression in glioma cells is upregulated at oxygen levels below <0.1%, the physiological relevance of such severe hypoxia warrants consideration. Not all regions of DMG and GBM tumours experience oxygen levels this low, instead, there is a gradient of oxygen levels within the tumour (Evans *et al.*, 2004). As such, using a single oxygen level may not accurately reflect the typical heterogenous oxygen gradients found within gliomas. Nonetheless, <0.1% O_2 remains a useful experimental model to study cellular behaviours under hypoxic stress response and radiation response under hypoxia.

C5aR1 mRNA expression was found to be specifically upregulated at <0.1% O_2, but not 1%, aligning with our previous findings that its induction is driven by UPR, rather than HIF signalling (Suwa *et al.*, 2025). HIF is said to be most active at 1% O_2, a condition

that does not typically activate UPR, hence, no changes in C5aR1 expression were observed. In contrast, <0.1% O_2 strongly induces ER stress, leading to UPR activation. To our surprise, we observed differential C5aR1 protein expression between our DMG and GBM models under severe hypoxia. We observed increased intracellular C5aR1 protein levels in LN229, but not in SF8628. Chemical induction of the UPR failed to elicit C5aR1 protein induction in SF8628 cells, even after timing optimisation (Figure 3.8). This discrepancy prompted us to question why C5aR1 mRNA was upregulated without corresponding protein upregulation. One possible explanation is post-transcriptional regulation, such as enhanced proteasomal degradation which may vary between cell lines. Under severe hypoxia, global translation repression is an adaptive mechanism that limits energy expenditure and protein accumulation. However, UPR activation selectively permits translation of proteins critical for survival under hypoxic stress. The absence of C5aR1 protein induction in SF8628 may reflect cell line- or glioma subtype-specific prioritisation of survival pathways, where C5aR1 is either less essential or subject to stricter translational control. It would be interesting to study if the absence of C5aR1 protein upregulation under severe hypoxia is also observed in other DMG cell lines.

C5aR1 receptor expression in SF8628 remains unchanged under severe hypoxia, accompanied with downregulated C5 ligand expression, which might explain the lack of significant changes in cell survival observed with Avacopan treatment under hypoxia, as opposed to the modest anti-survival effects observed in LN229 cells. This differential response between cell lines highlights heterogeneity in therapeutic response across HGG subtypes and underscores the importance of patient stratification when considering C5aR1-targeted therapies. Of note, when cell survival was assessed via clonogenic assays, cells were initially subjected to <0.1% O_2, followed by incubation at 21% O_2 for 10-14 days due to experimental constraints. This reoxygenation step introduces an additional

layer of cellular stress, potentially influencing cellular behaviours. Therefore, further investigation into the impact of reoxygenation in hypoxic HGG cells would be beneficial.

To assess C5aR1 receptor activation/inhibition, we used western blotting to detect changes in activation of NF-κB or MAPK pathways which are downstream of C5aR1, as shown in our previous study (Beach *et al.*, 2023). Although we acknowledge that these pathways are not exclusive to C5aR1, pRelA and pERK represent appropriate readouts for receptor activation. Another alternative to assess C5aR1 activation is via cyclic adenosine monophosphate (cAMP) assay which monitors production of cAMP resulted from GPCR activation. However, cAMP is also relatively non-specific to C5aR1 as it could be produced by any GPCRs.

A major challenge in detecting pRelA and pERK changes was optimising the timing of sample collection. Although we explored a range of timepoints during optimisation, the selected intervals may not have captured all potential signalling changes, and some event could have been missed. With that said, although NF-κB and MAPK signalling changes could occur within an hour after irradiation, we ultimately chose to harvest protein 24 h post-irradiation based on previous observations, and since significant signalling events are known to persist if initiated earlier (Hagan *et al.*, 2000; Sharma *et al.*, 2010). Another key limitation in interpreting our data lies in the concurrent downregulation of total and phosphorylated forms of RelA and ERK. The reduced total protein levels confound interpretation of phosphorylation changes as indicators of signalling activity. RNA-sequencing and pathway analysis in C5aR1 knockout colorectal cancer cells revealed broad suppression of protein translation pathways when C5aR1 is lost, which may also apply to HGG cells, though further validation is required.

We observed attenuation of both NF-κB and MAPK signalling pathways upon genetic silencing of C5aR1. However, pharmacological inhibition using C5aR1 antagonists predominantly attenuated MAPK activation, with minimal or inconsistent effects on NF-κB signalling. This differential downstream signalling implies that the mode of C5aR1 inhibition, genetic versus pharmacological, may elicit distinct signalling bias. Such functional selectivity has been found in GPCRs, including C5aR1, where different ligands or inhibitors could stabilise unique receptor conformations, leading to biased activation or suppression of downstream intracellular signalling pathways (Kenakin, 2011; Feng *et al.*, 2023). Specifically, C5aR1 could signal through various effector proteins, including heterotrimeric G proteins and β-arrestin, which can initiate separate cascades such as MAPK, NF-κB or PI3K/AKT signalling. The recruitment of specific effectors often depends on ligand structure, receptor conformation and duration of engagement. For example, recombinant C5a robustly activated NF-κB without altering MAPK, whereas Avacopan and PMX205 selectively attenuated MAPK signalling. These observations support the hypothesis that biased signalling at C5aR1 may underlie functional divergence observed with different inhibitor modalities. Future structural and proteomic studies could elucidate the mechanisms underpinnings of this pathway-selective modulation.

Due to limited availability of recombinant C5a, its use was mainly restricted to experiments specifically investigating C5a-C5aR1 signalling. Incorporating recombinant C5a as a control in more experiments, particularly under hypoxic or irradiation stress would have been beneficial. Upon addition of exogenous C5a proteins, NF-κB signalling changes were detectable within 2 hours. In contrast, a much longer pre-treatment duration was needed for our experiments with C5aR1 antagonists when we did not supplement the

culture media with recombinant or human C5a. One potential explanation would be the relatively low level of C5a present in our HGG culture. In the brain, sources of C5a include tumour cells, TAM, and other infiltrating immune cells. However, in our in vitro model, C5a is solely produced by glioma cells, and the reduced ligand availability may explain the need to prolong antagonist exposure before encountering hypoxic or irradiation stress to observe functional effects. Although we have not yet quantified the C5a protein level in our culture media due to technical challenges, intracellular C5 mRNA and protein were successfully detected in our cell lysates. We acknowledge that measuring C5a levels in the culture media, particularly in the conditioned media used for microglia experiments, would be important to confirm that C5a-C5aR1 signalling in the primary contributor to the effects we observed.

For irradiation studies, a single dose of 9 Gy was selected based on our prior work; however, clonogenic assays revealed physical limitations in colony formation above 6 Gy, raising concerns about the physiological relevance of the chosen dose. We subsequently confirmed via western blotting that 4 Gy irradiation elicited comparable Avacopan-induced signalling changes, thereby validating our experimental design. Nonetheless, future studies should consider including a lower irradiation dose that is uniform across different experiments, or fractionated doses to resemble clinical settings. In this study, we demonstrated the importance of C5aR1 in HGG survival and that Avacopan and PMX205 sensitise HGG cells to irradiation, even under hypoxia. However, expanding the panel of glioma models, particularly including more DMG cell lines, will be critical for assessing intertumoral variability. Due to culturing difficulties, we acknowledge that DMG cell lines were underrepresented in this study. Exploring C5aR1 inhibition in more HGG models may help identify responsive patient subsets, especially by incorporating cell lines with diverse mutation profiles, particularly those harbouring

MGMT or BRAF alterations that drive sustained NF-κB and MAPK signalling, to help assess how mutation status influences the efficacy of C5aR1 inhibition.

Another approach of modelling the hypoxic microenvironment is to utilise 3D spheroid cultures with hypoxic cores. Under severe hypoxia, Avacopan reduced cell survival in 2D cultures, but this effect was absent in LN229 spheroids despite confirmed hypoxic regions. This could be due to difference in oxygen levels. We could not measure the oxygen concentration within the spheroids and therefore could not verify if the core of spheroids reached <0.1% O_2. Given that C5aR1 is upregulated only at <0.1% O_2, the absence of response in spheroids may be attributed by insufficient hypoxic stress, and partial UPR activation. The divergent response observed between 2D monolayer cultures and 3D spheroid models underscore the importance of physiologically relevant TME models in preclinical assessment of therapeutic agents. While both PMX205 and Avacopan demonstrated radiosensitising effects in 2D cultures under normoxic and hypoxic conditions, these effects were not recapitulated in the 3D spheroid model. On the contrary, both inhibitors unexpectedly promoted spheroid growth, even under irradiation. This discrepancy may be attributed to the complex architecture of spheroids, which more accurately mimic the TME, including hypoxic gradients, limited drug penetration, and cell–cell interactions that could influence drug response. We did not validate whether the C5aR1 antagonists were functionally effective in 3D culture, and we could have optimised the dosage and treatment regimen. Furthermore, the pre-treatment duration before irradiation in 3D spheroids was shorter than our 2D models due to experimental constraints. Spheroids under different treatment conditions had to be irradiated when they were approximately the same size and we therefore could not leave the antagonists on for an extended period, in case they affected cell proliferation before irradiation. This shorter pre-treatment duration might also be part of the reason why different growth effects were

observed in between 2D and 3D cell models. The enhanced spheroid growth observed with C5aR1 blockade suggests that under certain conditions, C5aR1 may exert context-dependent effects, potentially restraining proliferation in hypoxia-adapted 3D tumour structures. However, there are other components in the glioma TME that express C5 and C5aR1, such as microglia and macrophages, which could influence the overall response to C5aR1 antagonists, and they are not present in our 3D model. Therefore, incorporating other TME components, and using in vivo models are necessary to more reliably predict physiologically relevant therapeutic efficacy.

After investigating the potential radiosensitisation role of C5aR1 in HGGs, we shifted our focus to microglia, which also express C5aR1. When assessing C5aR1 inhibition in irradiated microglia, we observed no significant changes in clonogenic survival, unlike what we observed in glioma cells which suggest a cell type-specific effect of PMX205 and Avacopan, and could be validated by genetic silencing of C5aR1. A piece of data we did not show in this study reveals that C5aR1 inhibition in glioma cells actually protect microglia from radiation-induced cytotoxicity due to certain glioma-derived proteins in the CM, meaning C5aR1 potentially has a radioprotective effects in microglia when they are in contact with HGG cells. The identity of potential glioma-derived proteins contributing to this radioprotective effect remains unclear and requires further exploration.

Our results show that microglia can support HGG viability via secretion of soluble factors, which aligns with previous reports (Liu *et al.*, 2021; Si *et al.*, 2024). However, Liu et al., (2021) specified that this pro-GBM function may be specific to HGG-associated microglia, a subpopulation not replicated in our culture system. Our hSV40 cells were not cultured in direct contact with glioma cells or glioma-conditioned media,

which are necessary for inducing HGG-MG phenotypes. Our model may therefore represent either resting or irradiation-activated microglia, rather than true-HGG-MG (Han *et al.*, 2016). Irradiation-activated microglia could act differently to actual HGG-MG and that microglia-promoted GBM growth could be different in vivo, when cells are in direct contact. Therefore, future studies incorporating direct co-culture systems could better replicate the glioma TME.

Upon irradiation, hSV40 microglia-like cells adopted a pro-inflammatory phenotype, similar to the phenotype described in HGG-AM (Liu *et al.*, 2022; Han *et al.*, 2016; Acharya *et al.*, 2016). C5aR1 inhibition in microglia successfully suppressed this radiation-induced inflammation, as evident by downregulation of several pro-inflammatory markers, which we expected from blocking anaphylatoxin signalling. These findings mirror studies in Alzheimer's Disease, where absence or inhibition of C5aR1 delays microglial polarisation to a pro-inflammatory phenotype (Gomez-Arboledas *et al.*, 2022; Hernandez *et al.*, 2017; Schartz *et al.*, 2023). This suppression of inflammatory responses suggests a shift away from the M1-like phenotype, and potentially reduced phagocytic activity, as phagocytosis is enhanced by inflammation (Neher *et al.*, 2011). This is supported by the work from Dr Lolita Singh in our group, which demonstrates significant reduction in phagocytosis in irradiated IMG cells upon PMX205 treatment (data not included). Reduction in phagocytosis had also been previously reported upon C5aR1 ablation (Hernandez *et al.*, 2017; Carvalho *et al.*, 2022). However, the exact mechanisms involved remain poorly defined, particularly in the context of HGG.

APOE has been implicated in inflammasome regulation, particularly the NLRP1 complex, leading to IL-1β secretion (Liu *et al.*, 2021). We observed increased APOE expression in irradiated microglia, which was then suppressed by C5aR1 inhibition. Previous spatial transcriptomics from our group comparing expression changes in irradiated intestines between WT and C5aR1 KO mice also revealed downregulation of APOE gene expression when C5aR1 is absent, further supporting the link with C5aR1 and APOE, which has not been reported in existing literature. APOE is overexpressed by many cancer types, including GBM, where it drives glioma progression and therefore we should investigate the novel link between C5aR1 and APOE expression in the future (Huang *et al.*, 2025; Nicoll *et al.*, 2003). However, the role of APOE in microglia polarisation is context- and isoform-dependent. In Alzheimer's disease, APOE4 promotes neurotoxicity and pro-inflammation responses of microglia by increasing the level of NLRP3 inflammasome and ROS (Liu *et al.*, 2024; Friedberg *et al.*, 2020). In contrast, in the context of GBM, APOE appears to foster an immunosuppressive M2-like TAM phenotype with anti-inflammatory properties, though no specific isoforms have been identified as the main contributor (Kemp *et al.*, 2021; Hui *et al.*, 2022; Huang *et al.*, 2025). In our model, APOE upregulation in irradiated microglia was associated with increased pro-inflammatory gene expression, and APOE downregulation in Avacopan-treated microglia was accompanied with concurrent suppression of many pro-inflammatory markers. Although we did not investigate the direct correlation between APOE and these inflammatory genes, our data suggests APOE appears to associate with inflammation, aligning with the studies in Alzheimer's disease rather than GBM. However, the role of APOE in these previous cancer-related studies utilised APOE knockout mice or gene silencing in cancer cells, rather than direct APOE modulation in microglia. Future studies employing direct APOE induction or silencing in microglia, ideally within co-culture

systems together with HGG cells, are needed to clarify its role in glioma-associated inflammation.

Currently, the link between APOE and nucleotide-binding domain, leucine-rich-containing gamily, pyrin domain-containing protein 3 (NLRP3) activation is more well-established than with NLRP1. There is strong evidence in Alzheimer's Disease that APOE in microglia activates NLRP3, resulting in secretion of pro-inflammatory caspase-1 mediated IL-1β (Liu *et al.*, 2024; Jin *et al.*, 2022; Li *et al.*, 2022). It is worth noting that both NLRP1 and NLRP3 leads to IL-1β secretion, and IL-1β also elevates the expression of APOE, forming a positive feedback loop (Liu *et al.*, 2011b). We therefore attempted to investigate if irradiation also activates NLRP3 in hSV40 cells. However, NLRP3 proteins were not detected in our hSV40 cells via western blotting under any tested conditions, so it is unlikely to be responsible for the secretion of IL-1β. Additionally, changes in NF-κB activity in microglia may also modulate 1β secretion and should be investigated in the future, as this pro-survival signalling pathway is often upregulated by irradiation (Kang *et al.*, 2021).

Despite the uncertainties linking APOE and IL-1β, we detected an increase in IL-1β secretion in irradiated microglia, which was suppressed by Avacopan. Addition of exogenous IL-1β promoted HGG cell proliferation and radioresistance, supporting its role in HGG progression. Our results support numerous studies reporting the pro-tumorigenic role of IL-1β in GBM (Shen *et al.*, 2021; Liu *et al.*, 2021; Fathima Hurmath, Ramaswamy and Nandakumar, 2014; Si *et al.*, 2024). To our knowledge, there is no existing literature reporting IL-1β as a radioresistance mediator in brain tumours, though there is one study which described IL-1β expression as indicator of cellular radioresistance in head and neck squamous cell carcinoma (Tiwari *et al.*, 2022). The exact mechanisms on how IL-1β

affects radiosensitivity remain unknown, but it could activate key pro-survival signalling pathways such as PI3K/AKT, NF-κB and MAPK, all of which have established roles in radioresistance (Shen *et al.*, 2021; Kulawik *et al.*, 2017; Hai Ping *et al.*, 2016; Pei *et al.*, 2016). It would be worth studying if IL-1β mediates radioresistance in HGGs by regulating these canonical signalling pathways. Moreover, genetic loss of IL-1β has been reported to reduce exhausted $CD8^+$ T cells and improves survival of GBM-bearing mice, highlighting an area worth exploring if we are to explore how C5aR1 inhibition could affect adaptive immunity (Chen *et al.*, 2023). However, it is important to note that the concentration of IL-1β detected in our microglia culture media was substantially lower than the effective concentration of recombinant IL-1β added to HGG cells, and we did not observe any radioresistance effects when recombinant IL-1β was added directly to unconditioned media. The overall pro-survival effects observed with our media co-culture system were more likely the result of a combination of multiple soluble factors secreted by microglia, rather than being mediated by IL-1β alone.

One thing to note is that we originally used hSV40 cell line as our human microglia model. However, both our group and our collaborator discovered that hSV40 as a microglia-like cell line lacks expression of typical myeloid markers such as TMEM119 and CD11b at the protein level. Due to these inconsistencies, hSV40 cells are best considered microglia-like rather than true microglia. Microglia culture might lose certain typical myeloid surface markers after repeated passages, flow cytometry at earliest available passages (passage 8) was attempted to detect classic M1/M2-like surface markers but also failed. More importantly, upon completion of the experiments included in this study, we discovered that the hSV40 cell line was of mouse origin rather than human, despite confirmation from the supplier. Given that Avacopan theoretically binds

to human C5aR1 with much higher affinity than mouse C5aR1, the species discrepancy limits the interpretation of the Avacopan data obtained using hSV40 cells. To address this limitation, we also utilised PBMC-derived MΦ as another TAM model they yielded results similar to those in hSV40 cells. However, these PBMCs were collected from healthy patients and differentiated into MΦ in the lab, therefore they might behave differently to the specific TAMs found in the HGG TME. We also have not yet tested Avacopan on these human MΦ. A better human microglia model would be highly beneficial for this study, and we are currently repeating key microglia experiments using human induced pluripotent stem cells-derived microglia, particularly given the human-specific activity of Avacopan. In general, C5aR1 knockout cell lines or mice would also be beneficial to study any potential off-target effects observed with C5aR1 antagonists.

Overall, our studies demonstrated a potential role in C5aR1 inhibition in enhancing the radiosensitivity of HGG cells. However, our findings are limited to in vitro models. While studies on cell lines offer valuable mechanistic insights, they do not account for the full complexity of the TME that exist in vivo, especially considering that C5aR1 is expressed on many immune cells. Future in vivo studies using orthotopic glioma models would be beneficial to validate the therapeutic relevance of C5aR1 inhibition in improving radiosensitivity of HGGs.

Appendices

Appendix A

A.1 Quantification of Western Blot analysis of C5aR1 knockdown in SF8628 cells under hypoxia

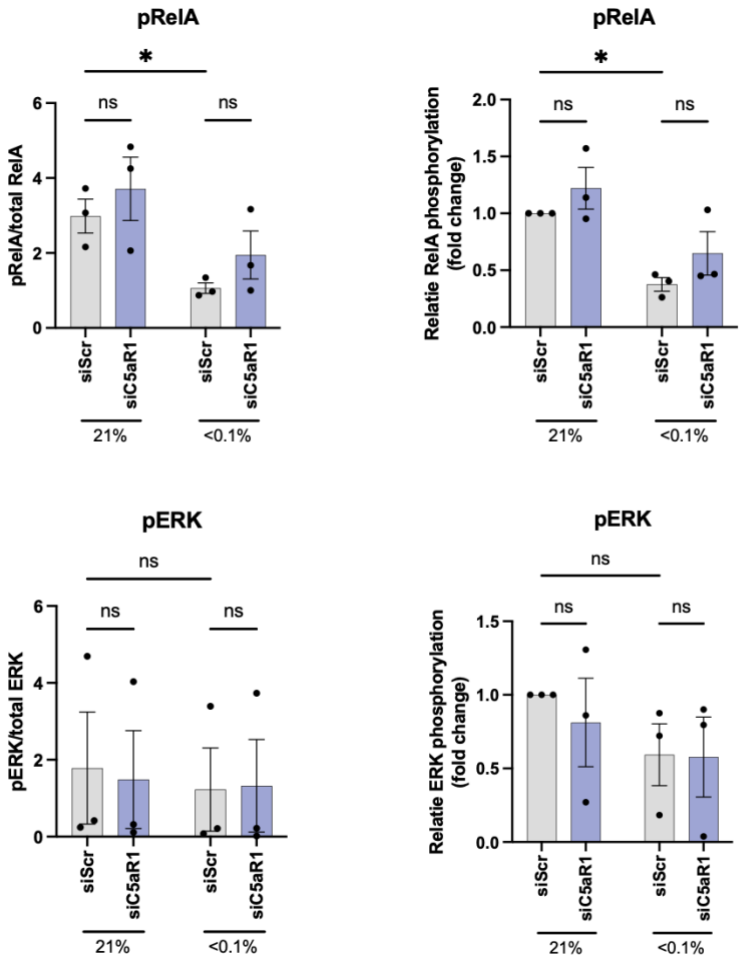

Figure A.1 Variable effects of C5aR1 knockdown on pro-survival signalling in SF8628

SF8628 cells were transfected with siScr or siC5aR1 for 72 hours before 16 h of exposure to 21% or <0.1% O_2. Western blotting was carried out using antibodies against pRelA, total RelA, pERK and total ERK. Band intensities were quantified and are presented in two ways: as the ratio of phosphorylated to total protein (left panel) and as fold change relative to control (right panel). Data presented as mean ± SEM of biological replicates. n=3. Statistical analysis used two-way ANOVA with Fisher's LSD test. *p≤0.05.

A.2 Optimisation of PMX205 treatment time

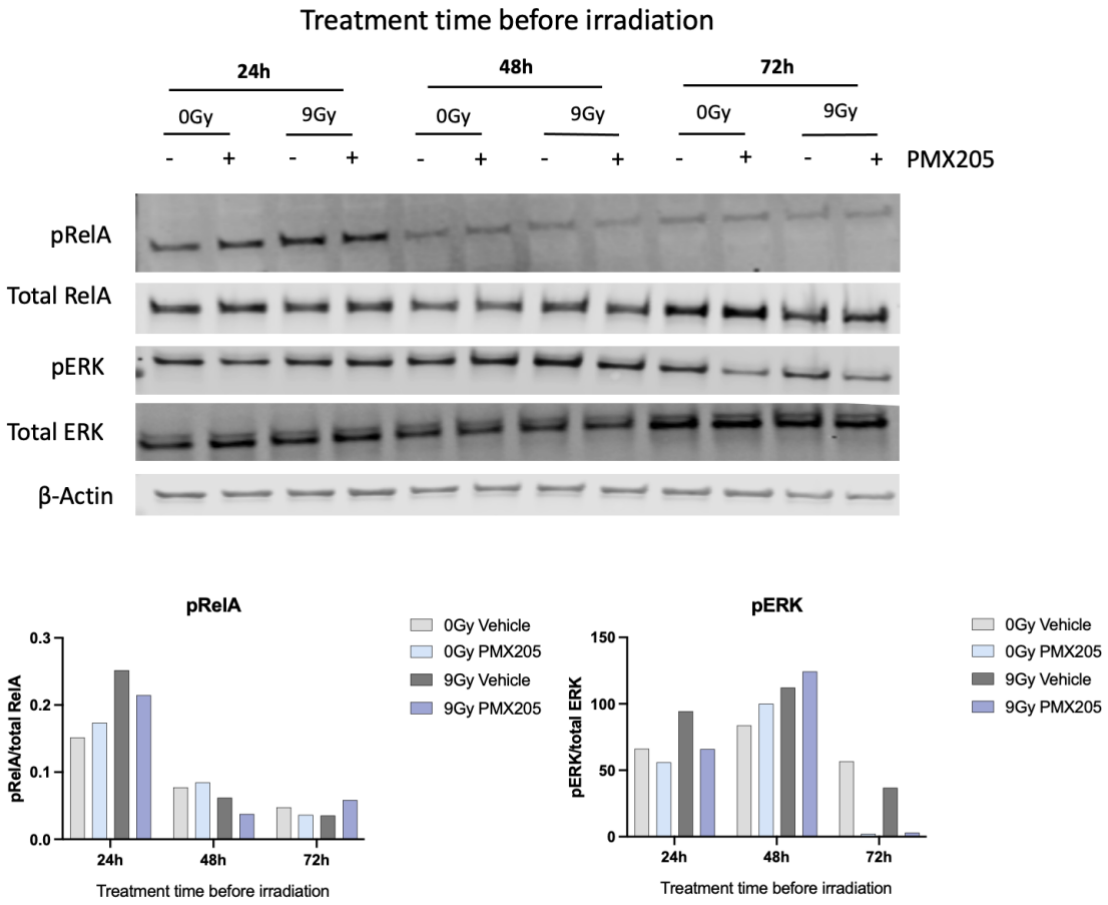

Figure A.2 Optimisation of PMX205 treatment time before irradiation with pro-survival signalling changes

Vehicle (water) or PMX205 was added to LN229 cells for 24, 48 or 72 h before 0 or 9 Gy irradiation. Samples were harvested 24 h post-irradiation. Western blotting was carried out with the antibodies indicated. β-actin was used as loading control. Band intensities were quantified and presented as the ratio of phosphorylated to total protein.

A.3 Quantification of Western Blot analysis of PMX205 treatment in SF8628 cells under irradiation

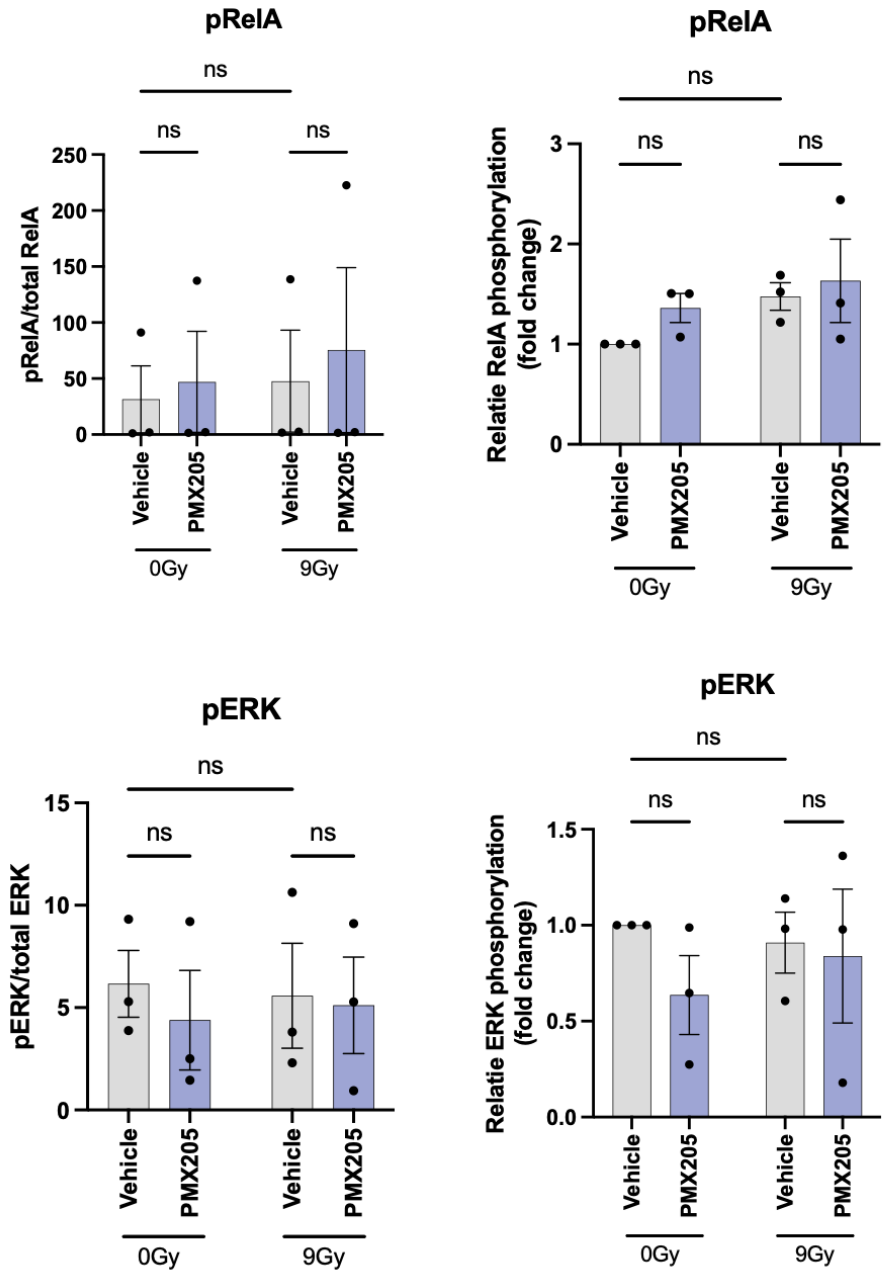

Figure A.3 PMX205 treatment had no significant impact on pro-survival signalling in SF8628

Vehicle (water) or PMX205 was added to SF8628 cells for 72 h before 0 or 9 Gy irradiation. Samples were harvested 24 h post-irradiation. Western blotting was carried out using antibodies against pRelA, total RelA, pERK and total ERK. Band intensities were quantified and are presented in two ways: as the ratio of phosphorylated to total protein (left panel) and as fold change relative to control (right panel). Data presented as mean ± SEM of biological replicates. n=3. Statistical analysis used two-way ANOVA with Fisher's LSD test.

A.4 Quantification of Western Blot analysis of Avacopan treatment in LN229 cells under irradiation

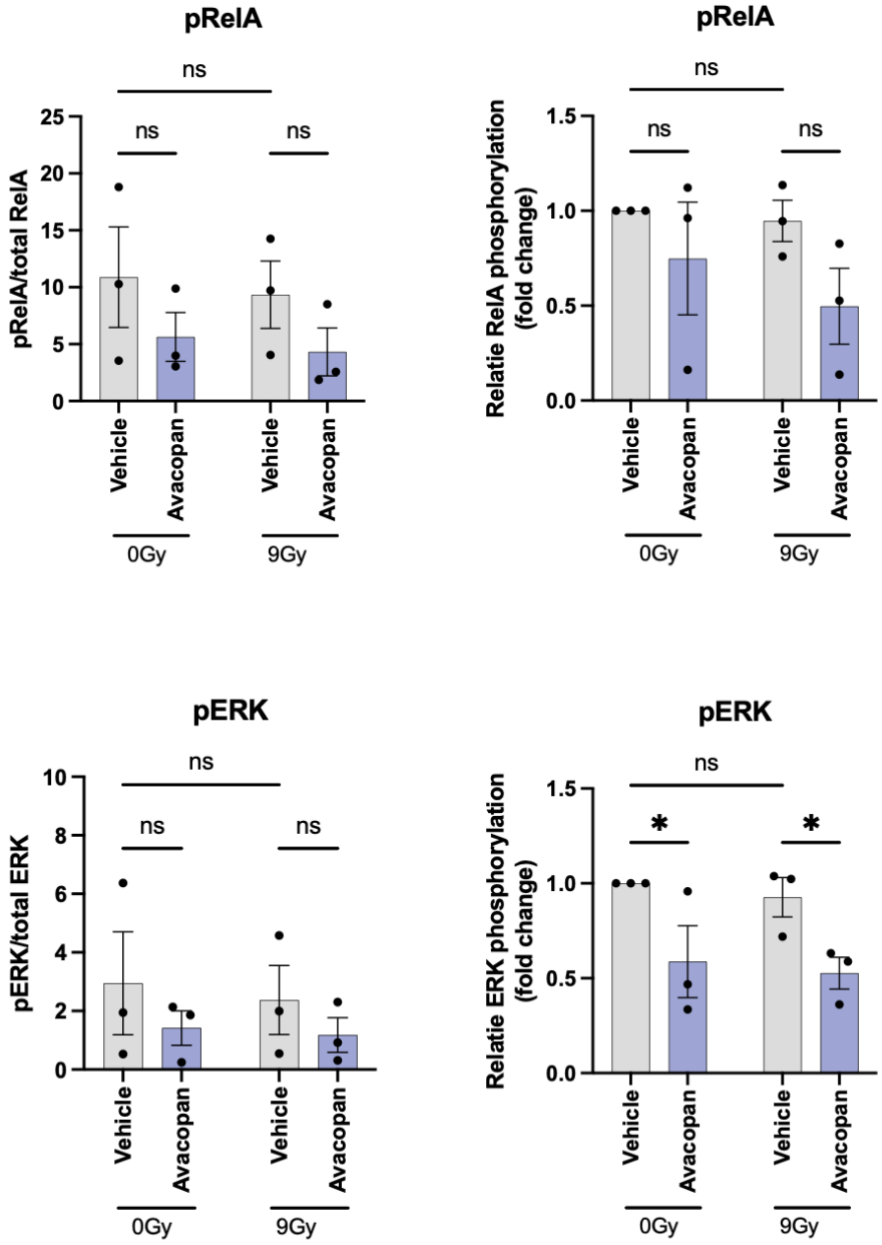

Figure A.4 Variable effects of Avacopan treatment on NF-κB signalling in LN229

Vehicle (DMSO) or Avacopan was added to LN229 cells for 24 h before 0 or 9 Gy irradiation. Samples were harvested 24 h post-irradiation. Western blotting was carried out using antibodies against pRelA, total RelA, pERK and total ERK. Band intensities were quantified and are presented in two ways: as the ratio of phosphorylated to total protein (left panel) and as fold change relative to control (right panel). Data presented as mean ± SEM of biological replicates. n=3. Statistical analysis used two-way ANOVA with Fisher's LSD test. *p≤0.05.

Appendix B

B.1 Validation of LPS as a control for inflammatory marker expression in IMG cells

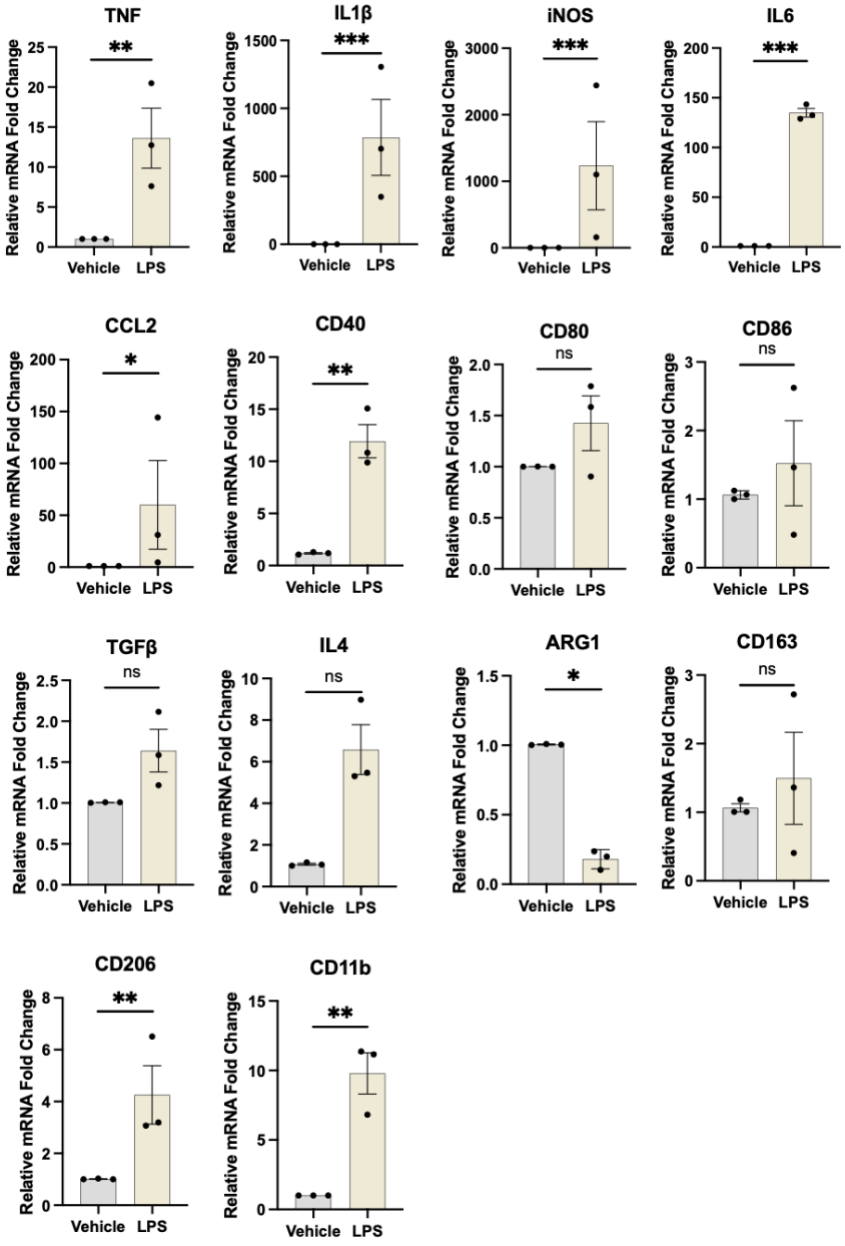

Figure B.1 Validation of LPS as a control for inflammatory marker expression in IMG cells

IMG cells were treated with vehicle (water) or LPS for 24 h before 0 or 9 Gy irradiation. mRNA expression of the indicated genes were assessed by qPCR 24 h post-irradiation. All mRNA levels were normalised to 18S and expressed as fold change relative to the expression of Vehicle. Data present as mean of biological replicates. n=3. Statistical analysis was performed on unnormalised values using unpaired t-test. *p≤0.05, **p≤0.01, ***p≤0.001.

B.2 Validation of LPS as a control for inflammatory marker expression in hSV40 cells

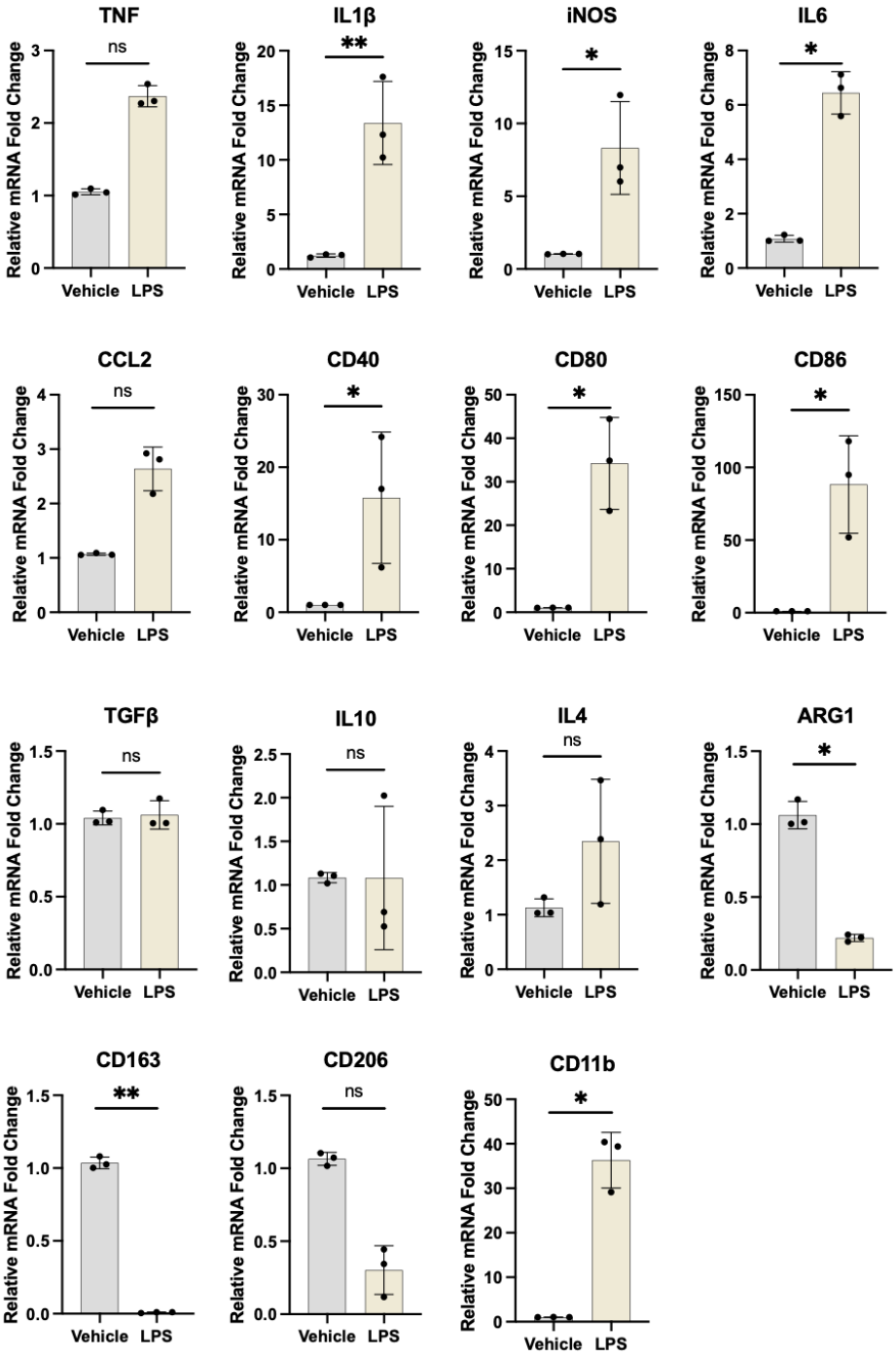

Figure B.2 Validation of LPS as a control for inflammatory marker expression in hSV40 cells

hSV40 cells were treated with vehicle (water) or LPS for 24 h before 0 or 9 Gy irradiation. mRNA expression of the indicated genes were assessed by qPCR 24 h post-irradiation. All mRNA levels were normalised to 18S and expressed as fold change relative to the expression of vehicle. Data present as mean of biological replicates. n=3. Statistical analysis was performed on unnormalised values using unpaired t-test. *p≤0.05, **p≤0.01.

References

Abd Elmaogod, E. A., Daoud, S. A., Mostafa, Z. M., Mohamed, E. and Mahmoud, M. (2022) 'Prognostic significance of HIF1-α immunohistochemical expression in gliomas and it's relation to IDH1 mutation status', *Beni-Suef Univ J Basic Appl Sci,* 11(140).

Acharya, M. M., Green, K. N., Allen, B. D., Najafi, A. R., Syage, A., Minasyan, H., Le, M. T., Kawashita, T., Giedzinski, E., Parihar, V. K., West, B. L., Baulch, J. E. and Limoli, C. L. (2016) 'Elimination of microglia improves cognitive function following cranial irradiation', *Sci Rep,* 6, pp. 31545.

Adermark, L., Lagström, O., Loftén, A., Licheri, V., Havenäng, A., Loi, E. A., Stomberg, R., Söderpalm, B., Domi, A. and Ericson, M. (2022) 'Astrocytes modulate extracellular neurotransmitter levels and excitatory neurotransmission in dorsolateral striatum via dopamine D2 receptor signaling', *Neuropsychopharmacology,* 47, pp. 1493–1502

Afashar-Kharghan, V. (2017) 'The role of the complement system in cancer', *The Journal of Clinical Investigation,* 127(3), pp. 780-789.

Alcantara Llaguno, S., Chen, J., Kwon, C. H., Jackson, E. L., Li, Y., Burns, D. K., Alvarez-Buylla, A. and Parada, L. F. (2009) 'Malignant astrocytomas originate from neural stem/progenitor cells in a somatic tumor suppressor mouse model', *Cancer Cell,* 15(1), pp. 45-56.

An, X. Q., Xi, W., Gu, C. Y. and Huang, X. (2018) 'Complement protein C5a enhances the β-amyloid-induced neuro-inflammatory response in microglia in Alzheimer's disease', *Med Sci (Paris),* 34 Focus issue F1, pp. 116-120.

Araki, K. and Nagata, K. (2011) 'Protein folding and quality control in the ER', *Cold Spring Harb Perspect Biol,* 3(11), pp. a007526.

Aspelund, A., Antila, S., Proulx, S. T., Karlsen, T. V., Karaman, S., Detmar, M., Wiig, H. and Alitalo, K. (2015) 'A dural lymphatic vascular system that drains brain interstitial fluid and macromolecules', *J Exp Med,* 212(7), pp. 991-999.

B'Chir, W., Maurin, A. C., Carraro, V., Averous, J., Jousse, C., Muranishi, Y., Parry, L., Stepien, G., Fafournoux, P. and Bruhat, A. (2013) 'The eIF2α/ATF4 pathway is essential for stress-induced autophagy gene expression', *Nucleic Acids Res,* 41(16), pp. 7683-99.

Babaloui, S., Najafi, M., Mozdarani, H., Borhani, S., Jaberi, R. and Aghili, M. (2022) 'Radiosensitization of Glioma Cells by Temozolomide (TMZ): A Colony Formation Assay', *J Biomed Phys Eng,* 12(1), pp. 43-50.

Bao, S., Wu, Q., McLendon, R. E., Hao, Y., Shi, Q., Hjelmeland, A. B., Dewhirst, M. W., Bigner, D. D. and Rich, J. N. (2006) 'Glioma stem cells promote radioresistance by preferential activation of the DNA damage response', *Nature,* 444(7120), pp. 756-60.

Bar, E. E., Lin, A., Mahairaki, V., Matsui, W. and Eberhart, C. G. (2010) 'Hypoxia increases the expression of stem-cell markers and promotes clonogenicity in glioblastoma neurospheres', *Am J Pathol,* 177(3), pp. 1491-502.

Barbero, S., Bajetto, A., Bonavia, R., Porcile, C., Piccioli, P., Pirani, P., Ravetti, J. L., Zona, G., Spaziante, R., Florio, T. and Schettini, G. (2002) 'Expression of the Chemokine Receptor CXCR4 and Its Ligand Stromal Cell-Derived Factor 1 in Human Brain Tumors and Their Involvement in Glial Proliferation *in Vitro*', *Annals of the New York Academy of Sciences,* 973, pp. 60-69.

Basak, O., Giachino, C., Fiorini, E., Macdonald, H. R. and Taylor, V. (2012) 'Neurogenic subventricular zone stem/progenitor cells are Notch1-dependent in their active but not quiescent state', *J Neurosci,* 32(16), pp. 5654-66.

Baskar, R., Dai, J., Nei, W., Yeo, R. and Yeoh, K.-W. (2014) 'Biological response of cancer cells to radiation treatment', *Frontiers in Molecular Biosciences,* 1(24).

Basu, R., Whitlock, B. M., Husson, J., Le Floc'h, A., Jin, W., Oyler-Yaniv, A., Dotiwala, F., Giannone, G., Hivroz, C., Biais, N., Lieberman, J., Kam, L. C. and Huse, M. (2016) 'Cytotoxic T Cells Use Mechanical Force to Potentiate Target Cell Killing', *Cell,* 165(1), pp. 100-110.

Beach, C., MacLean, D., Majorova, D., Melemenidis, S., Nambiar, D. K., Kim, R. K., Valbuena, G. N., Guglietta, S., Krieg, C., Darvish-Damavandi, M., Suwa, T., Easton, A., Hillson, L. V. S., McCulloch, A. K., McMahon, R. K., Pennel, K., Edwards, J., O'Cathail, S. M., Roxburgh, C. S., Dominigo, E., Moon, E. J., Jiang, D., Jiang, Y., Zhang, Q., Koong, A. C., Woodruff, T. M., Graves, E. E., Maughan, T., Buczacki, S. J. A., Stucki, M., Le, Q.-T., Leedham, S. J., Giaccia, A. J. and Olcina, M. M. (2023) 'Improving radiotherapy in immunosuppressive microenvironments by targeting complement receptor C5aR1', *J Clin Invest.,* 133(23), pp. e168277.

Bekker, P., Dairaghi, D., Seitz, L., Leleti, M., Wang, Y., Ertl, L., Baumgart, T., Shugarts, S., Lohr, L., Dang, T., Miao, S., Zeng, Y., Fan, P., Zhang, P., Johnson, D., Powers, J., Jaen, J., Charo, I. and Schall, T. J. (2016) 'Characterization of Pharmacologic and Pharmacokinetic Properties of CCX168, a Potent and Selective Orally Administered Complement 5a Receptor Inhibitor, Based on Preclinical Evaluation and Randomized Phase 1 Clinical Study', *PLoS One,* 11(10), pp. e0164646.

Berghoff, A. S., Kiesel, B., Widhalm, G., Rajky, O., Ricken, G., Wöhrer, A., Dieckmann, K., Filipits, M., Brandstetter, A., Weller, M., Kurscheid, S., Hegi, M. E., Zielinski, C. C., Marosi, C., Hainfellner, J. A., Preusser, M. and Wick, W. (2015) 'Programmed death ligand 1 expression and tumor-infiltrating lymphocytes in glioblastoma', *Neuro-Oncology,* 17(8), pp. 1064–1075.

Bertout, J. A., Patel, S. A. and Simon, M. C. (2008) 'The impact of O2 availability on human cancer', *Nat Rev Cancer,* 8(12), pp. 967-75.

Bhaskara, V. K., Mohanam, I., Rao, J. S. and Mohanam, S. (2012) 'Intermittent hypoxia regulates stem-like characteristics and differentiation of neuroblastoma cells', *PLoS One,* 7(2), pp. e30905.

Bhat, K. P. L., Balasubramaniyan, V., Vaillant, B., Ezhilarasan, R., Hummelink, K., Hollingsworth, F., Wani, K., Heathcock, L., James, J. D., Goodman, L. D., Conroy, S., Long, L., Lelic, N., Wang, S., Gumin, J., Raj, D., Kodama, Y., Raghunathan, A., Olar, A., Joshi, K., Pelloski, C. E., Heimberger, A., Kim, S. H., Cahill, D. P., Rao, G., Den

Dunnen, W. F. A., Boddeke, H., Phillips, H. S., Nakano, I., Lang, F. F., Colman, H., Sulman, E. P. and Aldape, K. (2013) 'Mesenchymal differentiation mediated by NF-κB promotes radiation resistance in glioblastoma', *Cancer Cell,* 24(3), pp. 331-46.

Blair, T., Baird, J., Bambina, S., Kramer, G., Gostissa, M., Harvey, C. J., Gough, M. J. and Crittenden, M. R. (2022) 'ICOS is upregulated on T cells following radiation and agonism combined with radiation results in enhanced tumor control', *Sci Rep,* 12(1), pp. 14954.

Blandin, A.-F., Durand, A., Littler, M., Tripp, A., Guérin, É., Ruhland, E., Obrecht, A., Keime, C., Fuchs, Q., Reita, D., Lhermitte, B., Coca, A., Jones, C., Lelong Rebel, I., Villa, P., Namer, I. J., Dontenwill, M., Guenot, D. and Entz-Werle, N. (2019) 'Hypoxic Environment and Paired Hierarchical 3D and 2D Models of Pediatric H*3.3*-Mutated Gliomas Recreate the Patient Tumor Complexity', *Cancers (Basel),* 11(12), pp. 1875.

Bommiasamy, H., Back, S. H., Fagone, P., Lee, K., Meshinchi, S., Vink, E., Sriburi, R., Frank, M., Jackowski, S., Kaufman, R. J. and Brewer, J. W. (2009) 'ATF6alpha induces XBP1-independent expansion of the endoplasmic reticulum', *J Cell Sci,* 122(Pt 10), pp. 1626-36.

Bowman, R. L., Klemm, F., Akkari, L., Pyonteck, S. M., Sevenich, L., Quail, D. F., Dhara, S., Simpson, K., Gardner, E. E., Iacobuzio-Donahue, C. A., Brennan, C. W., Tabar, V., Putin, P. H. and Joyce, J. A. (2016) 'Macrophage Ontogeny Underlies Differences in Tumor-Specific Education in Brain Malignancies', *Cell Reports,* 17(9), pp. 2445-2459.

Brennan, C. W., Verhaak, R. G., McKenna, A., Campos, B., Noushmehr, H., Salama, S. R., Zheng, S., Chakravarty, D., Sanborn, J. Z., Berman, S. H., Beroukhim, R., Bernard, B., Wu, C. J., Genovese, G., Shmulevich, I., Barnholtz-Sloan, J., Zou, L., Vegesna, R., Shukla, S. A., Ciriello, G., Yung, W. K., Zhang, W., Sougnez, C., Mikkelsen, T., Aldape, K., Bigner, D. D., Van Meir, E. G., Prados, M., Sloan, A., Black, K. L., Eschbacher, J., Finocchiaro, G., Friedman, W., Andrews, D. W., Guha, A., Iacocca, M., O'Neill, B. P., Foltz, G., Myers, J., Weisenberger, D. J., Penny, R., Kucherlapati, R., Perou, C. M., Hayes, D. N., Gibbs, R., Marra, M., Mills, G. B., Lander, E., Spellman, P., Wilson, R., Sander, C., Weinstein, J., Meyerson, M., Gabriel, S., Laird, P. W., Haussler, D., Getz, G. and Chin, L. (2013) 'The somatic genomic landscape of glioblastoma', *Cell,* 155(2), pp. 462-77.

Broekman, M. L., Maas, S. L. N., Abels, E. R., Mempel, T. R., Krichevsky, A. M. and Breakefield, X. O. (2018) 'Multidimensional communication in the microenvirons of glioblastoma', *Nat Rev Neurol,* 14(8), pp. 482-495.

Buckingham, S. C., Campbell, S. L., Haas, B. R., Montana, V., Robel, S., Ogunrinu, T. and Sontheimer, H. (2011) 'Glutamate Release by Primary Brain Tumors Induces Epileptic Activity', *Nat Med,* 17(10), pp. 1269–1274.

Buczkowicz, P. and Hawkins, C. (2015) 'Pathology, Molecular Genetics, and Epigenetics of Diffuse Intrinsic Pontine Glioma', *Front Oncol,* 5, pp. 147.

Cain, K., Brown, D. G., Langlais, C. and Cohen, G. M. (1999) 'Caspase activation involves the formation of the aposome, a large (approximately 700 kDa) caspase-activating complex', *J Biol Chem,* 274(32), pp. 22686-92.

Calzascia, T., Masson, F., di Berardino-Besson, W., Contassot, E., Wilmotte, R., Aurrand-Lions, M., Rüegg, C., Dietrich, P.-Y. and Walker, P. R. (2005) 'Homing Phenotypes of Tumor-Specific CD8 T Cells Are Predetermined at the Tumor Site by Crosspresenting APCs', *Immunity,* 22(2), pp. 175-84.

Cao, J., Dai, D. L., Yao, L., Yu, H. H., Ning, B., Zhang, Q., Chen, J., Cheng, W. H., Shen, W. and Yang, Z. X. (2012) 'Saturated fatty acid induction of endoplasmic reticulum stress and apoptosis in human liver cells via the PERK/ATF4/CHOP signaling pathway', *Mol Cell Biochem,* 364(1-2), pp. 115-29.

Carvalho, D. M., Temelso, S., Mackay, A., Pemberton, H. N., Rogers, R., Kessler, K., Izquierdo, E., Bjerke, L., Salom, J. F., Clarke, M., Grabovska, Y., Burford, A., Olaciregui, N. G., Boult, J. K., Molinari, V., Fofana, M., Proszek, P., Potente, E., Taylor, K. R., Chandler, C., Zebian, B., Bhangoo, R., Martin, A. J., Dabbous, B., Stapleton, S., Hettige, S., Marshall, L. V., Carceller, F., Mandeville, H. C., Vaidya, S. J., Al-Sarraj, S., Bridges, L. R., Johnston, R., Cryan, J., Farrell, M., Crimmins, D., Caird, J., Pears, J., Pericoli, G., Miele, E., Mastronuzzi, A., Locatelli, F., Carai, A., Robinson, S. P., Hubank, M., Monje, M., Moore, A. S., Hassall, T. E., Carcaboso, A. M., Lord, C. J., Vinci, M. and Jones, C. (2020) 'Drug screening linked to molecular profiling identifies novel dependencies in patient-derived primary cultures of paediatric high grade glioma and DIPG', *BioRxiv*.

Carvalho, K., Schartz, N. D., Balderrama-Gutierrez, G., Liang, H. Y., Chu, S. H., Selvan, P., Gomez-Arboledas, A., Petrisko, T. J., Fonseca, M. I., Mortazavi, A. and Tenner, A. J. (2022) 'Modulation of C5a-C5aR1 signaling alters the dynamics of AD progression', *J Neuroinflammation,* 19(1), pp. 178.

Chakraborty, M., Abrams, S. I., Camphausen, K., Liu, K., Scott, T., Coleman, C. N. and Hodge, J. W. (2003) 'Irradiation of tumor cells up-regulates Fas and enhances CTL lytic activity and CTL adoptive immunotherapy', *J Immunol,* 170(12), pp. 6338-47.

Chaligne, R., Gaiti, F., Silverbush, D., Schiffman, J. S., Weisman, H. R., Kluegel, L., Gritsch, S., Deochand, S. D., Gonzalez Castro, L. N., Richman, A. R., Klughammer, J., Biancalani, T., Muus, C., Sheridan, C., Alonso, A., Izzo, F., Park, J., Rozenblatt-Rosen, O., Regev, A., Suvà, M. L. and Landau, D. A. (2021) 'Epigenetic encoding, heritability and plasticity of glioma transcriptional cell states', *Nat Genet,* 53(10), pp. 1469-1479.

Chalmers, A. J., Ruff, E. M., Martindale, C., Lovegrove, N. and Short, S. C. (2009) 'Cytotoxic effects of temozolomide and radiation are additive- and schedule-dependent', *Int J Radiat Oncol Biol Phys,* 75(5), pp. 1511-9.

Chang, A. L., Miska, J., Wainwright, D. A., Dey, M., Rivetta, C. V., Yu, D., Kanji, D., Pitch, K. C., Qiao, J., Pytel, P., Han, Y., Wu, M., Zhang, L., Horbinski, C. M., Ahmed, A. U. and Lesniak, M. S. (2016) 'CCL2 Produced by the Glioma Microenvironment Is Essential for the Recruitment of Regulatory T Cells and Myeloid-Derived Suppressor Cells', *Cancer Res,* 76(19), pp. 5671–5682.

Chen, H. Y., Xu, L., Li, L. F., Liu, X. X., Gao, J. X. and Bai, Y. R. (2018) 'Inhibiting the CD8(+) T cell infiltration in the tumor microenvironment after radiotherapy is an important mechanism of radioresistance', *Sci Rep,* 8(1), pp. 11934.

Chen, M.-L., Pittet, M. J., Gorelik, L., Flavell, R. A., Weissleder, R., von Boehmer, H. and Khazaie, K. (2004) 'Regulatory T cells suppress tumor-specific CD8 T cell cytotoxicity through TGF-β signals i*n vivo*', *PNAS,* 102(2), pp. 419- 424

Chen, S., Li, X., Wang, H., Chen, G. and Zhou, Y. (2022) 'Anti-VEGFR2 monoclonal antibody(MSB0254) inhibits angiogenesis and tumor growth by blocking the signaling pathway mediated by VEGFR2 in glioblastoma', *Biochemical and Biophysical Research Communications,* 604(14), pp. 158-164.

Chen, W., Xia, T., Wang, D., Huang, B., Zhao, P., Wang, J., Qu, X. and Li, X. (2016) 'Human astrocytes secrete IL-6 to promote glioma migration and invasion through upregulation of cytomembrane MMP14 ', *Oncotarget,* 7, pp. 62425-62438.

Chen, Z., Feng, X., Heating, C. J., Alvarez Garcia, V., Nie, K., Pong, W. W., Rasmussen, R., Dwivedi, B., Seby, S., Wolf, S. A., Gutmann, D. H. and Hambardzumyan (2017) 'Cellular and Molecular Identity of Tumor-Associated Macrophages in Glioblastoma', *Cancer Res,* 77(9), pp. 2266-2278.

Chen, Z., Giotti, B., Kaluzova, M., Vallcorba, M. P., Rawat, K., Price, G., Herting, C. J., Pinero, G., Cristea, S., Ross, J. L., Ackley, J., Maximov, V., Szulzewsky, F., Thomason, W., Marquez-Ropero, M., Angione, A., Nichols, N., Tsankova, N. M., Michor, F., Shayakhmetov, D. M., Gutmann, D. H., Tsankov, A. M. and Hambardzumyan, D. (2023) 'A paracrine circuit of IL-1β/IL-1R1 between myeloid and tumor cells drives genotype-dependent glioblastoma progression', *J Clin Invest,* 133(22).

Chen, Z., Wang, J., Peng, P., Liu, G., Dong, M., Zhang, X., Zhang, Y., Yang, X., Wan, L., Xiang, W., Zhang, S., Zhang, B., Wu, Q., Yu, X. and Wan, F. (2024) 'Hypoxia-induced TGFBI maintains glioma stem cells by stabilizing EphA2', *Theranostics,* 14(15), pp. 5778-5792.

Chen, Z., Yuan, S.-J., Li, K., Zhang, Q., Li, T.-F., An, H.-C., Xu, H.-Z., Yue, Y., Han, M., Xu, Y.-H., Komatsu, N., Zhao, L. and Chen, X. (2020) 'Doxorubicin-polyglycerol-nanodiamond conjugates disrupt STAT3/IL-6-mediated reciprocal activation loop between glioblastoma cells and astrocytes', *Journal of Controlled Release,* 320, pp. 469-483.

Cheng, L., Huang, Z., Zhou, W., Wu, Q., Donnola, S., Liu, J. K., Fang, X., Sloan, A. E., Mao, Y., Lathia, J. D., Min, W., McLendon, R. R., Rich, J. N. and Bao, S. (2013) 'Glioblastoma Stem Cells Generate Vascular Pericytes to Support Vessel Function and Tumor Growth', *Cell,* 153(1), pp. 139-152.

Cho, M. S., Vasquez, H. G., Rupaimoole, R., Pradeep, S., Wu, S., Zand, B., Han, H.-D., Rodriguez-Aguayo, C., Bottsford-Miller, J., Huang, J., Miyake, T., Choi, H.-J., Dalton, H. J., Ivan, C., Baggerly, K., Lopez-Berestein, G., Sood, A. K. and Afshar-Kharghan, V. (2014) 'Autocrine Effects of Tumor-Derived Complement', *Cell Reports,* 6(6), pp. 1085-1095.

Choi, S. H., Stuckey, D. W., Pignatta, S., Reinshagen, C., Khalsa, J., Kaur, Roozendaa, N., Martinez-Quintanilla, J., Tamura, K., Keles, E. and Shah, K. (2017) 'Tumor Resection Recruits Effector T Cells and Boosts Therapeutic Efficacy of Encapsulated Stem Cells Expressing IFNβ in Glioblastomas', *Clin Cancer Res,* 23(22), pp. 7047–7058.

Chowdhury, R., Leung, I. K. H., Tian, Y.-M., Abboud, M. I., Ge, W., Domene, C., Cantrelle, F.-X., Landrieu, I., Hardy, A. P., Pugh, C. W., Ratcliffe, P. J., Claridge, T. D. W. and Schofield, C. J. (2016) 'Structural basis for oxygen degradation domain selectivity of the HIF prolyl hydroxylases', *Nat Commun,* 7, pp. 12673.

Clara, C., Afonso, Marie, S., K.N, de Almeida, J. R. W., Wakamatsu, A., Oba-Shinjo, S. M., Uno, M., Neville, M. and Rosemberg, S. (2014) 'Angiogenesis and expression of PDGF-C, VEGF, CD105 and HIF-1α in human glioblastoma', *Neuropathology,* 34(4), pp. 343-352.

Classen, F., Kranz, P., Riffkin, H., Pompsch, M., Wolf, A., Göpelt, K., Baumann, M., Baumann, J., Brockmeier, U. and Metzen, E. (2019) 'Autophagy induced by ionizing radiation promotes cell death over survival in human colorectal cancer cells', *Exp Cell Res,* 374(1), pp. 29-37.

Cockman, M. E., Masson, N., Mole, D. R., Jaakkola, P., Chang, G.-W., Clifford, S. C., Maher, E. R., Pugh, C. W., Ratcliffe, P. J. and Maxwell, P. H. (2000) 'Hypoxia Inducible Factor-α Binding and Ubiquitylation by the von Hippel-Lindau Tumor Suppressor Protein', *Journal of Biological Chemistry,* 275(33), pp. 25733-25741.

Collingridge, D. R., Piepmeier, J. M., Rockwell, S. and Knisely, J. P. (1999) 'Polarographic measurements of oxygen tension in human glioma and surrounding peritumoural brain tissue', *Radiother Oncol,* 53(2), pp. 127-31.

Coniglio, S. J., Eugenin, E., Dobrenis, K., Stanley, E. R., West, B. L., Symons, M. H. and Segall, J. (2012) 'Microglial Stimulation of Glioblastoma Invasion Involves Epidermal Growth Factor Receptor (EGFR) and Colony Stimulating Factor 1 Receptor (CSF-1R) Signaling', *Molecular Medicine,* 18(1), pp. 519-527.

Cooney , T., Lane, A., Bartels , U., Bouffet , E., Goldman , S., Leary , S. E. S., Foreman , N. K., Packer , R. J., Broniscer , A., Minturn, J., Shih, C.-S., Chintagumpala, M., Hassall, T., Gottardo, N. G., Dholaria, H., Hoffman, L., Chaney, B., Baugh, J., Doughman, R., Leach, J. L., Jones, B. V., Fouladi, M., Warren, K. E. and Monje, M. (2017) 'Contemporary survival endpoints: an International Diffuse Intrinsic Pontine Glioma Registry study', *Neuro-Oncology,* 19(9), pp. 1279–1280.

Corrales, L., Ajona, D., Rafail, S., Lasarte, Juan J, Riezu-Boj, J. I., Lambris, J. D., Rouzaut, A., Pajares, M. J., Moutuenga, L. M. and Pio, R. (2012) 'Anaphylatoxin C5a creates a favorable microenvironment for lung cancer progression', *J Immunol,* 189(9), pp. 4674-83.

Coulthard, L. G., Hawksworth, O. A., Li, R., Balachandran, A., Lee, J. D., Sepehrband, F., Kurniawan, N., Jeanes, A., Simmons, D. G., Wolvetang, E. and Woodruff, T. M. (2017) 'Complement C5aR1 Signaling Promotes Polarization and Proliferation of Embryonic Neural Progenitor Cells through PKCζ', *Journal of Neuroscience,* 37(22), pp. 5395-5407.

Crane, C. A., Ahn, B. J., Han, S. J. and Parsa, A. T. (2012) 'Soluble factors secreted by glioblastoma cell lines facilitate recruitment, survival, and expansion of regulatory T cells: implications for immunotherapy', *Neuro-Oncology,* 14(5), pp. 584-595.

Crane, C. A., Han, S. J., Barry, J. J., Ahn, B. J., Lanier, L. L. and Parsa, A. T. (2009) 'TGF-β downregulates the activating receptor NKG2D on NK cells and CD8 + T cells in glioma patients', *Neuro Oncol,* 12(1), pp. 7-13.

Culver, C., Sundqvist, A., Mudie, S., Melvin, A., Xirodimas, D. and Rocha, S. (2010) 'Mechanism of hypoxia-induced NF-kappaB', *Mol Cell Biol,* 30(20), pp. 4901-21.

Czabotar, P. E., Lessene, G., Strasser, A. and Adams, J. M. (2014) 'Control of apoptosis by the BCL-2 protein family: implications for physiology and therapy', *Nature Reviews Molecular Cell Biology volume,* 15, pp. 49-63.

da Fonseca, A. C. C., Romão, L., Amaral, R. F., Assad Khan, S., Lobo, D., Martins, S., Marcondes de Souza, J., Moura-Neto, V. and Lima, F. R. S. (2012) 'Microglial stress inducible protein 1 promotes proliferation and migration in human glioblastoma cells', *Neuroscience,* 200, pp. 130-141.

Deivasigamani, S., Miteva, M. T., Natale, S., Gutierrez-Barragan, D., Basilico, B., Di Anelantonio, S., Weinhard, L., Molotov, D., Deb, S., Pape, C., Bolasco, G., Galbusera, A., Asari, H., Gozzi, A., Ragozzino, D. and Gross, C. T. (2023) 'Microglia complement signaling promotes neuronal elimination and normal brain functional connectivity ', *Cerebral Cortex,* 33(21), pp. 10750–10760.

DeMartino, J. A., Van Riper, G., Sicilianos, S. J., Molineaux, C. J., Konteatisn, Z. D., Rosen, H. and Springer, M. S. (1994) 'The amino terminus of the human C5a receptor is required for high affinity C5a binding and for receptor activation by C5a but not C5a analogs', *The Journal of Biological Chemistry,* 269(May 20), pp. 14446–14450.

Dengler, V. L., Galbraith, M. and Espinosa, J. M. (2014) 'Transcriptional regulation by hypoxia inducible factors', *Crit Rev Biochem Mol Biol,* 49(1), pp. 1-15.

Ding, P., Li, L., Li, L., Lv, X., Zhou, D., Wang, Q., Chen, J., Yang, C., Xu, E., Dai, W., Zhang, X., Wang, N., Wang, Q., Zhang, W., Zhang, L., Zhou, Y., Gu, H., Lei, Q., Zhou, X. and Hu, W. (2020) 'C5aR1 is a master regulator in Colorectal Tumorigenesis via Immune modulation', *Theranostics,* 10(9), pp. 8619–8632.

Djuzenova, C. S., Fiedler, V., Memmel, S., Katzer, A., Hartmann, S., Krohne, G., Zimmermann, H., Scholz, C. J., Polat, B., Flentje, M. and Sukhorukov, V. L. (2015) 'Actin cytoskeleton organization, cell surface modification and invasion rate of 5 glioblastoma cell lines differing in PTEN and p53 status', *Exp Cell Res,* 330(2), pp. 346-357.

Dzwigonska, M., Rosa, P., Lipiec, S., Obrebski, T., Smyk, G., Kaza, B., Cyranowski, S., Ellert-Miklaszewska, A., Kominek, A., Malik, A. R., Piwocka, K., Mieczkowski, J., Kaminska, B. and Leszczynska, K. B. (2025) 'Hypoxic stress dysregulates functions of glioma-associated myeloid cells through epigenomic and transcriptional programs', *Cell Rep,* 44(9), pp. 116222.

Ehrnthaller, C., Ignatius, A., Gebhard, F. and Huber-Lang, M. (2011) 'New insights of an old defense system: structure, function, and clinical relevance of the complement system', *Mol Med,* 17(3-4), pp. 317-29.

Elvington, M., Scheiber, M., Yang, X., Lyons, K., Jacqmin, D., Wadsworth, C., Marshall, D., Vanek, K. and Tomlinson, S. (2014) 'Complement-Dependent Modulation of Antitumor Immunity following Radiation Therapy', *Cell Reports,* 8(3), pp. 818-830.

Evans, S. M., Jenkins, K. W., Jenkins, W. T., Dilling, T., Judy, K. D., Schrlau, A., Judkins, A., Hahn, S. M. and Koch, C. J. (2008) 'Imaging and analytical methods as applied to the evaluation of vasculature and hypoxia in human brain tumors', *Radiat Res,* 170(6), pp. 677-90.

Evans, S. M., Judy, K. D., Dunphy, I., Jenkins, W. T., Hwang, W. T., Nelson, P. T., Lustig, R. A., Jenkins, K., Magarelli, D. P., Hahn, S. M., Collins, R. A., Grady, M. S. and Koch, C. J. (2004) 'Hypoxia is important in the biology and aggression of human glial brain tumors', *Clin Cancer Res,* 10(24), pp. 8177-84.

Fang, Y., Zhang, H., Zhong, Y. and Ding, X. (2016) 'Prolyl hydroxylase 2 (PHD2) inhibition protects human renal epithelial cells and mice kidney from hypoxia injury', *Oncotarget,* 7(34), pp. 54317-54328.

Farin, A., Suzuki, S. O., Weiner, M., Goldman, J. E., Bruce, J. N. and Canoll, P. (2006) 'Transplanted glioma cells migrate and proliferate on host brain vasculature: A dynamic analysis', 53(8), pp. 799-808.

Fathima Hurmath, K., Ramaswamy, P. and Nandakumar, D. N. (2014) 'IL-1β microenvironment promotes proliferation, migration, and invasion of human glioma cells', *Cell Biol Int,* 38(12), pp. 1415-22.

Feng, H., Wang, J., Chen, W., Shan, B., Guo, Y., Xu, J., Wang, L., Guo, P. and Zhang, Y. (2016) 'Hypoxia-induced autophagy as an additional mechanism in human osteosarcoma radioresistance', *J Bone Oncol,* 5(2), pp. 67-73.

Feng, Y., Zhao, C., Deng, Y., Wang, H., Ma, L., Liu, S., Tian, X., Wang, B., Bin, Y., Chen, P., Yan, W., Fu, P. and Shah, Z. (2023) 'Mechanism of activation and biased signaling in complement receptor C5aR1', *Cell Research,* 33, pp. 312-324.

Ferrari, G., Cook, B., D, Terushkin, V., Pintucci, G. and Mignatti, P. (2009) 'Transforming growth factor-beta 1 (TGF-beta1) induces angiogenesis through vascular endothelial growth factor (VEGF)-mediated apoptosis', *J Cell Physiol,* 219(2), pp. 449-58.

Filbin, M. G., Tirosh, I., Hovestadt, V., Shaw, M. L., Escalante, L. E., Mathewson, N. D., Neftel, C., Frank, N., Pelton, K., Hebert, C. M., Haberler, C., Yizhak, K., Gojo, J., Egervari, K., Mount, C., van Galen, P., Bonal, D. M., Nguyen, Q. D., Beck, A., Sinai, C., Czech, T., Dorfer, C., Goumnerova, L., Lavarino, C., Carcaboso, A. M., Mora, J., Mylvaganam, R., Luo, C. C., Peyrl, A., Popović, M., Azizi, A., Batchelor, T. T., Frosch, M. P., Martinez-Lage, M., Kieran, M. W., Bandopadhayay, P., Beroukhim, R., Fritsch, G., Getz, G., Rozenblatt-Rosen, O., Wucherpfennig, K. W., Louis, D. N., Monje, M., Slavc, I., Ligon, K. L., Golub, T. R., Regev, A., Bernstein, B. E. and Suvà, M. L. (2018) 'Developmental and oncogenic programs in H3K27M gliomas dissected by single-cell RNA-seq', *Science,* 360(6386), pp. 331-335.

Fonseca, M. I., McGuire, S. O., Counts, S. E. and Tenner, A. J. (2013) 'Complement activation fragment C5a receptors, CD88 and C5L2, are associated with neurofibrillary pathology', *Journal of Neuroinflammation,* 10, pp. 803.

Fraser, D. A., Pisalyaput, K. and Tenner, A. J. (2010) 'C1q enhances microglial clearance of apoptotic neurons and neuronal blebs, and modulates subsequent inflammatory cytokine production', *Journal of Clinical Neurochemistry,* 112(3), pp. 733-743.

Freedman, S. J., Sun, Z. Y., Poy, F., Kung, A. L., Livingston, D. M., Wagner, G. and Eck, M. J. (2002) 'Structural basis for recruitment of CBP/p300 by hypoxia-inducible factor-1 alpha', *Proc Natl Acad Sci U S A,* 99(8), pp. 5367-72.

Friedberg, J. S., Aytan, N., Cherry, J. D., Xia, W., Standring, O. J., Alvarez, V. E., Nicks, R., Svirsky, S., Meng, G., Jun, G., Ryu, H., Au, R. and Stein, T. D. (2020) 'Associations between brain inflammatory profiles and human neuropathology are altered based on apolipoprotein E ε4 genotype', *Sci Rep,* 10(1), pp. 2924.

Frosina, G. (2023) 'Radiotherapy of high-grade gliomas: dealing with a stalemate', *Crit Rev Oncol Hematol,* 190, pp. 104110.

Gabrusiewicz, K., Ellert-Miklaszewska, A., Lipko, M., Sielska, M., Frankowska, M. and Kaminska, B. (2011) 'Characteristics of the Alternative Phenotype of Microglia/Macrophages and its Modulation in Experimental Gliomas', *PLoS One,* 6(8).

Gadwa, J., Bickett, T. E., Darragh, L. B., Knitz, M. W., Bhatia, S., Piper, M., Van Court, B., Bhuvane, S., Nguyen, D., Nangia, V., Kleczko, E. K., Nemenoff, R. A. and Karam, S. D. (2021) 'Complement C3a and C5a receptor blockade modulates regulatory T cell conversion in head and neck cancer', *Journal for ImmunoTherapy of Cancer,* 9(3).

Gallitto, M., Lazarev, S., Wasserman, I., Stafford, J. M., Wolden, S. L., Terezakis, S. A., Bindra, R. S. and Bakst, R. L. (2019) 'Role of Radiation Therapy in the Management of Diffuse Intrinsic Pontine Glioma: A Systematic Review', *Advances in Radiation Oncology,* 4(3), pp. 520-531.

Galluzzi, L. and Vitale, I. and Aaronson, S. A. and Abrams, J. M. and Adam, D. and Agostinis, P. and Alnemri, E. S. and Altucci, L. and Amelio, I. and Andrews, D. W. and Annicchiarico-Petruzzelli, M. and Antonov, A. V. and Arama, E. and Baehrecke, E. H. and Barlev, N. A. and Bazan, N. G. and Bernassola, F. and Bertrand, M. J. M. and Bianchi, K. and Blagosklonny, M. V. and Blomgren, K. and Borner, C. and Boya, P. and Brenner, C. and Campanella, M. and Candi, E. and Carmona-Gutierrez, D. and Cecconi, F. and Chan, F. K. and Chandel, N. S. and Cheng, E. H. and Chipuk, J. E. and Cidlowski, J. A. and Ciechanover, A. and Cohen, G. M. and Conrad, M. and Cubillos-Ruiz, J. R. and Czabotar, P. E. and D'Angiolella, V. and Dawson, T. M. and Dawson, V. L. and De Laurenzi, V. and De Maria, R. and Debatin, K. M. and DeBerardinis, R. J. and Deshmukh, M. and Di Daniele, N. and Di Virgilio, F. and Dixit, V. M. and Dixon, S. J. and Duckett, C. S. and Dynlacht, B. D. and El-Deiry, W. S. and Elrod, J. W. and Fimia, G. M. and Fulda, S. and García-Sáez, A. J. and Garg, A. D. and Garrido, C. and Gavathiotis, E. and Golstein, P. and Gottlieb, E. and Green, D. R. and Greene, L. A. and Gronemeyer, H. and Gross, A. and Hajnoczky, G. and Hardwick, J. M. and Harris, I. S. and Hengartner, M. O. and Hetz, C. and Ichijo, H. and Jäättelä, M. and Joseph, B. and Jost, P. J. and Juin, P. P. and Kaiser, W. J. and Karin, M. and Kaufmann, T. and Kepp, O. and Kimchi, A. and

Kitsis, R. N. and Klionsky, D. J. and Knight, R. A. and Kumar, S. and Lee, S. W. and Lemasters, J. J. and Levine, B. and Linkermann, A. and Lipton, S. A. and Lockshin, R. A. and López-Otín, C. and Lowe, S. W. and Luedde, T. and Lugli, E. and MacFarlane, M. and Madeo, F. and Malewicz, M. and Malorni, W. and Manic, G. and Marine, J. C. and Martin, S. J. and Martinou, J. C. and Medema, J. P. and Mehlen, P. and Meier, P. and Melino, S. and Miao, E. A. and Molkentin, J. D. and Moll, U. M. and Muñoz-Pinedo, C. and Nagata, S. and Nuñez, G. and Oberst, A. and Oren, M. and Overholtzer, M. and Pagano, M. and Panaretakis, T. and Pasparakis, M. and Penninger, J. M. and Pereira, D. M. and Pervaiz, S. and Peter, M. E. and Piacentini, M. and Pinton, P. and Prehn, J. H. M. and Puthalakath, H. and Rabinovich, G. A. and Rehm, M. and Rizzuto, R. and Rodrigues, C. M. P. and Rubinsztein, D. C. and Rudel, T. and Ryan, K. M. and Sayan, E. and Scorrano, L. and Shao, F. and Shi, Y. and Silke, J. and Simon, H. U. and Sistigu, A. and Stockwell, B. R. and Strasser, A. and Szabadkai, G. and Tait, S. W. G. and Tang, D. and Tavernarakis, N. and Thorburn, A. and Tsujimoto, Y. and Turk, B. and Vanden Berghe, T. and Vandenabeele, P. and Vander Heiden, M. G. and Villunger, A. and Virgin, H. W. and Vousden, K. H. and Vucic, D. and Wagner, E. F. and Walczak, H. and Wallach, D. and Wang, Y. and Wells, J. A. and Wood, W. and Yuan, J. and Zakeri, Z. and Zhivotovsky, B. and Zitvogel, L. and Melino, G. and Kroemer, G. (2018) 'Molecular mechanisms of cell death: recommendations of the Nomenclature Committee on Cell Death 2018', *Cell Death Differ,* 25(3), pp. 486-541.

Gelderman, K. A., Blok, V. T., Fleuren, G. J. and Gorter, A. (2002) 'The inhibitory effect of CD46, CD55, and CD59 on complement activation after immunotherapeutic treatment of cervical carcinoma cells with monoclonal antibodies or bispecific monoclonal antibodies', *Lab Invest,* 82(4), pp. 483-93.

Genard, G., Wera, A.-C., Huart, C., Le Calve, B., Penninckx, S., Fattaccioli, A., Tabarrant, T., Demazy, C., Ninane, N., Heuskin, A.-C., Lucas, S. and Michiels, C. (2018) 'Proton irradiation orchestrates macrophage reprogramming through NFκB signaling', *Cell Death Dis,* 9, pp. 728.

Ghosh, M., Shubham, S., Mandal, K., Trivedi, V., Chauhan, R. and Naseera, S. (2017) 'Survival and prognostic factors for glioblastoma multiforme: Retrospective single-institutional study', *Indian J Cancer,* 54(1), pp. 362-367.

Ginhoux, F., Greter, M., Leboeuf, M., Nandi, S., See, P., Gokhan, S., Mehler, M. F., Conway, S. J., Ng, L. G., Stanley, E. R., Samokhvalov, I. M. and Merad, M. (2010) 'Fate mapping analysis reveals that adult microglia derive from primitive macrophages', *Science,* 330(6005), pp. 841-5.

Golden, E. B., Pellicciotta, I., Demaria, S., Barcellos-Hoff, M. H. and Formenti, S. C. (2012) 'The convergence of radiation and immunogenic cell death signaling pathways', *Front Oncol,* 2, pp. 88.

Gomez-Arboledas, A., Carvalho, K., Balderrama-Gutierrez, G., Chu, S. H., Liang, H. Y., Schartz, N. D., Selvan, P., Petrisko, T. J., Pan, M. A., Mortazavi, A. and Tenner, A. J. (2022) 'C5aR1 antagonism alters microglial polarization and mitigates disease progression in a mouse model of Alzheimer's disease', *Acta Neuropathol Commun,* 10(1), pp. 116.

Gorelik, A., Sapir, T., Haffner-Krausz, R., Olender, T., Woodruff, T. M. and Reiner, O. (2017) 'Developmental activities of the complement pathway in migrating neurons', *Nature Communications,* 8, pp. 15096.

Grimes, D. R. and Partridge, M. (2015) 'A mechanistic investigation of the oxygen fixation hypothesis and oxygen enhancement ratio', *Biomed Phys Eng Express,* 1(4), pp. 045209.

Grochans, S., Cybulska, A. M., Simińska, D., Korbecki, J., Kojder, K., Chlubek, D. and Baranowska-Bosiacka, I. (2022) 'Epidemiology of Glioblastoma Multiforme-Literature Review', *Cancers (Basel),* 14(10).

Gu, J., Ding, J. Y., Lu, C. L., Lin, Z. W., Chu, Y. W., Zhao, G. Y., Guo, J. and Ge, D. (2013) 'Overexpression of CD88 predicts poor prognosis in non-small-cell lung cancer', *Lung Cancer,* 81(2), pp. 259-65.

Gunn, L., Ding, C., Liu, M., Ma, Y., Qi, C., Cai, Y., Hu, X., Aggarwal, D., Zhang, H.-g. and Yan, J. (2012) 'Opposing Roles for Complement Component C5a in Tumor Progression and the Tumor Microenvironment', *J Immunol,* 108(6), pp. 2985-94.

Guo, Y.-J., Pan, W.-W., Liu, S.-B., Shen, Z.-F., Xu, Y. and Hu, L.-L. (2020) 'ERK/MAPK signalling pathway and tumorigenesis (Review)', *Experimental and Therapeutic Medicine,* 19(3), pp. 1997-2007.

Gupta, A., Hossain, M. M., Miller, N., Kerin, M., Callagy, G. and Gupta, S. (2016) 'NCOA3 coactivator is a transcriptional target of XBP1 and regulates PERK-eIF2α-ATF4 signalling in breast cancer', *Oncogene,* 35(45), pp. 5860-5871.

Gupta, A., Probst, H. C., Vuong, V., Landshammer, A., Muth, S., Yagita, H., Schwendener, R., Pruschy, M., Knuth, A. and van den Broek, M. (2012) 'Radiotherapy promotes tumor-specific effector CD8+ T cells via dendritic cell activation', *J Immunol,* 189(2), pp. 558-66.

Hagan, M., Wang, L., Hanley, J. R., Park, J. S. and Dent, P. (2000) 'Ionizing radiation-induced mitogen-activated protein (MAP) kinase activation in DU145 prostate carcinoma cells: MAP kinase inhibition enhances radiation-induced cell killing and G2/M-phase arrest', *Radiat Res,* 153(4), pp. 371-83.

Hai Ping, P., Feng Bo, T., Li, L., Nan Hui, Y. and Hong, Z. (2016) 'IL-1β/NF-kb signaling promotes colorectal cancer cell growth through miR-181a/PTEN axis', *Arch Biochem Biophys,* 604, pp. 20-6.

Hall, E. J. and Giaccia, A. J. (2006) *Radiobiology for the Radiologist.* 6 edn. Philadelphia, PA, USA: Lippincott Williams & Wilkins.

Han, S., Zhang, C., Li, Q., Dong, J., Liu, Y., Huang, Y., Jiang, T. and Wu, A. (2014) 'Tumour-infiltrating CD4 + and CD8 + lymphocytes as predictors of clinical outcome in glioma', *Br J Cancer,* 110(10), pp. 2560–2568.

Han, W., Umekawa, T., Zhou, K., Zhang, X. M., Ohshima, M., Dominguez, C. A., Harris, R. A., Zhu, C. and Blomgren, K. (2016) 'Cranial irradiation induces transient microglia

accumulation, followed by long-lasting inflammation and loss of microglia', *Oncotarget,* 7(50), pp. 82305-82323.

Hanahan, D. (2022) 'Hallmarks of Cancer: New Dimensions', *Cancer Discov,* 12(1), pp. 31-46.

Hanahan, D. and Weinberg, R. A. (2000) 'The hallmarks of cancer', *Cell,* 100(1), pp. 57-70.

Hanahan, D. and Weinberg, R. A. (2011) 'Hallmarks of cancer: the next generation', *Cell,* 144(5), pp. 646-74.

Harding, H. P., Novoa, I., Zhang, Y., Zeng, H., Wek, R., Schapira, M. and Ron, D. (2000) 'Regulated translation initiation controls stress-induced gene expression in mammalian cells', *Mol Cell,* 6(5), pp. 1099-108.

Hassin, D., Garber, O. G., Meiraz, A., Schiffenbauer, Y. S. and Berke, G. (2011) 'Cytotoxic T lymphocyte perforin and Fas ligand working in concert even when Fas ligand lytic action is still not detectable', *Immunology,* 133(2), pp. 190-196.

He, W., Batty-Stuart, S., Lee, J. E. and Ohh, M. (2021) 'HIF-1α Hydroxyprolines Modulate Oxygen-Dependent Protein Stability Via Single VHL Interface With Comparable Effect on Ubiquitination Rate', *J Mol Biol,* 433(22), pp. 167244.

Heiland, D. H., Ravi, V. M., Behringer, S. P., Frenking, J. H., Wurm, J., Joseph, K., Garrelfs, N. W. C., Strähle, J., Heynckes, S., Grauvogel, J., France, P., Mader, I., Schneider, M., Potthoff, A.-L., Delev, D., Hofmann, U. G., Fung, C., Beck, J., Sankowski, R., Prinz, M. and Schnell, O. (2019) 'Tumor-associated reactive astrocytes aid the evolution of immunosuppressive environment in glioblastoma', *<i data-test="journal-title" style="box-sizing: inherit;">Nature Communications volume,* 10, pp. 2541.

Heiland, H., Haaker, G., Delev, D., Mercas, B., Masalha, W., Heynckes, S., A, G., Pferifer, D., Carro, S., Weyerbrock, A. and Schnell, P. M. (2017) 'Comprehensive analysis of PD-L1 expression in glioblastoma multiforme', *Oncotarget,* 8, pp. 42214-42225.

Hernandez, M. X., Jiang, S., Cole, T. A., Chu, S. H., Fonseca, M. I., Fang, M. J., Hohsfield, L. A., Torres, M. D., Green, K. N., Wetsel, R. A., Mortazavi, A. and Tenner, A. J. (2017) 'Prevention of C5aR1 signaling delays microglial inflammatory polarization, favors clearance pathways and suppresses cognitive loss', *Mol Neurodegener,* 12(1), pp. 66.

Hill, R. M., Fok, M., Grundy, G., Parsons, J. L. and Rocha, S. (2023) 'The role of autophagy in hypoxia-induced radioresistance', *Radiother Oncol,* 189, pp. 109951.

Hollien, J. and Weissman, J. S. (2006) 'Decay of endoplasmic reticulum-localized mRNAs during the unfolded protein response', *Science,* 313(5783), pp. 104-7.

Hu, B., Wang, Q., Wang, Y. A., Hua, S., Sauvé, C.-E. G., Ong, D., Lan, Z. D., Chang, Q., Ho, Y. W., Moreno Monasterio, M., Lu, X., Zhong, Y., Zhang, J., Deng, P., Tan, Z., Wang, G., Liao, W.-T., Corley, L. J., Yan, H., Zhang, J., You, Y., Liu, N., Cai, L., Finocchiaro, G., Phillips, J. J., Berger, M. S., Spring, D. J., Hu, J., Sulman, E. P., Fuller,

G. N., Chin, L., Verhaak, R. G. W. and DePinho, R. A. (2021) 'Epigenetic Activation of WNT5A Drives Glioblastoma Stem Cell Differentiation and Invasive Growth', *Cell,* 167(5), pp. 1 281 - 1295.

Hu, W. H., Hu, Z., Shen, X., Dong, L. Y., Zhou, W. Z. and Yu, X. X. (2016) 'C5a receptor enhances hepatocellular carcinoma cell invasiveness via activating ERK1/2-mediated epithelial-mesenchymal transition', *Exp Mol Pathol,* 100(1), pp. 101-8.

Huang, F., Zhao, J. L., Wang, L., Gao, C. C., Liang, S. Q., An, D. J., Bai, J., Chen, Y., Han, H. and Qin, H. Y. (2017) 'miR-148a-3p Mediates Notch Signaling to Promote the Differentiation and M1 Activation of Macrophages', *Front Immunol,* 8, pp. 1327.

Huang, O., Zhang, W., Zhi, Q., Xue, X., Liu, H., Shen, D., Geng, M., Xie, Z. and Jiang, M. (2015) 'Teriflunomide, an immunomodulatory drug, exerts anticancer activity in triple negative breast cancer cells', *Exp Biol Med (Maywood),* 240(4), pp. 426-37.

Huang, W., Li, W., Chen, X., Xiang, C. and Luo, K. (2025) 'APOE Drives Glioma Progression by Modulating CCL5/CCR5 Signaling in the Tumor Microenvironment and Inducing M2 Macrophage Polarization', *Immunobiology,* 230(3), pp. 152895.

Huber-Lang, M., Sarma, J. V., Zetoune, F. S., Rittirsch, D., Neff, T. A., McGuire, S. R., Lambris, J. D., Warner, R. L., Flierl, M. A., Hoesel, L. M., Gebhard, F., Younger, J. G., Drouin, S. M., Wetsel, R. A. and Ward, P. A. (2006) 'Generation of C5a in the absence of C3: a new complement activation pathway', *Nat Med,* 12(6), pp. 682-7.

Hui, B., Lu, C., Li, H., Hao, X., Liu, H., Zhuo, D., Wang, Q., Li, Z., Liu, L., Wang, X., Gu, Y. and Tang, W. (2022) 'Inhibition of APOE potentiates immune checkpoint therapy for cancer', *Int J Biol Sci,* 18(14), pp. 5230-5240.

Hussain, S. F., Yang, D., Suki, D., Grimm, E. and Heimberger, A. B. (2006) 'Innate immune functions of microglia isolated from human glioma patients', *Journal of Translational Medicine,* 4, pp. 15.

Inggas, M. A. M., Patel, U., Wijaya, J. H., Otinashvili, N., Menon, V. R., Iyer, A. K., Turjman, T., Dadwal, S., Gadaevi, M., Ismayilova, A., Gaddam, S. J., Arya, P., Upadhyay, N. and Kataria, S. (2025) 'The role of temozolomide as adjuvant therapy in glioblastoma management: a systematic review and meta-analysis', *BMC Cancer,* 25(1), pp. 399.

Izquierdo, E., Carvalho, D. M., Mackay, A., Temelso, S., Boult, J. K. R., Pericoli, G., Fernandez, E., Das, M., Molinari, V., Grabovska, Y., Rogers, R. F., Ajmone-Cat, M. A., Proszek, P. Z., Stubbs, M., Depani, S., O'Hare, P., Yu, L., Roumelioti, G., Choudhary, J. S., Clarke, M., Fairchild, A. R., Jacques, T. S., Grundy, R. G., Howell, L., Picton, S., Adamski, J., Wilson, S., Gray, J. C., Zebian, B., Marshall, L. V., Carceller, F., Grill, J., Vinci, M., Robinson, S. P., Hubank, M., Hargrave, D. and Jones, C. (2022) 'DIPG Harbors Alterations Targetable by MEK Inhibitors, with Acquired Resistance Mechanisms Overcome by Combinatorial Inhibition', *Cancer Discovery,* 12(3), pp. 712-729.

Jiang, Y., Zhao, J., Xu, J., Zhang, H., Zhou, J., Li, H., Zhang, G., Xu, K. and Jing, Z. (2022) 'Glioblastoma-associated microglia-derived exosomal circKIF18A promotes angiogenesis by targeting FOXC2', *Oncogene,* 41, pp. 3461–3473.

Jiao, Y., Cao, F. and Liu, H. (2022) 'Radiation-induced Cell Death and Its Mechanisms', *Health Phys,* 123(5), pp. 376-386.

Jin, P., Shin, S.-H., Chun, Y.-S., Shin, H.-W., Shin, Y. J., Lee, Y., Kim, D., Nam, D.-H. and Park, J.-W. (2018) 'Astrocyte-derived CCL20 reinforces HIF-1-mediated hypoxic responses in glioblastoma by stimulating the CCR6-NF-κB signaling pathway', *Oncogene,* 37, pp. 3070–3087.

Jin, Y., Liu, Y., Xu, L., Xu, J., Xiong, Y., Peng, Y., Ding, K., Zheng, S., Yang, N., Zhang, Z., Li, L., Tan, L., Song, H. and Fu, J. (2022) 'Novel role for caspase 1 inhibitor VX765 in suppressing NLRP3 inflammasome assembly and atherosclerosis via promoting mitophagy and efferocytosis', *Cell Death Dis,* 13(5), pp. 512.

Johung, T. B. and Monje, M. (2017) 'Diffuse Intrinsic Pontine Glioma: New Pathophysiological Insights and Emerging Therapeutic Targets', *Current Neuropharmacology,* 15(1), pp. 88-97.

Joseph, J. V., Conroy, S., Pavlov, K., Sontakke, P., Tomar, T., Eggens-Meijer, E., Balasubramaniyan, V., Wagemakers, M., den Dunnen, W. F. and Kruyt, F. A. (2015) 'Hypoxia enhances migration and invasion in glioblastoma by promoting a mesenchymal shift mediated by the HIF1α-ZEB1 axis', *Cancer Lett,* 359(1), pp. 107-16.

Jung, Y., Ahn, S.-H., Park, H., Park, S. H., Choi, K., Choi, C., Lee Kang, J. and Choi, Y.-H. (2018) 'MCP-1 and MIP-3α Secreted from Necrotic Cell-Treated Glioblastoma Cells Promote Migration/Infiltration of Microgli a ', *Cellular Physiology and Biochemistry,* 48(3), pp. 1332-1346.

Jurga, A. M., Paleczna, M. and Kuter, K. Z. (2020) 'Overview of General and Discriminating Markers of Differential Microglia Phenotypes', *Front Cell Neurosci,* 14, pp. 198.

Kang, A. R., Cho, J. H., Lee, N. G., Kwon, J. H., Song, J. Y., Hwang, S. G., Jung, I. S., Kim, J. S., Um, H. D., Oh, S. C. and Park, J. K. (2021) 'Radiation-induced IL-1β expression and secretion promote cancer cell migration/invasion via activation of the NF-κB-RIP1 pathway', *Biochem Biophys Res Commun,* 534, pp. 973-979.

Karimi Roshan, M., Belikov, S., Ix, M., Protti, N., Balducci, C., Dodel, R., Ross, J. A. and Lundholm, L. (2024) 'Fractionated alpha and mixed beam radiation promote stronger pro-inflammatory effects compared to acute exposure and trigger phagocytosis', *Front Cell Neurosci,* 18, pp. 1440559.

Kaur, B., Khwaja, F. W., Severson, E. A., Matheny, S. L., Brat, D. J. and Van Meir, E. G. (2005) 'Hypoxia and the hypoxia-inducible-factor pathway in glioma growth and angiogenesis', *Neuro-Oncology,* 7(2), pp. 134-153.

Kaur, E., Nair, J., Ghorai, A., Mishra, S. V., Achareker, A., Ketkar, M., Sarkar, D., Salunkhe, S., Rajendra, J., Gardi, N., Desai, S., Iyer, P., Thorat, R., Dutt, A., Moiyadi, A. and Dutt, S. (2020) 'Inhibition of SETMAR–H3K36me2–NHEJ repair axis in residual disease cells prevents glioblastoma recurrence', *Neuro-Oncology,* 22(12), pp. 1785–1796.

Kawashima, T., Yashiro, M., Kasashima, H., Terakawa, Y., Uda, T., Nakaja, K., Umaba, R., Tanoue, Y., Tamrakar, S. and Ohata, K. (2019) 'Oligodendrocytes Up-regulate the

Invasive Activity of Glioblastoma Cells *via* the Angiopoietin-2 Signaling Pathway', *Anticancer research,* 39(2), pp. 577-584.

Kemp, S. B., Carpenter, E. S., Steele, N. G., Donahue, K. L., Nwosu, Z. C., Pacheco, A., Velez-Delgado, A., Menjivar, R. E., Lima, F., The, S., Espinoza, C. E., Brown, K., Long, D., Lyssiotis, C. A., Rao, A., Zhang, Y., Pasca di Magliano, M. and Crawford, H. C. (2021) 'Apolipoprotein E Promotes Immune Suppression in Pancreatic Cancer through NF-κB-Mediated Production of CXCL1', *Cancer Res,* 81(16), pp. 4305-4318.

Kenakin, T. (2011) 'Functional selectivity and biased receptor signaling', *J Pharmacol Exp Ther,* 336(2), pp. 296-302.

Kesselring, R., Thiel, A., Pries, R., Fichtner-Feigl, S., Brunner, S., Seidel, P., Bruchhage, K. L. and Wollenberg, B. (2014) 'The complement receptors CD46, CD55 and CD59 are regulated by the tumour microenvironment of head and neck cancer to facilitate escape of complement attack', *Eur J Cancer,* 50(12), pp. 2152-61.

Kil, W. J., Cerna, D., Burgan, W. E., Beam, K., Carter, D., Steeg, P. S., Tofilon, P. J. and Camphausen, K. (2008) 'In vitro and In vivo Radiosensitization Induced by the DNA Methylating Agent Temozolomide', *Clinical Cancer Research,* 14(3), pp. 931-938.

Killela, P. J., Reitman, Z. J., Jiao, Y., Bettegowda, C., Agrawal, N., Diaz, L. A., Jr., Friedman, A. H., Friedman, H., Gallia, G. L., Giovanella, B. C., Grollman, A. P., He, T. C., He, Y., Hruban, R. H., Jallo, G. I., Mandahl, N., Meeker, A. K., Mertens, F., Netto, G. J., Rasheed, B. A., Riggins, G. J., Rosenquist, T. A., Schiffman, M., Shih Ie, M., Theodorescu, D., Torbenson, M. S., Velculescu, V. E., Wang, T. L., Wentzensen, N., Wood, L. D., Zhang, M., McLendon, R. E., Bigner, D. D., Kinzler, K. W., Vogelstein, B., Papadopoulos, N. and Yan, H. (2013) 'TERT promoter mutations occur frequently in gliomas and a subset of tumors derived from cells with low rates of self-renewal', *Proc Natl Acad Sci U S A,* 110(15), pp. 6021-6.

Kim, J.-K., Jin, X., Sohn, Y.-W., Jin, X., Jeon, H.-Y., Kim, E.-J., Ham, S. W., Jeon, H.-M., Chang, S.-Y., Oh, S.-Y., Yin, J., Kim, S.-H., Park, J. B., Nakano, I. and Kim, H. (2014) 'Tumoral RANKL activates astrocytes that promote glioma cell invasion through cytokine signaling', *Cancer Letters,* 353(2), pp. 194-200.

Komohara, Y., Ohnishi, K., Kuratsu, J. and Takeya, M. (2008) 'Possible involvement of the M2 anti-inflammatory macrophage phenotype in growth of human gliomas', *The Journal of Pathology,* 216(1), pp. 15-24.

Kopp, M. C., Larburu, N., Durairaj, V., Adams, C. J. and Ali, M. M. U. (2019) 'UPR proteins IRE1 and PERK switch BiP from chaperone to ER stress sensor', *Nat Struct Mol Biol,* 26(11), pp. 1053-1062.

Krshnan, L., van de Weijer, M. L. and Carvalho, P. (2022) 'Endoplasmic Reticulum-Associated Protein Degradation', *Cold Spring Harb Perspect Biol,* 14(12).

Ku, M.-C., Wolf, S. A., Respondek, D., Matyash, V., Pohlmann, A., Waiczies, S., Waiczies, H., Niendorf, T., Synowitz, M., Glass, R. and Kettenmann, H. (2013) 'GDNF mediates glioblastoma-induced microglia attraction but not astrogliosis', *Acta Neuropathologica,* 125(4), pp. 609-620.

Kulawik, A., Engesser, R., Ehlting, C., Raue, A., Albrecht, U., Hahn, B., Lehmann, W. D., Gaestel, M., Klingmüller, U., Häussinger, D., Timmer, J. and Bode, J. G. (2017) 'IL-1β-induced and p38(MAPK)-dependent activation of the mitogen-activated protein kinase-activated protein kinase 2 (MK2) in hepatocytes: Signal transduction with robust and concentration-independent signal amplification', *J Biol Chem,* 292(15), pp. 6291-6302.

Kumar, V., Lee, J. D., Clark, R. J., Noakes, P. G., Taylor, S. M. and Woodruff, T. M. (2020) 'Preclinical Pharmacokinetics of Complement C5a Receptor Antagonists PMX53 and PMX205 in Mice', *ACS Omega,* 5(5), pp. 2345-2354.

Kučera, J., Netušilová, J., Sladeček, S., Lánová, M., Vašíček, O., Štefková, K., Navrátilová, J., Kubala, L. and Pacherník, J. (2017) 'Hypoxia Downregulates MAPK/ERK but Not STAT3 Signaling in ROS-Dependent and HIF-1-Independent Manners in Mouse Embryonic Stem Cells', *Oxid Med Cell Longev,* 2017, pp. 4386947.

Kwak, J. W., Laskowski, J., Li, H. Y., McSharry, M. B., Sippel, T. R., Bullock, B. L., Johnson, A. M., Poczobutt, J. M., Neuwelt, A. J., Malkoski, S. P., Weiser-Evans, M. C., Lambris, J. D., Clambey, E. T., Thurman, J. M. and Nemenoff, R. A. (2018) 'Complement Activation via a C3a Receptor Pathway Alters CD4 + T Lymphocytes and Mediates Lung Cancer Progression', *Cancer Res,* 78(1), pp. 143-156.

Lau, J., Ilkhanizadeh, S., Wang, S., Miroshnikova, Y., A, Salvatierra, N. A., Wong, R., A, Schmidt, C., Weaver, V. M., Weiss, W. A. and Persson, A. I. (2015) 'STAT3 Blockade Inhibits Radiation-Induced Malignant Progression in Glioma

', *Cancer Res,* 75(20), pp. 4302-4311.

Lavoie, H., Gagnon, J. and Therrien, M. (2020) 'ERK signalling: a master regulator of cell behaviour, life and fate', *Nature Reviews Molecular Cell Biology,* 21, pp. 607-632.

Lavoie, J. N., L'Allemain, G., Brunet, A., Müller, R. and Pouysségur, J. (1996) 'Cyclin D1 expression is regulated positively by the p42/p44MAPK and negatively by the p38/HOGMAPK pathway', *J Biol Chem,* 271(34), pp. 20608-16.

Lecoultre, M., Chliate, S., Espinoza, F. I., Tankov, S., Dutoit, V. and Walker, P. R. (2024) 'Radio-chemotherapy of glioblastoma cells promotes phagocytosis by macrophages in vitro', *Radiotherapy and Oncology,* 190, pp. 110049.

Lee, A. H., Scapa, E. F., Cohen, D. E. and Glimcher, L. H. (2008) 'Regulation of hepatic lipogenesis by the transcription factor XBP1', *Science,* 320(5882), pp. 1492-6.

Lee, K. S. W., Zhang, Q., Suwa, T., Clark, H. and Olcina, M. M. (2025) 'The role of the complement system in the response to cytotoxic therapy', *Semin Immunol,* 77, pp. 101927.

Lenin, S., Ponthier, E., Scheer, K. G., Yeo, E. C. F., Tea, M. N., Ebert, L. M., Oksdath Mansilla, M., Poonnoose, S., Baumgartner, U., Day, B. W., Ormsby, R. J., Pitson, S. M. and Gomez, G. A. (2021) 'A Drug Screening Pipeline Using 2D and 3D Patient-Derived In Vitro Models for Pre-Clinical Analysis of Therapy Response in Glioblastoma', *Int J Mol Sci,* 22(9).

Li, M. D., Burns, T. C., Kumar, S., Morgan, A. A., Sloan, S. A. and Palmer, T. D. (2015) 'Aging-like changes in the transcriptome of irradiated microglia', *Glia,* 63(5), pp. 754-67.

Li, P., Nijhawan, D., Budihardjo, I., Srinivasula, S. M., Ahmad, M., Alnemri, E. S. and Wang, X. (1997) 'Cytochrome c and dATP-dependent formation of Apaf-1/caspase-9 complex initiates an apoptotic protease cascade', *Cell,* 91(4), pp. 479-89.

Li, P., Zhang, D., Shen, L., Dong, K., Wu, M., Ou, Z. and Shi, D. (2016) 'Redox homeostasis protects mitochondria through accelerating ROS conversion to enhance hypoxia resistance in cancer cells', *Sci Rep,* 6, pp. 22831.

Li, P., Zhou, C., Xu, L. and Xiao, H. (2013) 'Hypoxia enhances stemness of cancer stem cells in glioblastoma: an in vitro study', *Int J Med Sci,* 10(4), pp. 399-407.

Li, R., Li, G., Deng, L., Liu, Q., Dai, J., Shen, J. and Zhang, J. (2010) 'IL-6 augments the invasiveness of U87MG human glioblastoma multiforme cells via up-regulation of MMP-2 and fascin-1 ', *Oncology Reports,* 23, pp. 1553-1559.

Li, S., Fang, Y., Zhang, Y., Song, M., Zhang, X., Ding, X., Yao, H., Chen, M., Sun, Y., Ding, J., Wang, Q., Lu, M., Wu, G. and Hu, G. (2022) 'Microglial NLRP3 inflammasome activates neurotoxic astrocytes in depression-like mice', *Cell Rep,* 41(4), pp. 111532.

Li, X. X., Kumar, V., Clark, R. J., Lee, J. D. and Woodruff, T. M. (2020a) 'The "C3aR Antagonist" SB290157 is a Partial C5aR2 Agonist', *Front Pharmacol,* 11, pp. 591398.

Li, X. X., Lee, J. D., Massey, N. L., Guan, C., Robertson, A. A. B., Clark, R. J. and Woodruff, T. M. (2020b) 'Pharmacological characterisation of small molecule C5aR1 inhibitors in human cells reveals biased activities for signalling and function', *Biochemical Pharmacology,* 180, pp. 114156.

Li, Y., Jiang, W., Niu, Q., Sun, Y., Meng, C., Tan, L., Song, C., Qiu, X., Liao, Y. and Ding, C. (2019) 'eIF2α-CHOP-BCl-2/JNK and IRE1α-XBP1/JNK signaling promote apoptosis and inflammation and support the proliferation of Newcastle disease virus', *Cell Death Dis,* 10(12), pp. 891.

Li, Z., Bao, S., Wu, Q., Wang, H., Eyler, C., Sathornsumetee, S., Shi, Q., Cao, Y., Lathia, J., McLendon, R. E., Hjelmeland, A. B. and Rich, J. N. (2009) 'Hypoxia-inducible factors regulate tumorigenic capacity of glioma stem cells', *Cancer Cell,* 15(6), pp. 501-13.

Li, Z., Meng, X., Wu, P., Zha, C., Han, B., Li, L., Sun, N., Qi, T., Qin, J., Zhang, Y., Tian, K., Li, S., Yang, C., Ren, L., Ming, J., Wang, P., Song, Y., Jiang, C. and Cai, J. (2021) 'Glioblastoma Cell–Derived lncRNA-Containing Exosomes Induce Microglia to Produce Complement C5, Promoting Chemotherapy Resistance ', *Cancer Immunol Res,* 9(12), pp. 1383–1399.

Lian, H., Litvinchuk, A., Chiang, A. C.-A., Aithmitti, N., Jankowsky, J. and Zheng, H. (2016) 'Astrocyte-Microglia Cross Talk through Complement Activation Modulates Amyloid Pathology in Mouse Models of Alzheimer's Disease', *J.Neurosci,* 36(2), pp. 577-89.

Liau, B. B., Sievers, C., Donohue, L. K., Gillespie, S. M., Flavahan, W. A., Miller, T. E., Venteicher, A. S., Hebert, C. H., Carey, C. D., Rodig, S. J., Shareef, S. J., Najm, F. J.,

van Galen, P., Wakimoto, H., Cahill, D. P., Rich, J. N., Aster, J. C., Suvà, M. L., Patel, A. P. and Bernstein, B. E. (2017) 'Adaptive Chromatin Remodeling Drives Glioblastoma Stem Cell Plasticity and Drug Tolerance', *Cell Stem Cell,* 20(2), pp. 233-246.e7.

Lieberman, N. A. P., DeGolier, K., Kovar, H. M., Davis, A., Hoglund, V., Stevens, J., Winter, C., Deutsch, G., Furlan, S. N., Vitanza, N. A., Leary, S. E. S. and Crane, C. A. (2019) 'Characterization of the immune microenvironment of diffuse intrinsic pontine glioma: implications for development of immunotherapy', *Neuro Oncol,* 21(1), pp. 83-94.

Lim, E.-J., Kim, S., Oh, Y., Such, Y., Kaushik, N., Lee, J.-H., Lee, H.-J., Kim, M.-J., Park, M.-J., Kim, R.-K., Cha, J., Kim, S. H., Shim, J.-K., Choi, J., Chang, J. H., Hong, Y. K., Huh, Y. M., Kim, P., Kang, S.-G. and Lee, S.-J. (2020) 'Crosstalk between GBM cells and mesenchymal stemlike cells promotes the invasiveness of GBM through the C5a/p38/ZEB1 axis', *Neuro-Oncology,* 22(10), pp. 1452–1462.

Lim, J. Y., Gerber, S. A., Murphy, S. P. and Lord, E. M. (2014) 'Type I interferons induced by radiation therapy mediate recruitment and effector function of CD8(+) T cells', *Cancer Immunol Immunother,* 63(3), pp. 259-71.

Lin, G. L., Nagaraja, S., Filbin, M. G., Suvà, M. L., Vogel, H. and Monje, M. (2018) 'Non-inflammatory tumor microenvironment of diffuse intrinsic pontine glioma', *Acata Neuropathologica Communications,* 6(51).

Lin, Y. and Wu, Z. (2023) 'Hypoxia-inducible factor 1α (HIF-1α)-activated Gli1 induces invasion and EMT by H3K4 methylation in glioma cells', *Oncologie,* 25(1), pp. 71-79.

Liu, C., Sage, J. C., Miller, M. R., Verhaak, R. G., Hippenmeyer, S., Vogel, H., Foreman, O., Bronson, R. T., Nishiyama, A., Luo, L. and Zong, H. (2011a) 'Mosaic analysis with double markers reveals tumor cell of origin in glioma', *Cell,* 146(2), pp. 209-21.

Liu, H., Kim, H. R., Deepak, R. N. V. K., Wang, L., Chung, K. Y., Fan, H., Wei, Z. and Zhang, C. (2018) 'Orthosteric and allosteric action of the C5a receptor antagonists', *Nature Structural & Molecular Biology,* 25, pp. 472-481.

Liu, H., Sun, Y., Zhang, Q., Jin, W., Gordon, R. E., Zhang, Y., Wang, J., Sun, C., Wang, Z. J., Qi, X., Zhang, J., Huang, B., Gui, Q., Yuan, H., Chen, L., Xiaodong, M., Fang, C., Liu, Y.-q., Yu, X. and Feng, S. (2021) 'Pro-inflammatory and proliferative microglia drive progression of glioblastoma', *Cell Reports,* 36(11), pp. 109718.

Liu, L., Aboud, O., Jones, R. A., Mrak, R. E., Griffin, W. S. and Barger, S. W. (2011b) 'Apolipoprotein E expression is elevated by interleukin 1 and other interleukin 1-induced factors', *J Neuroinflammation,* 8, pp. 175.

Liu, L., Cash, T. P., Jones, R. G., Keith, B., Thompson, C. B. and Simon, M. C. (2006) 'Hypoxia-induced energy stress regulates mRNA translation and cell growth', *Mol Cell,* 21(4), pp. 521-31.

Liu, Q., Huang, Y., Duan, M., Yang, Q., Ren, B. and Tang, F. (2022) 'Microglia as Therapeutic Target for Radiation-Induced Brain Injury', *Int J Mol Sci,* 23(15).

Liu, X. T., Chen, X., Zhao, N., Geng, F., Zhu, M. M. and Ren, Q. G. (2024) 'Synergism of ApoE4 and systemic infectious burden is mediated by the APOE-NLRP3 axis in Alzheimer's disease', *Psychiatry Clin Neurosci,* 78(9), pp. 517-526.

Liu, Y., Hou, X., Liu, M., Yang, Z., Bi, Y., Zou, H., Wu, J., Che, H., Li, C., Wang, X., Wang, K., Zhong, C., Zhang, J., Yu, T., Bian, Q., Chai, S., Liu, H., Ai, J. and Zhao, S. (2016) 'XBP1 silencing decreases glioma cell viability and glycolysis possibly by inhibiting HK2 expression', *J Neurooncol,* 126(3), pp. 455-62.

Liu, Z., Ma, Y., Cui, Q., Xu, J., Tang, Z., Wang, Y., He, C. and Wang, X. (2020) 'Toll-like receptor 4 plays a key role in advanced glycation end products-induced M1 macrophage polarization', *Biochem Biophys Res Commun,* 531(4), pp. 602-608.

Lohr, J., Ratliff, T., Huppertz, A., Ge, Y., Dictus, C., Ahmadi, R., Grau, S., Hiraoka, N., Eckstein, V., Ecker, R. C., Korff, T., von Deimling, A., Unterberg, A., Beckhove, P. and Herold-Mende, C. (2011) 'Effector T-Cell Infiltration Positively Impacts Survival of Glioblastoma Patients and Is Impaired by Tumor-Derived TGF-β', *Clin Cancer Res,* 17(13), pp. 4296–4308.

Louis, D. N., Perry, A., Wesseling, P., Brat, D. J., Cree, I. A., Figarella-Branger, D., Hawkins, C., Ng, H. K., Pfister, S. M., Reifenberger, G., Soffietti, R., von Deimling, A. and Ellison, D. W. (2021) 'The 2021 WHO Classification of Tumors of the Central Nervous System: a summary', *Neuro Oncol,* 23(8), pp. 1231-1251.

Louveau, A., Smirnov, I., Keyes, T. J., Eccles, J. D., Rouhani, S. J., Peske, J. D., Derecki, N. C., Castle, D., Mandell, J. W., Lee, K. S., Harris, T. H. and Kipnis, J. (2015) 'Structural and functional features of central nervous system lymphatic vessels', *Nature,* 523, pp. 337–341.

Lubbers, R., Van Essen, M. F., Van Kooten, C. and Trouw, L. A. (2017) 'Production of complement components by cells of the immune system', *Clinical & Experimental Immunology,* 188(2), pp. 183–194.

Lyu, X., Zhang, M., Li, G., Cai, Y. and Qiao, Q. (2019) 'Interleukin-6 production mediated by the IRE1-XBP1 pathway confers radioresistance in human papillomavirus-negative oropharyngeal carcinoma', *Cancer Sci,* 110(8), pp. 2471-2484.

Mackay, A., Burford, A., Carvalho, D., Izquierdo, E., Fazal-Salom, J., Taylor, K. R., Bjerke, L., Clarke, M., Vinci, M., Nandhabalan, M., Temelso, S., Popov, S., Molinari, V., Raman, P., Waanders, A. J., Han, H. J., Gupta, S., Marshall, L., Zacharoulis, S., Vaidya, S., Mandeville, H. C., Bridges, L. R., Martin, A. J., Al-Sarraj, S., Chandler, C., Ng, H.-K., Li, X., Mu, K., Trabelsi, S., Brahim, D. H. m., Kisljakov, A. N., Konovalov, D. M., Moore, A. S., Carcaboso, A. M., Sunol, M., De Torres, C., Cruz, O., Mora, J., Shats, L. I., Stavale, J. N., Bidinotto, L. T., Reis, R. M., Entz-Werle, N., Farrell, M., Cryan, J., Crimmins, D., Caird, J., Pears, J., Monje, M., Debily, M.-A., Castel, D., Grill, J., Hawkins, C., Nikbakht, H., Jabado, N., Baker, S. J., Pfister, S. M., Jones, D. T. W., Fouladi, M., Von Bueren, A. O., Baudis, M., Resnick, A. and Jones, C. (2017) 'Integrated Molecular Meta-Analysis of 1,000 Pediatric High-Grade and Diffuse Intrinsic Pontine Glioma', *Cancer Cell,* 32(4), pp. 520-537.

Madden, E., Logue, S. E., Healy, S. J., Manie, S. and Samali, A. (2019) 'The role of the unfolded protein response in cancer progression: From oncogenesis to chemoresistance', *Biol Cell,* 111(1), pp. 1-17.

Mahaney, B. L., Meek, K. and Lees-Miller, S. P. (2009) 'Repair of ionizing radiation-induced DNA double strand breaks by non-homologous end-joining', *Biochem J,* 417(3), pp. 639–650.

Malmström, A., Grønberg, B. H., Marosi, C., Stupp, R., Frappaz, D., Schultz, H., Abacioglu, U., Tavelin, B., Lhermitte, B., Hegi, M. E., Rosell, J. and Henriksson, R. (2012) 'Temozolomide versus standard 6-week radiotherapy versus hypofractionated radiotherapy in patients older than 60 years with glioblastoma: the Nordic randomised, phase 3 trial', *Lancet Oncol,* 13(9), pp. 916-26.

Mangogna, A., Belmonte, B., Agostinis, C., Zacchi, P., Iacopino, D. G., Martorana, A., Rodolico, V., Bonazza, D., Zanconati, F., Kishore, U. and Bulla, R. (2019) 'Prognostic Implications of the Complement Protein C1q in Gliomas', *Frontiers in Immunology,* 10, pp. 2366.

Marampon, F., Gravina, G. L., Di Rocco, A., Bonfili, P., Di Staso, M., Fardella, C., Polidoro, L., Ciccarelli, C., Festuccia, C., Popov, V. M., Pestell, R. G., Tombolini, V. and Zani, B. M. (2011) 'MEK/ERK inhibitor U0126 increases the radiosensitivity of rhabdomyosarcoma cells in vitro and in vivo by downregulating growth and DNA repair signals', *Mol Cancer Ther,* 10(1), pp. 159-68.

Marcus, H. J., Carpenter, K. L. H., Price, S. J. and Hutchinson, P. J. (2010) 'In vivo assessment of high-grade glioma biochemistry using microdialysis: a study of energy-related molecules, growth factors and cytokines', *Journal of Neuro-Oncology,* 97, pp. 11-23.

Markarian, M., Krattli, R. P., Jr., Baddour, J. D., Alikhani, L., Giedzinski, E., Usmani, M. T., Agrawal, A., Baulch, J. E., Tenner, A. J. and Acharya, M. M. (2021) 'Glia-Selective Deletion of Complement C1q Prevents Radiation-Induced Cognitive Deficits and Neuroinflammation', *Cancer Res,* 81(7), pp. 1732-1744.

Markiewski, M. M., DeAngelis, R. A., Benecia, F., Ricklin-Lichtsteiner, S. K., Koutoulai, A., Gerard, C., Coukos, G. and Lambris, J. D. (2008) 'Modulation of the anti-tumor immune response by complement', *Nat Immunol,* 9(11), pp. 1225-35.

Markovic, D. S., Glass, R., Synowitz, M., van Rooijen, N. and Kettenmann, H. (2005) 'Microglia Stimulate the Invasiveness of Glioma Cells by Increasing the Activity of Metalloprotease-2', *Journal of Neuropathology & Experimental Neurology,* 64(9), pp. 754–762.

Markovic, D. S., Vinnakota, K., Chirasani, S., Synowitz, M., Raguet, H., Stock, K., Silwa, M., Lehmann, S., Kälin, R., van Rooijen, N., Holmebeck, K., Heppner, F. L., Kiwit, J., Matyash, V., Lehnardt, S., Kaminska, B., Glass, R. and Kettenmann, H. (2009) 'Gliomas induce and exploit microglial MT1-MMP expression for tumor expansion', *Proc Natl Acad Sci U S A,* 16(30), pp. 12530-12535.

Matsuoka, Y., Nakayama, H., Yoshida, R., Hirosue, A., Nagata, M., Tanaka, T., Kawahara, K., Sakata, J., Arita, H., Nakashima, H., Shinriki, S., Fukuma, D., Ogi, H., Hiraki, A., Shinohara, M., Toya, R. and Murakami, R. (2016) 'IL-6 controls resistance to radiation by suppressing oxidative stress via the Nrf2-antioxidant pathway in oral squamous cell carcinoma', *Br J Cancer,* 115(10), pp. 1234-1244.

McIntyre, A., Patiar, S., Wigfield, S., Li, J. L., Ledaki, I., Turley, H., Leek, R., Snell, C., Gatter, K., Sly, W. S., Vaughan-Jones, R. D., Swietach, P. and Harris, A. L. (2012) 'Carbonic anhydrase IX promotes tumor growth and necrosis in vivo and inhibition enhances anti-VEGF therapy', *Clin Cancer Res,* 18(11), pp. 3100-11.

Mei, X., Chen, Y.-S., Chen, F.-R., Xi, S.-Y. and Chen, Z.-P. (2017) 'Glioblastoma stem cell differentiation into endothelial cells evidenced through live-cell imaging', *Neuro-Oncology,* 19(8), pp. 1109–1118.

Menegakis, A., Klompmaker, R., Vennin, C., Arbusà, A., Damen, M., van den Broek, B., Zips, D., van Rheenen, J., Krenning, L. and Medema, R. H. (2021) 'Resistance of Hypoxic Cells to Ionizing Radiation Is Mediated in Part via Hypoxia-Induced Quiescence', *Cells,* 10(3).

Meng, X., Duan, C., Pang, H., Chen, Q., Han, B., Zha, C., Dinislam, M., Wu, P., Li, Z., Zhao, S., Wang, R., Lin, L., Jiang, C. and Cai, J. (2019) 'DNA damage repair alterations modulate M2 polarization of microglia to remodel the tumor microenvironment via the p53-mediated MDK expression in glioma', *EBioMedicine,* 41, pp. 185-199.

Mosser, D. M. and Edwards, J. P. (2008) 'Exploring the full spectrum of macrophage activation', *Nature Reviews Immunology,* **8**, pp. 958–969

Mou, Y., Hu, Y., Guolian, X., Wenjian, Z., Yang, J., Chen, L., Cao, H., Min, C., Deng, J., Dai, P., Zhu, H. and Wang, L. (2023) 'Glioma angiogenesis is boosted by ELK3 activating the HIF-1/VEGF-A signaling axis', *BMC Cancer,* 23, pp. 662.

Muthukrishnan, S. D., Kawaguchi, R., Nair, P., Prasad, R., Qin, Y., Johnson, M., Wang, Q., VanderVeer-Harris, N., Pham, A., Alvarado, A. G., Condro, M. C., Gao, F., Gau, R., Castro, M. G., Lowenstein, P. R., Deb, A., Hinman, J. D., Pajonk, F., Burns, T. C., Goldman, S. A., Geschwind, D. H. and Kornblum, H. I. (2022) 'P300 promotes tumor recurrence by regulating radiation-induced conversion of glioma stem cells to vascular-like cells', *Nature Communications,* 13, pp. 6202.

Müller, A., Brandenburg, S., Turkowski, K., Müller, S. and Vajkoczy, P. (2015) 'Resident microglia, and not peripheral macrophages, are the main source of brain tumor mononuclear cells', *Int. J. Cancer,* 137, pp. 278-288.

Nabizadeh, J. A., Manthey, H. D., Panagides, N., Steyn, F. J., Lee, J. D., Li, X. X., Akhir, F. N. M., Chen, W., Boyle, G. M., Taylor, S. M., Woodruff, T. M. and Rolfe, B. E. (2019) 'C5a receptors C5aR1 and C5aR2 mediate opposing pathologies in a mouse model of melanoma', *The FASEB Journal,* 33, pp. 11060-11071.

Navarria, P., Ascolese, A. M., Tomatis, S., Reggiori, G., Clerici, E., Villa, E., Maggi, G., Bello, L., Pessina, F., Cozzi, L. and Scorsetti, M. (2016) 'Hypofractionated Stereotactic

Radiation Therapy in Recurrent High-Grade Glioma: A New Challenge', *Cancer Res Treat,* 48(1), pp. 37-44.

Neher, J. J., Neniskyte, U., Zhao, J. W., Bal-Price, A., Tolkovsky, A. M. and Brown, G. C. (2011) 'Inhibition of microglial phagocytosis is sufficient to prevent inflammatory neuronal death', *J Immunol,* 186(8), pp. 4973-83.

Nejo, T., Matsushita, H., Karasaki, T., Nomura, M., Saito, K., Tanaka, S., Takayanagi, S., Hana, T., Takahashi, S., Kitagawa, Y., Koike, T., Kobayashi, Y., Nagae, G., Yamamoto, S., Ueda, H., Tatsuno, K., Narita, Y., Nagane, M., Ueki, K., Nishikawa, R., Aburatani, H., Mukasa, A., Saito, N. and Kakimi, K. (2019) 'Reduced Neoantigen Expression Revealed by Longitudinal Multiomics as a Possible Immune Evasion Mechanism in Glioma', *7,* 7(*Cancer Immunol Res*), pp. 1148–1161.

Nicoll, J. A., Zunarelli, E., Rampling, R., Murray, L. S., Papanastassiou, V. and Stewart, J. (2003) 'Involvement of apolipoprotein E in glioblastoma: immunohistochemistry and clinical outcome', *Neuroreport,* 14(15), pp. 1923-6.

Nunez-Cruz, S., Gimotty, P. A., Guerra, M. W., Connolly, D. C., Wu, Y.-Q., DeAngelis, R. A., Lambirs, J. D., Coukos, G. and Scholler, N. (2012) 'Genetic and pharmacologic inhibition of complement impairs endothelial cell function and ablates ovarian cancer neovascularization', *Neoplasia,* 14(11), pp. 994-1004.

Ohh, M., Park, C. W., Ivan, M., Hoffman, M. A., Kim, T. Y., Huang, L. E., Pavletich, N., Chau, V. and Kaelin, W. G. (2000) 'Ubiquitination of hypoxia-inducible factor requires direct binding to the beta-domain of the von Hippel-Lindau protein', *Nat Cell Biol,* 2(7), pp. 423-7.

Oliveira, F. D., de Campos, R. P., Pereira, L. C., Meira, L. B. and Lenz, G. (2024) 'Expression of key unfolded protein response genes predicts patient survival and an immunosuppressive microenvironment in glioblastoma', *Translational Medicine Communications,* 9(1), pp. 5.

Ortiz, R., Perazzoli, G., Cabeza, L., Jiménez-Luna, C., Luque, R., Prados, J. and Melguizo, C. (2021) 'Temozolomide: An Updated Overview of Resistance Mechanisms, Nanotechnology Advances and Clinical Applications', *Curr Neuropharmacol,* 19(4), pp. 513-537.

Osman, A. M., Sun, Y., Burns, T. C., He, L., Kee, N., Oliva-Vilarnau, N., Alevyzaki, A., Zhou, K., Louhivuori, L., Uhlén, P., Hedlund, E., Betsholtz, C., Lauschke, V. M., Kele, J. and Blomgren, K. (2020) 'Radiation Triggers a Dynamic Sequence of Transient Microglial Alterations in Juvenile Brain', *Cell Rep,* 31(9), pp. 107699.

Ostrom, Q. T., Patil, N., Cioffi, G., Waite, K., Kruchko, C. and Barnholtz-Sloan, J. S. (2020) 'CBTRUS Statistical Report: Primary Brain and Other Central Nervous System Tumors Diagnosed in the United States in 2013-2017', *Neuro Oncol,* 22(12 Suppl 2), pp. iv1-iv96.

Ostrom, Q. T., Price, M., Neff, C., Cioffi, G., Waite, K. A., Kruchko, C. and Barnholtz-Sloan, J. S. (2023) 'CBTRUS Statistical Report: Primary Brain and Other Central Nervous

System Tumors Diagnosed in the United States in 2016-2020', *Neuro Oncol,* 25(12 Suppl 2), pp. iv1-iv99.

Palmieri, E. M., Gonzalez-Cotto, M., Baseler, W. A., Davies, L. C., Ghesquière, B., Maio, N., Rice, C. M., Rouault, T. A., Cassel, T., Higashi, R. M., Lane, A. N., Fan, T. W., Wink, D. A. and McVicar, D. W. (2020) 'Nitric oxide orchestrates metabolic rewiring in M1 macrophages by targeting aconitase 2 and pyruvate dehydrogenase', *Nat Commun,* 11(1), pp. 698.

Pandey, S., Maharana, J., Li, X. X., Woodruff, T. M. and Shukla, A. K. (2020) 'Emerging Insights into the Structure and Function of Complement C5a Receptors', *Trends Biochem Sci,* 45(8), pp. 693-705.

Park, B. V., Freeman, Z. T., Ghasemzadeh, A., Chattergoon, M. A., Rutebemberwa, A., Steigner, J., Winter, M. E., Huynh, T. V., Sebald, S. M., Lee, S.-J., Pan, F., Pardon, D. M. and Cox, A. L. (2016) 'TGFβ1-Mediated SMAD3 Enhances PD-1 Expression on Antigen-Specific T Cells in Cancer ', *Cancer Discovery,* 6(12), pp. 1366–1381.

Park, J., Kim, C. G., Shim, J.-K., Kim, J. H., Lee, H., Lee, J. E., Kim, M. H., Haam, K., Jung, I., Park, S.-H., Chang, J. H., Shin, E.-C. and Kang, S.-G. (2018) 'Effect of combined anti-PD-1 and temozolomide therapy in glioblastoma', *Oncoimmunology,* 8(1), pp. e1525243.

Park, J., Yea, J. W. and Park, J. W. (2020) 'Hypofractionated radiotherapy versus conventional radiotherapy for diffuse intrinsic pontine glioma', *Medicine (Baltimore),* 99(42), pp. e22721.

Pei, H. P., Tan, F. B., Liu, L., Yu, N. H. and Zhu, H. (2016) 'IL-1β/NF-kb signaling promotes colorectal cancer cell growth through miR-181a/PTEN axis', *Arch Biochem Biophys,* 604, pp. 20-6.

Perillo, B., Di Donato, M., Pezone, A., Di Zazzo, E., Giovannelli, P., Galasso, G., Castoria, G. and Migliaccio, A. (2020) 'ROS in cancer therapy: the bright side of the moon', *Exp Mol Med,* 52(2), pp. 192-203.

Phuphanich, S., Supko, J. G., Carson, K. A., Grossman, S. A., Burt Nabors, L., Mikkelsen, T., Lesser, G., Rosenfeld, S., Desideri, S. and Olson, J. J. (2010) 'Phase 1 clinical trial of bortezomib in adults with recurrent malignant glioma', *J Neurooncol,* 100(1), pp. 95-103.

Piao, C., Zhang, W. M., Li, T. T., Zhang, C. C., Qiu, S., Liu, Y., Liu, S., Jin, M., Jia, L. X., Song, W. C. and Du, J. (2018) 'Complement 5a stimulates macrophage polarization and contributes to tumor metastases of colon cancer', *Exp Cell Res,* 366(2), pp. 127-138.

Platten, M., Kretz, A., Naumann, U., Aulwurm, S., Egashira, K., Isenmann, S. and Weller, M. (2003) 'Monocyte chemoattractant protein–1 increases microglial infiltration and aggressiveness of gliomas', *Annals of Neurology,* 54(3), pp. 388-392.

Prinz, M. and Priller, J. (2014) 'Microglia and brain macrophages in the molecular age: from origin to neuropsychiatric disease', *Nat Rev Neurosci,* 15(5), pp. 300-12.

Proescholdt, M. A., Merrill, M. J., Stoerr, E.-M., Lohmeier, A., Pohl, F. and Brawanski, A. (2012) 'Function of carbonic anhydrase IX in glioblastoma multiforme', *Neuro-Oncology,* 14(11), pp. 1357–1366.

Qiang, L., Wu, T., Zhang, H. W., Lu, N., Hu, R., Wang, Y. J., Zhao, L., Chen, F. H., Wang, X. T., You, Q. D. and Guo, Q. L. (2012) 'HIF-1α is critical for hypoxia-mediated maintenance of glioblastoma stem cells by activating Notch signaling pathway', *Cell Death Differ,* 19(2), pp. 284-94.

Qiao, Q., Sun, C., Han, C., Han, N., Zhang, M. and Li, G. (2017) 'Endoplasmic reticulum stress pathway PERK-eIF2α confers radioresistance in oropharyngeal carcinoma by activating NF-κB', *Cancer Sci,* 108(7), pp. 1421-1431.

Rahpeymai, Y., Hietala, M. A., Wilhelmsson, U., Fotheringham, A., Davies, I., Nilsson, A.-K., Zwirner, J., Wetsel, R. A., Gerard, C., Pekny, M. and Pekna, M. (2006) 'Complement: a novel factor in basal and ischemia-induced neurogenesis', *The EMBO Journal,* 25, pp. 1364 - 1374.

Ren, J., Xu, B., Ren, J., Liu, Z., Cai, L., Zhang, X., Wang, W., Li, S., Jin, L. and Ding, L. (2023) 'The Importance of M1-and M2-Polarized Macrophages in Glioma and as Potential Treatment Targets', *Brain Sciences,* 13(9), pp. 1269.

Revel, M., Daugan, M. V., Sautés-Fridman, C., Fridman, W. H. and Roumenina, L. T. (2020) 'Complement System: Promoter or Suppressor of Cancer Progression?', *Antibodies,* 9(4), pp. 57.

Ricklin, D., Hajishengallis, G., Yang, K. and Lambris, J. D. (2010) 'Complement: a key system for immune surveillance and homeostasis', *Nat Immunol,* 11(9), pp. 785-97.

Robertson, N., Rappas, M., Doré, A. S., Brown, J., Bottegoni, G., Koglin, M., Cansfield, J., Jazayeri, A., Cooke, R. M. and Marshall, F. H. (2018) 'Structure of the complement C5a receptor bound to the extra-helical antagonist NDT9513727', *Nature,* 553, pp. 111-114.

Romero-Ramirez, L., Cao, H., Regalado, M. P., Kambham, N., Siemann, D., Kim, J. J., Le, Q. T. and Koong, A. C. (2009) 'X box-binding protein 1 regulates angiogenesis in human pancreatic adenocarcinomas', *Transl Oncol,* 2(1), pp. 31-8.

Rosberg, R., Smolag, K. I., Sjölund, J., Johansson, E., Bergelin, C., Wahldén, J., Pantazopoulou, V., Ceberg, C., Pietras, K., Blom, A. M. and Pietras, A. (2024) 'Hypoxia-induced Complement Component 3 Promotes Aggressive Tumor Growth in the Glioblastoma Microenvironment', *JCI Insight,* 9(19), pp. e179854.

Roumenina, L. T., Daugan, M. V., Petitprez, F., Sautès-Fridman, C. and Fridman, W. H. (2019) 'Context-dependent roles of complement in cancer', *Nature Reviews Cancer,* 19, pp. 698-715.

Rübe, C. E., Wilfert, F., Uthe, D., Schmid, K. W., Knoop, R., Willich, N., Schuck, A. and Rübe, C. (2002) 'Modulation of radiation-induced tumour necrosis factor alpha (TNF-alpha) expression in the lung tissue by pentoxifylline', *Radiother Oncol,* 64(2), pp. 177-87.

Safa, A. R., Saadatzadeh, M. R., Cohen-Gadol, A. A., Pollok, K. E. and Bijangi-Vishehsaraei, K. (2015) 'Glioblastoma stem cells (GSCs) epigenetic plasticity and interconversion between differentiated non-GSCs and GSCs', *Genes Dis,* 2(2), pp. 152-163.

Said, H. M., Hagemann, C., Staab, A., Stojic, J., Kühnel, S., Vince, G. H., Flentje, M., Roosen, K. and Vordermark, D. (2007) 'Expression patterns of the hypoxia-related genes osteopontin, CA9, erythropoietin, VEGF and HIF-1α in human glioma i*n vitro* and i*n vivo*', *Radiotherapy & Oncology,* 83(3), pp. 398-405.

Sattler, R., Tyler, B., Hoover, B., Coddington, L. T., Recinos, V., Hwang, L., Brem, H. and Rothstein, J. D. (2013) 'Increased expression of glutamate transporter GLT-1 in peritumoral tissue associated with prolonged survival and decreases in tumor growth in a rat model of experimental malignant gliom a', *J Neurosurg,* 119(4), pp. 878-886.

Schafer, D. P., Lehrman, E. K., Kautzman, A. G., Koyama, R., Mardinly, A. R., Yamasaki, R., Ransohoff, R. M., Greenberg, M. E., Barres, B. A. and Stevens, B. (2012) 'Microglia Sculpt Postnatal Neural Circuits in an Activity and Complement-Dependent Manner', *Neuron,* 74(4), pp. 691-705.

Schartz, N. D., Liang, H. Y., Carvalho, K., Chu, S. H., Mendoza-Arvilla, A., Petrisko, T. J., Gomez-Arboledas, A., Mortazavi, A. and Tenner, A. J. (2023) 'C5aR1 antagonism suppresses inflammatory glial gene expression and alters cellular signaling in an aggressive Alzheimer's model', *bioRxiv*.

Schraufstatter, I. U., DiScipio, R. G., Zhao, M. and Khaldoyanidi, S. K. (2009) 'C3a and C5a Are Chemotactic Factors for Human Mesenchymal Stem Cells, Which Cause Prolonged ERK1/2 Phosphorylation', *J Immunol* 182(6), pp. 3827–3836.

Schüller, U., Iglauer, P., Dorostkar, M. M., Mawrin, C., Herms, J., Giese, A., Glatzel, M. and Neumann, J. E. (2021) 'Mutations within FGFR1 are associated with superior outcome in a series of 83 diffuse midline gliomas with H3F3A K27M mutations', *Acta Neuropathol,* 141(2), pp. 323-325.

Scole, A.-M., Johswich, K.-O., Morgan, B. P., Klos, A. and Monk, P. N. (2009) 'The human complement fragment receptor, C5L2, is a recycling decoy receptor', *Molecular Immunology,* 46(6), pp. 1149-1162.

Scott-Hewitt, N., Mahoney, M., Huang, Y., Korte, N., Yvanka de Soysa, T., Wilton, D. K., Knorr, E., Mastro, K., Chang, A., Zhang, A., Melville, D., Schenone, M., Hartigan, C. and Stevens, B. (2024) 'Microglial-derived C1q integrates into neuronal ribonucleoprotein complexes and impacts protein homeostasis in the aging brain', *Cell,* 187(16), pp. 4193-4212.e24.

Shamas-Din, A., Kale, J., Leber, B. and Andrews, D. W. (2013) 'Mechanisms of action of Bcl-2 family proteins', *Cold Spring Harb Perspect Biol,* 5(4), pp. a008714.

Shambharkar, P. B., Blonska, M., Pappu, B. P., Li, H., You, R., Sakural, H., Darnay, B. G. and Lin, X. (2007) 'Phosphorylation and ubiquitination of the IκB kinase complex by two distinct signaling pathways', *The EMBO Journal,* 26(7), pp. 1794-1805.

Sharma, D., Sandur, S. K., Rashmi, R., Maurya, D. K., Suryavanshi, S., Checker, R., Krishnan, S. and Sainis, K. B. (2010) 'Differential activation of NF-κB and nitric oxide in lymphocytes regulates in vitro and in vivo radiosensitivity', *Mutat Res,* 703(2), pp. 149-57.

Shen, C. K., Huang, B. R., Yeh, W. L., Chen, C. W., Liu, Y. S., Lai, S. W., Tseng, W. P., Lu, D. Y. and Tsai, C. F. (2021) 'Regulatory effects of IL-1β in the interaction of GBM and tumor-associated monocyte through VCAM-1 and ICAM-1', *Eur J Pharmacol,* 905, pp. 174216.

Shen, H., Mudassar, F., Ma, S., Wang, X., Nguyen, S., Bal, N., Huynh, Q. S., Wang, D., Chang, C., Ing, P., Varikatt, W., Lai, J., Gloss, B., Holst, J., O'Neill, G. M., Gee, H., Cook, K. M. and Hau, E. (2025) 'Inhibition of mitochondrial bioenergetics and hypoxia to radiosensitize diffuse intrinsic pontine glioma', *Neuro Oncol,* 27(4), pp. 1061-1075.

Shen, J., Chen, X., Hendershot, L. and Prywes, R. (2002) 'ER stress regulation of ATF6 localization by dissociation of BiP/GRP78 binding and unmasking of Golgi localization signals', *Dev Cell,* 3(1), pp. 99-111.

Shu, C., Zha, H., Long, H., Wang, X., Yang, F., Gao, J., Hu, C., Zhou, L., Guo, B. and Zhu, B. (2020) 'C3a-C3aR signaling promotes breast cancer lung metastasis via modulating carcinoma associated fibroblasts', *J Exp Clin Cancer Res,* 39(1), pp. 11.

Si, J., Guo, J., Zhang, X., Li, W., Zhang, S., Shang, S. and Zhang, Q. (2024) 'Hypoxia-induced activation of HIF-1alpha/IL-1beta axis in microglia promotes glioma progression via NF-κB-mediated upregulation of heparanase expression', *Biol Direct,* 19(1), pp. 45.

Siciliano, A. J., Rollins, T. E., Demartino, J., Konteatis, Z., Malkowitz, L., Van Riper, G., Bondy, S., Rosen, H. and Springer, M. S. (1994) 'Two-site binding of C5a by its receptor: an alternative binding paradigm for G protein-coupled receptors', *Proc. Natl. Acad. Sci. USA,* 91, pp. 1214-1218.

Sielska, M., Przanowski, P., Wylot, B., Gabrusiewicz, K., Maleszewska, M., Kijewska, M., Zawadzka, M., Kucharska, J., Vinnakota, K., Kettenmann, H., Kotulska, K., Grajkowska, W. and Kaminska, B. (2013) 'Distinct roles of CSF family cytokines in macrophage infiltration and activation in glioma progression and injury response', *The Journal of Pathology,* 230(3).

Simanshu, D. K., Nissley, D. V. and McCormick, F. (2017) 'RAS Proteins and Their Regulators in Human Disease', *Cell,* 170(1), pp. 17-33.

Soda, Y., Marumoto, T., Friedmann-Morvinski, D. and Verma, I. M. (2011) 'Transdifferentiation of glioblastoma cells into vascular endothelial cells', *PNAS,* 108(11), pp. 4274-4280.

Sodji, Q. H., Nambiar, D. K., Viswanathan, V., von Eybe, R., Colburg, D., Binkley, M. S., Li, C. G., Olcina, M. M., Chang, D. T., Le, Q.-T. and Giaccia, A. J. (2022) 'The Combination of Radiotherapy and Complement C3a Inhibition Potentiates Natural Killer cell Functions Against Pancreatic Cancer', *Cancer Res Commun.,* 2(7), pp. 725-738.

Song, Y., Wu, K. Y., Wu, W., Duan, Z. Y., Gao, Y. F., Zhang, L. D., Chong, T., Garstka, M. A., Zhou, W. and Li, K. (2018) 'Epithelial C5aR1 Signaling Enhances Uropathogenic

Escherichia coli Adhesion to Human Renal Tubular Epithelial Cells', *Front Immunol,* 9, pp. 949.

Sta, M., Sylva-Steenland, R. M. R., Casula, M., de Jong, J. M. B. V., Troost, D., Aronica, E. and Baas, F. (2011) 'Innate and adaptive immunity in amyotrophic lateral sclerosis: Evidence of complement activation', *Neurobiology of Disease,* 42(3), pp. 211-220.

Stellwagen, D. and Malenka, R. C. (2006) 'Synaptic scaling mediated by glial TNF-α', *Nature,* 440, pp. 1054–1059.

Stewart, R. D., Yu, V. K., Georgakilas, A. G., Koumenis, C., Park, J. H. and Carlson, D. J. (2011) 'Effects of Radiation Quality and Oxygen on Clustered DNA Lesions and Cell Death', *Radiation Research,* 176(5), pp. 587-602.

Strainic, M. G., Shevach, E. M., An, F., Lin, F. and Medof, M. E. (2013) 'Absent C3a and C5a receptor signaling into CD4 + T cells enables auto-inductive TGF-β1 signaling and induction of Foxp3 + T regulatory cells', *Nat Immunol,* 14(2), pp. 162-71.

Stupp, R., Hegi, M. E., Mason, W. P., van den Bent, M. J., Taphoorn, M. J., Janzer, R. C., Ludwin, S. K., Allgeier, A., Fisher, B., Belanger, K., Hau, P., Brandes, A. A., Gijtenbeek, J., Marosi, C., Vecht, C. J., Mokhtari, K., Wesseling, P., Villa, S., Eisenhauer, E., Gorlia, T., Weller, M., Lacombe, D., Cairncross, J. G. and Mirimanoff, R. O. (2009) 'Effects of radiotherapy with concomitant and adjuvant temozolomide versus radiotherapy alone on survival in glioblastoma in a randomised phase III study: 5-year analysis of the EORTC-NCIC trial', *Lancet Oncol,* 10(5), pp. 459-66.

Stupp, R., Mason, W. P., van den Bent, M. J., Weller, M., Fisher, B., Taphoorn, M. J., Belanger, K., Brandes, A. A., Marosi, C., Bogdahn, U., Curschmann, J., Janzer, R. C., Ludwin, S. K., Gorlia, T., Allgeier, A., Lacombe, D., Cairncross, J. G., Eisenhauer, E. and Mirimanoff, R. O. (2005) 'Radiotherapy plus concomitant and adjuvant temozolomide for glioblastoma', *N Engl J Med,* 352(10), pp. 987-96.

Su, Y., Liu, J., Tian, Y., Dong, H., Shi, M., Zhang, J., Li, W., Huang, Q., Xiang, N., Wang, C., He, L., Hu, L., Haberman, A. M., Liu, H. and Yang, X. (2024) 'HIF-1α Mediates Immunosuppression and Chemoresistance in Colorectal Cancer by Inhibiting CXCL9, -10 and -11', *Biomed Pharmacother,* 173, pp. 116427.

Surace, L., Lysenko, V. L., Fontana, A. O., Cecconi, V., Janssen, H., Bicvic, A., Okoniewski, M., Pruschy, M., Dummer, R., Neefjes, J., Knuth, A., Gupta, A. and Den Broek, M. (2015) 'Complement Is a Central Mediator of Radiotherapy-Induced Tumor-Specific Immunity and Clinical Response', *Immunity,* 42(2), pp. 767-777.

Suwa, T., Lee, K. S., Chai, I. J., Clark, H. O. L., MacLean, D. J., Machado, N., Rodriguez-Berriguete, G., Singh, L., Higgins, G. S., Hammond, E. M. and Olcina, M. M. (2025) 'UPR-induced intracellular C5aR1 promotes adaptation to the hypoxic tumour microenvironment', *Cell Death Dis,* 16(1), pp. 547.

Tabatabaei, P., Visse, E., Bergström, P., Brännström, T., Siesjö, P. and Bergenheim, A. T. (2017) 'Radiotherapy induces an immediate inflammatory reaction in malignant glioma: a clinical microdialysis study', *J Neurooncol,* 131(1), pp. 83-92.

Tailor, A., Estephan, H., Parker, R., Woodhouse, I., Abdulghani, M., Nicastri, A., Jones, K., Salatino, S., Muschel, R., Humphrey, T., Giaccia, A. and Ternette, N. (2022) 'Ionizing Radiation Drives Key Regulators of Antigen Presentation and a Global Expansion of the Immunopeptidome', *Mol Cell Proteomics,* 21(11), pp. 100410.

Takano, T., Lin, J. H.-C., Arcuino, G., Gao, Q., Yang, J. and Nedergaard, M. (2001) 'Glutamate release promotes growth of malignant gliomas', *Nature Medicine,* 7, pp. 1010-1015.

Tam, A. B., Koong, A. C. and Niwa, M. (2014) 'Ire1 has distinct catalytic mechanisms for XBP1/HAC1 splicing and RIDD', *Cell Rep,* 9(3), pp. 850-8.

Tamura, K., Aoyagi, M., Ando, N., Ogishima, T., Wakimoto, H., Yamamoto, M. and Ohno, K. (2013) 'Expansion of CD133-positive glioma cells in recurrent de novo glioblastomas after radiotherapy and chemotherapy', *J Neurosurg,* 119(5), pp. 1145-55.

Taylor, C. T. and Scholz, C. C. (2022) 'The effect of HIF on metabolism and immunity', *Nat Rev Nephrol,* 18(9), pp. 573-587.

Taylor, K. R., Mackay, A., Truffaux, N., Butterfield, Y., Morozova, O., Philippe, C., Castel, D., Grasso, C. S., Vinci, M., Carvalho, D., Carcaboso, A. M., de Torres, C., Cruz, O., Mora, J., Entz-Werle, N., Ingram, W. J., Monje, M., Hargrave, D., Bullock, A. N., Puget, S., Yip, S., Jones, C. and Grill, J. (2014) 'Recurrent activating ACVR1 mutations in diffuse intrinsic pontine glioma', *Nat Genet,* 46(5), pp. 457-461.

Teresa Pinto, A., Laranjeiro Pinto, M., Patrícia Cardoso, A., Monteiro, C., Teixeira Pinto, M., Filipe Maia, A., Castro, P., Figueira, R., Monteiro, A., Marques, M., Mareel, M., Dos Santos, S. G., Seruca, R., Adolfo Barbosa, M., Rocha, S. and José Oliveira, M. (2016) 'Ionizing radiation modulates human macrophages towards a pro-inflammatory phenotype preserving their pro-invasive and pro-angiogenic capacities', *Sci Rep,* 6, pp. 18765.

Thornberry, N. A., Bull, H. G., Calaycay, J. R., Chapman, K. T., Howard, A. D., Kostura, M. J., Miller, D. K., Molineaux, S. M., Weidner, J. R., Aunins, J. and et al. (1992) 'A novel heterodimeric cysteine protease is required for interleukin-1 beta processing in monocytes', *Nature,* 356(6372), pp. 768-74.

Tiwari, D. K., Hannen, R., Unger, K., Kohl, S., Heß, J., Lauber, K., Subtil, F. S. B., Dikomey, E., Engenhart-Cabillic, R. and Schötz, U. (2022) 'IL1 Pathway in HPV-Negative HNSCC Cells Is an Indicator of Radioresistance After Photon and Carbon Ion Irradiation Without Functional Involvement', *Front Oncol,* 12, pp. 878675.

Tomita, Y., Shimazu, Y., Somasundaram, A., Tanaka, Y., Takata, N., Ishi, Y., Gadd, S., Hashizume, R., Angione, A., Pinero, G., Hambardzumyan, D., Brat, D. J., Hoeman, C. M. and Becher, O. J. (2022) 'A novel mouse model of diffuse midline glioma initiated in neonatal oligodendrocyte progenitor cells highlights cell-of-origin dependent effects of H3K27M', *Glia,* 70(9), pp. 1681-1698.

Treps, L., Perret, R., Edmond, S., Ricard, D. and Gavard, J. (2017) 'Glioblastoma stem-like cells secrete the pro-angiogenic VEGF-A factor in extracellular vesicles', *Journal of Extracellular Vesicles,* 6(1), pp. 1359479.

Tsuchiya, Y., Saito, M., Kadokura, H., Miyazaki, J. I., Tashiro, F., Imagawa, Y., Iwawaki, T. and Kohno, K. (2019) 'Correction: IRE1-XBP1 pathway regulates oxidative proinsulin folding in pancreatic β cells', *J Cell Biol,* 218(5), pp. 1764.

Ueda, R., Fujita, M., Zhu, X., Sasaki, K., Kastenhuber, E. R., Kohanbash, G., McDonald, H. A., Harper, J., Lonning, S. and Okada, H. (2009) 'Systemic Inhibition of Transforming Growth Factor-β in Glioma-Bearing Mice Improves the Therapeutic Efficacy of Glioma-Associated Antigen Peptide Vaccines', *Clin Cancer Res,* 15(21), pp. 6551–6559.

Upton, J. P., Wang, L., Han, D., Wang, E. S., Huskey, N. E., Lim, L., Truitt, M., McManus, M. T., Ruggero, D., Goga, A., Papa, F. R. and Oakes, S. A. (2012) 'IRE1α cleaves select microRNAs during ER stress to derepress translation of proapoptotic Caspase-2', *Science,* 338(6108), pp. 818-22.

Vadrevu, S. K., Chintala, N. K., Sharma, S. K., Sharma, P., Cleveland, C., Riediger, L., Manne, S., Fairlie, D. P., Gorczyca, W., Almanza, O., Karbowniczek, M. and Markiewski, M. M. (2014) 'Complement C5a Receptor Facilitates Cancer Metastasis by Altering T-Cell Responses in the Metastatic Niche', *Cancer Res,* 74(13), pp. 3454–65.

van Hooren, L., Handgraaf, S. M., Kloosterman, D. J., Karimi, E., van Mil, L. W. H. G., Gassama, A. A., Gomez Solsona, B., de Groot, M. H. P., Brandsma, D., Quail, D. F., Walsh, L. A., Borst, G. R. and Akkari, L. (2023) 'CD103 + regulatory T cells underlie resistance to radio-immunotherapy and impair CD8 + T cell activation in glioblastoma', *Nature,* 4, pp. 665–681.

Vanan, M. I. and Eisenstat, D. D. (2015) 'DIPG in Children – What Can We Learn from the Past?', *Frontiers in Oncology,* 5.

Venkatesh, H. S., John, T. B., Caretti, V., Noll, A., Tang, Y., Nagaraja, S., Gibson, E. M., Mount, C. W., Polepalli, J., Mitra, S. S., Woo, P. J., Malenka, R. C., Vogel, H., Bredel, M., Mallick, P. and Monje, M. (2015) 'Neuronal Activity Promotes Glioma Growth through Neuroligin-3 Secretion', *Cell,* 161(4), pp. 803-816.

Venkatesh, H. S., Tam, L. T., Woo, P., J, Lennon, J., Nagaraja, S., Gillespie, S. M., Ni, J., Duveau, D. Y., Morris, P. J., Zhao, J. J., Thomas, C. J. and Monje, M. (2017) 'Targeting neuronal activity-regulated neuroligin-3 dependency in high-grade glioma', *Nature,* 549, pp. 533-537.

Voshart, D. C., Oshima, T., Jiang, Y., van der Linden, G. P., Ainslie, A. P., Reali Nazario, L., van Buuren-Broek, F., Scholma, A. C., van Weering, H. R. J., Brouwer, N., Sewdihal, J., Brouwer, U., Coppes, R. P., Holtman, I. R., Eggen, B. J. L., Kooistra, S. M. and Barazzuol, L. (2024) 'Radiotherapy induces persistent innate immune reprogramming of microglia into a primed state', *Cell Rep,* 43(2), pp. 113764.

Wainwright, D. A., Chang, A. L., Dey, M., Balyasnikova, I. V., Kim, C. K., Tobias, A., Cheng, Y., Kim, J. W., Qiao, J., Zhang, L., Han, Y. and Lesniak, M. S. (2014) 'Durable therapeutic efficacy utilizing combinatorial blockade against IDO, CTLA-4 and PD-L1 in mice with brain tumors', *Clin Cancer Res,* 20(20), pp. 5290–5301.

Walmsley, S. R., Print, C., Farahi, N., Peyssonnaux, C., Johnson, R. S., Cramer, T., Sobolewski, A., Condliffe, A. M., Cowburn, A. S., Johnson, N. and Chilvers, E. R. (2005)

'Hypoxia-induced neutrophil survival is mediated by HIF-1alpha-dependent NF-kappaB activity', *J Exp Med,* 201(1), pp. 105-15.

Wang, H., Jiang, H., Van De Gucht, M. and De Ridder, M. (2019) 'Hypoxic Radioresistance: Can ROS Be the Key to Overcome It?', *Cancers (Basel),* 11(1).

Wang, M. and Kaufman, R. J. (2016) 'Protein misfolding in the endoplasmic reticulum as a conduit to human disease', *Nature,* 529(7586), pp. 326-35.

Wang, S.-C., Hong, J.-H., Hsueh, C. and Chiang, C.-S. (2012) 'Tumor-secreted SDF-1 promotes glioma invasiveness and TAM tropism toward hypoxia in a murine astrocytoma model', *Laboratory Investigation,* 92(1), pp. 151-162.

Warren, K. E. (2012) 'Diffuse intrinsic pontine glioma: poised for progress', *Frontiers in Oncology,* 2, pp. 205.

Waters, S. M., Brodbeck, R. M., Steflik, J., Yu, J., Baltazar, C., Peck, A. E., Severance, D., Zhang, L. Y., Currie, K., Chenard, B. L., Hutchison, A. J., Maynard, G. and Krause, J. E. (2005) 'Molecular Characterization of the Gerbil C5a Receptor and Identification of a Transmembrane Domain V Amino Acid That Is Crucial for Small Molecule Antagonist Interaction', *Journal of Biological Chemistry,* 280(49), pp. 40617-40623.

Watkins, S., Robel, S., Kimbrough, I. F., Robert, S. M., Ellis-Davies, G. and Sontheimer, H. (2014) 'Disruption of astrocyte–vascular coupling and the blood–brain barrier by invading glioma cells', *Nature Communications,* 5, pp. 4196.

Wei, J., Zhu, K., Yang, Z., Zhou, Y., Xia, Z., Ren, J., Zhao, Y., Wu, G. and Liu, C. (2023) 'Hypoxia-Induced Autophagy Is Involved in Radioresistance via HIF1A-Associated Beclin-1 in Glioblastoma Multiforme', *Heliyon,* 9(1), pp. e12820.

Wei, Q., Singh, O., Ekinci, C., Gill, J., Li, M., Mamatjan, Y., Karimi, S., Bunda, S., Mansouri, S., Aldape, K. and Zadeh, G. (2021) 'TNFα secreted by glioma associated macrophages promotes endothelial activation and resistance against anti-angiogenic therapy', *Acta Neuropathol Commun,* 9(1), pp. 67.

Weidemann, A. and Johnson, R. S. (2008) 'Biology of HIF-1α', *Cell Death Differ,* 15, pp. 621-627.

Werbrouck, C., Evangelista, C. C. S., Lobón-Iglesias, M.-J., Barret, E., Le Teuff, G., Merlevede, J., Brusini, R., Kergrohen, T., Mondini, M., Bolle, S., Varlet, P., Beccaria, K., Boddaert, N., Puget, S., Grill, J. and Debily, M.-A. (2019) 'TP53 Pathway Alterations Drive Radioresistance in Diffuse Intrinsic Pontine Gliomas (DIPG) ', *Clinical Cancer Research,* 25(22), pp. 6788-6800.

Wesolowska, A., Kwiatkowska, A., Slomnicki, L., Dembinski, M., Master, A., Silwa, M., Franciszkiewicz, K., Chouaib, S. and Kaminska, B. (2007) 'Microglia-derived TGF-β as an important regulator of glioblastoma invasion—an inhibition of TGF-β-dependent effects by shRNA against human TGF-β type II receptor', *27*, pp. 918-930.

Wick, W., Platten, M., Meisner, C., Felsberg, J., Tabatabai, G., Simon, M., Nikkhah, G., Papsdorf, K., Steinbach, J. P., Sabel, M., Combs, S. E., Vesper, J., Braun, C., Meixensberger, J., Ketter, R., Mayer-Steinacker, R., Reifenberger, G. and Weller, M.

(2012) 'Temozolomide chemotherapy alone versus radiotherapy alone for malignant astrocytoma in the elderly: the NOA-08 randomised, phase 3 trial', *Lancet Oncol,* 13(7), pp. 707-15.

Wu, A., Wei, J., Kong, L.-Y., Wang, Y., Priebe, W., Qiao, W., Sawaya, R. and Heimberger, A. B. (2010) 'Glioma cancer stem cells induce immunosuppressive macrophages/microglia', *Neuro-Oncology,* 12(11), pp. 1113–1125.

Wu, M., Wu, L., Wu, W., Zhu, M., Li, J., Wang, Z., Li, J., Ding, R., Liang, Y., Li, L., Zhang, T., Huang, B., Cai, Y., Li, K., Li, L., Zhang, R., Hu, B., Lin, F., Wang, X., Zheng, S., Chen, J., You, Y., Jiang, T., Zhang, J., Chen, H. and Wang, Q. (2023) 'Phagocytosis of Glioma Cells Enhances the Immunosuppressive Phenotype of Bone Marrow–Derived Macrophages', *Cancer Res,* 83(5), pp. 771–785.

Wu, P., Tian, T., Zhao, J., Song, Q., Wu, X., Guo, Y., Yu, Y., Tan, S. and Xia, H. (2021) 'IRE1α-JNK pathway-mediated autophagy promotes cell survival in response to endoplasmic reticulum stress during the initial phase of hepatic steatosis', *Life Sci,* 264, pp. 118668.

Wu, S., Du, R., Gao, C., Kang, J., Wen, J. and Sun, T. (2018) 'The role of XBP1s in the metastasis and prognosis of hepatocellular carcinoma', *Biochem Biophys Res Commun,* 500(3), pp. 530-537.

Xue, J., Dong, J. H., Huang, G. D., Qu, X. F., Wu, G. and Dong, X. R. (2014) 'NF-κB signaling modulates radiation-induced microglial activation', *Oncol Rep,* 31(6), pp. 2555-60.

Yamamori, T., Yasui, H., Yamazumi, M., Wada, Y., Nakamura, Y., Nakamura, H. and Inanami, O. (2012) 'Ionizing radiation induces mitochondrial reactive oxygen species production accompanied by upregulation of mitochondrial electron transport chain function and mitochondrial content under control of the cell cycle checkpoint', *Free Radic Biol Med,* 53(2), pp. 260-70.

Yang, H., Niemeijer, M., van de Water, B. and Beltman, J. B. (2020) 'ATF6 Is a Critical Determinant of CHOP Dynamics during the Unfolded Protein Response', *iScience,* 23(2), pp. 100860.

Yang, T., Li, J., Cheng, X., Lu, Q., Farooq, Z., Fu, Y., Lv, S., Nan, W., Yu, B., Duan, J., Zhang, Y., Fu, Y., Jiang, H., McCormick, P. J., Li, Y. and Zhang, J. (2024) 'Structural analysis of the human C5a-C5aR1 complex using cryo-electron microscopy', *Journal of Structural Biology,* 216(3), pp. 108117.

Ye, J., Rawson, R. B., Komuro, R., Chen, X., Davé, U. P., Prywes, R., Brown, M. S. and Goldstein, J. L. (2000) 'ER stress induces cleavage of membrane-bound ATF6 by the same proteases that process SREBPs', *Mol Cell,* 6(6), pp. 1355-64.

Yeom, K. W., Lober, R. M., Nelson Jr, M. D., Panigraphy, A. and Blüml, S. (2015) 'Citrate concentrations increase with hypoperfusion in pediatric diffuse intrinsic pontine glioma ', *Journal of Neuro-Oncology,* 122, pp. 383-389.

Yoshida, H., Matsui, T., Yamamoto, A., Okada, T. and Mori, K. (2001) 'XBP1 mRNA is induced by ATF6 and spliced by IRE1 in response to ER stress to produce a highly active transcription factor', *Cell,* 107(7), pp. 881-91.

Yu, C.-F., Chen, F.-H., Lu, M.-H., Hong, J.-H. and Chiang, C.-S. (2017) 'Dual roles of tumour cells-derived matrix metalloproteinase 2 on brain tumour growth and invasion', *British Journal of Cancer,* 117, pp. 1828-1836.

Yu, J.-R., LeRoy, G., Bready, D., Frenster, J. D., Saldaña-Meyer, R., Jin, Y., Descostes, N., Stafford, J. M., Placantonakis, D. G. and Reinberg, D. (2021) 'The H3K36me2 writer-reader dependency in H3K27M-DIPG', *7,* 29.

Yuan, M., Wang, C., Wu, Y., Qiao, L., Deng, G., Liang, N., Chen, F., Liu, L., Chen, Y., Yang, Y., Wang, H., Liu, T., Yang, X., Zhang, Y., Lv, Y., Suwinski, R., Hu, P., Zhang, Y. and Zhang, J. (2023) 'Targeting complement C5a to improve radiotherapy sensitivity in non-small cell lung cancer', *Translational Lung Cancer Research,* 12(5), pp. 1093-1107.

Yun, E. J., Kim, D., Kim, S., Hsieh, J. T. and Baek, S. T. (2023) 'Targeting Wnt/β-catenin-mediated upregulation of oncogenic NLGN3 suppresses cancer stem cells in glioblastoma', *Cell Death Dis,* 14(7), pp. 423.

Zanoni, M., Sarti, A. C., Zamagni, A., Cortesi, M., Pignatta, S., Arienti, C., Tebaldi, M., Sarnelli, A., Romeo, A., Bartolini, D., Tosatto, L., Adinolfi, E., Tesei, A. and Di Virgilio, F. (2022) 'Irradiation causes senescence, ATP release, and P2X7 receptor isoform switch in glioblastoma', *Cell Death Dis,* 13(1), pp. 80.

Zeng, J., See, A. P., Phallen, J., Jackson, C. M., Belcaid, Z., Ruzevick, J., Durham, N., Meyer, C., Harris, T. J., Albesiano, E., Pradilla, G., Ford, E., Wong, J., Hammers, H. J., Mathios, D., Tyler, B., Brem, H., Tran, P. T., Pardoll, D., Drake, C. G. and Lim, M. (2013a) 'Anti-PD-1 blockade and stereotactic radiation produce long-term survival in mice with intracranial gliomas', *Int J Radiat Oncol Biol Phys,* 86(2), pp. 343-9.

Zeng, L., Xiao, Q., Chen, M., Margariti, A., Martin, D., Ivetic, A., Xu, H., Mason, J., Wang, W., Cockerill, G., Mori, K., Li, J. Y., Chien, S., Hu, Y. and Xu, Q. (2013b) 'Vascular endothelial cell growth-activated XBP1 splicing in endothelial cells is crucial for angiogenesis', *Circulation,* 127(16), pp. 1712-22.

Zhang, G., Dong, Z., Prager, B. C., Kim, L. J., Wu, Q., Gimple, R. C., Wang, X., Bao, S., Hamerlik, P. and Rich, J. N. (2019) 'Chromatin remodeler HELLS maintains glioma stem cells through E2F3 and MYC', *JCI Insight,* 4(7).

Zhang, J., Sarkar, S., Cua, R., Zhou, Y., Hader, W. and Yong, V. W. (2012) 'A dialog between glioma and microglia that promotes tumor invasiveness through the CCL2/CCR2/interleukin-6 axis', *Carcinogenesis,* 33(2), pp. 312–319.

Zhang, J., Stevens, M. F. and Bradshaw, T. D. (2012) 'Temozolomide: mechanisms of action, repair and resistance', *Curr Mol Pharmacol,* 5(1), pp. 102-14.

Zhang, W., Shi, X., Peng, Y., Wu, M., Zhang, P., Xie, R., Wu, Y., Yan, Q., Liu, S. and Wang, J. (2015) 'HIF-1α Promotes Epithelial-Mesenchymal Transition and Metastasis through Direct Regulation of ZEB1 in Colorectal Cancer', *PLoS One,* 10(6), pp. e0129603.

Zhang, Y., Kang, T., Wang, Y., Song, C., Li, H., Mi, H., Li, Y., Dong, M., Ma, X., Zhu, H., Cheng, L., Zhang, P., Chen, Z., Zhou, L., Wu, Q., Mao, F., Wang, B., Zhang, S., Shu, K., Wan, F., Zhou, W., Rich, J. N., Shen, J., Xiao, Q. and Yu, X. (2024) 'A low level of tumor necrosis factor α in tumor microenvironment maintains the self-renewal of glioma stem cells by Vasorin-mediated glycolysis', *Neuro Oncol,* 26(12), pp. 2256-2271.

Zhang, Y. C., Huo, F. C., Wei, L. L., Gong, C. C., Pan, Y. J., Mou, J. and Pei, D. S. (2017) 'PAK5-mediated phosphorylation and nuclear translocation of NF-κB-p65 promotes breast cancer cell proliferation in vitro and in vivo', *J Exp Clin Cancer Res,* 36(1), pp. 146.

Zheng, Z., Su, J., Bao, X., Wang, H., Bian, C., Zhao, Q. and Jiang, X. (2023) 'Mechanisms and applications of radiation-induced oxidative stress in regulating cancer immunotherapy', *Front Immunol,* 14, pp. 1247268.

Zhou, J., Li, C., Yao, W., Alsiddig, M. C., Huo, L., Liu, H. and Miao, Y. L. (2018) 'Hypoxia-inducible factor-1α-dependent autophagy plays a role in glycolysis switch in mouse granulosa cells', *Biol Reprod,* 99(2), pp. 308-318.

Zhou, X., He, L., Wu, C., Zhang, Y., Wu, X. and Yin, Y. (2017) 'Serine alleviates oxidative stress via supporting glutathione synthesis and methionine cycle in mice', *Mol Nutr Food Res,* 61(11).

Zou, W., Wolchok, J. D. and Chen, L. (2016) 'PD-L1 (B7-H1) and PD-1 Pathway Blockade for Cancer Therapy: Mechanisms, Response Biomarkers and Combinations', *Sci Transl Med,* 8(328), pp. 328rv4.